



CISM COURSES AND LECTURES NO. 315
INTERNATIONAL CENTRE FOR MECHANICAL SCIENCES

NONLINEAR WAVES IN REAL FLUIDS

EDITED BY

A. KLUWICK

SPRINGER - VERLAG
WIEN - NEW YORK

University of Nebraska, Lincoln - Libraries



R0218929595

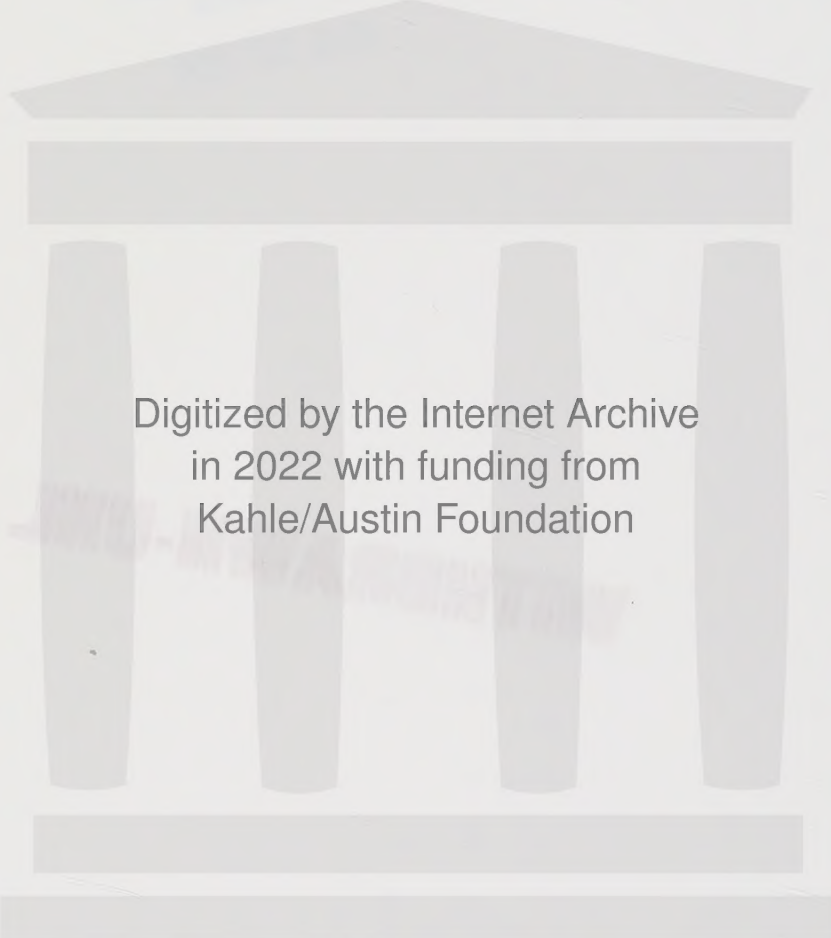


2000x2000

UNIVERSITY OF NEBR.
LIBRARIES

AUG 22 1991

WITHDRAWN-UNL



Digitized by the Internet Archive
in 2022 with funding from
Kahle/Austin Foundation

<https://archive.org/details/nonlinearwavesin0000unse>

COURSES AND LECTURES - No. 315



NONLINEAR WAVES IN
REAL FLUIDS

EDITED BY

A. KLUWICK

TECHNICAL UNIVERSITY OF VIENNA

SPRINGER - VERLAG



WIEN - NEW YORK

Le spese di stampa di questo volume sono in parte coperte da
contributi del Consiglio Nazionale delle Ricerche.

This volume contains 159 illustrations.

This work is subject to copyright.

All rights are reserved,
whether the whole or part of the material is concerned
specifically those of translation, reprinting, re-use of illustrations,
broadcasting, reproduction by photocopying machine
or similar means, and storage in data banks.
© 1991 by CISM, Udine
Printed in Italy

In order to make this volume available as economically and as
rapidly as possible the authors' typescripts have been
reproduced in their original forms. This method unfortunately
has its typographical limitations but it is hoped that they in no
way distract the reader.

ISBN 3-211-82277-1 Springer Verlag Wien-New York
ISBN 0-387-82277-1 Springer Verlag New York-Wien

PREFACE

The study of materials which exhibit new and unconventional properties is of central importance for the development of advanced and refined technologies in many fields of engineering science. In this connection there has been a rapidly growing interest in real fluid effects on wave phenomena in the past few years. Here the notation “real” is not meant simply to infer the incorporation of dissipative mechanisms such as internal friction, heat conduction, etc. which are neglected in studies dealing with ideal fluids. Rather, it signals the occurrence of new effects which are present even in situations where dissipation plays an insignificant role. A prominent example is provided by Beth-Zel'dovich-Thompson (BZT) fluids which have the distinguishing feature that they exhibit negative nonlinearity over a finite range of temperatures and pressures in the vapour phase. However, two phase flows with and without phase change are an even richer source of new unexpected and previously thought impossible phenomena.

The present volume contains the lecture notes presented during a course at the International Centre for Mechanical Sciences in Udine. Topics covered by these lecture notes include waves in gases near the critical point, waves in retrograde fluids, temperature waves in superfluid helium and density waves in suspensions of particles in liquids. Clearly, the aim of the various contributions is twofold. First, they are intended to provide scientists and engineers working in these and related areas with an overview of various new physical phenomena as for example expansion shocks, sonic shocks, shock splitting, evaporation and liquefaction shocks, ... and the experimental techniques needed to study these phenomena. Second an attempt is made to discuss aspects of their

mathematical modeling with special emphasis on properties which these phenomena have in common. In this respect model equations such as the modified Burgers equation, the Burgers Korteweg de Vries equation are seen to play a key role as far as the propagation of weakly nonlinear waves is concerned. However, methods for treating finite amplitude effects are outlined also.

The authors would like to thank the members of CISM and in particular Prof. Kaliszky, Prof. Bianchi, Prof. Tasso and Dr. Bertozzi for their advice and help during the preparation of this volume.

A. Kluwick

CONTENTS

	Page
Preface	
Small-amplitude finite-rate waves in fluids having both positive and negative nonlinearity by A. Kluwick	1
Nonlinear acoustics of bubbly liquids by D.G. Crighton	45
Nonlinear waves in aerosols and dusty gases by D.G. Crighton	69
Nonlinear waves in fluidized beds by D.G. Crighton	83
Nonclassical dynamics of classical gases by M.S. Cramer	91
Liquid-vapor adiabatic phase changes and related phenomena by P.A. Thompson	147
Nucleation, condensation and evaporation in waves and jets by G.E.A. Meier	215
Waves in superfluid Helium by W. Fiszdon	273

SMALL-AMPLITUDE FINITE-RATE WAVES IN FLUIDS HAVING BOTH POSITIVE AND NEGATIVE NONLINEARITY

A. Kluwick

Technical University Vienna, Vienna, Austria

Abstract

The present study deals with weakly nonlinear progressive waves in which the local value of the fundamental derivative Γ changes sign. The unperturbed medium is taken to be at rest and in a state such that Γ is small and of the order of the wave amplitude. A weak shock theory is developed to treat inviscid motions in channels of constant and slowly varying area of crossection. Furthermore, the method of multiple scales is used to account for thermoviscous effects which are of importance inside shock layers and acoustic boundary layers. New phenomena of interest include shocks having sonic conditions either upstream or downstream of the shock, collisions between expansion and compression shocks and shocks which terminate at a finite distance from their origin.

1. Introduction

As pointed out by Hayes [1] the socalled fundamental derivative

$$\Gamma(\tilde{\varrho}, \tilde{s}) = \frac{1}{\tilde{c}} \frac{\partial(\tilde{c} \tilde{\varrho})}{\partial \tilde{\varrho}} \Big|_{\tilde{s}}$$

plays a key role as far as the propagation of weakly nonlinear acoustic waves is concerned. Here $\tilde{c} = \sqrt{(\partial \tilde{p}/\partial \tilde{\varrho})_{\tilde{s}}}$ is the local speed of sound and \tilde{p} , $\tilde{\varrho}$ and \tilde{s} are the

pressure, the density and the entropy; throughout, dimensional quantities will be denoted by $\tilde{\cdot}$.

If Γ is positive at every point of the body of the fluid considered, parts of an acoustic wave carrying higher values of the excess pressure propagate faster than those where the pressure disturbances are smaller. As a consequence, compression shocks are the only discontinuities capable of propagating in the fluid while any (imposed) expansion discontinuity immediately disintegrates into a wave fan. Perfect gases are one important member of this class of fluids, Γ then being a positive constant. Therefore, if the undisturbed state of the fluid is characterized by a point in the $\tilde{p}, 1/\tilde{\varrho}$ -plane (Fig. 1) which is sufficiently far from the saturation line one expects Γ to be positive. If Γ is negative in the whole body of fluid considered, however, wavefronts will steepen backwards and expansion or rarefaction shocks are the only discontinuities capable of forming and propagating in the fluid. Fluids of this type have been studied first by Bethe [2] and independently by Zel'dovich [3] who showed that Van der Waals gases exhibit regions of negative nonlinearity near the critical point provided the specific heats take on sufficiently large values. An important recent study is due to Thompson and Lambrakis [4] who gave specific examples of real fluids having $\Gamma < 0$ which include hydrocarbons and fluorocarbons of moderate complexity. The properties of fluorocarbons have been investigated also by Cramer [5] who applied the Martin Hou equation to determine the fundamental derivative. Each of seven commercially available fluorocarbons were found to have a region of negative nonlinearity large enough to include the critical isotherm.

The studies mentioned so far confirm that Γ can, in fact, change sign for a class of single-phase fluids. This occurs on a line in the $\tilde{p}, 1/\tilde{\varrho}$ -plane to which we shall refer to as the transition line and its neighbourhood as the transition zone. When the unperturbed state of the fluid is sufficiently far from this zone, every point on a given wave or pulse will correspond to either positive or negative values of Γ . If Γ is positive the results predicted by the classical theory of nonlinear acoustics hold. Moreover, these results can be generalized quite easily to cover the range of strictly negative nonlinearity $\Gamma < 0$. However, when the unperturbed state is sufficiently close to the transition line relative to the wave amplitude, the local value of Γ may change sign inside the wave. As a consequence, one portion of the wave would correspond to $\Gamma > 0$ and another to $\Gamma < 0$ and as shown by Borisov, Borisov, Kutateladze and Nakoryakov [6] and by Cramer and Kluwick [7] the behaviour of the wave can then be qualitatively different from that obtained when the sign of Γ remains unchanged.

In the present study an attempt is being made to briefly outline the main

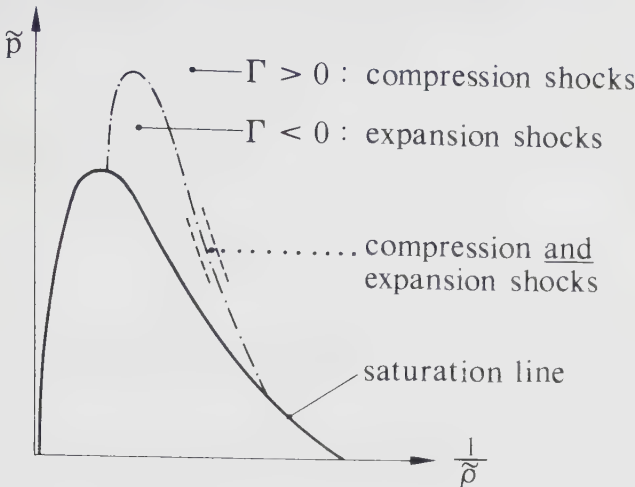


Figure 1: Regions of $\Gamma > 0$ and $\Gamma < 0$ in the \tilde{p} , $1/\tilde{\rho}$ -plane

properties of small-amplitude finite-rate waves in media having both positive and negative, e.g. having mixed nonlinearity. Waves in single phase fluids are treated in sections 2, 3 and 4. Effects of mixed nonlinearity, however, are not restricted to such media. Indeed, they have been encountered first in studies dealing with two phase flows, Kynch [8], Slis, Willemse and Kramers [9]. In section 4, therefore, the results holding for single phase fluids are extended to cover more general situations including among others wave motions in two phase systems and superfluid Helium.

2. Weakly nonlinear plane waves with mixed nonlinearity

As a starting point let us consider waves which are governed by the one-dimensional version of the classical Navier-Stokes-equations

$$\frac{\partial \tilde{\rho}}{\partial t} + \tilde{u} \frac{\partial \tilde{\rho}}{\partial \tilde{x}} + \tilde{\rho} \frac{\partial \tilde{u}}{\partial \tilde{x}} = 0 \quad (2.1)$$

$$\tilde{\rho} \left[\frac{\partial \tilde{u}}{\partial t} + \tilde{u} \frac{\partial \tilde{u}}{\partial \tilde{x}} \right] + \frac{\partial \tilde{p}}{\partial \tilde{x}} = \frac{\partial}{\partial \tilde{x}} [(\tilde{\lambda} + 2\tilde{\mu}) \frac{\partial \tilde{u}}{\partial \tilde{x}}] \quad (2.2)$$

$$\tilde{\rho} \tilde{T} \left[\frac{\partial \tilde{s}}{\partial \tilde{t}} + \tilde{u} \frac{\partial \tilde{s}}{\partial \tilde{x}} \right] = (\tilde{\lambda} + 2\tilde{\mu}) \left(\frac{\partial \tilde{u}}{\partial \tilde{x}} \right)^2 + \frac{\partial}{\partial \tilde{x}} (\tilde{k} \frac{\partial \tilde{T}}{\partial \tilde{x}}) \quad (2.3)$$

where $\tilde{\rho}$, \tilde{p} , \tilde{T} , \tilde{s} and \tilde{u} denote the density, the pressure, the absolute temperature, the entropy and the velocity of the fluid and the quantities \tilde{k} , $\tilde{\mu}$ and $\tilde{\lambda}$ are the thermal conductivity and the first and second viscosity, respectively. We shall mostly be concerned with the lossless limit of the governing equations, i.e. $\tilde{\mu}$, $\tilde{\lambda}$,

$\tilde{k} = 0$ which then have to be supplemented by the shock jump conditions

$$\tilde{v}[\tilde{\varrho}] = [\tilde{\varrho}\tilde{u}] \quad (2.4)$$

$$(\tilde{v} - \tilde{u}_a)(\tilde{v} - \tilde{u}_b) = \frac{[\tilde{p}]}{[\tilde{\varrho}]} \quad (2.5)$$

$$[\tilde{h}] = \frac{1}{2}(\tilde{V}_a + \tilde{V}_b)[\tilde{p}] \quad (2.6)$$

$$[\tilde{s}] \geq 0 \quad (2.7)$$

where $\tilde{V} = 1/\tilde{\varrho}$, and \tilde{h} and \tilde{v} are the specific enthalpies and the shock speed. The brackets denote jumps, i.e. $[Q] = Q_a - Q_b$ and the subscripts a and b refer to conditions after and before the shock.

The unperturbed state will be taken to be uniform and at rest $\tilde{u} = 0$, $\tilde{\varrho} = \tilde{\varrho}_o$, $\tilde{s} = \tilde{s}_o$. It is then convenient to introduce the nondimensional quantities

$$\begin{aligned} x &= \frac{\tilde{x}}{\tilde{L}}, \quad t = \frac{\tilde{c}_o}{\tilde{L}}\tilde{t}, \quad u = \frac{\tilde{u}}{\tilde{c}_o}, \quad v = \frac{\tilde{v}}{\tilde{c}_o}, \\ s &= \frac{\tilde{s}}{\tilde{c}_{vo}}, \quad p = \frac{\tilde{p} - \tilde{p}_o}{\tilde{\varrho}_o \tilde{c}_o^2}, \quad \varrho = \frac{\tilde{\varrho}}{\tilde{\varrho}_o}, \quad T = \frac{\tilde{T}}{\tilde{T}_o}, \\ h &= \frac{\tilde{h}}{\tilde{c}_o^2}, \quad V = \tilde{V}\tilde{\varrho}_o, \\ \lambda &= \frac{\tilde{\lambda}}{\tilde{\lambda}_o}, \quad \mu = \frac{\tilde{\mu}}{\tilde{\mu}_o}, \quad k = \frac{\tilde{k}}{\tilde{k}_o}. \end{aligned} \quad (2.8)$$

Here \tilde{L} is a characteristic wavelength and the subscript o denotes quantities evaluated at the unperturbed state. Substitution of (2.8) into equations (2.1), (2.2) and (2.3) yields

$$\frac{\partial \varrho}{\partial t} + u \frac{\partial \varrho}{\partial x} + \varrho \frac{\partial u}{\partial x} = 0 \quad (2.9)$$

$$\varrho \left[\frac{\partial u}{\partial t} + u \frac{\partial u}{\partial x} \right] + \frac{\partial p}{\partial x} = \frac{1}{Re} \frac{\partial}{\partial x} \left[(\frac{\tilde{\lambda}_o}{\tilde{\mu}_o} \lambda + 2\mu) \frac{\partial u}{\partial x} \right] \quad (2.10)$$

$$\varrho T \left[\frac{\partial s}{\partial t} + u \frac{\partial s}{\partial x} \right] = \frac{1}{Re} \left\{ E \left(\frac{\tilde{\lambda}_o}{\tilde{\mu}_o} \lambda + 2\mu \right) \left(\frac{\partial u}{\partial x} \right)^2 + \frac{\gamma_o}{Pr} \frac{\partial}{\partial x} \left(k \frac{\partial T}{\partial x} \right) \right\} \quad (2.11)$$

where $\bar{\gamma}_o$ is the ratio of the specific heats $\tilde{c}_{po}/\tilde{c}_{vo}$ and

$$Re = \frac{\tilde{\varrho}_o \tilde{c}_o \tilde{L}}{\tilde{\mu}_o}, \quad Pr = \frac{\tilde{\mu}_o \tilde{c}_{po}}{\tilde{k}_o}, \quad E = \frac{c_o^2}{\tilde{T}_o \tilde{c}_{vo}} \quad (2.12)$$

are the Reynolds, Prandtl and Eckert numbers. The jump conditions (2.4), (2.5), (2.6) and (2.7) assume the form

$$v[\varrho] = [\varrho u] \quad (2.13)$$

$$(v - u_a)(v - u_b) = \frac{[p]}{[\varrho]} \quad (2.14)$$

$$[h] = \frac{1}{2}(V_a + V_b)[p] \quad (2.15)$$

$$[s] \geq 0 . \quad (2.16)$$

In the following we investigate approximate solutions of the governing equations describing weakly nonlinear waves, i.e.

$$|u| = O(\varepsilon)$$

where $\varepsilon \ll 1$ is a small perturbation parameter.

The right hand sides of the governing equations (2.9), (2.10) and (2.11) vanish in the lossless limit $Rc \rightarrow \infty$ with x, t kept fixed. One then obtains a set of hyperbolic equations which can be written in the form

$$\varrho \frac{du}{dt} \pm c \frac{d\varrho}{dt} = -\alpha \frac{\partial s}{\partial x} \quad \text{on} \quad \frac{dx}{dt} = u \pm c \quad (2.17)$$

$$\frac{ds}{dt} = 0 \quad \text{on} \quad \frac{dx}{dt} = u \quad (2.18)$$

where

$$\alpha = \frac{\tilde{c}_{vo}}{\tilde{\varrho}_o \tilde{c}_o^2} \frac{\dot{\beta} \hat{T} \tilde{\varrho} \tilde{c}^2}{\tilde{c}_p} , \quad \dot{\beta} = -\frac{1}{\tilde{\varrho}} \frac{\partial \tilde{\varrho}}{\partial \hat{T}} \Big|_{\tilde{p}} . \quad (2.19)$$

Owing to the neglect of the thermoviscous effects, the entropy s is constant on particle paths. The entropy of a fluid particle, however, increases when it passes through a shock front. For the case of weak shocks which are of interest here, Bethe [2] has shown that

$$[s] = \frac{\Gamma_b}{6\hat{T}_b \tilde{\varrho}_b \tilde{c}_b^6} [\tilde{p}]^3 + o([\tilde{p}]^3) \quad (2.20)$$

if $\Gamma_b = O(1)$. In this case which has been studied extensively in the past (e.g. Germain [10], Whitham [11], Lighthill [12], Crighton [13], Kluwick [14], Sachdev [15] the nonlinear distortion of the wave profile is of importance over propagation distances and times of order $1/\varepsilon$.

Here we assume that the unperturbed state is characterized by a point in the transition zone of Fig. 1, i.e.

$$\varrho = 1, \quad s = s_o : \quad \Gamma_o = \varepsilon \hat{\Gamma}, \quad \hat{\Gamma} = O(1), \quad \Lambda_o = \frac{\partial}{\partial \varrho} \left(\frac{c}{\varrho} \Gamma \right) \Big|_s = O(1). \quad (2.21)$$

It can then be shown that the correct lowest order expression for the entropy jumps across weak shocks is given by (Cramer and Kluwick [6]).

$$[\tilde{s}] = \frac{\tilde{c}_o^2 [\tilde{\varrho}]^3}{6 \tilde{T}_o \tilde{\varrho}_o^3} \left\{ \Gamma_o + \frac{\Lambda_o}{2} \left(\frac{\tilde{\varrho}_b - \tilde{\varrho}_o}{\tilde{\varrho}_o} + \frac{\tilde{\varrho}_a - \tilde{\varrho}_o}{\tilde{\varrho}_o} \right) \right\} + o\left(\left(\frac{\tilde{\varrho} - \tilde{\varrho}_o}{\tilde{\varrho}_o}\right)^4\right). \quad (2.22)$$

Thus, in the transition zone, the size of the entropy jump across weak shocks is fourth order in the density/pressure jump. Furthermore, it is found that the nonlinear distortion of the wave profile is of importance over propagation distances and times of order $1/\varepsilon^2$ rather than $1/\varepsilon$ if (2.21) is satisfied. Equation (2.22) can then be used to show that the entropy term appearing in (2.17) is negligible small as far as the calculation of the leading order terms of the expansions

$$\begin{aligned} u &= \varepsilon u_1 + \varepsilon^2 u_2 + \varepsilon^3 u_3 + o(\varepsilon^3) \\ c &= 1 + \varepsilon c_1 + \varepsilon^2 c_2 + \varepsilon^3 c_3 + o(\varepsilon^3) \\ \varrho &= 1 + \varepsilon \varrho_1 + \varepsilon^2 \varrho_2 + \varepsilon^3 \varrho_3 + o(\varepsilon^3) \\ s &= \frac{\tilde{s}_o}{c_{o,\varepsilon}} + \varepsilon^4 s_4 + o(\varepsilon^4) \end{aligned} \quad (2.23)$$

is concerned.

To derive the leading order approximation of the transport equation governing the evolution of one dimensional unidirectional waves the various terms of (2.23) are assumed to be functions of $\xi = x - t$, $\tau_o = t$ and the slow time $\tau_1 = \varepsilon^2 t$. Substitution into the governing equations and elimination of secular terms then yields

$$\frac{\partial u_1}{\partial \tau_1} + (\hat{\Gamma} + \frac{\Lambda_o}{2} u_1) u_1 \frac{\partial u_1}{\partial \xi} = 0. \quad (2.24)$$

By making use of the transformed quantities

$$\hat{u} = \frac{\Lambda_o}{\hat{\Gamma}} u_1, \quad \hat{\xi} = \frac{\Lambda_o}{\hat{\Gamma}^2} \xi, \quad \tau = \tau_1 \quad (2.25)$$

the parameters Λ_o and $\hat{\Gamma}$ are eliminated from equation (2.24). One then obtains

$$\frac{\partial \hat{u}}{\partial \tau} + (\hat{u} + \frac{\hat{u}^2}{2}) \frac{\partial \hat{u}}{\partial \hat{\xi}} = 0. \quad (2.26)$$

Furthermore, evaluation of the jump conditions (2.4) to (2.7) using the results for the first and second order terms entering equations (2.23) yields the correct lowest order approximation to the shock speed

$$\frac{d\hat{\xi}}{d\tau} = \frac{1}{2} \frac{[\hat{u}^2]}{[\hat{u}]} + \frac{1}{6} \frac{[\hat{u}^3]}{[\hat{u}]} . \quad (2.27)$$

It is convenient to write equation (2.26) in the form of a kinematic wave equation (e.g. Lighthill and Whitham [16])

$$\frac{\partial \hat{u}}{\partial \tau} + \frac{\partial \hat{j}}{\partial \hat{\xi}} = 0 , \quad \hat{j} = \frac{\hat{u}^2}{2} + \frac{\hat{u}^3}{6} . \quad (2.28)$$

Consequently

$$\frac{d\hat{\xi}}{d\tau} = \frac{d\hat{j}}{d\hat{u}} \text{ along characteristics,} \quad (2.29)$$

$$\frac{d\hat{\xi}}{d\tau} = \frac{[\hat{j}]}{[\hat{u}]} \text{ along shock fronts.}$$

These relationships can be represented graphically by plotting the curve $\hat{j} = \hat{j}(\hat{u})$. According to (2.29) the slope of this curve is directly related to the characteristic speed corresponding to the value of \hat{u} considered while the slope of a straight line connecting two points of this curve equals the speed of a shock having the velocity jump $[\hat{u}]$, Fig. 2.

Let us assume that the point (1) of Fig. 2 characterizes the state downstream of a shock and that the state upstream of the shock varies. If the shock is very weak as in case (a) the wave pattern in the $\hat{\xi}, \tau$ -plane is qualitatively similar to that following from the theory of classical nonlinear acoustics. However, if the value of \hat{u}_b decreases further the slope of the characteristic before the shock is seen to decrease also while the slope of the shock front is found to increase. This finally leads to the limiting case (b) where the slopes of the shock front and the characteristic before the shock are equal - shocks of this kind will be termed sonic shocks. For even smaller values of \hat{u}_b the naive application of the graphical construction used so far would lead to a wave pattern of the form depicted in (c): the upstream characteristics emanate from the shock front. Discontinuities of this strength can, of course, be imposed in the form of initial or boundary conditions. They cannot, however, form in an interior point of the $\hat{\xi}, \tau$ -plane and thus will be discarded from the following considerations. One thus obtains the result shown in (d): jump discontinuities which exceed the critical strength - characterized by the

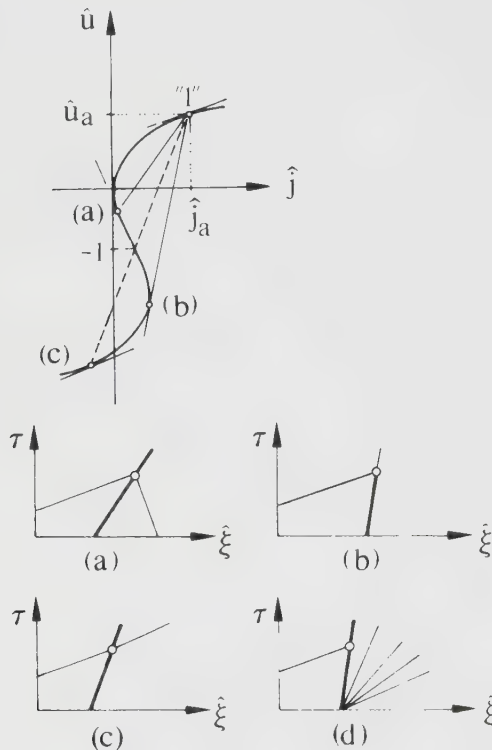


Figure 2: Plot of \hat{j} versus \hat{u} , equation (2.28)

occurrence of sonic conditions before the shock - immediately disintegrate into a sonic shock and a wave fan. Solutions to (2.29) containing shocks will therefore be considered permissible only if the condition

$$\left. \frac{d\hat{\xi}}{d\tau} \right|_a > \left. \frac{d\hat{\xi}}{d\tau} \right|_{shock} \geq \left. \frac{d\hat{\xi}}{d\tau} \right|_b \quad (2.30)$$

is satisfied along each shock front.

Condition (2.30) is equivalent to the entropy condition of Lax [17] and has been suggested also by Germain [18] and in the context of viscoelastic shear waves by Lee-Bapty [19] and Crighton [20].

The relationship (2.30) may be used to show that permissible pairs of \hat{u}_a, \hat{u}_b lie between the lines $\hat{u}_b = \hat{u}_a$ and $\hat{u}_b = -(\hat{u}_a + 3)/2$ for $\Lambda_o > 0$, and between $\hat{u}_b = \hat{u}_a$ and $\hat{u}_b = -(2\hat{u}_a + 3)$ for $\Lambda_o < 0$, Cramer and Kluwick [7]. These results

are depicted in Fig. 3 where the shaded regions denote forbidden (\hat{u}_a, \hat{u}_b) pairs.

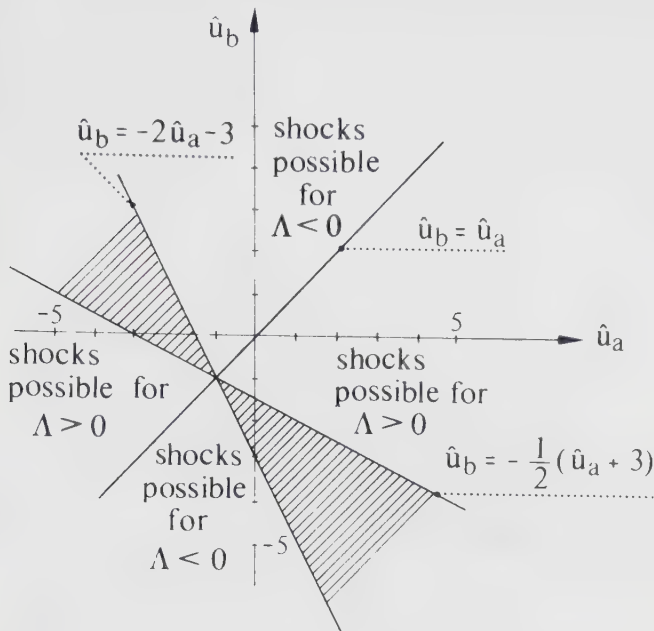


Figure 3: Regions of admissible shock waves in the \hat{u}_b , \hat{u}_a -plane

To illustrate the behaviour of shock waves we now discuss briefly three different cases of square pulses:

$$\tau = 0 : \hat{u} = \begin{cases} A & -1 \leq \xi \leq 1 \\ 0 & \text{elsewhere} . \end{cases} \quad (2.31)$$

In the first case, shown in Fig. 4, A is taken to be positive. As in the case of a perfect gas, the jump discontinuity imposed at $\xi = 1, \tau = 0$ leads to the formation of a compression shock while an expansion fan emanates from the point $\xi = -1, \tau = 0$. The leading shock is weakened by its interaction with the wave fan. At large time, therefore, the velocity disturbances inside the pulse are small and (2.29) reduce to the equations of the classical weak shock theory. Accordingly, the final decay will always be that of the classical theory, i.e.

$$[\hat{u}] \sim K\tau^{-1/2} \quad \text{as } \tau \rightarrow \infty \quad (2.32)$$

where K is an integration constant, provided $\hat{\Gamma} \neq 0$. Similar results are obtained for negative pulses $A \geq -1$. Of course, the roles of expansion fan and compression

shock are interchanged as far as their position in the $\hat{\xi}, \tau$ -plane is concerned but otherwise nothing exciting happens.

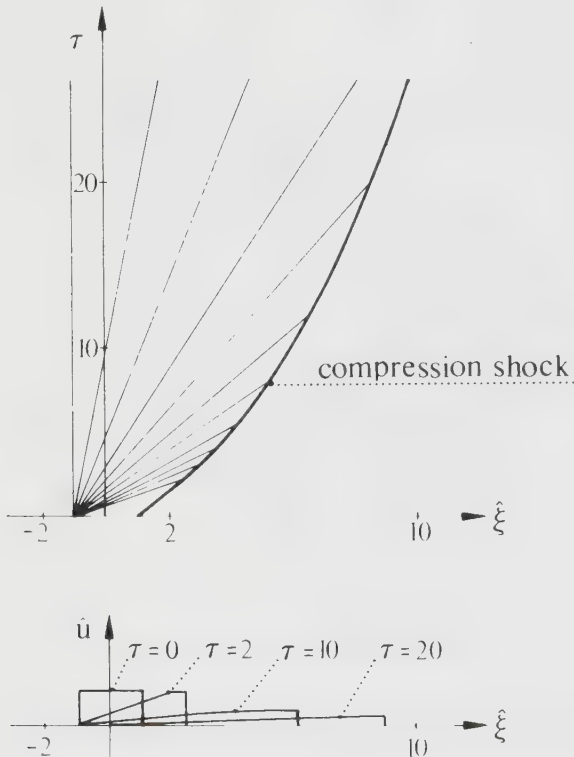


Figure 4: Wave evolution for $A = 1$

Interesting new effects, however, arise if the amplitude of a negative pulse is larger than 1. Specifically we consider $A = -2.2$, Fig. 5. This value is found to be too large for a single leading expansion fan and, therefore, a weaker expansion fan followed by a sonic expansion shock forms at $\hat{\xi} = 1, \tau = 0$. Similarly, the amplitude of the pulse is too large for a permissible trailing compression shock. As a consequence, a compression fan terminated by a sonic compression shock is seen to be generated at $\hat{\xi} = -1, \tau = 0$. The sonic expansion shock is weakened by its interaction with the compression fan. In order to stay sonic the expansion shock has to emanate characteristic lines which leave the shock front in the tangential direction. In this way a so-called precursor is formed (points inside the precursor region are no longer connected directly with the initial data but the information propagates along characteristics which cross sonic shocks). Since the compression

and the expansion shocks propagate with different speeds they finally collide at time τ_c which leads to another new phenomenon as can be seen from the plots of the wave profiles for various values of τ . According to classical theory, two merging shocks result in a single shock with larger amplitude. In contrast, the collision of an expansion and a compression shock is found to lead to a discontinuous reduction of the shock strength. For values $\tau \gg \tau_c$ the waveprofile approaches a linear sawtooth and the shock strength decays as $\tau^{-1/2}$ just as in the case of a classical fluid.

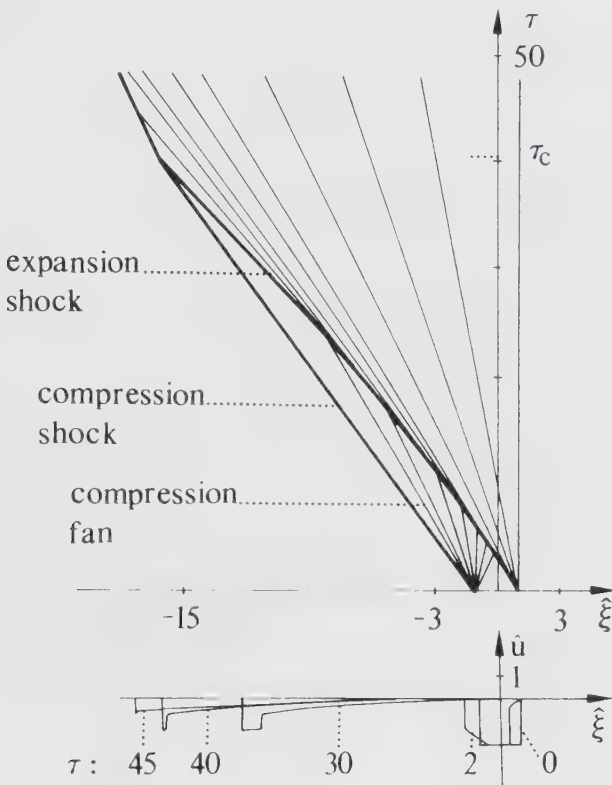


Figure 5: Wave evolution for $A = -2.2$

Finally, the special cases where either Λ_o or $\hat{\Gamma}$ are zero have to be mentioned briefly. As expected, the case $\hat{\Gamma} \neq 0$ is essentially the same as the classical theory and the solution for $\hat{\Gamma} = 0, \Lambda_o \neq 0$ closely resemble those described above in the limit $|A| \rightarrow \infty$. However, in the latter case, the shock-fan interaction leads to a different decay law than the $t^{-1/2}$ law of the classical theory. For a square pulse one obtains

$$[\hat{u}] \sim K\tau^{-1/3} \quad (2.33)$$

for all values of τ after the interaction begins.

Supplementing the brief outline of the properties of single pulses let us consider next one example of a periodic wavetrain. The case that the value of the fundamental derivative Γ vanishes in the unperturbed state has been studied by Lee-Baptist and Crighton [21] in the different context of viscoelastic waves and by Kluwick and Koller [22] for the case of acoustic waves. Introducing the variables

$$\alpha = u_1 , \hat{x} = \xi , \hat{t} = \Lambda_o \tau \quad (2.34)$$

equation (2.24) with $\hat{\Gamma} = 0$ reduces to

$$\frac{\partial \alpha}{\partial \hat{t}} + \frac{1}{2} \alpha^2 \frac{\partial \alpha}{\partial \hat{x}} = 0 . \quad (2.35)$$

If the initial wave profile is a periodic square wave, as shown in Fig. 6, the solution can be expressed in closed form. However, the results are rather lengthy and thus will not be displayed here in detail.

Since $\hat{\Gamma} = 0$, the nonlinear correction to the unperturbed sound speed is proportional to α^2 . Consequently, positive and negative disturbances of the same size propagate with the same speed thus leading to a wave pattern which repeats itself after half of the wavelength and to the occurrence of expansion and compression shocks of equal strength. Inspection of (2.35) indicates that $\bar{t} = A^2 \hat{t}$ rather than \hat{t} is the appropriate time where A denotes the amplitude of the wave at $\hat{t} = 0$. Furthermore, inspection of the plot $j = \alpha^3/6$ versus α shows that the jump discontinuities imposed at $\hat{t} = 0$ exceed the maximum strength of permissible shocks. Therefore, they immediately disintegrate into sonic shocks followed by wave-fans. This can also be seen from the waveprofiles which are plotted for several values of \bar{t} . Sonic shocks and wave fans start to interact at $\bar{t} \geq T_1 = 8/3$. For $T_1 \leq \bar{t} \leq T_2$, $T_2 = 2^{17/3}/3 \approx 16.932\dots$ the position of shock fronts can be calculated from the relationship

$$\hat{x}_s = K \bar{t}^4 \pm n , \quad n = 1, 2, \dots \quad K = 2^{5/4}/3^{3/4} = 1.043\dots . \quad (2.36)$$

As is the case of single pulses the interaction between sonic shocks and wave fans leads to the formation of precursor regions. In contrast to this case, however, these regions now cover the whole \hat{x} -axis if $\bar{t} \geq T_2$.

A characteristic which leaves a sonic shock at time $t \geq T_2$ will merge with the upstream sonic shock at time $t_2 = t_1 + \tau(t_1)$. Evaluation of the jump conditions for sonic shocks then shows that the motion of shock front for $t \geq T_2$ can be described by the set of equations

$$\hat{x}_s(t + \tau(t)) = \hat{x}_s(t) + \dot{\hat{x}}_s(t) \tau(t) - 1$$

$$\dot{\hat{x}}_s(t + \tau(t)) = \frac{1}{4} \dot{\hat{x}}_s(t) \quad (2.37)$$

The special solution

$$\hat{x}_s = \frac{1}{3 - \ln 4} \ln \bar{t} + const \quad (2.38)$$

describes the asymptotic behaviour of the shocks in the limit $\bar{t} \rightarrow \infty$ and is seen to be in good agreement with the exact solution.

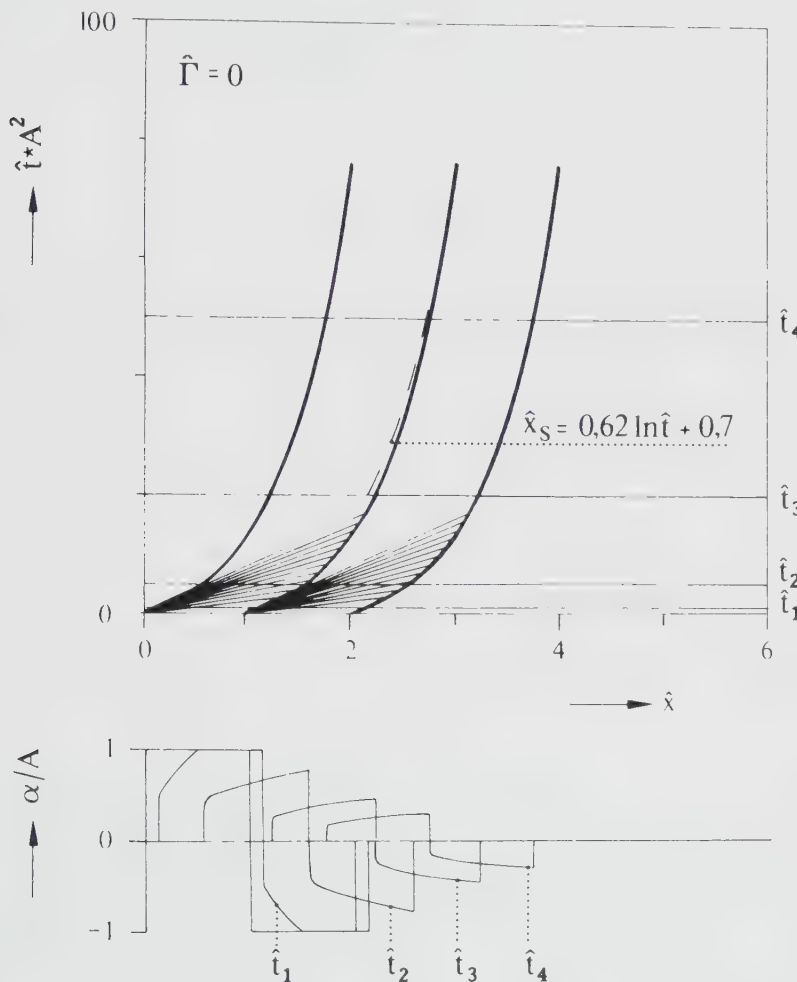


Figure 6: Evolution of periodic square wave for $\hat{\Gamma} = 0$

The results discussed so far have shown that the appearance of a cubic non-

linearity in the evolution equation for weakly nonlinear waves leads to a number of new effects. Most important, it was found that not all shock discontinuities satisfying the jump conditions (2.13) - (2.16) are physically sensible and it was argued that permissible shocks have to satisfy, in addition, the wave speed ordering relationship (2.30). In view of the importance of this relationship for the evolution of general waves it seems desirable to develop a second line of argument based on the full set of governing equations (2.9), (2.10) and (2.11) rather than its inviscid version.

To derive the evolution equation for weakly nonlinear-weakly dissipative waves, asymptotic expansions of the form (2.23) will be used for the various field quantities. However, the dissipative terms on the right hand side of equations (2.10) and (2.11) generate an order ε^3 perturbation to the entropy. Thus the expansion for s in (2.23) has to be replaced by

$$s = \frac{\tilde{s}_o}{\tilde{c}_{po}} + \varepsilon^3 s_3 + \varepsilon^4 s_4 + o(\varepsilon^4). \quad (2.39)$$

Furthermore, we shall require that $Re = O(\varepsilon^{-2})$ in order that thermoviscous effects be noticeable over the same timescale as the nonlinearity.

Elimination of secular terms entering the third order approximation then yields, Cramer and Kluwick [7]

$$\frac{\partial \hat{u}}{\partial \tau} + (1 + \frac{1}{2}\hat{u})\hat{u} \frac{\partial \hat{u}}{\partial \hat{\xi}} = \frac{\delta \Lambda_o^2}{2\hat{\Gamma}^4} \frac{\partial^2 \hat{u}}{\partial \hat{\xi}^2} \quad (2.40)$$

where

$$\delta = \frac{1}{\varepsilon^2 Re} (2 + \frac{\tilde{\lambda}_o}{\tilde{\mu}_o} + \frac{\tilde{\beta}_o^2 \tilde{T}_o \tilde{c}_o^2}{Pr \tilde{c}_{po}}), \quad \beta_o = -\frac{1}{\tilde{\varrho}} \frac{\partial \tilde{\varrho}}{\partial \tilde{T}} \Big|_{\tilde{s}=\tilde{s}_o} \quad (2.41)$$

are essentially the acoustic diffusivity for a general fluid and the thermal expansion coefficient.

Evaluation of the energy equation (2.3) shows that the leading order term of the entropy disturbance is proportional to the negative slope of the density profile. As a consequence, the entropy distributions of rarefaction shocks exhibit regions of negative entropy perturbations. The required netto increase of entropy across any permissible shock is provided by the higher order contribution ε^4 , s_4 , in agreement with the results of weak shock theory.

In contrast to the case of the classical Burgers equation which can be linearized by the Cole-Hopf transformation, powerful analytical methods which allow to calculate exact solutions of the modified Burgers equation (2.40) are not known

at present. In the absence of such exact methods, Cramer, Kluwick, Watson and Pelz [23] have resorted to numerical techniques. Here we are mainly concerned with the thermoviscous shock structure for fluids in the vicinity of the transition line. To this end we consider solutions of (2.40) representing waves of constant form

$$\hat{u} = \hat{u}(\eta) , \quad \eta = \hat{\xi} - S\tau \quad (2.42)$$

where S denotes the unknown shock speed, Cramer and Kluwick [7], Cramer [24]. Equation (2.40) then reduces to

$$\frac{\delta\Lambda_o^2}{2\hat{\Gamma}^4} \frac{d^2\hat{u}}{d\eta^2} = (\hat{u} + \frac{1}{2}\hat{u}^2 - S)\frac{d\hat{u}}{d\eta} . \quad (2.43)$$

Appropriate boundary conditions are

$$\hat{u} \rightarrow \hat{u}_b \text{ as } \eta \rightarrow \infty \quad (2.44)$$

$$\hat{u} \rightarrow \hat{u}_a \text{ as } \eta \rightarrow -\infty .$$

It is convenient to introduce the scaled quantities

$$G = \frac{2}{[\hat{u}]} \left(\hat{u} - \frac{\hat{u}_a + \hat{u}_b}{2} \right) , \quad \hat{\eta} = \frac{\hat{\Gamma}^4 [\hat{u}]^2}{12\delta\Lambda_o^2} \eta . \quad (2.45)$$

One then obtains the boundary value problem

$$\begin{aligned} G' &= (G^2 - 1)(G + B) \\ G &\rightarrow -1 \text{ as } \hat{\eta} \rightarrow \infty \\ G &\rightarrow +1 \text{ as } \hat{\eta} \rightarrow -\infty \\ G(0) &= 0 \end{aligned} \quad (2.46)$$

where

$$B = \frac{6}{[\hat{u}]} \left(1 + \frac{\hat{u}_a + \hat{u}_b}{2} \right) . \quad (2.47)$$

It can be shown that solutions to equations (2.46) exist for $B \geq 1$ only. Furthermore, a simple analysis shows that this condition requires (2.30) to be satisfied for all permissible shocks.

Equations (2.46) can be solved in closed form. Shock profiles for various values of B are plotted in Fig. 7. If $B \gg 1$, i.e. if the quadratic nonlinearity dominates over the cubic nonlinearity, the solution deviates only slightly from the Taylor profile of classical fluids. For decreasing values of B the shock thickness is seen to increase

and the shock profiles are no longer antisymmetric with respect to the origin $\hat{\eta} = 0$. Still, the disturbances decay exponentially far upstream and downstream provided $B > 1$. However, in the limiting case $B = 1$ which corresponds to sonic conditions upstream of the shock the solution approaches the upstream asymptote algebraically rather than exponentially.

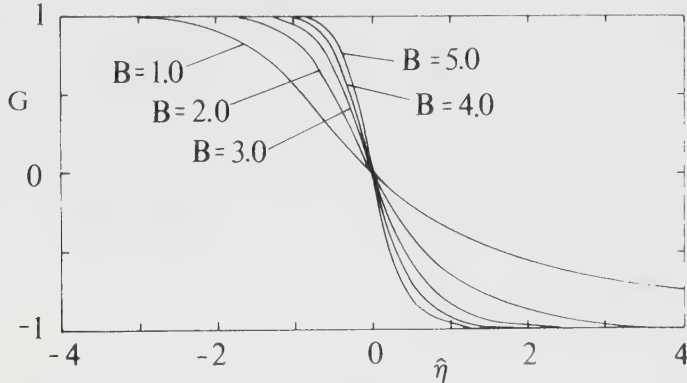


Figure 7: Shock structure. $B = 1.0$ corresponds to a shock having sonic conditions as $\hat{\eta} \rightarrow \infty$

The results summarized so far hold if $\Gamma_o = O(\varepsilon)$ and $\Lambda_o = O(1)$. However, there exists at least one point on the $\Gamma = 0$ curve in the $\tilde{p}, 1/\tilde{\varrho}$ -plane (Fig. 1) where the slope of this curve is tangent to the corresponding isentrope, e.g. where $\Gamma_o = \Lambda_o = 0$. In order to study nonlinear waves which cause small perturbations of this state the order of magnitude relations (2.21) have to be replaced by

$$\begin{aligned}\Gamma_o &= \varepsilon^2 \hat{\Gamma} , \quad \hat{\Gamma} = O(1) \\ \Lambda_o &= \varepsilon \hat{\Lambda} , \quad \hat{\Lambda} = O(1) \\ \Sigma_o &\equiv \frac{\partial^2}{\partial \varrho^2} \left(\frac{c}{\varrho} \Gamma \right) \Big|_s = O(1)\end{aligned}\tag{2.48}$$

As a consequence, nonlinear effects are of importance over propagation distances and times of order $1/\varepsilon^3$ rather than $1/\varepsilon^2$ as earlier. Furthermore, it is easily seen that the entropy increase across weak shocks is of order ε^5 if (2.48) is satisfied.

The derivation of the appropriate evolution equation for weakly nonlinear waves subjected to conditions (2.48) proceeds along the same lines leading to equation (2.40) and the details will, therefore, be omitted. Introducing the scaled quantities

$$\tau = \varepsilon^3 t, \hat{\xi} = \frac{\hat{\Lambda}}{\hat{\Gamma}^2}(x - t), \hat{u} = \frac{\hat{\Lambda}}{\hat{\Gamma}} u_1 \quad (2.49)$$

where as before $u = \varepsilon u_1 + o(\varepsilon)$ one finally obtains

$$\frac{\partial \hat{u}}{\partial \tau} + \left(1 + \frac{\hat{u}}{2} + \frac{K\hat{u}^2}{6}\right)\hat{u} \frac{\partial \hat{u}}{\partial \hat{\xi}} = \frac{\delta \hat{\Lambda}^2}{2\hat{\Gamma}^4} \frac{\partial^2 \hat{u}}{\partial \hat{\xi}^2} \quad (2.50)$$

Herein, K and δ respectively, denote the additional similarity parameter

$$K = \frac{\Sigma_o \hat{\Gamma}^2}{\hat{\Lambda}^2} > 0 \quad (2.51)$$

and the diffusivity of sound written in the form

$$\delta = \frac{1}{\varepsilon^3 Re} \left(2 + \frac{\tilde{\lambda}_o}{\tilde{\mu}_o} + \frac{\tilde{\beta}_o \tilde{T}_o \tilde{c}_o}{Pr \tilde{c}_{po}}\right) \quad (2.52)$$

taking care of the requirement $Re = O(\varepsilon^{-3})$ which is needed to ensure that thermoviscous and nonlinear effects are of importance over the same timescale.¹

In the lossless limit $\delta = 0$ equation (2.50) reduces to the kinematic wave equation

$$\frac{\partial \hat{u}}{\partial \tau} + \frac{\partial j}{\partial \hat{\xi}} = 0, \quad j = \frac{\hat{u}^2}{2} + \frac{\hat{u}^3}{6} + \frac{K\hat{u}^4}{12}. \quad (2.53)$$

The properties of equations (2.50) and (2.53) are currently under investigation and the results will be published elsewhere. However, inspection of the graph j versus \hat{u} , Fig. 8, already indicates the occurrence of new phenomena not covered by equations (2.40) and (2.28). These phenomena include (i) sonic shock - fan - sonic shock combinations, Fig. 8a, and (ii) shocks having sonic conditions upstream and downstream of the front, Fig. 8 b.

Finally, it should be noted that sonic shock - fan - sonic shock configurations and double sonic shocks similar to those shown in Fig. 8a and Fig. 8b have been observed in studies dealing with gravity settling (Shannon and Tory [25]) and evaporation waves in retrograde fluids (Thompson, Chaves, Meier, Kim and Speckmann [26]), respectively. In both cases, however, the occurrence of these phenomena is limited to waves of finite amplitudes.

¹An equivalent version of equation (2.50) has recently been used by Cramer and Crickenberger [27] to study the dissipative structure of weak shock waves.

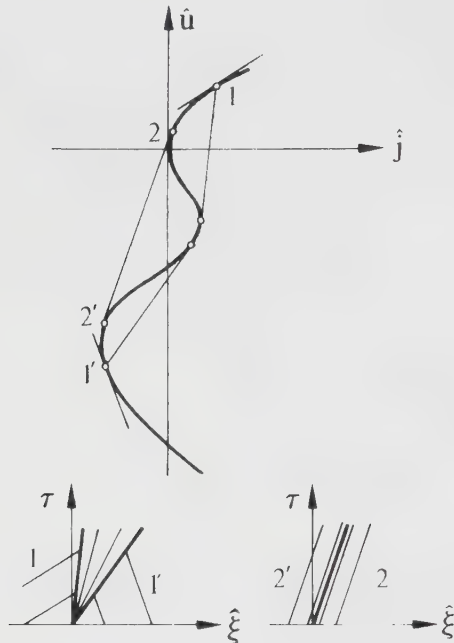


Figure 8: Plot of \hat{j} versus \hat{u} , equation (2.53)

3. Small-amplitude finite-rate waves in channels with slowly varying cross section

In generalization of the problem treated in section 2 we consider waves propagating in a channel with varying cross-sectional area. Let x , t , u , c denote the distance along the channel axis, the time, the axial velocity component and the speed of sound nondimensional with the wavelength \tilde{L} , \tilde{L}/\tilde{c}_o , and \tilde{c}_o respectively. In addition $A(x)$ denotes the cross-sectional area of the channel which will be assumed to vary slowly so that the wave motion is quasi-one-dimensional. The governing equations for isentropic flow can then be written in the form

$$\begin{aligned} (\Gamma - 1)c \frac{\partial u}{\partial x} + \frac{\partial c}{\partial t} + u \frac{\partial c}{\partial x} + uc(\Gamma - 1) \frac{d}{dx} \ln A &= 0 \\ \frac{\partial u}{\partial t} + u \frac{\partial u}{\partial x} + \frac{c}{\Gamma - 1} \frac{\partial c}{\partial x} &= 0 . \end{aligned} \tag{3.1}$$

Special cases included in equations (3.1) are cylindrical and spherical waves

having

$$\frac{d}{dx} \ln A = \frac{\sigma}{x}, \quad \sigma = 1, 2. \quad (3.2)$$

As in section 2 the considerations will be limited to small-amplitude finite-rate waves characterized by the perturbation parameter $\varepsilon \ll 1$. In contrast to the case of planar wave however, u and c cannot, in general, be represented by asymptotic series of the same form in the whole x, t -plane. For example, inspection of the linear solution for spherical waves generated by a pulsating sphere the radius of which is small compared to the wavelength

$$x = \varepsilon R(t) : \quad u = \varepsilon \frac{dR(t)}{dt}, \quad \varepsilon \ll 1 \quad (3.3)$$

shows that there exists an inner region $x = 0(\varepsilon)$ where the disturbances of the field quantities are of different order of magnitude: $u = 0(\varepsilon)$, $c - 1 = 0(\varepsilon^2)$. In contrast, u and $c - 1$ are of the same order of magnitude in the far field region $x \gg 1$ where the jump conditions across weak shocks are satisfied automatically to leading order

$$u \sim \frac{1}{\Gamma_o - 1}(c - 1) \sim \varepsilon^3 \frac{F(\zeta_1)}{x} \quad (3.4)$$

$$F(\zeta_1) = R^2(\zeta_1) \frac{dR(\zeta_1)}{d\zeta_1}, \quad \zeta_1 = t - x.$$

Equation (3.4) is not only valid at large distances but also near the wavefront $\zeta_1 = 0$. Both conditions can be summarized to the single requirement $\zeta_1/x \ll 1$ which means that the distance from the wave front must be small compared to the radius of curvature of the wave front. By differentiation of (3.4) one then obtains

$$\left| \frac{\partial u}{\partial x} \right| \ll \left| \frac{\partial u}{\partial \zeta_1} \right|. \quad (3.5)$$

Equation (3.5) states that the magnitude of the rate of change of u along $\zeta_1 = \text{const.}$ is small compared to the magnitude of the rate of change of u with ζ_1 for x fixed.

Obviously, the physical significance of (3.5) is not restricted to the linear solution. If ζ_1 is replaced by the exact outgoing characteristic we expect that

$$\left| \frac{\partial u}{\partial x} \right| \ll \left| \frac{\partial u}{\partial \xi} \right| \quad (3.6)$$

in the far field $\xi/x \ll 1$. Waves satisfying (3.6) are said to be relatively undistorted (Varley and Cumberbatch [28]) or to represent progressive waves, (Germain [10]).

As shown by Varley and Cumberbatch [28] the governing equs. (3.1) admit asymptotic expansions which proceed in powers of a small perturbation parameter if the wave under consideration is relatively undistorted. To this end it will be assumed that the relative changes of A over one wave length are small

$$A = A(\hat{x}) , \quad \hat{x} = \sigma(\varepsilon)x , \quad \sigma \ll 1 . \quad (3.7)$$

In order that nonlinear effects and effects due to changes of the crossectional area are of equal importance we must require that $\sigma = O(\varepsilon)$ if the fluid has strictly positive or negative nonlinearity ($\Gamma = O(1)$) while $\sigma = O(\varepsilon^2)$ if $\Gamma = O(\varepsilon)$ as considered here.

Appropriate asymptotic expansions for the velocity perturbation and the speed of sound are given by

$$\begin{aligned} u &= \varepsilon u_1(\zeta, \hat{x}) + \varepsilon^2 u_2(\zeta, \hat{x}) + \varepsilon^3 u_3(\zeta, \hat{x}) + o(\varepsilon^3) \\ c &= 1 + \varepsilon c_1(\zeta, \hat{x}) + \varepsilon^2 c_2(\zeta, \hat{x}) + \varepsilon^3 c_3(\zeta, \hat{x}) + o(\varepsilon^3) \end{aligned} \quad (3.8)$$

where

$$\hat{x} = \varepsilon^2 x , \quad \zeta = t - x + x_o \text{ and } A = A(\hat{x}) . \quad (3.9)$$

Substitution into the governing equations (3.1) yields the first order transport equation, Kluwick and Czemetschka [29]

$$\frac{\partial u_1}{\partial \hat{x}} - (\hat{\Gamma} + \frac{\Lambda_o}{2} u_1) u_1 \frac{\partial u_1}{\partial \zeta} + \frac{u_1}{2A} \frac{dA}{d\hat{x}} = 0 . \quad (3.10)$$

As in the case of media having strictly positive or negative nonlinearity, (e.g. Crighton [13]) the term containing the spatial variation of $A(\hat{x})$ can be eliminated by introducing the transformed quantity

$$v = u_1 \sqrt{A(\hat{x})} . \quad (3.11)$$

One then obtains

$$\frac{\partial v}{\partial \hat{x}} - \left(\frac{\hat{\Gamma}}{\sqrt{A}} + \frac{\Lambda_o}{2A} v \right) v \frac{\partial v}{\partial \zeta} = 0 . \quad (3.12)$$

It is no longer possible, however, to eliminate the explicit occurrence of $A(\hat{x})$ in the transport equation for v by means of a simple coordinate transformation $z = z(\hat{x})$. Making use of the transformed quantities

$$\hat{v} = v \frac{\Lambda_o}{\hat{\Gamma}} , \quad \hat{\zeta} = \frac{\Lambda_o}{\hat{\Gamma}^2} \zeta \quad (3.13)$$

leads to

$$\frac{\partial \hat{v}}{\partial \hat{x}} - \left(\frac{\hat{v}}{\sqrt{A}} + \frac{\hat{v}^2}{2A} \right) \frac{\partial \hat{v}}{\partial \hat{\zeta}} = 0. \quad (3.14)$$

Equation (3.14) can also be written in divergence form, e.g. in the form of a kinematic wave equation

$$\frac{\partial \hat{v}}{\partial \hat{x}} + \frac{\partial \hat{j}}{\partial \hat{\zeta}} = 0, \quad \hat{j} = -\frac{\hat{v}^2}{2\sqrt{A}} - \frac{\hat{v}^3}{6A}. \quad (3.15)$$

The formal solution to this equation is given by

$$\hat{v} = \text{const.} \quad \text{on} \quad \frac{d\hat{\zeta}}{d\hat{x}} = -\frac{\hat{v}}{\sqrt{A}} - \frac{\hat{v}^2}{2A}. \quad (3.16)$$

Due to the formation of shock discontinuities, however, this relationship is not sufficient, in general, to determine the unique solution of a given boundary or initial value problem. Rather it has to be combined with appropriate jump conditions which have been already discussed in detail in section 2 dealing with planar waves. Although these conditions hold unchanged, the variation of the wave amplitude associated with the variation of the crosssectional area $A(\hat{x})$ may, nevertheless, lead to the occurrence of an interesting new phenomenon.

To this end it will be assumed that $A(\hat{x})$ increases with distance: $A(\hat{x}) \rightarrow \infty$, $\hat{x} \rightarrow \infty$, as for example in the case of outgoing spherical or cylindrical waves. Since \hat{v} is constant along characteristic curves, the scaled velocity perturbation $\hat{u} = \hat{v}/\sqrt{A}$ then decays during the wave propagation process.

Let us consider first the properties of a single shock front initiated by the boundary condition

$$\hat{x} = \hat{x}_o : \begin{cases} \hat{u} = \hat{u}_o, & \hat{\zeta} > 0 \\ \hat{u} = 0, & \hat{\zeta} < 0 \end{cases}. \quad (3.17)$$

If $\hat{u}_o > 0$ one obtains a single compression shock. Due to the assumption that $A(\hat{x})$ is a growing function of \hat{x} the shock decays but still its strength vanishes only in the limit $\hat{x} \rightarrow \infty$. This result of classical nonlinear acoustics has been expressed by Hayes in the following way: "old shocks never die, they are like soldiers and only fade away".

If $-3 < \hat{u}_o < 0$ the jump discontinuity imposed at $\hat{x} = \hat{x}_o$ partly or fully disintegrates into a wave fan but a single negative shock is generated if $\hat{u}_o < -3$. Again the shock strength is found to decrease as \hat{x} increases. As a consequence, the conditions for a sonic shock will be reached at some distances $\hat{x} = \hat{x}_s$. For $\hat{x} > \hat{x}_s$,

therefore, a sonic shock forming a precursor emerges from the initially single shock front. Moreover, the sonic shock must vanish at a finite distance $\hat{x} = \hat{x}_{St} > \hat{x}_s$ following from the requirement, that the scaled velocity perturbation \hat{u} immediately downstream of the shock front assumes the value $\hat{u}_{St} = -1$ corresponding to the inflection point of the graph \hat{j}/\sqrt{A} versus \hat{u} , Fig. 9.

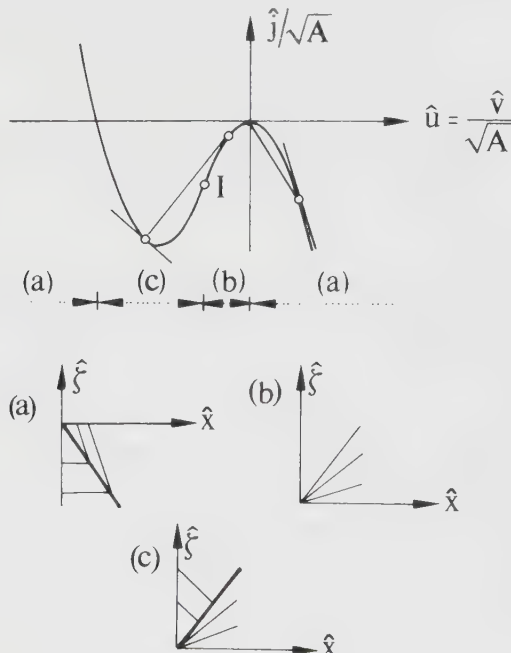


Figure 9: Plot of \hat{j}/\sqrt{A} versus \hat{u} , equation (3.15)

As a specific example of this phenomenon we consider the case of spherical waves. It is sufficient to treat the regime $-3 \leq \hat{u}_o \leq 1$. As a consequence, a wave fan emanates from the point $\hat{x} = \hat{x}_o$, $\hat{s} = 0$ in the \hat{x} , \hat{s} -plane, inside which the scaled velocity perturbations at $\hat{x} = \hat{x}_o$ decrease from $\hat{u} = 0$ to $\hat{u} = -\hat{u}_1 = -(\hat{u}_o + 3)/2$, Fig. 10. As already mentioned, this wave fan is terminated by a sonic shock. Characteristics starting in the perturbed region downstream the shock merge with the shock front forming a nonvanishing angle, in general. The upstream characteristics, however, leave the sonic shock front in the tangential direction thus leading to the formation of a precursor region clearly visible in Fig. 10.

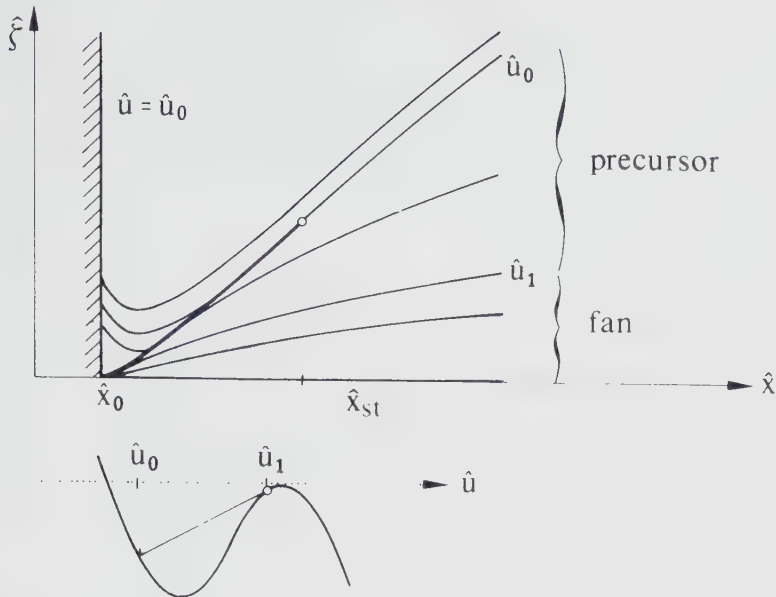


Figure 10: Schematic of wave pattern generated by a contracting sphere:
 $-3 \leq \hat{u}_o \leq -1$

Utilizing the jump condition $\hat{u}_b = -\frac{1}{2}(3 + \hat{u}_a)$ for sonic shocks it is possible to derive an analytical expression for the shock path

$$\hat{\zeta} = -\frac{1}{8}(\hat{x}_o \hat{u}_o)^2 \left(\frac{1}{\hat{x}_o} - \frac{1}{\hat{x}} \right) - \frac{1}{4} \hat{x}_o \hat{u}_o \ln \left(\frac{\hat{x}}{\hat{x}_o} \right) + \frac{3}{8} (\hat{x} - \hat{x}_o) . \quad (3.18)$$

Along this curve in the $\hat{\zeta}, \hat{x}$ -plane the shock strength varies according to

$$[\hat{u}] = \frac{3}{2}(\hat{u}_a + 1) = \frac{3}{2} \left(\hat{u}_o \frac{\hat{x}_o}{\hat{x}} + 1 \right) \quad (3.19)$$

and vanishes at the point

$$\hat{x}_{st} = -\hat{x}_o \hat{u}_o \quad (3.20)$$

$$\hat{\zeta}_{st} = -\frac{(\hat{x}_o \hat{u})^2 + 3}{8 \hat{x}_o} (\hat{u}_o + 1) - \frac{\hat{x}_o \hat{u}_o}{4} \ln(-\hat{u}_o)$$

where the precursor region and the region formed by the characteristics emanating from $\hat{x} = \hat{x}_o$ for $\hat{\zeta} > 0$ merge smoothly.

Three examples for the evolution of spherical square pulses satisfying the boundary conditions

$$\hat{x} = 2 : \begin{cases} \hat{u} = o & \text{for } \hat{\zeta} < 0 \\ \hat{u} = \hat{u}_o & \text{for } 0 \leq \hat{\zeta} \leq 4 \\ \hat{u} = 0 & \text{for } \hat{\zeta} > 4 \end{cases}$$

are shown in Figs. 11, 12 and 13.

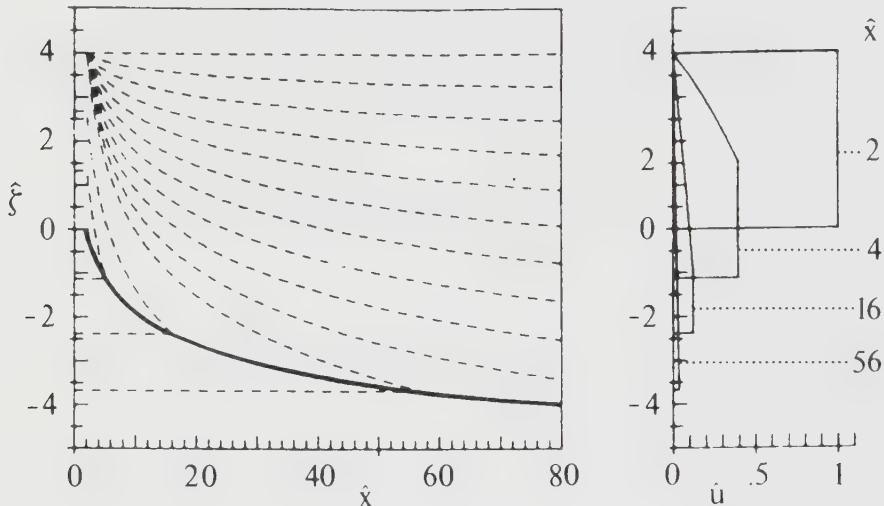
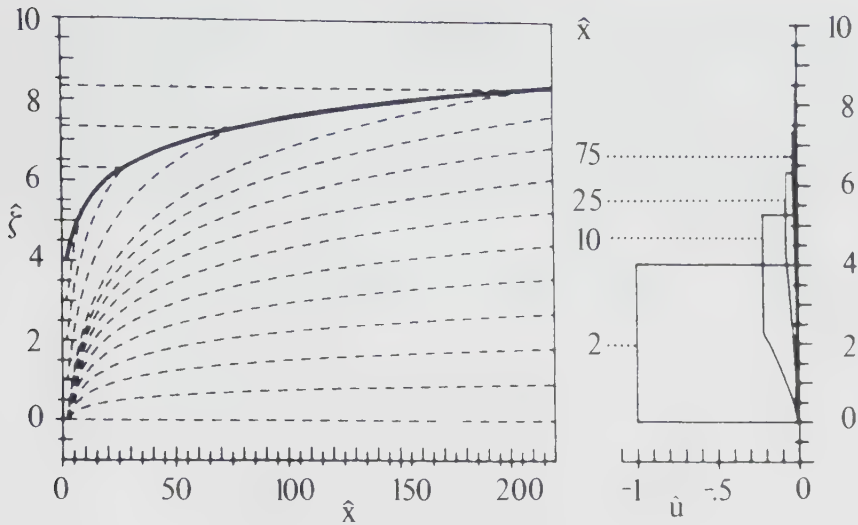
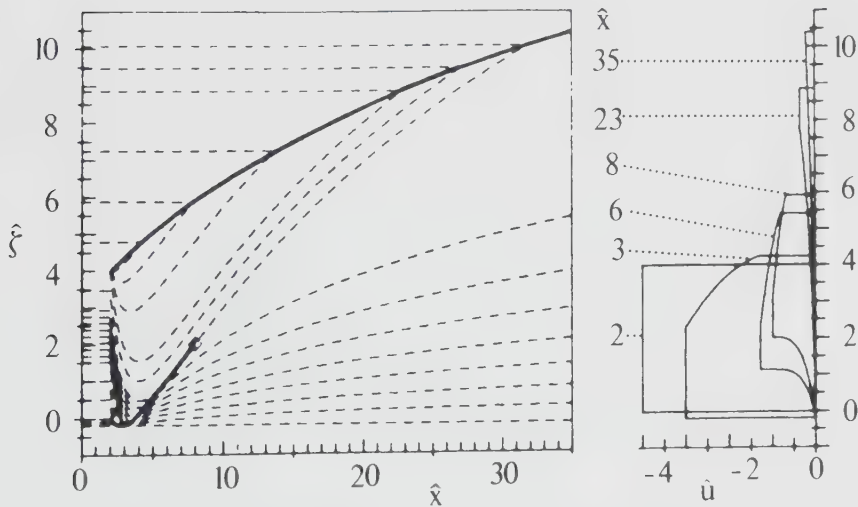


Figure 11: Wave evolution for $\hat{u}_o = 1$

If $\hat{u}_o > 0$ the pulse is headed by a positive shock while the discontinuous reduction of the velocity at $\hat{x} = 2, \hat{\zeta} = 4$ leads to the formation of a wave fan. The results are qualitatively similar to those holding in a medium having quadratic nonlinearity. In particular it is seen that the initial square pulse is eventually transformed into a linear sawtooth as $\hat{x} \rightarrow \infty$.

If $-1 \leq \hat{u}_o < 0$, the behaviour of the wave is again essentially the same as the classical theory, this is illustrated in Fig. 12 for the case $\hat{u}_o = -1$.

Finally, the evolution of a negative pulse with $\hat{u}_o = -4$ is depicted in Fig. 13. The jump discontinuity imposed at $\hat{x} = 2, \hat{\zeta} = 0$ then is strong enough to generate a single negative shock. The increase of the cross sectional area slows the shock which propagates with the unperturbed speed of sound in the $\hat{x}, \hat{\zeta}$ plane when $\hat{u} = -3$. At larger values of \hat{x} its strength and speed is determined by requiring that the conditions before the shock are sonic. The sonic shock terminates at $\hat{x} = 8$ and

Figure 12: Wave evolution for $\hat{u}_o = -1$ Figure 13: Wave evolution for $\hat{u}_o = -4$

the corresponding smooth velocity distribution exhibits a plateau region generated by the characteristics carrying constant values of $\hat{v}_o = \hat{u}_o \hat{x}_o$. However, this plateau region vanishes when the characteristic leaving the endpoint of the sonic shock merges with the trailing shock. At large distances $\hat{x} \rightarrow \infty$ the distribution inside

the precursor approaches a linear sawtooth.

In Fig. 13 the length of the pulse was chosen such that the sonic shock terminates before it interacts with the trailing shock. If the length/amplitude of the pulse is sufficiently small/large both shocks will collide as in the case of planar waves discussed earlier. In both cases, however, the trailing shock extends up to $\hat{x} = \infty$. Since the velocity disturbances decay as $\hat{x} \rightarrow \infty$ the quadratic term in equ. (3.14) eventually dominates over the cubic term thus leading to the $\hat{x}^{-1}(\ln \hat{x})^{-1/2}$ decay law of the classical theory, provided $\hat{\Gamma} \neq 0$.

4. Dispersive wall-friction effects on high frequency waves

Nonlinear effects on the propagation of acoustic effects can be studied most easily if one considers the evolution of one-dimensional unidirectional waves. The case that the medium under consideration is a perfect gas has been investigated extensively in the past and most of the basic problems have essentially been solved. As pointed out in sections 1 and 2, however, a rapidly growing interest concerning fluids with more complicated thermodynamic properties can be observed, quite recently. Meanwhile a number of interesting results - mostly dealing with one-dimensional simple waves - have been derived. All of these theoretical predictions have still to be tested experimentally² but, unfortunately, one-dimensional plane waves are difficult to simulate in any laboratory set up. Of course, this presents no difficulty if one considers the limiting case of an inviscid medium; a one-dimensional wave can then, for example, be generated inside a rigid tube by means of an oscillating piston. If the tube is filled with a perfect gas and if the piston performs harmonic oscillations nonlinear effects will eventually transform the initially sinusoidal wave train into a linear sawtooth. Early experiments by McKittrick, Blackstock and Wright [30] have shown, however, that the actually observed wave form may differ substantially from the theoretical result obtained by means of inviscid theory. Specifically, they found that there existed a slope discontinuity near the pressure minimum but that the region of positive excess pressure was perfectly smooth. Correctly, McKittrick et al [30] conjectured that these deviations from the inviscid result were due to dispersive rather than dissipative thermoviscous effects. Moreover, by adopting the assumption that the flow field can be split into a thin viscous wall layer and an essentially inviscid core region if the wave frequency is sufficiently high, Blackstock [31] was able to derive a generalized wave equation including a dispersive memory term. Unfortunately, however, no solutions of this model equation were given. Making use of a linear

²Rarefaction shocks originating from a near critical state of Freon-13 have been generated by Borisov et al [6]. Since the flow appears to have entered the two phase region the existence of negative shocks in single phase gases has still to be demonstrated, however.

momentum argument first proposed by Chester [32] in his study of resonant oscillations in closed tubes, the same model equation was derived independently by Crighton [13] and by Keller [33] but again no comparison between experimental and theoretical results was performed. In this section we want (i) to sketch a more systematic derivation of the appropriate model equation, (ii) to investigate some properties of its solutions and (iii) to compare these solutions with available experimental data by Pestorius [34].

It will be assumed that the velocity disturbances caused by the wave and characterized by the amplitude \tilde{u}_{max} are small compared to the unperturbed speed of sound \tilde{c}_o so that

$$\varepsilon = \frac{\tilde{u}_{max}}{\tilde{c}_o} \ll 1 \quad (4.1)$$

is a small perturbation parameter. Furthermore, it will be assumed that the wave is only weakly damped. This requires two additional parameters

$$\beta = \frac{\tilde{L}}{\tilde{R}} \sqrt{\frac{\tilde{\nu}}{\tilde{R}^2 \tilde{\omega}}} \ll 1, \quad \gamma = \sqrt{\frac{\tilde{\nu}}{\tilde{c}_o \tilde{L}}} \ll 1 \quad (4.2)$$

to be small (Gittler and Kluwick [35], Kluwick and Gittler [36]). Here \tilde{L} , \tilde{R} , $\tilde{\omega}$ and $\tilde{\nu}$ denote the characteristic wave length, the radius of the tube, the frequency of the oscillating piston and the kinematic viscosity of the fluid. Finally, it will be assumed that the thermodynamic properties of the medium are such that the nonlinear terms entering the long time evolution equation may be both positive or negative $\Gamma_o = \varepsilon \hat{\Gamma}$, $\hat{\Gamma} = O(1)$, $\Lambda_o = O(1)$.

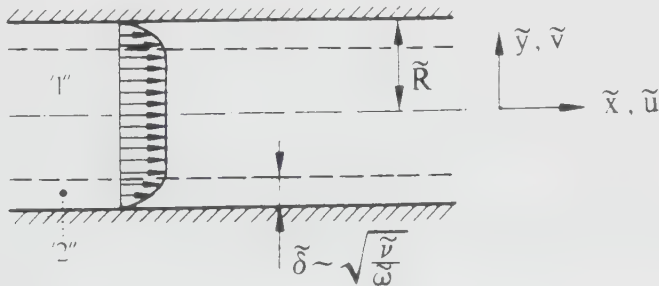


Figure 14: Schematic of flow structure

It has been pointed out already that an asymptotic theory of high frequency waves in liquid/gas filled tubes requires the treatment of two different regions. As

indicated in Fig. 14 thermoviscous effects are small inside the core region which comprises most of the crossectional area but have to be taken into account to leading order in a thin layer adjacent to the wall.

Let us consider first the properties of the wave motion inside the predominantly inviscid core region. To this end it is convenient to introduce the nondimensional quantities

$$\begin{aligned} x &= \frac{\tilde{x}}{\tilde{L}}, \quad y = \frac{\tilde{y}}{\tilde{R}}, \quad t = \frac{\tilde{c}_o}{\tilde{L}} \tilde{t}, \\ u &= \frac{\tilde{u}}{\tilde{c}_o}, \quad v = \frac{\tilde{v}}{\tilde{c}_o}, \quad c = \frac{\tilde{c}}{\tilde{c}_o}, \\ \varrho &= \frac{\tilde{\varrho}}{\tilde{\varrho}_o}, \quad T = \frac{\tilde{T}}{\tilde{T}_o}, \quad p = \frac{\tilde{p} - \tilde{p}_o}{\tilde{\varrho}_o \tilde{c}_o^2} \end{aligned} \quad (4.3)$$

where (in addition to the variables defined earlier) y , v and T denote the distance in the radial direction, the radial velocity component and the temperature.

Since it will be assumed that the wave under consideration propagates to the right, the axial coordinate x is replaced by the distance $\xi = x - t$ measured in a coordinate system moving with the unperturbed sound speed. Furthermore, in addition to the time $\tau_o = t$ we define an appropriate slow time

$$\tau_1 = \varepsilon^2 t, \quad \tau_2 = \beta t, \quad \tau_3 = \gamma t \quad (4.4)$$

for each of the perturbation parameters introduced earlier.

Asymptotic expansions of the form

$$u = \varepsilon u_1 + \varepsilon^2 u_2 + \varepsilon [\varepsilon^2 u_{31} + \beta u_{32} + \gamma u_{33}] + \dots \quad (4.5)$$

are assumed to hold for u , $c - 1$, $\varrho - 1$ and $T - 1$. Since the occurrence of the radial velocity component is caused by the thermoviscous wall layer the leading order term of the expansion for v is $O(\varepsilon\beta)$ rather than $O(\varepsilon)$:

$$v = \varepsilon\beta v_{32} + \dots \quad (4.6)$$

Insertion of the expansions (4.5), (4.6) into the full Navier-Stokes equation shows that secular terms enter the third order solution unless u_1 satisfies the transport equation

$$\frac{\partial u_1}{\partial t} + [1 + \varepsilon^2(\hat{\Gamma} u_1 + \frac{\Lambda_o}{2} u_1^2)] \frac{\partial u_1}{\partial x} = -\beta v_{32}|_{y=1} + \gamma \frac{\delta}{2} \frac{\partial^2 \hat{u}_1}{\partial x^2}$$

$$\delta = 2 + \frac{\tilde{\lambda}_o}{\tilde{\mu}_o} + \frac{\tilde{\beta}_o^2 \tilde{T}_o \tilde{c}_o^2}{Pr \tilde{c}_{po}} \quad (4.7)$$

where $v_{32}|_{y=1}$ is yet unknown.

To determine the value of the radial velocity component at $y = 1$ it is necessary to investigate the properties of the wall layer region. Appropriate independent variables characterizing this region are $x, Y = (1 - y)/\beta$ and t . The leading order terms of the expansions of the field quantities are assumed to be of the form

$$\begin{aligned} u &= \varepsilon(u_1 + u_{1b}) + \dots \\ v &= \varepsilon\beta v_{1b} + \dots \\ \varrho &= 1 + \varepsilon(\varrho_1 + \varrho_{1b}) + \dots \\ T &= 1 + \varepsilon(T_1 + T_{1b}) + \dots \end{aligned} \quad (4.8)$$

where the subscripts 1 and $1b$ denote the leading order y independent disturbances inside the core region and the boundary layer corrections, respectively.

Substitution into the full set of Navier-Stokes equations yields

$$\begin{aligned} \frac{\partial \varrho_{1b}}{\partial t} + \frac{\partial u_{1b}}{\partial x} + \frac{\partial v_{1b}}{\partial Y} &= 0 \\ \frac{\partial u_{1b}}{\partial t} - \frac{\partial^2 u_{1b}}{\partial Y^2} &= 0 \\ \frac{\partial T_{1b}}{\partial t} - \frac{1}{Pr} \frac{\partial^2 T_{1b}}{\partial Y^2} &= 0. \end{aligned} \quad (4.9)$$

Since the pressure disturbances do not vary across the wall layer to leading order it follows immediately that the boundary layer correction term must vanish. Solutions to equations (4.9) can be obtained by means of standard methods, e.g. heaviside calculus. In the case of constant wall temperature the radial velocity component at the outer edge $Y \rightarrow \infty$ of the wall layer is given by the relationship

$$v_{1b} \sim \frac{1}{\sqrt{\pi}} [1 + \frac{\tilde{\beta}_o \tilde{T}_o G_o}{\sqrt{Pr}}] \int_{-\infty}^t \frac{\partial u_1(x_1, \tau)}{\partial x} \frac{d\tau}{\sqrt{t - \tau}} \quad Y \rightarrow \infty \quad (4.10)$$

where G_o denotes the Grueneisen parameter $G = \left. \frac{\varrho \partial T}{T \partial \varrho} \right|_s$ evaluated in the unperturbed reference state. Using the matching condition $v_{1b}|_{Y \rightarrow \infty} = -v_{32}|_{y=1}$ one obtains

the final form of the evolution equation for weakly damped high frequency waves having both positive and negative nonlinearity

$$\begin{aligned} \frac{\partial u}{\partial t} + (1 + a u + b u^2) \frac{\partial u}{\partial x} &= c \int_{-\infty}^t \frac{\partial u(x, \tau)}{\partial x} \frac{d\tau}{\sqrt{t - \tau}} + d \frac{\partial^2 u}{\partial x^2}, \\ a &= \varepsilon^2 \hat{\Gamma}, \\ b &= \varepsilon^2 \frac{\Lambda_o}{2}, \\ c &= \frac{\beta}{\sqrt{\pi}} \left(1 + \frac{\tilde{\beta}_o \tilde{T}_o \tilde{G}_o}{\sqrt{Pr}}\right), \\ d &= \frac{\gamma}{2} \left(2 + \frac{\tilde{\lambda}_o}{\tilde{\mu}_o} + \frac{\tilde{\beta}_o^2 \tilde{T}_o \tilde{G}_o}{Pr \tilde{c}_{po}}\right), \end{aligned} \quad (4.11)$$

where the subscript 1 has been dropped. From (4.11) the special case of a perfect gas is recovered if

$$\hat{\Gamma} = \frac{\gamma_o + 1}{2\varepsilon}, \quad \Lambda_o = 0, \quad \tilde{\beta}_o \tilde{T}_o \tilde{G}_o = \gamma_o - 1. \quad (4.12)$$

Solutions to the lossless version of equation (4.11) have been discussed in detail in sect. 2. Unfortunately, however, exact solutions become rare if one adds thermoviscous effects. Nimmo and Crighton [37] have provided a comprehensive discussion of the application of B"acklund transformations to a general class of parabolic equations. The conclusion of this study is that, except for relatively simple extensions of the classical quadratic Burgers equation, such transformations are not useful in generating exact solutions. Thus, in the absence of such exact procedures one has to resort the numerical techniques, in general. Some analytical results can, however, be derived if the wave under consideration is a wave of constant form, Gittler and Kluwick [38].

Spectral as well as finite difference methods have been used to obtain numerical solutions of the evolution equation (4.11), Gittler and Kluwick [35]. The first technique is most suitable for the investigation of infinite periodic wavetrains while the properties of single pulses are studied more conveniently by means of finite difference schemes. Fig. 15 shows the comparison between numerical results and the experimental data obtained by Pestorius [34]. The experiments were performed in a tube filled with air and harmonic waves with a frequency of 2000 Hz and an amplitude of 142 db were generated by means of a loudspeaker. The radius of the tube was 2.54 cm and the waveform was recorded at a distance of 18.59 m

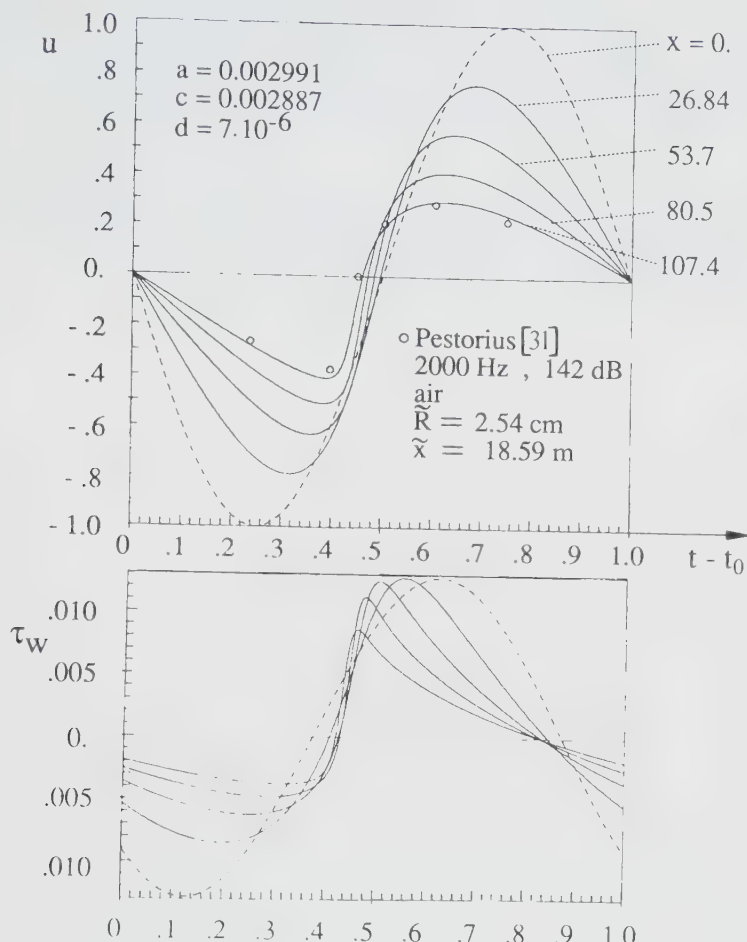


Figure 15: Evolution of the velocity distribution inside the core region (a) and the wall shear stress distribution (b)

which corresponds to a distance of approximately 107 wavelengths. The values of the parameters a , b and c determined from the experimental data are $a = 0.00299$, $b = 0$, $c = 0.002887$. 80 Fourier terms were used in the calculations and in order to suppress oscillations near the shock, the parameter d was given a small value $d = 7 \cdot 10^{-6}$. In Fig. 15a the evolution of the wave is shown starting with the initial profile at $x = 0$ up to the final profile $x = 107.4$. Very good agreement between the calculated profile and the experimental data at $x = 107.4$ given by the open circles is observed.

In addition to the velocity distribution, the wall shear stress distribution is plotted in Fig.15b. Initially, there is a phase lag of 45° between u and τ_w . With increasing distance from the loudspeaker, however, the maximum of the wall shear stress distribution is seen to decrease much more slowly than that of the velocity distribution.

As an example of the numerical solutions obtained by means of the finite difference scheme we consider wavetrains generated by a piston which is at rest for $t < 0$ but performs harmonic oscillations for $t \geq 0$:

$$x = 0 : u = \begin{cases} 0 & \text{for } t < 0 \\ \sin 2\pi t & \text{for } t \geq 0 \end{cases} . \quad (4.13)$$

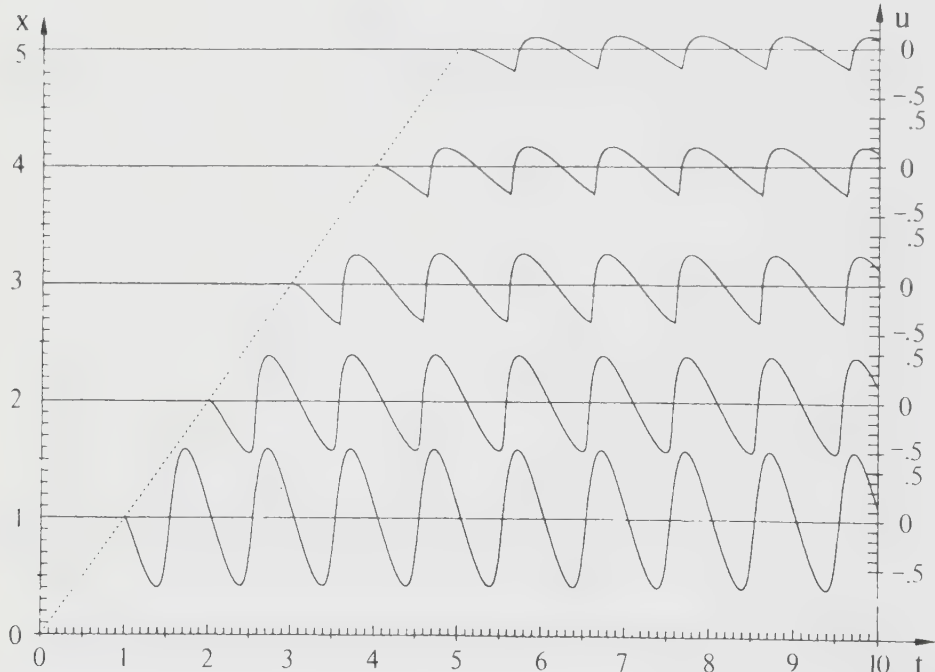


Figure 16: Wave evolution for $a = 0.1$; $b = 0$; $c = 0.1$; $d = 3 \cdot 10^{-5}$

Results for a fluid with strictly positive nonlinearity are summarized in Fig. 16. Here the neutral characteristic, indicated by the dotted line, separates the unperturbed region before the wave and the wavetrain. Since the same u -scaling is used at each x -station, the decay of the wave amplitude due to the presence

of the acoustic boundary layer is clearly visible. Furthermore, since the fluid has positive nonlinearity, portions of the wave with $u > 0$ steepen and shocks form at $x = x_s \approx 2.75$. For larger values of x the characteristic profile of a wave subjected to dispersive wall friction effects, i.e. a slope discontinuity near the pressure minimum and a smooth region of positive excess pressure is obtained.

Fig. 17 shows how the evolution of the wave train is changed if the medium under consideration has negative nonlinearity. Owing to $a < 0$ the initially sinusoidal wavetrain steepens backward leading to the formation of negative shocks which - as expected - are followed by a completely smooth further decrease of u .

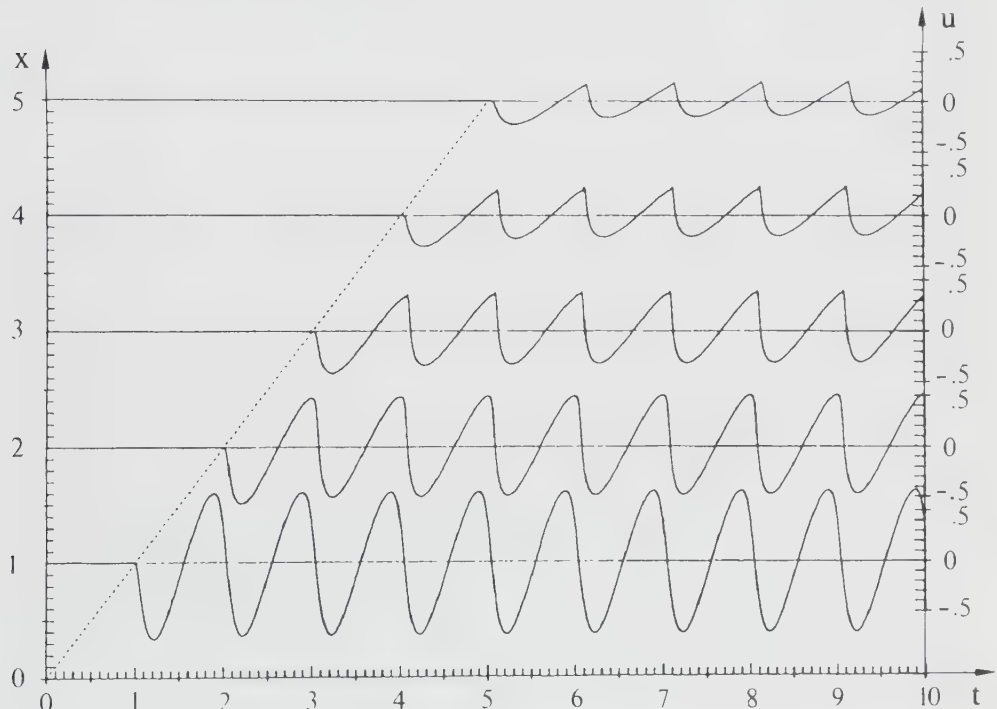


Figure 17: Wave evolution for $a = -0.1$; $b = 0$; $c = 0.1$; $d = 3 \cdot 10^{-5}$

The evolution of sinusoidal waves in media having cubic nonlinearity, depicted in Fig. 18, is more complicated. Here the full line indicates the solution of the lossless version of equation (4.11) with a small diffusivity added to suppress oscillations near shock fronts. Owing to the absence of a quadratic nonlinearity, compression and expansion shocks of equal strength are generated and the wave is seen to approach the asymptotic profile shown in section 2 very rapidly. Ad-

ding the integral memory term leads to the results indicated by the dotted lines. Investigation of waves of constant form for $a = 0$ has shown that they exist in form of compression/expansion shocks followed by positive/negative acceleration waves, Gittler and Kluwick [38]. As far as the propagation of periodic waves is concerned one, therefore, expects waves with perfectly smooth portions of positive and negative excess pressure to form. This is seen to be in complete agreement with the numerical computations. Since the boundary layer memory term exhibits dispersive as well as dissipative effects the wave amplitude is seen to decay more rapidly as in the purely inviscid case and eventually a sinusoidal wave profile is recovered at large distances from the piston.

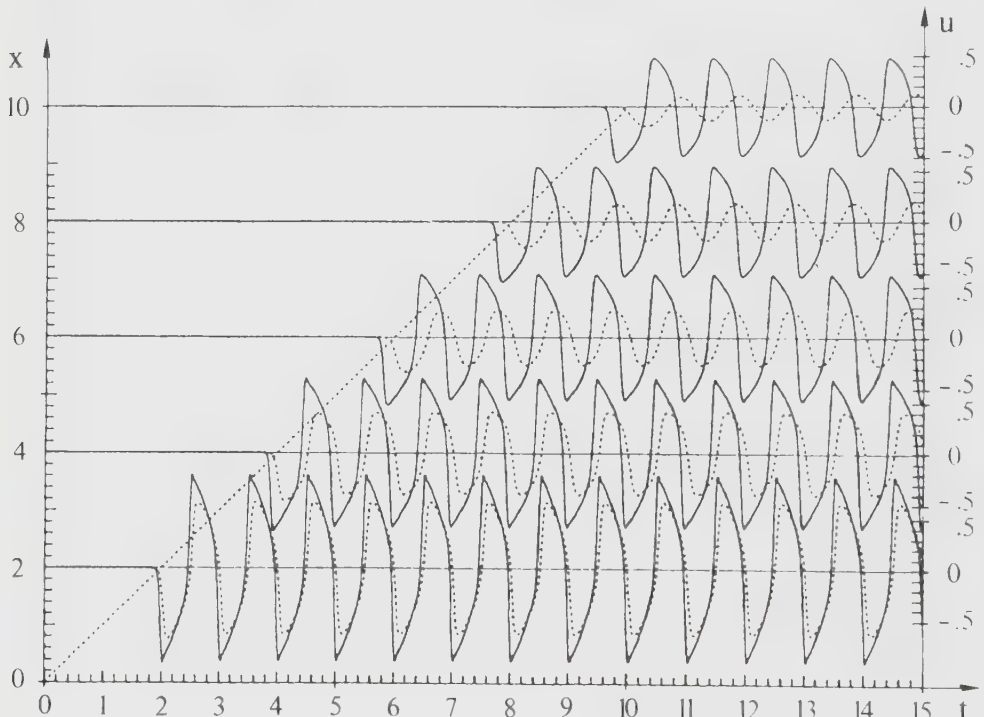


Figure 18: Wave evolution for $a = 0$; $b = 0.2$; $d = 1 \cdot 10^{-5}$; — $c = 0$; ··· $c = 0.0005$

Following this brief discussion of periodic wavetrains let us consider one example of a single pulse, Fig. 19. In terms of the scaled velocity perturbation \hat{u} introduced in section 2 the wave amplitude is -2.2 and the inviscid solution indicated by the full line, therefore, is identical with the results shown in Fig. 5. Again the disintegration of the jumps imposed at $t = 0$ into sonic shocks and wavefans is clearly visible. If boundary layer effects are accounted for, however, the behaviour

of the wave is seen to change drastically. In particular, it is found that the presence of the viscous wall layer causes the sonic expansion shock to decay very rapidly and the numerical results seem to indicate that it terminates at a finite distance from the piston. For larger values of x the wave profile is completely smooth and exhibits a long dispersive tail.

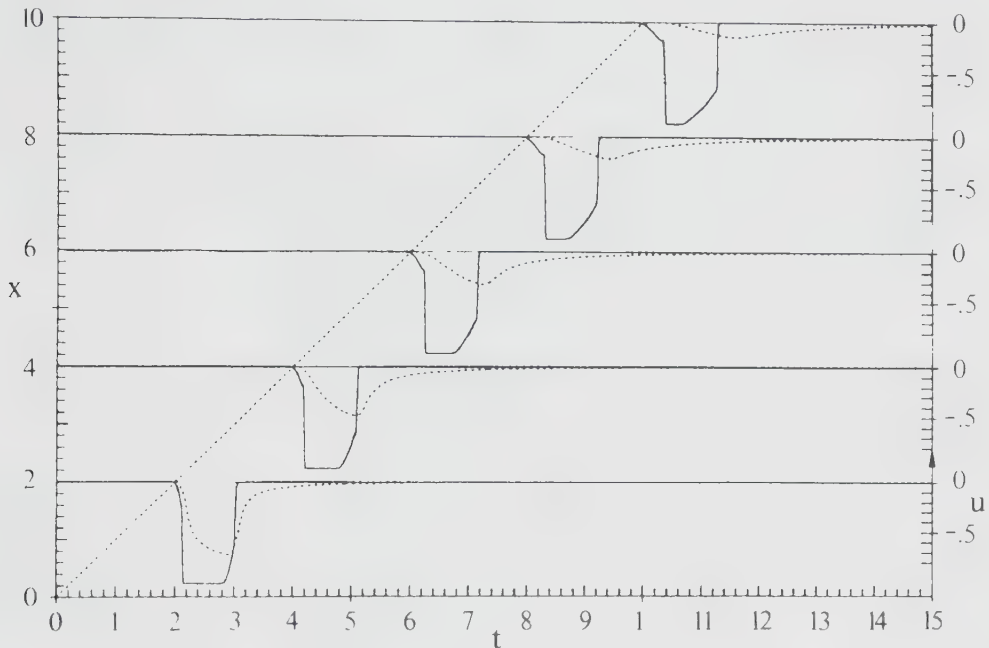


Figure 19: Wave evolution for $a = 0.18$; $b = 0.2$; $d = 1 \cdot 10^{-4}$; — $c = 0$; ··· $c = 0.1$

5. Further generalizations

The significance of the transport equation (3.10) derived for single phase fluids having mixed nonlinearity can be extended considerably. To this end we consider wave motions governed by the system of quasilinear first order partial differential equations

$$\frac{\partial \bar{u}}{\partial t} + \bar{A}^k(\bar{u}) \frac{\partial \bar{u}}{\partial x^k} = 0 \quad , \quad k = 1, 2, 3 \quad (5.1)$$

the components of the vector $\bar{u}(u^1, u^2, \dots, u^p)$ include the flow velocity as well as the various other field quantities entering the specific problem under investigation. t, x^k and \bar{A}^k denote the time, cartesian coordinates and matrices $(p \times p)$ which depend on \bar{u} only.

The system of governing equations (5.1) is said to exhibit solutions which describe progressive waves “if there exists a family of propagating surfaces $\xi = \text{const}$ (also termed wavelets), with

$$F(t, x^k) = \xi \quad (5.2)$$

such that the magnitude of the rate of change of \bar{u} when x^k is moving with such a surface is small compared with the magnitude of the rate of change of \bar{u} when x^k is kept fixed”, Germain [10].

In the case of weakly nonlinear progressive waves, which is of interest here, we assume small disturbances to a uniform rest state $u = \bar{u}_o$ so that

$$u = u_o + \varepsilon u_1 + o(\varepsilon)$$

$$A^k = A_o^k + \varepsilon A_1^k + o(\varepsilon) \quad (5.3)$$

where the nondimensional parameter $\varepsilon \ll 1$ is a measure of the wave amplitude. Furthermore, it is assumed that the disturbances u_1, u_2, \dots are functions of t, x^k and the fast variable

$$\xi = \frac{\xi}{\varepsilon^n} \quad (5.4)$$

with $n = 1$ or $n = 2$.

Substitution of (5.3) into (5.1) shows that the equation for \bar{u}_1 has a nontrivial solution if

$$\det C_o = 0, \quad C_{oij} = \delta_{ij} \frac{\partial F}{\partial t} + A_{oij}^k \frac{\partial F}{\partial x^k}. \quad (5.5)$$

As a consequence, wavelets $\xi = \text{const}$ must be characteristic surfaces of the set of governing equations (5.1). Introducing the (normalized) left and right eigenvectors

$$\bar{l} \bar{C}_o = \bar{C}_o \bar{r} = \bar{0}, \quad \bar{l} \bar{r} = 1 \quad (5.6)$$

the result for \bar{u}_1 can be written in the form

$$\bar{u}_1 = \alpha(\xi, s) \bar{r} \quad (5.7)$$

The socalled amplitude factor α which is a function of ξ and the distance s measured along geometric rays of characteristic surfaces $F(t, x^k) = \text{const}$ (Fig 20), remains unknown at this stage of analysis. In order to complete the first order solution it is necessary to work out the solvability condition for \bar{u}_2 or \bar{u}_3 if $n = 1$ or 2, respectively. The value of n entering the definition (5.4) of the fast variable

and the form of the resulting transport equation for α is found to depend on the order of magnitude of the quantity

$$\Gamma = l_i B_{oijl}^k \frac{\partial F}{\partial x^k} r_j r_l$$

with

$$B_{oijl}^k = \frac{\partial A_{ij}^k}{\partial u_l} (\bar{u}_o) . \quad (5.8)$$

If $\Gamma = O(1)$, the nonlinear deformation of the wave profile is noticeable over propagation distances $s = O(1/\varepsilon)$, Fig. 20. A suitable choice of the fast variable ξ is then given by ξ/ε and one recovers the classical result that the variation of the amplitude factor α along geometric rays is governed by a differential equation with quadratic nonlinearity, e.g. Germain [10]

$$\frac{\partial \alpha}{\partial s} - \Gamma \alpha \frac{\partial \alpha}{\partial \xi} + \alpha K = 0 .$$

$$K = l_i A_{oij}^k \frac{\partial r_j}{\partial x^k} . \quad (5.9)$$

Herein K is a known function of s once the wave geometry has been specified. However, if Γ is small and of the order of the wave amplitude

$$\Gamma = \varepsilon \hat{\Gamma} , \quad \hat{\Gamma} = O(1) \quad (5.10)$$

nonlinear effects will be of importance only at much larger distances $s = O(1/\varepsilon^2)$ thus implying $n = 2$. It can then be shown that the appropriate generalization of the classical result (5.9) is given by Kluwick [39]

$$\frac{\partial \alpha}{\partial s} - (\hat{\Gamma} + \frac{\Lambda_o}{2} \alpha) \alpha \frac{\partial \alpha}{\partial \xi} + \alpha K = 0 . \quad (5.11)$$

The definition of the quantity Λ_o closely resembles the relationship derived by Sen and Cramer [40] in their study of strictly one-dimensional wave propagation processes.

It should be noted that (5.11) is of essentially the same form as the evolution equation (3.10) describing the propagation of acoustic waves in channels with slowly varying cross section.

Equations of the form (5.1) describe a large variety of different physical problems. Applications of the theory outlined in this section include, for example,

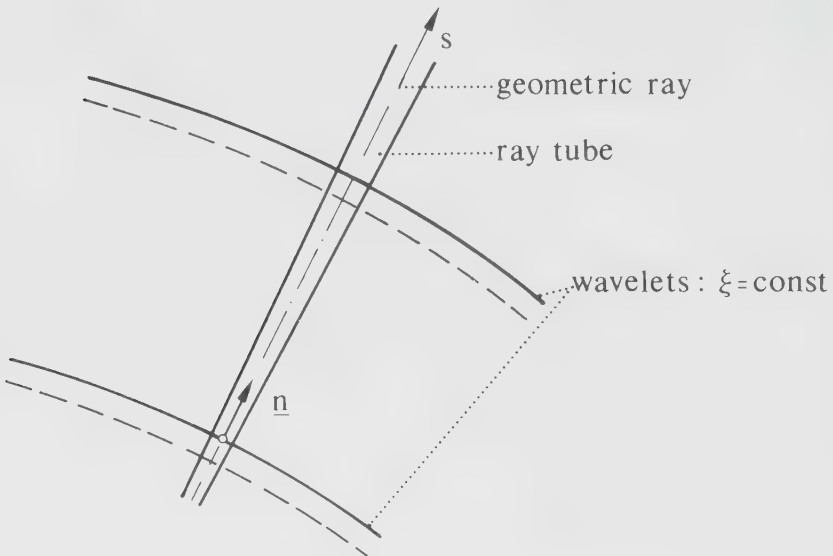


Figure 20: Wave geometry

the investigation of weak second sound waves in superfluid helium, Cramer and Sen [41], and of small amplitude kinematic waves in suspensions of particles in fluids, Kluwick [42]. In the latter case an evolution equation of the form (2.26) applies if the particle concentration α_0 in the unperturbed state differs only slightly from the value corresponding to the inflexion point of the driftflux curve. Adopting the driftflux relationship proposed by Richardson and Zaki [43]

$$j_{pf} = v_\infty \alpha (1 - \alpha)^n \quad (5.12)$$

where v_∞ , α and n denote the terminal settling velocity of a single particle in an unconfined medium, the particle concentration and a positive constant, respectively, this condition can be expressed in the form $|2 - (n - 1)\alpha_0| = 0(\varepsilon)$, $\varepsilon \ll 1$.

Experimental investigations of weak kinematic shocks in fluidized beds have been performed among others by Slis, Willemse and Kramers [9] and Verloop, Hertjes and Lerk [44]. In particular, Verloop et al [44] recorded the response of the interphase between suspension and clear liquid to a sudden change of the liquid flux in order to determine whether a single shock or a shock fan combination was generated. Fig. 21 summarizes their results which correspond to an increase of the fluid flux for the two test cases $n = 3.01$ and $n = 3.85$, respectively. Comparison with the theoretical limits of permissible shocks following from equation

(2.30) yields reasonable agreement, especially if one takes into account that it is difficult to distinguish experimentally between a single shock and a shock which is followed by a thin wave fan, Fig. 21. More recently the propagation of expansion shocks have been investigated experimentally by Didwania and Homsy [45]. As can be seen from Fig. 21 the criterion (2.30) which limits the strength of jump discontinuities is satisfied in all cases.

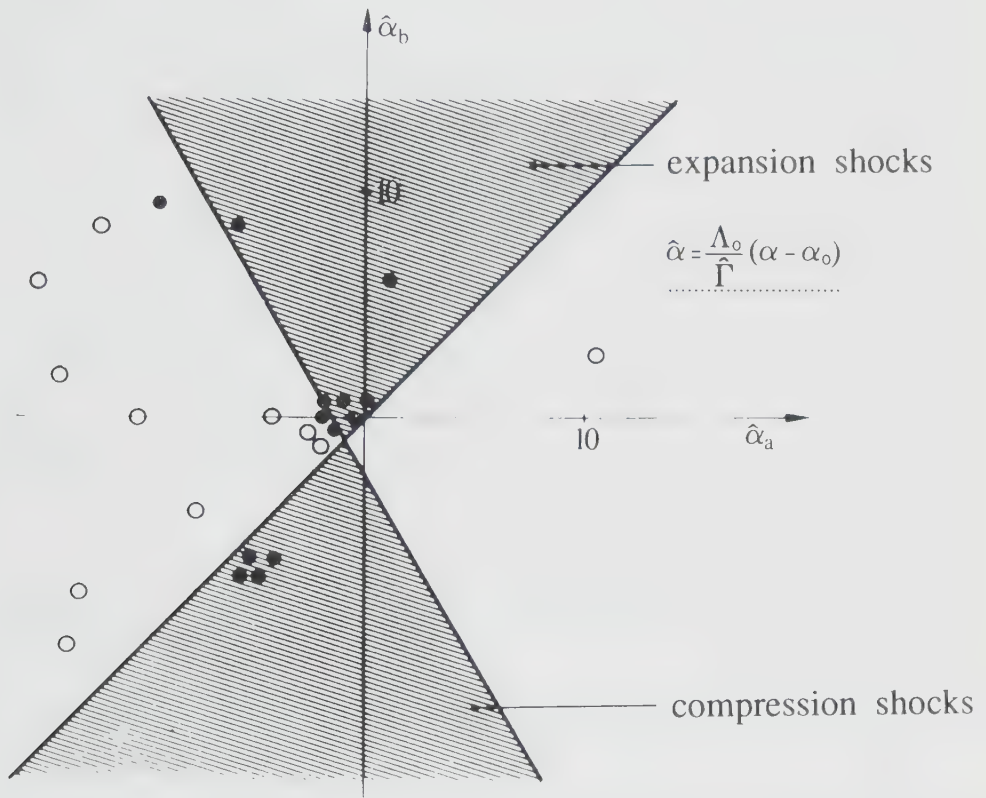


Figure 21: Stability of weak jump discontinuities in suspensions of particles in fluids. Values of $\hat{\alpha}_a$ and $\hat{\alpha}_b$ in shaded regions satisfy (2.30).

- single shock [44][45]
- shock-fan combination [44]

Inertia and internal friction effects are neglected in the strictly kinematic approach to the study of wave motions in suspensions of particles in fluids sketched so far. As shown by Kluwick [42], however, these effects can be retained in a theory

of weakly nonlinear long waves if a suitable defined Froude number is small. One then obtains the result that the appropriate generalization of (2.26) is the modified Burgers-Korteweg de Vries equation

$$\frac{\partial \hat{\alpha}}{\partial \tau} + (\hat{\alpha} + \frac{\hat{\alpha}^2}{2}) \frac{\partial \hat{\alpha}}{\partial \hat{\xi}} = \delta \frac{\partial^2 \hat{\alpha}}{\partial \hat{\xi}^2} - \gamma \frac{\partial^3 \hat{\alpha}}{\partial \hat{\xi}^3}. \quad (5.13)$$

Most interesting, it is found that the coefficient δ of the diffusive term may change sign. A similar conclusion was reached by Kluwick [46], Kurdynomov and Sergeev [47] and Crighton [48] who studied voidage waves governed by the Burgers-Korteweg de Vries equation which holds if the particle concentration α_0 is sufficiently far from the value α_i characterizing the inflection point of the drift flux curve.

Solutions of the modified Burgers-Korteweg de Vries equations (5.13) describing waves of constant form have been discussed briefly by Kluwick [42]. In agreement with the results holding for the modified Korteweg de Vries equation (Kakutani and Yamasaki [49], Miles [50]) soliton solutions are expected to form in the limit $\delta \rightarrow 0+$ but the characteristic features of solutions of both the Burgers-Korteweg de Vries equation and the modified Burgers-Korteweg de Vries equation in the unstable regime $\delta < 0$ do not appear to be known at present. Clearly, more analytical as well as numerical work will be necessary to elucidate these features which might shed some light on the formation of voidage instabilities observed quite frequently in fluidized beds.

References

- [1] Hayes, W.D. (1960) Gasdynamic discontinuities, Princeton Series on High Speed Aerodynamics and Jet Propulsion, Princeton University Press, Princeton, New Jersey.
- [2] Bethe, H.A. (1942) The theory of shock waves for an arbitrary equation of state, Office Sci.Res. & Dev.Rep. 545.
- [3] Zel'dovich, Ya.B. (1946) On the possibility of rarefaction shock waves, Zh. Eksp. Teor. Fiz. **4**, pp. 363-364.
- [4] Thompson, P.A. and Lambrakis, K.C. (1973) Negative shock waves, J.Fluid Mech., **60**, pp. 187-208.
- [5] Cramer, M.S. (1990) Negative Nonlinearity in Selected Fluorocarbons. Submitted to The Physics of Fluids (A).
- [6] Borisov, A.A., Borisov, Al.A. Kutateladze, S.S. and Nakoryakov, V.E. (1983) Rarefaction shock wave near the critical liquid-vapour point. J.Fluid Mech. **126**, pp. 59-73.

- [7] Cramer, M.S. and Kluwick A. (1984) On the propagation of waves exhibiting both positive and negative nonlinearity. *J.Fluid Mech.* **142**, pp. 9-37.
- [8] Kynch, G.J. (1952) A Theory of Sedimentation. *Trans. of the Faraday Soc.* **48**, pp. 166-176.
- [9] Slis, P.L., Willemse, Th.W., Kramers, H. (1959) The response of the level of a liquid fluidized bed to a sudden change in the fluidizing velocity. *Appl.Sci.Res., Sed A*, **8**, pp. 209-218.
- [10] Germain, P. (1971) Progressive waves, 14th Ludwig-Prandtl-memorial lecture. Mannheim, *Jahrbuch 1971 der DGLR*, pp. 11-30.
- [11] Whitham, G.B. (1974) Linear and nonlinear waves. John Wiley and Sons.
- [12] Lighthill, M.J. (1978) Waves in Fluids. Cambridge University Press.
- [13] Crighton, D.G. (1979) Model equations of nonlinear acoustics. *Ann.Rev.Fluid Mech.* **11**, pp. 11-33.
- [14] Kluwick A. (1981) The analytical method of characteristics. *Progress in Aerospace Sciences*, **19**, pp. 197-313.
- [15] Sachdev, P.L. (1987) Nonlinear diffusive waves. Cambridge University Press.
- [16] Lighthill, M.J. and Whitham, G.B. (1955) On kinematic waves: I. Flood movement in long rivers. *Proc.Roy.Soc.Lond. A* **299**, 281-316.
- [17] Lax, P.D. (1971) Shock waves and entropy. In: *Contributions to Nonlinear Functional Analysis* (ed. E.H.Zarantonello), Academic Press, New York.
- [18] Germain, P. (1972) Advances in Applied Mechanics **12**, pp. 131-184.
- [19] Lee-Bapty I.P. (1981) Ph.D. dissertation, Leeds University, England.
- [20] Crighton, D.G. (1982) Propagation of non-uniform shock waves over large distances. In: *Proc. IUTAM Symp. on Nonlinear Deformation Waves* (ed. U. Nigul & J.Engelbrecht), Springer.
- [21] Lee-Bapty I.P. and Crighton, D.G. (1987) Nonlinear Wave Motion Governed by the Modified Burgers Equation. *Phil.Trans.R.Soc.Lond. A*, **323**, pp. 173-209.
- [22] Kluwick, A. and Koller, F (1988) Ausbreitung periodischer Wellen kleiner Amplitude in Gasen mit grossen spezifischen Waermen, *ZAMM* **68** (1988) 5, T 306 - 307.

-
- [23] Cramer, M.S., Kluwick, A. Watson, L.T. and Pelz, W. (1986) Dissipative waves in fluids having both positive and negative nonlinearity, *J.Fluid Mech.* **169**, pp. 329-336.
 - [24] Cramer, M.S. (1987) Structure of weak shocks in fluids having embedded regions of negative nonlinearity. *Phys.Fluids* **30**, pp. 3034-3044.
 - [25] Shannon, P.T. and Tory, E.M. (1965) Settling of slurries. *Ind. Engng. Chem.* **57**, pp. 18 - 25.
 - [26] Thompson, P.A., Chaves, H., Meier, G.E.A., Kim, Y.G. and Speckmann, H.D. (1987) Wave splitting in a fluid of large heat capacity. *J. Fluid Mech.* **185**, pp. 385 - 414.
 - [27] Cramer, M.S. and Crickenberger, A.B. (1990) The Dissipative Structure of Shock Waves in Dense Gases. Submitted to *J. Fluid Mech.*
 - [28] Varley, E. and Cumberbatch, E. (1966) Non-linear, high frequency sound waves. *J.Inst. Maths. Applies.*, **2**, pp. 133-143.
 - [29] Kluwick, A., Czemetschka, E. (1989) Kugel- und Zylinderwellen in Medien mit positiver und negativer Nichtlinearität, GAMM-Tagung Karlsruhe, BRD, 28. - 31. 3. 1989.
 - [30] McKittrick, J.L.; Blackstock, D.T. and Wright, W.M. (1967) Profile of repeated shock waves in a tube. *J.Acoust.Soc.Amer.* **42**, pp. 1153.
 - [31] Blackstock, D.T. (1972) Nonlinear Acoustic (Theoretical), in: *Amer. Inst. Phys. Handbook*, D. Gray Ed. (McGraw-Hill Book Co., Inc., New York), ch 3n, pp. 3-183 through 3-205.
 - [32] Chester, W. (1969) Resonant oscillations in closed tubes, *J.Fluid Mech.* **18**, pp. 44-64.
 - [33] Keller, J.J. (1981) Propagation of simple non-linear waves in gas filled tubes with friction. *ZAMP* **32**, pp. 170-181.
 - [34] Pestorius, F.M. (1973) Propagation of plane acoustic noise of finite amplitude. Technical Report, Applied Research Laboratories, The Univ. of Texas at Austin, ARL-TR-73-23.
 - [35] Gittler, Ph. and Kluwick, A. (1989) Dispersive Wandreibungseffekte bei hochfrequenten Wellen in gasgefüllten Rohren, *ZAMM* **69**, 6, T 578 - T 579.

- [36] Kluwick, A. and Gittler, Ph. (1989) Dispersive wall-friction effects on high frequency waves in media having both positive and negative nonlinearity, Proceed. of the Euromech Colloquium 240, Dispersive waves in dissipative fluids, Bologna, Italy, August 30 - September 2, 1988, pp. 34-37.
- [37] Nimmo, J.J.C. and Crighton, D.G. (1982) Bäcklund transformations for nonlinear parabolic equations: the general results. Proc.Roy.Soc.Lond. A 384, pp. 381-401.
- [38] Gittler, Ph. and Kluwick, A. (1990) On the propagation of weakly nonlinear high frequency waves in tubes filled with dense gases, to be published.
- [39] Kuwick, A. (1990) Weakly nonlinear progressive waves having mixed nonlinearity, to be published.
- [40] Sen, and Cramer, M.S. (1987) A General Scheme for the Derivation of Evolution Equations Describing Mixed Nonlinearity, VPI-E-87-16 Report.
- [41] Cramer, M.S. and Sen (1990) The Equation Governing Mixed Nonlinearity and Double-Shocks in Superfluid Helium, submitted to J. Fluid Mech.
- [42] Kluwick, A. (1990) Weakly nonlinear kinematic waves in suspensions of particles in fluids, Acta Mechanica, in press.
- [43] Richardson, J.F., Zaki, W.N. (1954) Sedimentation and Fluidization: Part I., Trans. Inst. Chem. Engrs. **32**, 35-53.
- [44] Verloop, J., Heertjes, P.M., Lerk, L.A. (1974) The velocity and stability of large porosity fluctuations in homogeneous fluidized systems. Chem.Engng. Sci. **29**, pp. 1109-1114.
- [45] Didwania, A., Homsy, G.M. (1980) Fluidization, ed. J.R. Grace and J.M. Matsen, Plenum 1980, pp. 109-116.
- [46] Kluwick, A. (1983) Small-amplitude Finite-rate Waves in Suspensions of Particles in Fluids, ZAMM **63**, pp. 161-171.
- [47] Kurdyumov, V.N. and Sergeev, Yu.A. (1987) Propagation of nonlinear Waves in a fluidized bed in the presence of interaction between the particles of the dispersed phase. Fluid Dynamics **22**, No 2, pp. 235-242.
- [48] Crighton, D.G. (1991) Nonlinear waves in fluidized beds. In: Nonlinear Waves in Real Fluids (A. Kluwick, ed.), Springer Verlag 1991.
- [49] Kakutani, T. and Yamasaki, N. (1978) Solitary Waves on a Two-Layer Fluid. J. of the Physical Soc. of Japan, **45**, pp 674-679.
- [50] Miles, J.W. (1979) On internal solitary waves. Tellus **31**, pp. 456-462.

NONLINEAR ACOUSTIC OF BUBBLY LIQUIDS

D. G. Crighton
University of Cambridge, Cambridge, UK

ABSTRACT

This chapter deals with the propagation of nonlinear acoustic waves in dilute suspensions of air bubbles in water. It begins with a discussion of the dependence of the sound speed on bubble volume concentration and on frequency, and of the Rayleigh equation for the oscillations of an isolated bubble. Then the Korteweg-de Vries and Nonlinear Klein-Gordon equations are derived for nonlinear waves at low and at high frequency, respectively, and typical features of solutions of these equations are outlined.

1. INTRODUCTION

Bubbly liquids, with even small volume concentrations of small air bubbles, have very unusual hydrodynamic and acoustic properties. Extreme near-field pressures can be developed from the highly nonlinear oscillation of bubbles in an unsteady environment, while as far as the acoustics are concerned, small concentrations of bubbles can lead to sound speeds at low frequencies which are much lower than the pure water sound speed (by perhaps a factor of 10 or more) and even lower than the pure air sound speed. At moderate frequencies the sound speed can become even lower, essentially vanishing for a range of frequencies around the bubble resonance frequency, and then for still higher frequencies taking very large values, greater than the pure water sound speed. Dissipation is significant at all but the lower frequencies, and especially around the resonance frequency. These features have stimulated much work on sound propagation in bubbly liquids, the scattering and transmission of sound by clouds of bubbles (as in boundary layers and wakes), the generation of sound by turbulence in bubbly liquids, and the propagation of finite-amplitude sound pulses – which have a shock wave and/or *soliton* structure which is not possible in pure water or pure air.

2. SOUND SPEED IN BUBBLY LIQUIDS – LOW FREQUENCIES

Let ρ_ℓ, ρ_g be the liquid and gas densities in a suspension of gas bubbles in liquid (no relative motion between bubbles and liquid). The bubbles are assumed small, and sparsely distributed on the scale of a bubble radius, but sufficiently densely distributed on a macroscopic scale that they determine the properties of a continuum mixture of density ρ . The volume concentration of bubbles is assumed to be a uniform α ; α is the fraction of unit volume of mixture occupied by gas.

Then the continuum density is

$$\rho = (1 - \alpha)\rho_\ell + \alpha\rho_g , \quad (2.1)$$

and the assumption of no relative motion implies that the mass of gas in unit mass of mixture is constant, i.e.

$$\alpha\rho_g/\rho = \text{constant} . \quad (2.2)$$

Under equilibrium conditions (i.e., for frequencies well below any bubble resonance frequencies), pressure is uniform throughout liquid and bubbles, and (cf. van Wijngaarden [1]) we can calculate the mixture sound speed c from the definition

$$c^2 = dp/d\rho$$

and the definitions $c_g^2 = dp/d\rho_g$, $c_\ell^2 = dp/d\rho_\ell$ of the gas and liquid sound speeds c_g, c_ℓ . From (2.1)

$$\frac{d\rho}{dp} = \frac{(1-\alpha)}{c_\ell^2} + \frac{\alpha}{c_g^2} + (\rho_g - \rho_\ell) \frac{d\alpha}{dp} ,$$

and from (2.2)

$$\alpha \rho_g = \left(\frac{\alpha \rho_g}{\rho} \right) \rho$$

where the bracketed factor is constant, so that

$$\rho_g \frac{d\alpha}{dp} + \frac{\alpha}{c_g^2} = \left(\frac{\alpha \rho_g}{\rho} \right) \frac{d\rho}{dp} ,$$

giving

$$\frac{d\alpha}{dp} = \left(\frac{\alpha}{(1-\alpha)\rho_\ell + \alpha \rho_g} \right) \frac{d\rho}{dp} - \frac{\alpha}{\rho_g c_g^2} .$$

Elimination of $d\alpha/dp$ gives

$$\frac{1}{c^2} = \frac{(1-\alpha)^2}{c_\ell^2} + \frac{\alpha^2}{c_g^2} + \alpha(1-\alpha) \left\{ \frac{\rho_\ell^2 c_\ell^2 + \rho_g^2 c_g^2}{\rho_\ell \rho_g c_\ell^2 c_g^2} \right\} . \quad (2.3)$$

As $\alpha \rightarrow 0$, $c \rightarrow c_\ell$; and as $\alpha \rightarrow 1$, $c \rightarrow c_g$. However, the transition from c_ℓ to c_g is not monotonic, and for quite modest values of α , c drops to values not only much less than c_ℓ , but indeed much less than c_g , before recovering from below to the pure gas value c_g as $\alpha \rightarrow 1$. In (2.3) we can approximate the last term by

$$\alpha(1-\alpha)\rho_\ell/\rho_g c_g^2$$

and this is then seen to dominate both of the first two terms on the right of (2.3) unless α is very close to 1 or 0. Thus

$$c^2 \simeq \frac{\rho_g c_g^2}{\alpha(1-\alpha)\rho_\ell} ,$$

and $c_g^2 = p_0/\rho_g$ or $c_g^2 = \gamma p_0/\rho_g$ with γ the gas specific heat ratio, according as isothermal or adiabatic changes are assumed to take place in the bubbles. Then

$$c^2 \simeq \frac{\gamma p_0}{\alpha(1-\alpha)\rho_\ell} , \quad (2.4)$$

with $\gamma = 1$ for isothermal behaviour. This predicts a minimum of c as a function of α , for given p_0 and ρ_ℓ ; this occurs at $\alpha = 0.5$, corresponding to closely packed bubbles, and gives $c = 20$ m/s for water at 1 bar. The figure below, due to Campbell & Pitcher [2], shows that the theory gives results in reasonable agreement with experiment, $\gamma = 1$ giving the best agreement.

Note that $c \ll c_\ell$; and that $c < c_g$ is easily possible for quite small values of α . If $\alpha = 0.01$ at $p_0 = 1$ bar, then $c = 100$ m/s.

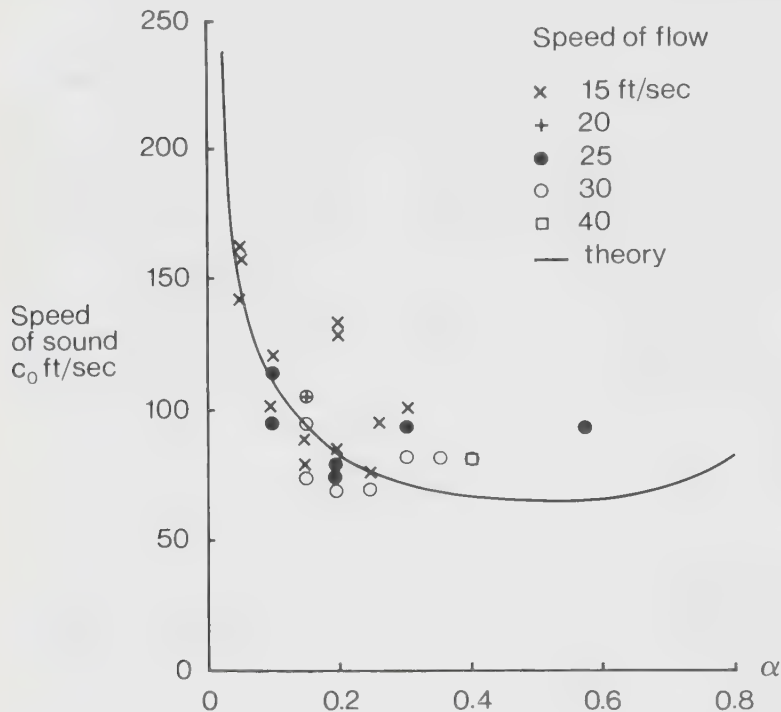


Figure 1

Theory and experimental measurement for low frequency sound speed c_0 (ft/sec) as a function of α . Speed of flow (water tunnel flow, gas injection at a grid) indicated by symbols. After Campbell & Pitcher [2].

3. MOTION IN THE NEIGHBOURHOOD OF A SINGLE BUBBLE

Consider a single bubble at rest apart from radial, spherically symmetric oscillations, in infinite otherwise homogeneous liquid. Assume first that the liquid is strictly incompressible, inviscid and non-heat-conducting. Conditions in the bubble are often assumed nonetheless to be isothermal, on the basis that an adiabatic compression of the whole mixture produces only a small temperature rise in the liquid, and higher temperatures produced in the bubble are rapidly reduced by conduction across the boundary of the bubble.

If r is distance from the bubble, whose radius is $R(t)$, then the potential in the liquid is

$$\phi = -R^2 \dot{R}/r \quad , \quad (3.1)$$

and the pressure $p(r, t)$ follows from Bernoulli's integral

$$\frac{\partial \phi}{\partial t} + \frac{p}{\rho_\ell} + \frac{1}{2} \left(\frac{\partial \phi}{\partial r} \right)^2 = \frac{p_\infty}{\rho_\ell}$$

as

$$p = p_\infty + \rho_\ell \left\{ \frac{R^2 \ddot{R}}{r} + \frac{2R \dot{R}^2}{r} - \frac{1}{2} \frac{R^4 \dot{R}^2}{r^4} \right\} \quad , \quad (3.2)$$

where p_∞ is the ambient pressure. Now if p_g is the (uniform) pressure in the bubble and T the surface tension,

$$p_g = p(R) + \frac{2T}{R} \quad ,$$

while if the gas behaves isothermally,

$$p_g R^3 = p_0 R_0^3$$

where p_0 and R_0 are the pressure and radius with no motion, so that

$$p_0 = p_\infty + \frac{2T}{R_0} \quad .$$

These equations lead to an equation, first found by Lord Rayleigh, for oscillation of a bubble of equilibrium radius R_0 in liquid at pressure p_∞ :

$$R \ddot{R} + \frac{3}{2} \dot{R}^2 + \frac{p_\infty}{\rho_\ell} \left(1 - \frac{R_0^3}{R^3} \right) + \frac{2T}{\rho_\ell R} \left(1 - \frac{R_0^2}{R^2} \right) = 0 \quad . \quad (3.3)$$

There has been much analytical and numerical work done recently on this equation and generalisations of it, particularly with regard to its nonlinear aspects and the possibility of chaotic response to single-frequency perturbations of p_∞ (see Lauterborn [3,4]).

For *small* oscillations we put $R = R_0 + S(t)$ and linearise to get

$$\ddot{S} + \omega_0^2 S = 0$$

where the bubble resonance (or Minnaert) frequency is

$$\omega_0 = \left(\frac{3p_\infty}{\rho_\ell R_0^2} + \frac{4T}{\rho_\ell R_0^3} \right)^{1/2} . \quad (3.4)$$

The effect of the surface tension term here and elsewhere is small unless the bubble radius is less than about 10^{-5} m, and it will in future be neglected.

General inclusion of compressibility is complicated; we deal just with the linear problem. Then the potential satisfies

$$(\nabla^2 + k_0^2)\phi = 0$$

where we assume $\exp(-i\omega t)$ time dependence and write $k_0 = \omega/c_0$ with c_0 the fluid sound speed. The monopole solution is

$$\phi = Ar^{-1} \exp ik_0 r$$

and imposing $\partial\phi/\partial r = -i\omega S$ at $r = R_0$, calculating p from the linearised Bernoulli equation and equating it to the linearised gas pressure, gives

$$\ddot{S} + \omega^2 S = 0$$

for free oscillations, where now

$$\omega^2 = \frac{3p_\infty}{\rho_\ell R_0^2} (1 - ik_0 R_0) . \quad (3.5)$$

Since the radius R_0 is always small compared with the acoustic scale k_0^{-1} in water, we get

$$\omega_1 = \left(\frac{3p_\infty}{\rho_\ell R_0^2} \right)^{\frac{1}{2}}, \quad \omega_2 = -\omega_1 \left(\frac{k_0 R_0}{2} \right) ,$$

if $\omega = \omega_1 + i\omega_2$, $\text{Im } \omega_2 < 0$ corresponding to radiation damping. For forced oscillations, with ambient pressure $p_\infty + p'_\infty \exp(-i\omega t)$, the response $S \exp(-i\omega t)$ is given by

$$(-\omega^2 + \omega_1^2 - 2i\delta\omega)S = -p'_\infty / \rho_\ell R_0 ,$$

where the damping factor is

$$\delta = \omega_1 \left(\frac{k_0 R_0}{2} \right)$$

and ensures a finite response at resonance, $\omega = \omega_1$.

The damping factor in the bubble response equation is not always dominated by radiation damping. Other damping mechanisms (each important in some parameter range) include (i) viscous dissipation in the radial fluid motion generated by the bubble, (ii) viscous dissipation in the relative motion between the bubble and the exterior fluid, (iii) thermal conduction across the bubble wall, (iv) surface chemistry mechanisms. None of these is always negligible, but the relative importance of them depends sensitively and differently on the actual distribution of bubble sizes.

4. SOUND SPEED IN BUBBLY LIQUID - DISPERSIVE EFFECTS

At non-zero frequencies, the equilibrium assumptions no longer hold, and in particular, the pressures inside the bubbles and in the surrounding liquid cannot be taken as equal because of the inertia of the fluid near each bubble. We consider first linear bubble oscillations, in the absence of surface tension and dissipation, in which case the mean pressure p_0 is the same in bubbles and liquid. We also assume that all bubbles have the same equilibrium radius R_0 .

Introduce the following:

$$\begin{aligned}
 & \text{mixture density } \rho = \rho_0 + \rho' \\
 & \text{pressure in liquid } p = p_0 + p' \\
 & \text{liquid density } \rho_\ell = \rho_{\ell 0} + \rho'_\ell \\
 & \text{pressure in gas } p_g = p_0 + p'_g \\
 & \text{volume concentration } \alpha = \alpha_0 + \alpha' \\
 & \text{liquid and gas velocity } u = u' \\
 & \text{bubble number density } n = n_0 + n' \\
 & \text{bubble radius } R = R_0 + R' .
 \end{aligned} \tag{4.1}$$

Mass conservation for the mixture requires

$$\frac{\partial \rho}{\partial t} + u \frac{\partial \rho}{\partial x} + \rho \frac{\partial u}{\partial x} = 0 , \tag{4.2}$$

and momentum conservation for the mixture requires

$$\rho \frac{\partial u}{\partial t} + \rho u \frac{\partial u}{\partial x} + \frac{\partial p}{\partial x} = 0 . \tag{4.3}$$

Conservation of bubbles (in a suspension) requires

$$\frac{\partial n}{\partial t} + u \frac{\partial n}{\partial x} + n \frac{\partial u}{\partial x} = 0 . \tag{4.4}$$

The linearised versions of these equations are

$$\frac{\partial \rho'}{\partial t} + \rho_0 \frac{\partial u'}{\partial x} = 0 \quad , \quad (4.5)$$

$$\rho_0 \frac{\partial u'}{\partial t} + \frac{\partial p'}{\partial x} = 0 \quad , \quad (4.6)$$

$$\frac{\partial n'}{\partial t} + n_0 \frac{\partial u'}{\partial x} = 0 \quad . \quad (4.7)$$

If we neglect the gas contribution $\alpha \rho_g$ to ρ , then

$$\rho = (1 - \alpha) \rho_\ell \quad , \text{ which gives}$$

$$\rho_0 = (1 - \alpha_0) \rho_\ell \quad , \quad \rho' = (1 - \alpha_0) \rho'_\ell - \frac{\alpha' \rho_0}{(1 - \alpha_0)} \quad . \quad (4.8)$$

The fluctuation ρ'_ℓ in liquid density can be related to p' through the liquid sound speed,

$$p' = c_\ell^2 \rho'_\ell \quad , \quad (4.9)$$

and the linearised version of the Rayleigh equation is

$$p'_g - p' = \frac{\rho_0}{(1 - \alpha_0)} R_0 \ddot{R}' \quad (4.10)$$

where the pressure p_∞ in the Rayleigh equation has been taken to be the mixture/liquid pressure p . Next, the relation $\alpha = \frac{4}{3}\pi R^3 n$ gives

$$\alpha_0 = \frac{4}{3}\pi R_0^3 n_0 \quad , \quad \alpha' = 4\pi R_0^2 n_0 R' + \frac{4}{3}\pi R_0^3 n' \quad . \quad (4.11)$$

Finally, if isothermal conditions prevail in the bubbles, then

$$p_g R^3 = p_0 R_0^3 \quad ,$$

or in linearised form,

$$p'_g R_0^3 + 3p_0 R_0^2 R' = 0 \quad . \quad (4.12)$$

Equations (4.5) - (4.12) are a set of eight homogeneous equations for the eight fluctuations. The *dispersion relation* for waves $\exp(ikx - i\omega t)$ is found to be

$$\frac{k^2}{\omega^2} = \frac{(1 - \alpha_0)^2}{c_\ell^2} + \frac{1}{c_0^2(1 - \frac{\omega^2}{\omega_0^2})} \quad , \quad (4.13)$$

where the left side is $1/c_p^2$ with c_p the phase speed at frequency ω , and where on the right c_0 refers to the low-frequency sound speed, given by (2.4) with $\gamma = 1$;

$$\omega_0 = \left(\frac{3p_0}{\rho_{\ell 0} R_0^2} \right)^{\frac{1}{2}}$$

is again the bubble resonance frequency (the bubbles being assumed all to have the same radius R_0).

For $\omega \ll \omega_0$ we get $c_p(\omega) \simeq c_0$, but we also see that c_p vanishes at $\omega = \omega_0$, and its real part then remains zero up to a higher frequency given approximately (for $\alpha_0 \ll 1$) by

$$\omega \simeq \omega_0 \left(\frac{c_\ell}{c_0} \right). \quad (4.14)$$

In the forbidden frequency band $(\omega_0, \omega_0 c_\ell / c_0)$, c_p is purely imaginary, the motion is purely reactive, and p' and u' are $\pi/2$ out of phase; no energy is propagated or absorbed. For frequencies just above the value in (4.14), c_p is again real, but now very large, and for still higher values of ω , c_p remains above c_ℓ , approaching $c_\ell/(1 - \alpha_0)$ from above as $\omega \rightarrow \infty$. We observe that while at low frequencies the bubbles make the mixture less stiff than water, the bubbles make the mixture more stiff than water when driven at frequencies above their resonance frequency.

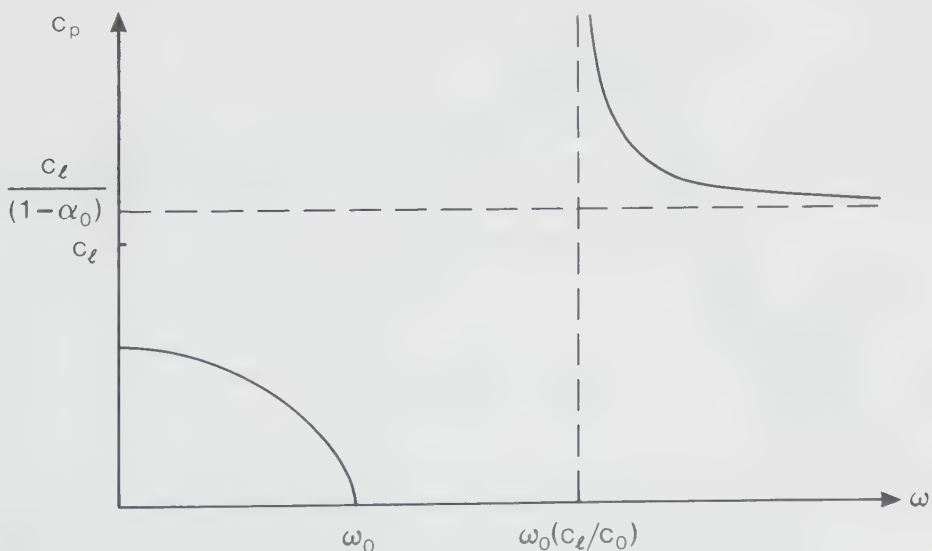


Figure 2

Schematic plot of the variation of phase speed $c_p(\omega)$ with frequency ω , for a distribution of bubbles with identical sizes, and with neglect of all dissipative effects.

Naturally, dissipation removes the singular behaviour seen above, though the trends illustrated there have certainly been seen in experiments – in particular, in one and the same experiment, with a fixed low concentration but with varying frequency, the initial decrease in c_p (below a value c_0 , itself much smaller than the pure liquid sound speed) followed by a sharp increase to values much higher than the liquid sound speed, followed finally by a gradual decrease towards the liquid sound speed, have all been observed. See Figure 3, taken from [1], with data from Fox, Curley & Larson [5]. If dissipation is modelled by the inclusion of a damping factor δ , as earlier, the modification to (4.13) is found to be

$$\frac{k^2}{\omega^2} = \frac{(1 - \alpha_0)^2}{c_\ell^2} + \frac{1}{c_0^2 \left\{ (1 - \frac{\omega^2}{\omega_0^2}) - 2i\delta \frac{\omega}{\omega_0} \right\}} \quad . \quad (4.15)$$

The prediction of (4.15) for $\text{Re } c_p$ is shown on Figure 3, for $\delta = 0.5$ and $\alpha_0 = 2 \times 10^{-4}$. The broken line represents the prediction for bubbles all of identical radius $R_0 = 1.2 \times 10^{-4}\text{m}$, the solid line a theoretical prediction for the actual bubble distribution with this R_0 as the mean radius.

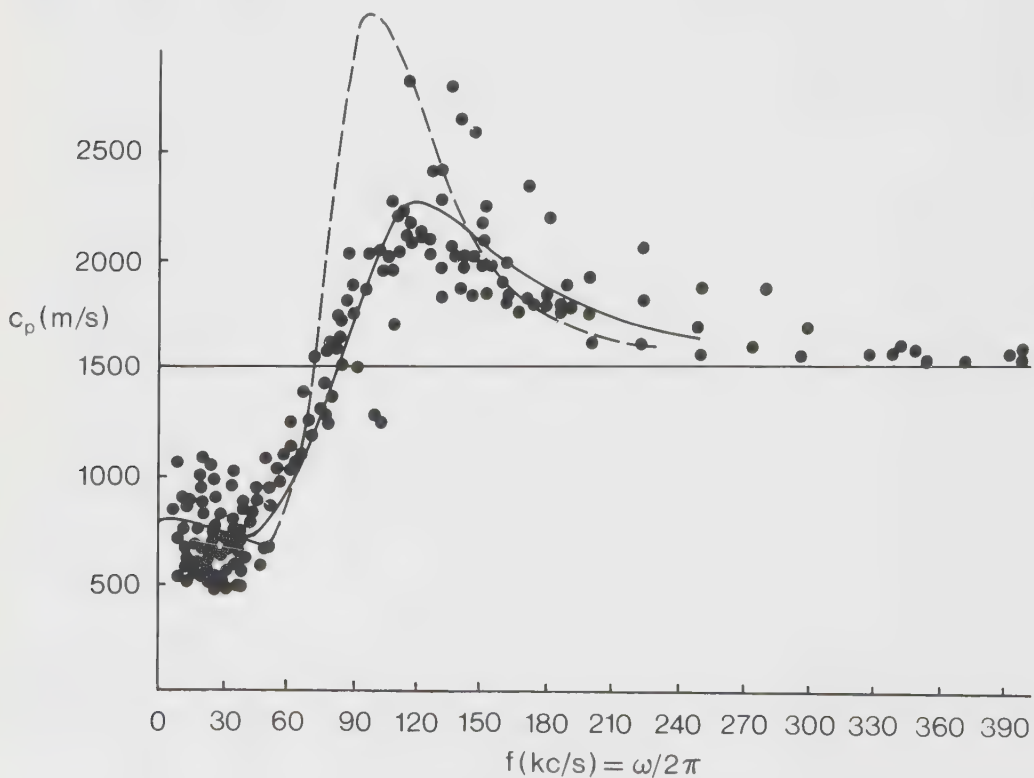


Figure 3

Variation of $\text{Re } c_p$ with ω , theory and experiment. For details see text.

5. WEAKLY NONLINEAR WAVES

We again make the splitting of (4.1), of all the field quantities into mean and fluctuating parts, but instead of keeping only linear terms in the fluctuations, as in (4.5)-(4.12), we also keep quadratic terms – although at first we just treat them as formal source terms.

Thus we have

$$\frac{\partial \rho'}{\partial t} + \rho_0 \frac{\partial u'}{\partial x} + W_1 = 0 \quad , \quad (5.1)$$

$$W_1 = \frac{\partial}{\partial x} \rho' u' \quad .$$

$$\frac{\partial n'}{\partial t} + n_0 \frac{\partial u'}{\partial x} + W_2 = 0 \quad , \quad (5.2)$$

$$W_2 = \frac{\partial}{\partial x} n' u' \quad ,$$

$$\rho_0 \frac{\partial u'}{\partial t} + \frac{\partial p'}{\partial x} + W_3 = 0 \quad , \quad (5.3)$$

$$W_3 = \rho' \frac{\partial u'}{\partial t} + \rho_0 u' \frac{\partial u'}{\partial x} \quad .$$

Again neglecting the gas contribution to the mass,

$$\rho' = (1 - \alpha_0) \rho'_\ell - \alpha' \rho_{\ell 0} \quad , \quad (5.4)$$

with $\rho_0 = (1 - \alpha_0) \rho_{\ell 0}$

We need a nonlinear version of the equation of state for water, and here it is common, and adequate, to take an adiabatic equation, as for air, but with an effective exponent $\Gamma \sim 7$. Thus

$$(p' + p_0)/p_0 = \left[(\rho'_\ell + \rho_{\ell 0})/\rho_{\ell 0} \right]^\Gamma \quad ,$$

which in quadratic approximation gives

$$p' = c_\ell^2 \rho'_\ell + \frac{c_\ell^2(\Gamma - 1)}{2\rho_{\ell 0}} \rho'^2_\ell \quad , \quad (5.5)$$

and when the linear term in ρ'_ℓ is eliminated between (5.4) and (5.5) we have

$$\rho' = -\alpha' \frac{\rho_0}{(1 - \alpha_0)} + \frac{(1 - \alpha_0)}{c_\ell^2} p' + W_4 \quad , \quad (5.6)$$

$$W_4 = -\frac{(1 - \alpha_0)(\Gamma - 1)}{2\rho_{\ell 0}} \rho'^2_\ell \quad .$$

In the Rayleigh equation

$$p_g - p = \rho_{\ell 0} R \ddot{R} + \frac{3}{2} \rho_{\ell 0} \dot{R}^2 ,$$

we note first that the coefficients have been given *constant* values $\rho_{\ell 0}$, and we agree further to take only a *linear* approximation to this equation, because it is the only equation in which *dispersive* terms appear, and our aim is to balance linear dispersive effects against quadratically nonlinear effects. Thus we take

$$p'_g - p' = \rho_{\ell 0} R_0 \ddot{R}' . \quad (5.7)$$

The final equations are quadratically nonlinear versions of (4.11) and (4.12), and are

$$\alpha' = \left(\frac{3}{R_0} R' + \frac{n'}{n_0} \right) \alpha_0 + W_5 , \quad (5.8)$$

$$W_5 = 4\pi(R_0^2 R' n' + R_0 n_0 R'^2) ,$$

and

$$p'_g R_0 + 3p_0 R' + W_6 = 0 , \quad (5.9)$$

$$W_6 = 3p'_g R' + 3p_0 R'^2 / R_0 .$$

We can eliminate linear R' terms between (5.8) and (5.9) to give

$$\alpha' = -\frac{\alpha_0}{p_0} p'_g + \frac{n'}{n_0} \alpha_0 + W_7 , \quad (5.10)$$

$$W_7 = W_5 - \alpha_0 W_6 / p_0 R_0 .$$

and then we need only take linear terms from (5.9) to eliminate R' from (5.7), giving

$$p' = (1 + \frac{1}{\omega_0^2} \frac{\partial^2}{\partial t^2}) p'_g \quad (5.11)$$

in terms of the bubble resonance frequency again.

Now, treating the W_i for the moment as known, the object is to obtain a linear wave equation for one of the variables $(\rho', u', n', p', \alpha', \rho'_{\ell}, p'_g)$ alone. It seems simplest to use p'_g , and one eliminates successively α', p', ρ', n' and u' (ρ'_{ℓ} and R' having been already eliminated). Thus one arrives at

$$\frac{1}{c_0^2} \frac{\partial^2 p'_g}{\partial t^2} + \left(1 + \frac{1}{\omega_0^2} \frac{\partial^2}{\partial t^2} \right) \left[\frac{(1 - \alpha_0)^2}{c_\ell^2} \frac{\partial^2 p'_g}{\partial t^2} - \frac{\partial^2 p'_g}{\partial x^2} \right] = Q \quad , \quad (5.12)$$

with the definitions $c_0 = (p_0/\alpha_0 \rho_0)^{\frac{1}{2}}$ of the low-frequency sound speed (as in (2.4) with $\alpha_0 \ll 1$), and

$$Q = -(1 - \alpha_0) \frac{\partial W_1}{\partial t} - \frac{\rho_0 \alpha_0}{n_0} \frac{\partial W_2}{\partial t} + \frac{\partial W_3}{\partial x} \\ -(1 - \alpha_0) \frac{\partial^2 W_4}{\partial t^2} + \rho_0 \frac{\partial^2 W_7}{\partial t^2} \quad (5.13)$$

of the quadratically nonlinear terms.

The linear operator on the left of (5.12) has precisely the dispersion relation (4.13), with low-frequency sound speed c_0 and high-frequency sound speed $c_\infty = c_\ell/(1 - \alpha_0)$. Acoustic propagation in bubbly liquid is strongly dispersive except at very low and very high frequencies. This means that nonlinear effects are of no general significance (for weakly nonlinear waves) except at very high or very low frequencies – because nonlinearity generates integral harmonics and combination harmonics which, at general frequencies, all travel at different speeds from each other and from the fundamental. Therefore they do not experience the kind of resonant interaction which occurs when dispersion is absent and which leads, over large times and distances, to dramatic distortion of the wave shape. Therefore a “weakly nonlinear theory” which can predict such long-time dramatic changes (leading even to the production of shock discontinuities from smooth initial data) must address itself to circumstances in which dispersion is weak. The low and high frequency limits here give rise to quite different weakly-nonlinear, weakly-dispersive phenomena, and we have to analyse (5.12) separately for the two cases.

6. LOW FREQUENCY WAVES – THE KdV EQUATION

Take the low-frequency limit $\partial^2/\partial t^2 \ll \omega_0^2$ in (5.12), and use also $c_0 \ll c_\ell$ to get

$$\left(\frac{1}{c_0^2} \frac{\partial^2}{\partial t^2} - \frac{\partial^2}{\partial x^2} \right) p'_g = Q \quad . \quad (6.1)$$

Now consider a weakly nonlinear wave, propagating in the x -direction. In such a wave, the low-frequency linear non-dispersive relations give

$$p'_g = p' = \rho_0 c_0 u' = \rho_0 c_0^2 n'/n_0 \\ = c_0^2 \rho' = -\rho_\ell c_0^2 \alpha' \quad .$$

and that all are functions (locally) of $x - c_0 t$, so that in this approximation $\partial/\partial t =$

$-c_0 \partial/\partial x$. These relations may be used to approximate Q further, in a way consistent with the underlying weak-nonlinearity, weak-dispersion limit. This gives

$$Q = -\frac{1}{\alpha_0 \rho_0 c_0^3} \frac{\partial^2}{\partial x \partial t} p_g'^2 \quad (6.2)$$

and a wave equation

$$\left(\frac{\partial}{\partial t} + c_0 \frac{\partial}{\partial x} \right) \left(\frac{\partial}{\partial t} - c_0 \frac{\partial}{\partial x} \right) p_g' = c_0^2 Q \quad ,$$

where we approximate the second factor by $2\partial/\partial t$ and integrate once with respect to t to obtain the nonlinear simple wave equation

$$\frac{\partial p_g'}{\partial t} + c_0 \frac{\partial p_g'}{\partial x} + \frac{1}{\alpha_0 \rho_0 c_0} p_g' \frac{\partial p_g'}{\partial x} = 0 \quad , \quad (6.3)$$

or, in terms of velocity $u = u' = p_g'/\rho_0 c_0$,

$$\frac{\partial u}{\partial t} + c_0 \frac{\partial u}{\partial x} + \frac{1}{\alpha_0} u \frac{\partial u}{\partial x} = 0 \quad . \quad (6.4)$$

This shows the enhancing effect of bubbles in relation to nonlinear distortion in two ways. First, for $\alpha_0 \ll 1$ the nonlinear term is much larger (for given u) than in pure liquid, where the corresponding term would be $[(\Gamma + 1)/2]u\partial u/\partial x$ with $\Gamma \sim 7$. Second, since $c_0 \ll c_\ell$ the distance for significant nonlinear distortion of a wave of given frequency is much smaller in physical units than in the case of pure liquid.

Equation (6.3) includes no dispersive term to offset the nonlinear steepening. Returning to (5.12), we include

$$-\frac{1}{\omega_0^2} \frac{\partial^4 p_g'}{\partial x^2 \partial t^2}$$

as the dominant dispersive term, but we continue to approximate Q as in (6.2). Then further approximating

$$-\frac{1}{\omega_0^2} \frac{\partial^4 p_g'}{\partial x^2 \partial t^2} \quad \text{by} \quad + \frac{c_0}{\omega_0^2} \frac{\partial^4 p_g'}{\partial x^3 \partial t}$$

and integrating out the time-derivative as before, we get

$$\frac{\partial p_g'}{\partial t} + c_0 \frac{\partial p_g'}{\partial x} + \frac{1}{\alpha_0 \rho_0 c_0} p_g' \frac{\partial p_g'}{\partial x} + \frac{c_0^3}{2\omega_0^2} \frac{\partial^3 p_g'}{\partial x^3} = 0 \quad ,$$

or

$$\frac{\partial u}{\partial t} + c_0 \frac{\partial u}{\partial x} + \frac{1}{\alpha_0} u \frac{\partial u}{\partial x} + \frac{c_0^3}{2\omega_0^2} \frac{\partial^3 u}{\partial x^3} = 0 \quad . \quad (6.5)$$

This is the famous *Korteweg-de Vries equation*, first derived in 1895 as a model for long waves of finite amplitude on the free surface of a channel of water, but since obtained in many applications (fluid and solid mechanics, magnetohydrodynamics, plasma physics, ...) – and in fact wherever the basic nonlinearity is quadratic convective ($u \partial u / \partial x$) and where the basic long wave dispersion is cubic, $\omega \sim c_0 k + \beta k^3$ say, as $k \rightarrow 0$.

The KdV equation was the first equation to be completely integrated (in 1967) by a new technique, the *Inverse Spectral* (or Scattering) *Transform*. This technique is amply described in many of the recent texts on soliton mathematics; for a simple introduction see Drazin & Johnson [6]. It reveals the following physically significant facts.

1. If the initial distribution of u (equivalent to p) is everywhere negative (initial rarefaction wave), then $u(x, t)$ develops into an oscillatory wavetrain whose amplitude decays algebraically with t , and in which the phase and group velocities of all components are negative when seen from a frame of reference travelling at speed c_0 in the positive x -direction. The situation is qualitatively and quantitatively similar to that for the linear KdV equation with the same initial condition.
2. If $u(x, 0) \not\prec 0$ everywhere, then in general the negative-propagating decaying oscillatory wavetrain (or “radiation”) will be produced, together with a finite number of “solitons”. These are inherently nonlinear features (not produced if $u(x, 0)$ is too small in some sense), which do not decay or disperse as t increases, and which propagate (relative to the sound speed c_0) with positive velocity, in the opposite direction to the radiation. The solitons each have $u(x, t) > 0$ and are localised pressure pulses of compression, with sech^2 profile and a propagation speed (relative to c_0) proportional to amplitude (and a width inversely proportional to $(\text{amplitude})^{1/2}$). Solitons with different velocities will interact with each other but perfectly regain their shape, size and identity (apart from a possible phase shift) after interaction. They are thus ubiquitous, long-lived features of the KdV field $u(x, t)$. The next figure illustrates this behaviour. In the upper figure (cf. [7]) a series of solitons is produced (from some initial condition like $u(x, 0) = u_0 \exp(-x^2/\ell^2)$ provided u_0 is large enough) and since amplitude and speed of a soliton are proportional, the soliton peaks lie roughly on a straight line. In the lower figure, u_0 is not large enough for solitons to be produced, and instead the left-propagating decaying dispersive wavetrain is seen. The predictions of Inverse Spectral Transform theory for the number and propagation speed of solitons produced by some initial disturbance have been quite well confirmed in experiments (see Kuznetsov et al [7], Noordzij [8]).

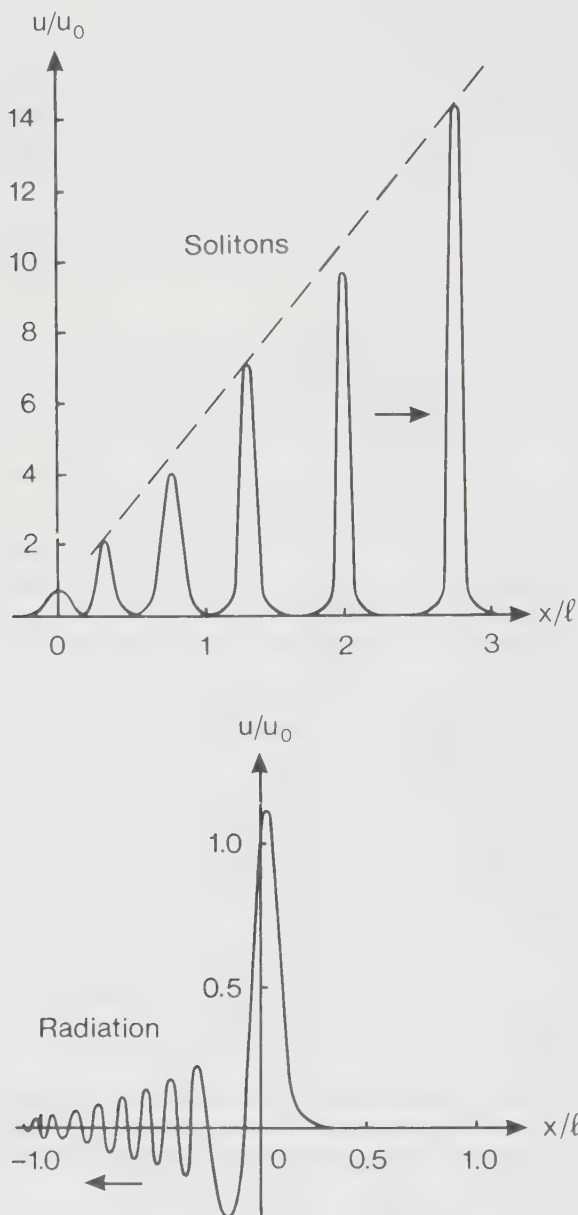


Figure 4

Evolution of the solution of KdV from initial data $u(x, 0) = u_0 \exp(-x^2/\ell^2)$. In the top diagram (u_0 sufficiently large and positive) a definite number of solitons emerges. In the lower diagram (small u_0 or any $u_0 < 0$) only a left-propagating decaying wavetrain ("radiation") is produced. From [7].

7. DISSIPATION AND DISPERSION – THE BKdV EQUATION

Viscous dissipation, acoustic radiation loss and thermal dissipation can also all be approximately included (see van Wijngaarden [1] and other references given there), and the result is a fusion of the Burgers and Korteweg de Vries equations,

$$\frac{\partial u}{\partial t} + c_0 \frac{\partial u}{\partial x} + \frac{1}{\alpha_0} u \frac{\partial u}{\partial x} - \eta \frac{\partial^2 u}{\partial x^2} + \frac{c_0^3}{2\omega_0^2} \frac{\partial^3 u}{\partial x^3} = 0 \quad , \quad (7.1)$$

where η is an effective diffusivity with contributions from all three damping mechanisms. The BKdV equation is not an integrable equation, and only one exact solution has been obtained in closed form. This is a very recent discovery; see [9, 10]. For some special values of the parameters the travelling wave ordinary differential equation for $f, u = f(x - Vt)$, is integrable and an exact explicit solution is obtained in the form

$$u = -2\eta \frac{\partial}{\partial x} \ln F \quad , \quad F = 1 + \exp(\lambda x + \mu t + \nu)$$

for some particular λ, μ and any ν . This describes a monotonic shock wave transition, very similar to that in a non-dispersive medium, for which Burgers equation applies and where the *general* solution is of the form $u = -2\eta \partial/\partial x \ln F$ where F is the general solution of the linear equation

$$\frac{\partial F}{\partial t} + c_0 \frac{\partial F}{\partial x} - \eta \frac{\partial^2 F}{\partial x^2} = 0 \quad .$$

In the absence of general exact solutions, progress on (7.1) needs numerical and asymptotic work. The computations of Kuznetsov et al [7] show (see Figure 5) that for a fixed coefficient of dispersion and small diffusivity, soliton-like features are produced, but without the clear separation of pure solitons (top diagram), whereas when the diffusivity coefficient is increased by a factor 15 (lower diagram) no solitons are seen and the wave propagates essentially as it would in a dispersionless medium.

One definite prediction can be made analytically. Consider a shock transition from $u = 0$ ahead to $u = U$ behind. We have $u = f(X)$, $X = x - Vt$, and

$$V = c_0 + \frac{1}{2\alpha_0} U \quad .$$

$$-Vf + c_0 f + \frac{1}{2\alpha_0} f^2 - \eta f' + \beta f'' = 0$$

$$\text{where } ' \equiv d/dX \text{ and } \beta = c_0^3/2\omega_0^2 > 0 \quad .$$

Linearising about the front of the wave, where f is small, we get $f(X) \sim \exp(\lambda X)$,

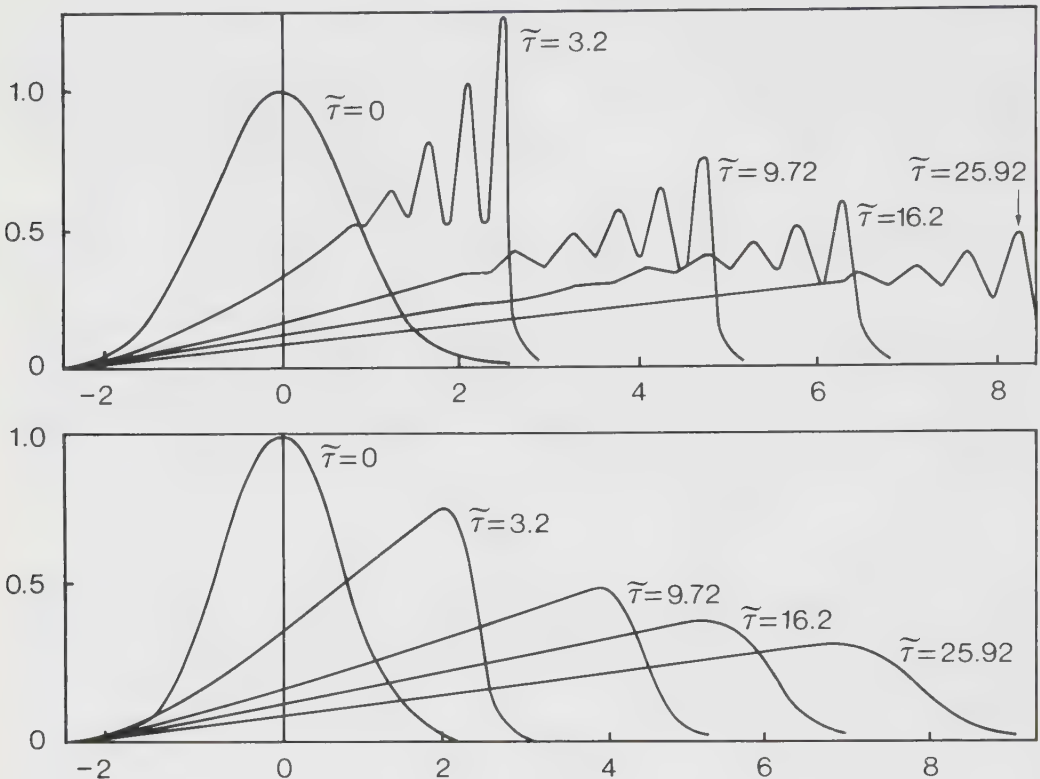


Figure 5

Evolution of solutions of BKdV, same initial data as in Figure 4. Each curve is labelled by a dimensionless time $\tilde{\tau}$. The diffusivity coefficient for the lower diagram exceeds that for the upper diagram by a factor 15. For details see [7].

$$\lambda = \frac{\eta \pm \sqrt{\eta^2 + 2U\beta/\alpha_0}}{2\beta} ,$$

where the acceptable root has the negative square root and implies that the approach to $u = 0$ is monotonic. Linearising, with $f = U + g$, about the back of the shock, we find

$$g(X) \sim \exp(\lambda X) , \quad \lambda = \frac{\eta \pm \sqrt{\eta^2 - 2U\beta/\alpha_0}}{2\beta} ,$$

and the transition on the high-pressure side of the shock is *oscillatory* if $\beta > \eta^2\alpha_0/2U$. Oscillatory shock waves in gas bubble/water mixtures have been observed experimentally; see Figure 6, with data taken from experiments conducted by Kuznetsov et al [7].

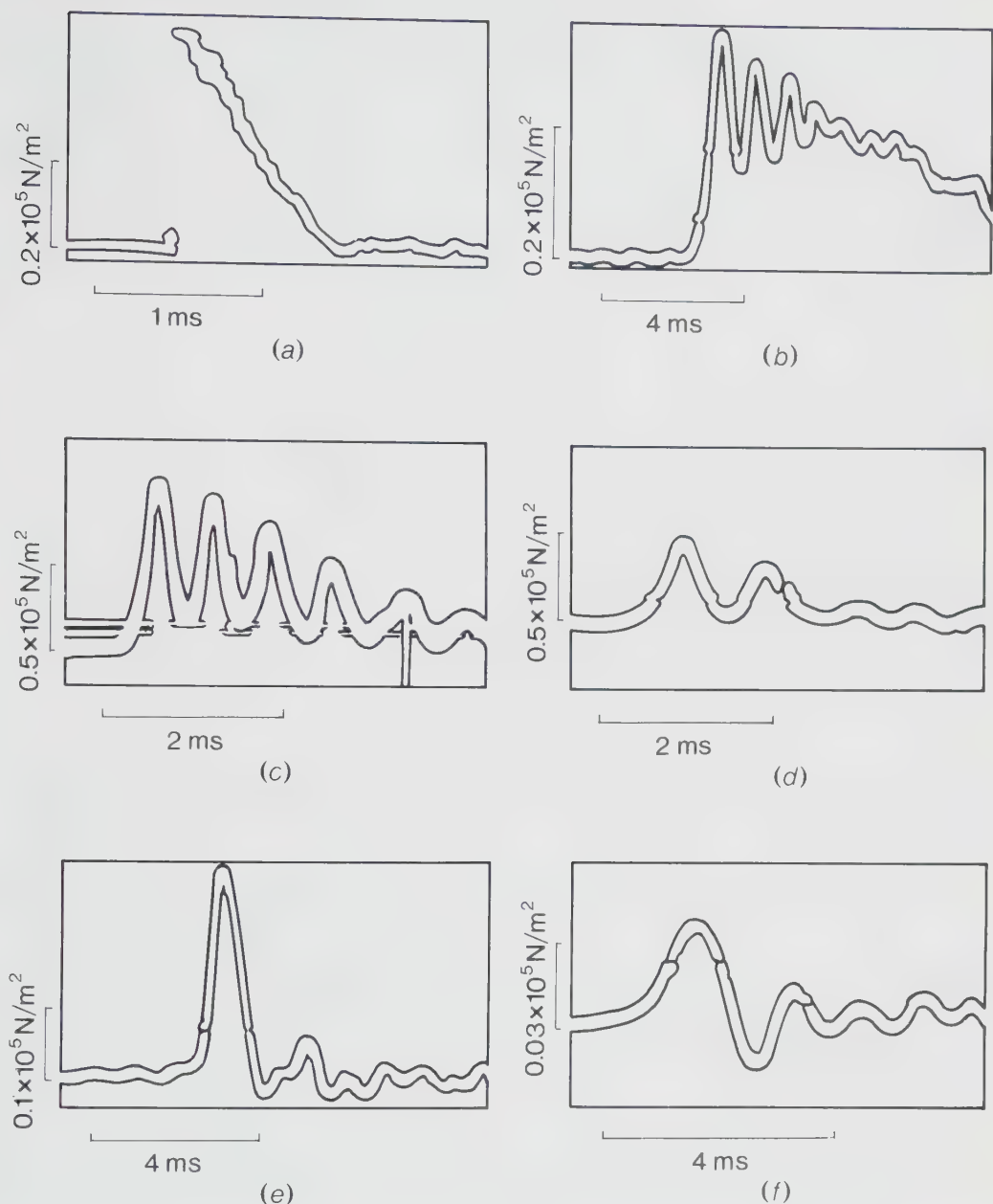


Figure 6

Experimental observations (see [7]) of oscillatory shock and soliton features in propagation of pressure pulses in liquid with CO_2 bubbles.

8. HIGH FREQUENCY WAVES – THE NLKG EQUATION

Take the limit $E = \frac{1}{\omega_0} \frac{\partial}{\partial t} \gg 1$ in (5.12) and keep the dominant linear dispersive term,

$$\frac{1}{c_\infty^2} \frac{\partial^2 p_g'}{\partial t^2} + \frac{\omega_0^2}{c_0^2} p_g' - \frac{\partial^2 p_g'}{\partial x^2} = E^{-2} Q . \quad (8.1)$$

To simplify Q , we have in the high frequency limit,

$$\begin{aligned} p_g' &= 0 , \quad p' = \rho_0 c_\infty u' = \rho_0 c_\infty^2 n' / n_0 \\ &= c_\infty^2 \rho' = \rho_0 c_\infty^2 \alpha' / \alpha_0 , \end{aligned}$$

giving (in terms first of p')

$$Q = (1 - \alpha_0) \frac{\partial^2}{\partial t^2} \left[\frac{p'^2}{\rho_0 c_\infty^4} \frac{(\Gamma + 1 - 2\alpha_0)}{(1 - \alpha_0)^2} \right] .$$

Now take $\partial^2 / \partial t^2$ of (8.1), use $p' \simeq \frac{1}{\omega_0^2} \frac{\partial^2 p_g'}{\partial t^2}$ and use the above form for Q , and we get

$$\begin{aligned} &\frac{1}{c_\infty^2} \frac{\partial^2 p'}{\partial t^2} - \frac{\partial^2 p'}{\partial x^2} + \frac{\omega_0^2}{c_0^2} p' \\ &= \frac{(\Gamma + 1 - 2\alpha_0)}{2(1 - \alpha_0)} \frac{1}{\rho_0 c_\infty^4} \frac{\partial^2}{\partial t^2} (p'^2) \end{aligned}$$

and then, making the usual reduction for propagation purely in the x -direction, we get, for u ,

$$\frac{\partial}{\partial x} \left[\frac{\partial u}{\partial t} + c_\infty \frac{\partial u}{\partial x} + \frac{(\Gamma + 1 - 2\alpha_0)}{2(1 - \alpha_0)} u \frac{\partial u}{\partial x} \right] - \frac{\omega_0^2 c_\infty}{2c_0^2} u = 0 . \quad (8.2)$$

Equation (8.2) will be called the Nonlinear Klein-Gordon equation (NLKG). Little is known about this equation; it appears not to be integrable.

Analytical, perturbation and numerical studies of NLKG have been done by Leonard [11] and Hunter & Tan [12]. Several significant features are identified by both authors.

1. There are periodic travelling waves of any positive velocity (relative to c_∞); there are no bounded travelling waves with positive velocity (relative to c_∞) that are not periodic; and there are no bounded travelling waves with negative velocity (relative to c_∞).
2. For each positive velocity of travelling waves (relative to c_∞) there is a continuous family of periodic travelling waves, each having a different period or wavelength and a different amplitude determined by the wavelength. There is no bounded solution if the amplitude exceeds a critical value. The limiting wave

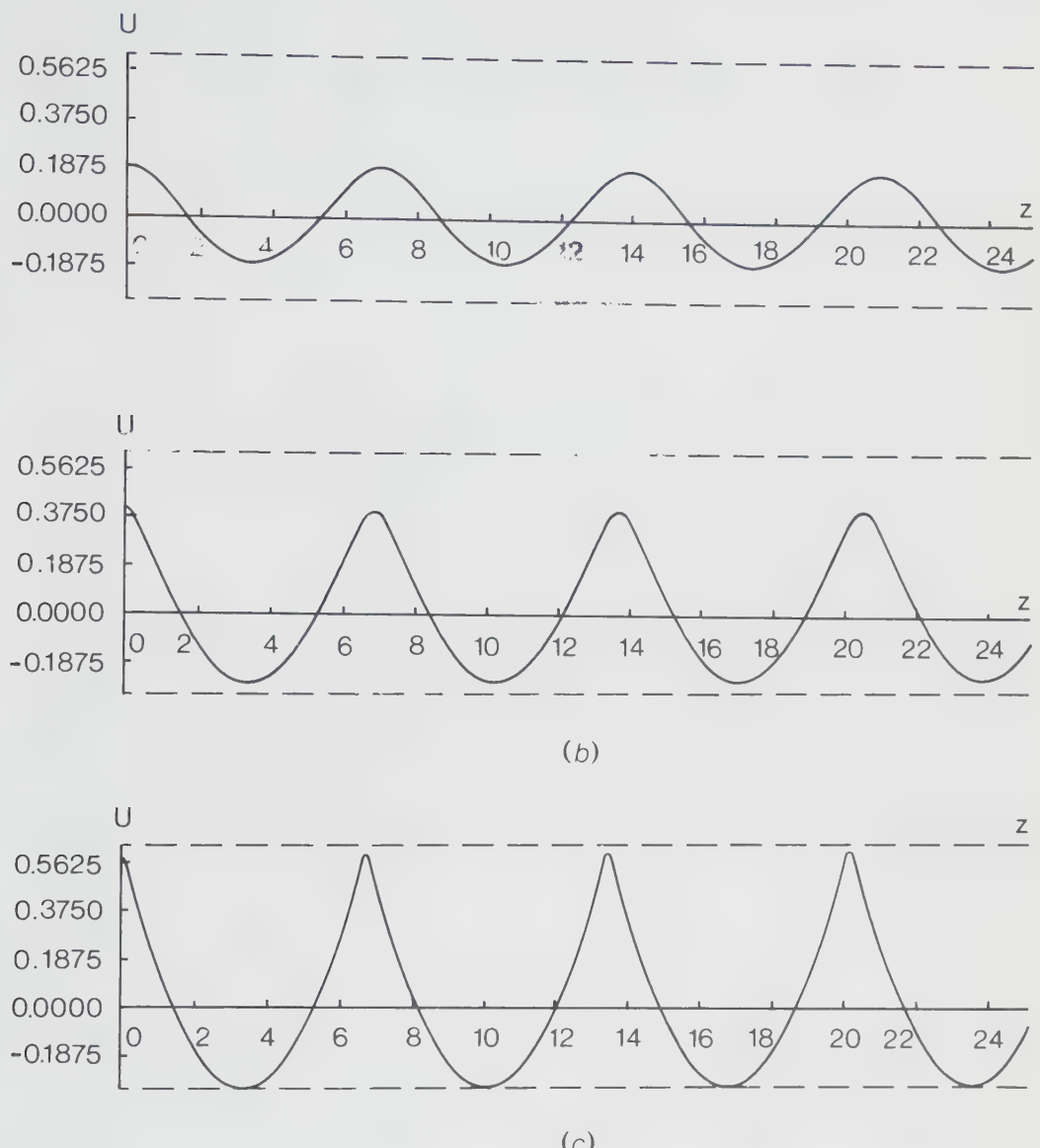


Figure 7

Travelling wave profiles for the NLKG equation, computed by Leonard [11].

has mean level $u = 0$, crests in $u = a$, troughs in $u = -a/2$, wave speed a and wavelength $6a^{1/2}$, in units and coordinates for which (8.2) takes the form

$$\frac{\partial}{\partial x} \left[\frac{\partial u}{\partial t} + u \frac{\partial u}{\partial x} \right] - u = 0 \quad . \quad (8.3)$$

The limiting wave has a corner at its crests, and there

$$\frac{\partial u}{\partial x} = \pm \sqrt{\frac{a(a+2)}{2}} \quad .$$

All this follows from straightforward phase-plane analysis of (8.3) for $u = f(z)$, $z = x - at$ (see the studies by Leonard [11] and Hunter & Tan [12]). The diagrams below in Figure 7 (from Leonard) give travelling wave profiles for three different amplitudes, the lowest corresponding to near-linear behaviour, the highest to almost the limiting corner-wave condition.

Numerical integration of (8.3) by Leonard, and by Hunter & Tan, for periodic initial conditions, shows that in general shocks will be formed. In contrast to KdV, the dispersion associated with NLKG becomes weaker as the wave steepens and generates higher Fourier components, and in general cannot prevent shock formation. However, as time increases, the shocks decay, and the wave approaches one of the limiting continuous travelling waves. Once the shocks have disappeared, no further decay of the wave occurs. See Figure 8 below (from Hunter & Tan [12]). An interesting (unsolved) problem is that of relating the amplitude and speed of the final limiting wave to those of the original wave.

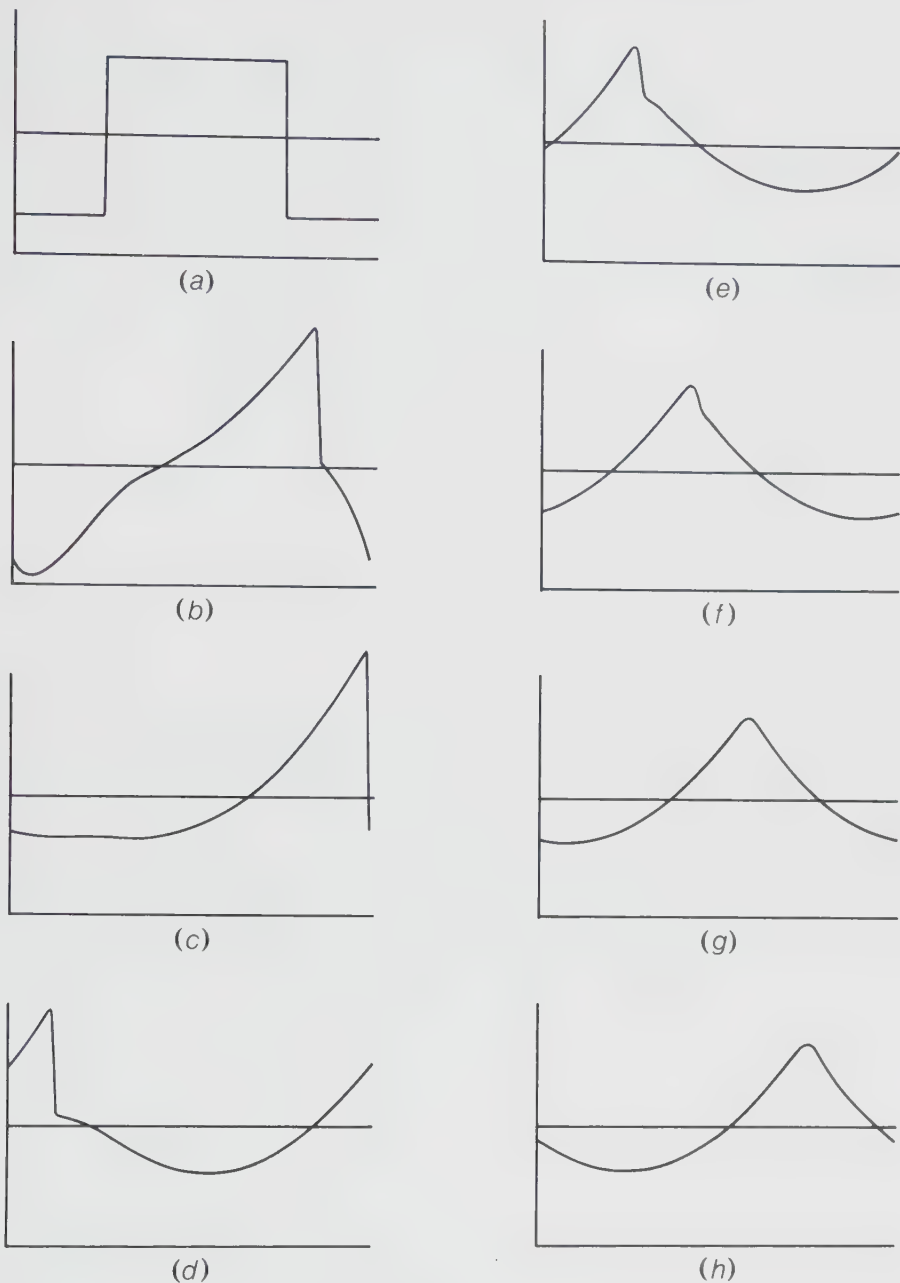


Figure 8

Typical features in the evolution of a solution to NLKG with periodic initial conditions (from Hunter & Tan [12]).

REFERENCES

1. van Wijngaarden, L. 1972 "One-dimensional flow of liquids containing small gas bubbles", *Ann. Rev. Fluid Mech.* **4**, 369-396.
2. Campbell, I.J. & Pitcher, A.S. 1954 Symposium at Admiralty Research Laboratory, Middlesex.
3. Lauterborn, W. 1976 "Numerical investigation of nonlinear oscillations of gas bubbles in liquids", *J. Acoust. Soc. Am.* **59**, 283-293.
4. Lauterborn, W. 1986 "Acoustic turbulence". In "Frontiers in Physical Acoustics", ed. D. Sette, 124-144, North-Holland, Amsterdam.
5. Fox, F.E., Curley, S.R. & Larson, G.S. 1955 "Phase velocity and absorption measurements in water containing air bubbles", *J. Acoust. Soc. Am.* **27**, 534-539.
6. Drazin, P.G. & Johnson, R.S. 1989 "Solitons: an introduction", Cambridge University Press.
7. Kuznetsov, V.V., Nakoryakov, V.E., Pokusaev, B.G. & Schreiber, I.R. 1978 "Propagation of perturbations in a gas-liquid mixture", *J. Fluid Mech.* **85**, 85-96.
8. Noordzij, L. 1971 "Shock waves in bubble/liquid mixtures". In Proc. IUTAM Symposium on "Non-steady Flow of Water at High Speeds", eds. L.I. Sedov & Yu.G. Stepanov, 369-383.
9. Jeffrey, A. & Xu, S. 1989 "Exact solutions to the Korteweg-de Vries-Burgers equation", *Wave Motion* **11**, 55-564.
10. McIntosh, L. 1990 "Single-phase averaging and travelling wave solutions of the modified Burgers-Korteweg-de Vries equation", *Phys. Lett. A* **143**, 57-61.
11. Leonard, S.R. 1988 "The propagation of nonlinear waves in a bubbly liquid", Ph.D. thesis, University of Leeds.
12. Hunter, J.K. & Tan, K.P. 1988 Private communication.

NONLINEAR WAVES IN AEROSOLS AND DUSTY GASES

D. G. Crighton

University of Cambridge, Cambridge, UK

ABSTRACT

A two-phase medium composed of air and fine dust or aerosol particles is a relaxing medium, with two relaxing degrees of freedom, corresponding to exchange of momentum and heat between the phases. Model equations for the propagation of weakly nonlinear waves in such a medium are derived, with allowance for finite rates of relaxation. Characteristic features are discussed, in particular the possibility that shock formation may be altogether prevented in some circumstances, and the possibility that shocks that do form may be either fully or partly dispersed.

1. BASIC MODEL

Here the model we discuss is that of a two-phase system, with an ordinary fluid phase (usually gas), and a solid phase of fine rigid particles [1,2]. The particles have negligible volume concentration, but significant mass loading. Heat and momentum transfer occurs between the phases, but no mass transfer. Such a system is a simple *relaxing medium*, with two relaxing “degrees of freedom”, with relaxation processes (adjustment of the particle phase velocity and temperature to those of the surrounding gas phase) which can be easily understood. It serves as a useful model for phenomena which occur in a polyatomic (but essentially single phase) gas, where one or more of the molecular degrees of freedom is not always in equilibrium, but relaxes under acoustic perturbation just as the velocity and temperature of the solid phase do in the dusty gas model. A common example of relaxation processes at the molecular level arises in the relaxation of the vibrational degree of freedom of the diatomic (dumbbell) nitrogen molecule.

We introduce the gas velocity u' , gas density ρ' , particle phase velocity v' , particle number density n' , position x' , time t' , gas pressure p' , gas temperature T' , particle phase temperature θ' . Assume the gas is perfect, $p' = R\rho'T'$, and is itself a non-relaxing thermoviscous gas of viscosity μ and thermal conductivity κ . The usual constant volume and constant pressure specific heats are c_p , c_v ; $\gamma = c_p/c_v$, $R = c_p - c_v$. The heat capacity of unit mass of the aerosol phase is c . The aerosol or dust consists of identical rigid particles of mass m . No thermal motion is associated with the particles, no mutual interaction, and there is no “partial pressure” in the particle phase. Only one-dimensional problems will be considered here.

2. BASIC EQUATIONS OF MOTION

Mass conservation in the gas phase requires

$$\frac{\partial \rho'}{\partial t'} + u' \frac{\partial \rho'}{\partial x'} + \rho' \frac{\partial u'}{\partial x'} = 0 \quad , \quad (2.1)$$

and momentum conservation for the gas phase requires

$$\rho' \frac{\partial u'}{\partial t'} + \rho' u' \frac{\partial u'}{\partial x'} + \frac{\partial p'}{\partial x'} = \frac{4}{3} \mu \frac{\partial^2 u'}{\partial x'^2} + n' F' \quad . \quad (2.2)$$

Here F' is the force on the gas exerted by a single particle. For spherical particles of radius R_0 , under a low Reynolds number assumption,

$$F' = 6\pi\mu R_0(v' - u') \quad . \quad (2.3)$$

Other forms for F' may be appropriate, depending on the parameters involved. The energy equation for the gas is

$$\begin{aligned} \rho' c_v \left(\frac{\partial T'}{\partial t'} + u' \frac{\partial T'}{\partial x'} \right) - \kappa \frac{\partial^2 T'}{\partial x'^2} = \\ \frac{4}{3} \mu \left(\frac{\partial u'}{\partial x'} \right)^2 - p' \frac{\partial u'}{\partial x'} + n' Q' + n' F' (v' - u') . \end{aligned} \quad (2.4)$$

Here, in addition to the usual production terms for the clean gas, there are terms giving the heat transfer $n' Q'$ to the gas, per unit time, from the n' particles in unit volume, and the rate of heat production from the working of the forces exerted by these particles.

Mass conservation in the aerosol phase is expressed by

$$\frac{\partial n'}{\partial t'} + v' \frac{\partial n'}{\partial x'} + n' \frac{\partial v'}{\partial x'} = 0 , \quad (2.5)$$

Momentum conservation in the aerosol phase by

$$m \left(\frac{\partial v'}{\partial t'} + v' \frac{\partial v'}{\partial x'} \right) = -F' , \quad (2.6)$$

and the heat transfer (energy) equation for the particle phase is

$$mc \left(\frac{\partial \theta'}{\partial t'} + v' \frac{\partial \theta'}{\partial x'} \right) = -Q' . \quad (2.7)$$

A possible assumption for Q' is given by Newton's law of cooling, with Nusselt number 2,

$$Q' = 4\pi\kappa R_0(\theta' - T') , \quad (2.8)$$

though as with the momentum transfer, other mechanisms and models may be appropriate in some parameter ranges.

Suppose now that boundary or initial data provide a time scale ω^{-1} say. A velocity scale is $c_0 = (\gamma RT_0)^{1/2}$, the clean gas sound speed, and length scale is c_0/ω , and other scales are provided by the ambient (uniform) state variables p_0 , ρ_0 , T_0 , n_0 . Thus we define

$$\begin{aligned} x = \frac{\omega x'}{c_0} , \quad t = \omega t' , \quad u = \frac{u'}{c_0} , \quad v = \frac{v'}{c_0} , \\ n = \frac{n'}{n_0} , \quad \rho = \frac{\rho'}{\rho_0} , \quad p = \frac{p'}{p_0} , \quad T = \frac{T'}{T_0} , \quad \theta = \frac{\theta'}{T_0} . \end{aligned}$$

Then, with the specific assumed forms (2.3) for F' and (2.8) for Q' , the six governing equations become

$$\frac{\partial \rho}{\partial t} + u \frac{\partial \rho}{\partial x} + \rho \frac{\partial u}{\partial x} = 0 , \quad (2.9)$$

$$\rho \frac{\partial u}{\partial t} + \rho u \frac{\partial u}{\partial x} + \frac{1}{\gamma} \frac{\partial}{\partial x} \rho T = \delta_M \frac{\partial^2 u}{\partial x'^2} + \alpha M n(v - u) , \quad (2.10)$$

$$\rho \frac{\partial T}{\partial t} + \rho u \frac{\partial T}{\partial x} - \delta_T \frac{\partial^2 T}{\partial x^2} = \delta \gamma (\gamma - 1) \left(\frac{\partial u}{\partial x} \right)^2 - (\gamma - 1) \rho T \frac{\partial u}{\partial x} + M H \beta n (\theta - T) + M \alpha n \gamma (\gamma - 1) (v - u)^2 . \quad (2.11)$$

$$\frac{\partial n}{\partial t} + v \frac{\partial n}{\partial x} + n \frac{\partial v}{\partial x} = 0 , \quad (2.12)$$

$$\frac{\partial v}{\partial t} + v \frac{\partial v}{\partial x} + \alpha (v - u) = 0 , \quad (2.13)$$

$$\frac{\partial \theta}{\partial t} + v \frac{\partial \theta}{\partial x} + \beta (\theta - T) = 0 . \quad (2.14)$$

These are six equations for ρ, u, T, n, v, θ ; the gas pressure follows then from $p = \rho T$.

Dimensionless parameters appearing in these equations are

$$\delta_M = \frac{4 \nu \omega}{3 c_0^2} = \text{dimensionless diffusivity of momentum of gas},$$

$$\delta_T = \frac{\kappa \omega}{\rho_0 c_v c_0^2} = \text{dimensionless diffusivity of heat of gas},$$

$\alpha = (\omega \tau_M)^{-1}$; $\tau_M = m/(6\pi\mu R_0)$ is the velocity relaxation time for the particles.

$\beta = (\omega \tau_T)^{-1}$; $\tau_T = mc/(4\pi\kappa R_0)$ is the thermal relaxation time for the particles.

$M = mn_0/\rho_0$ = mass loading in equilibrium,

$H = c/c_v$ = ratio of specific heats of solid and gas phases.

3. REDUCTION TO A SINGLE EQUATION

Write $\rho = 1 + \rho^*$, $u = 0 + u^*$, $v = 0 + v^*$, $T = 1 + T^*$, $\theta = 1 + \theta^*$. $n = 1 + n^*$ and retain quadratically nonlinear terms in (*). Also regard δ_M, δ_T and M as $O(*)$, but $\alpha, \beta, \gamma, \kappa$ will be taken fixed, $O(1)$. This is the weakly-nonlinear, weakly-diffusive, “weakly-dusty” gas limit. There is, however, no frequency restriction, i.e. we are dealing with a *finite rate* model (cf. [2]).

Dropping the (*), the equations are

$$\frac{\partial \rho}{\partial t} + \frac{\partial u}{\partial x} = W_1 , \quad (3.1)$$

$$\frac{\partial u}{\partial t} + \frac{1}{\gamma} \frac{\partial}{\partial x} (p + T) = W_2 , \quad (3.2)$$

$$\frac{\partial T}{\partial t} + (\gamma - 1) \frac{\partial u}{\partial x} = W_3 , \quad (3.3)$$

$$\frac{\partial n}{\partial t} + \frac{\partial v}{\partial x} = W_4 , \quad (3.4)$$

$$\frac{\partial v}{\partial t} + \alpha (v - u) = W_5 , \quad (3.5)$$

$$\frac{\partial \theta}{\partial t} + \beta (\theta - T) = W_6 , \quad (3.6)$$

with

$$\begin{aligned}
 W_1 &= -\frac{\partial}{\partial x}(\rho u) \quad , \\
 W_2 &= -\rho \frac{\partial u}{\partial t} - u \frac{\partial u}{\partial x} - \frac{1}{\gamma} \frac{\partial}{\partial x}(\rho T) + \delta_M \frac{\partial^2 u}{\partial x^2} + \alpha M(v - u) \quad , \\
 W_3 &= -\rho \frac{\partial T}{\partial t} - u \frac{\partial T}{\partial x} + \delta_T \frac{\partial^2 T}{\partial x^2} - (\gamma - 1)(\rho + T) \frac{\partial u}{\partial x} \\
 &\quad + M H \beta(\theta - T) \quad , \\
 W_4 &= -\frac{\partial}{\partial x}(n v) \quad , \\
 W_5 &= -v \frac{\partial v}{\partial x} \quad , \\
 W_6 &= -v \frac{\partial \theta}{\partial x} \quad .
 \end{aligned}$$

Eliminating ρ and T we get

$$\frac{\partial^2 u}{\partial t^2} - \frac{\partial^2 u}{\partial x^2} = \frac{\partial W_2}{\partial t} - \frac{1}{\gamma} \frac{\partial}{\partial x}(W_1 + W_3) \quad .$$

On the right we now approximate, using the relations $u = \rho = T/(\gamma - 1)$, $\partial/\partial t + \partial/\partial x = 0$, which are appropriate to a linear plane wave, propagating to the right in clean non-diffusive gas. This gives

$$\begin{aligned}
 \frac{\partial^2 u}{\partial t^2} - \frac{\partial^2 u}{\partial x^2} &= -\frac{\partial^2}{\partial t \partial x} u^2 + \delta_M \frac{\partial^3 u}{\partial x^2 \partial t} \\
 -M \frac{\partial^2 v}{\partial t^2} - \frac{\gamma - 1}{\gamma} \delta_T \frac{\partial^3 u}{\partial x^3} &+ (\gamma - 1) \frac{\partial}{\partial x}(u \frac{\partial u}{\partial x}) + \frac{MH}{\gamma} \frac{\partial^2 \theta}{\partial x \partial t} \quad .
 \end{aligned}$$

We replace the operator on the left in the same approximation by

$$2 \frac{\partial}{\partial t} \left(\frac{\partial}{\partial t} + \frac{\partial}{\partial x} \right)$$

and integrate with respect to t to get

$$\frac{\partial u}{\partial t} + \frac{\partial u}{\partial x} + \frac{\gamma + 1}{2} u \frac{\partial u}{\partial x} = \frac{1}{2} \Delta \frac{\partial^2 u}{\partial x^2} - M \frac{\partial v}{\partial t} + \frac{MH}{2\gamma} \frac{\partial \theta}{\partial x} \quad .$$

Now operate on this equation with

$$\left(\frac{\partial}{\partial t} + \alpha \right) \left(\frac{\partial}{\partial t} + \beta \right)$$

and use the linear versions of (3.5), (3.6), to get

$$\begin{aligned} & \left(\frac{\partial}{\partial t} + \alpha \right) \left(\frac{\partial}{\partial t} + \beta \right) \left[\frac{\partial u}{\partial t} + \frac{\partial u}{\partial x} + \frac{\gamma+1}{2} u \frac{\partial u}{\partial x} - \frac{1}{2} \Delta \frac{\partial^2 u}{\partial x^2} \right] \\ &= \frac{M}{2} \left\{ \alpha \left(\frac{\partial}{\partial t} + \beta \right) + \beta H \left(\frac{\gamma-1}{\gamma} \right) \left(\frac{\partial}{\partial t} + \alpha \right) \right\} \frac{\partial u}{\partial x} . \end{aligned} \quad (3.7)$$

Again, on the right of (3.7), or in $u \partial u / \partial x$ and $\partial^2 u / \partial x^2$, the replacement of $\partial / \partial x$ by $-\partial / \partial t$ may be made, as convenient. The “total” diffusivity appearing in (3.7) is what (in physical units) Lighthill [3] called the “*diffusivity of sound*”, and is given by

$$\Delta = \delta_M + \frac{\gamma-1}{\gamma} \delta_T .$$

If $\alpha = \beta = 0$ (i.e. $\omega \tau_M, \omega \tau_T \rightarrow \infty$), or if $M = 0$, we have

$$\frac{\partial u}{\partial t} + \frac{\partial u}{\partial x} + \frac{\gamma+1}{2} u \frac{\partial u}{\partial x} - \frac{1}{2} \Delta \frac{\partial^2 u}{\partial x^2} = 0 ,$$

which is just *Burgers equation* for one-dimensional nonlinear wave propagation in a thermoviscous gas. The sound speed in physical units is c_0 , the clean gas speed, and in this infinite frequency limit the aerosol or dust particles play no role; they are “*frozen*”, and the frozen sound speed is

$$a_\infty = c_0 . \quad (3.8)$$

In the low frequency limit $\partial / \partial t \rightarrow 0$ (or $\alpha, \beta \rightarrow \infty$) we have, on the other hand,

$$\begin{aligned} & \frac{\partial u}{\partial t} + \frac{\partial u}{\partial x} + \frac{\gamma+1}{2} u \frac{\partial u}{\partial x} - \frac{1}{2} \Delta \frac{\partial^2 u}{\partial x^2} \\ &= \frac{M}{2} \left(1 + \frac{\gamma-1}{\gamma} H \right) \frac{\partial u}{\partial x} . \end{aligned}$$

This indicates that the non-dimensional sound speed for linear waves at frequencies ω much smaller than either of the “*relaxation frequencies*” τ_M^{-1}, τ_T^{-1} , is

$$1 - \frac{M}{2} \left(1 + \frac{\gamma-1}{\gamma} H \right)$$

and thus in physical units the low-frequency or “*equilibrium*” sound speed is

$$a_0 = a_\infty \left\{ 1 - \frac{M}{2} \left(1 + \frac{\gamma-1}{\gamma} H \right) \right\} . \quad (3.9)$$

(This is easy to understand if the heat transfer effect is omitted; then $a_0 = c_0 (1 - \frac{M}{2})$ which, for $M \ll 1$, is just a statement that $a_0^2 = dp/dp$ with $\rho = \rho_0 (1 + M)$. The effect of the particulate phase at low frequencies is simply to increase the density by a factor $(1 + M)$, with no other effect.)

If a further term is kept in the low frequency limit (by operating on (3.7) with $(\partial/\partial t - \alpha)(\partial/\partial t - \beta)$) we get

$$\begin{aligned} \frac{\partial u}{\partial t} + \left\{ 1 - \frac{M}{2} \left(1 + \frac{\gamma-1}{\gamma} H \right) \right\} \frac{\partial u}{\partial x} + \frac{\gamma+1}{2} u \frac{\partial u}{\partial x} \\ = \left\{ \frac{\Delta}{2} + \frac{M}{2} \left(\frac{1}{\alpha} + H \frac{\gamma-1}{\gamma} \frac{1}{\beta} \right) \right\} \frac{\partial^2 u}{\partial x^2} , \end{aligned} \quad (3.10)$$

which is again Burgers equation, but now with an additional “bulk diffusivity” represented by the coefficient $\left(\frac{M}{2}\right)\left(\frac{1}{\alpha} + H \frac{\gamma-1}{\gamma} \frac{1}{\beta}\right)$. This may be very much larger than the molecular diffusivity, and then it will lead to increased shock wave thicknesses, as compared with those in a clean gas.

The full equation (3.7), with two relaxation operators for momentum and heat, has not been studied, beyond the results above. In the case $\alpha = \beta$ ($\tau_M = \tau_T = \tau$), one of the operators can be integrated out, and then, in physical variables, we get

$$\begin{aligned} (1 + \tau \frac{\partial}{\partial t}) \left\{ \frac{\partial u}{\partial t} + (a_\infty + \frac{\gamma+1}{2} u) \frac{\partial u}{\partial x} - \frac{1}{2} \delta \frac{\partial^2 u}{\partial x^2} \right\} \\ = (a_\infty - a_0) \frac{\partial u}{\partial x} . \end{aligned} \quad (3.11)$$

Here a_∞ and a_0 are the frozen and equilibrium sound speeds, defined in (3.8) and (3.9), and

$$\delta = \frac{4}{3} \frac{\nu}{c_0} + \frac{\kappa}{\rho_0 c_0 c_v}$$

is the dimensional (molecular) diffusivity of sound. Equation (3.11) is a standard form of *relaxing gas equation*, derived originally (Polyakova, Soluyan & Khokhlov [4], Blythe [5], Ockendon & Spence [6]) for a clean gas with one degree of freedom which can relax on a finite time scale to thermodynamic non-equilibrium. (In a simple model, air is such a gas, and the relaxing degree of freedom is associated with the vibrational modes of nitrogen or with the formation and relaxation of diatomic oxygen, O_2 ; see the extensive review by Johannessen & Hodgson [7].) The dusty gas or aerosol is an example where the relaxation takes place on the macroscopic scale, and arises from the inertia of the particulate phase and its finite (non-zero) heat capacity.

4. SHOCK FORMATION IN A DUSTY GAS

An interesting (incompletely solved) problem is that of shock formation in a dusty gas, or relaxing medium. Consider the much-studied sinusoidal wave problem

of nonlinear acoustics, in which, in physical units,

$$u = \epsilon c_0 \sin \omega x / c_0 \quad \text{at } t = 0 .$$

For the clean gas, and in the absence of thermoviscous diffusion, shock formation takes place at time takes place at time

$$t_* = \left(\frac{2}{\gamma + 1} \right) \frac{c_0}{\omega} \frac{1}{\epsilon} .$$

What, for the same initial condition, is the shock-formation time for the aerosol or dusty gas?

One can see that, for $\omega\tau \ll 1$ there is no finite t_* at which a triple-valued wave would form in the absence of molecular diffusivity. For then, by the steps that led to (3.10), equation (3.11) can be reduced to the Burgers equation

$$\frac{\partial u}{\partial t} + \left(a_0 + \frac{\gamma + 1}{2} u \right) \frac{\partial u}{\partial x} - a_\infty \tau (a_\infty - a_0) \frac{\partial^2 u}{\partial x^2} = 0 ,$$

in which the relaxation process acts as a bulk viscosity and ensures that solutions remain single-valued for all time. On the other hand, for $\omega\tau \rightarrow \infty$ (and again for $\delta = 0$) (3.11) is equivalent to

$$\begin{aligned} & \tau \frac{\partial}{\partial t} \left\{ \frac{\partial u}{\partial t} + \left(a_\infty + \frac{\gamma + 1}{2} u \right) \frac{\partial u}{\partial x} \right\} \\ &= (a_\infty - a_0) \frac{\partial u}{\partial x} \simeq - \left(\frac{a_\infty - a_0}{a_\infty} \right) \frac{\partial u}{\partial t} , \end{aligned}$$

i.e. to an equation sometimes called the *Varley-Rogers* equation,

$$\frac{\partial u}{\partial t} + \left(a_\infty + \frac{\gamma + 1}{2} u \right) \frac{\partial u}{\partial x} + \left(\frac{a_\infty - a_0}{a_\infty \tau} \right) u = 0 . \quad (4.1)$$

Since $a_\infty > a_0$, this is formally the same as the weakly nonlinear wave equation for propagation down an exponential horn whose cross-section increases exponentially with propagation distance. There is thus the possibility that if the “flare constant” $(a_\infty - a_0)/a_\infty$ is large enough, nonlinear steepening may be reduced so that a shock cannot be formed in finite time. This is seen from the characteristic solution to (4.1),

$$u(x, t) = u_0(\phi) \exp(-\lambda t) ,$$

$$x - a_\infty t = \phi + \frac{\gamma + 1}{2} u_0(\phi) \left(\frac{1 - e^{-\lambda t}}{\lambda} \right)$$

where the initial function is $u_0(\phi) = \epsilon c_0 \sin \omega \phi / c_0$, and $\lambda = (a_\infty - a_0)/a_\infty \tau$. The mapping from x to ϕ is initially one-valued, and will remain one-valued for $0 \leq t < \infty$ provided

$$1 + \frac{\gamma + 1}{2} \frac{1}{\lambda} u'_0(\phi) > 0$$

i.e. provided

$$\frac{\epsilon \omega}{\lambda} \frac{\gamma + 1}{2} < 1 .$$

In terms of the mass loading M , initial Mach number ϵ and dimensionless frequency $\omega \tau$, this is

$$\frac{M}{\epsilon} > \frac{\gamma + 1}{(1 + \frac{\gamma-1}{\gamma} H)} \omega \tau . \quad (4.2)$$

This indicates the powerful role which the aerosol relaxation may have on nonlinear steepening, although strictly condition (4.2) cannot be achieved in our model, which assumes small comparable values of M and ϵ , and, here, a large value of $\omega \tau$.

For other conditions, no criterion analogous to (4.2) has been found, and in general any criterion like (4.2) will involve the three parameters M, ϵ and $\omega \tau$ independently (only in the limit $\omega \tau \rightarrow \infty$ does the problem involve M, ϵ in the ratio M/ϵ only). Davidson & Scott [1] try (effectively) to solve (3.11) by a perturbation series in amplitude,

$$u = \epsilon c_0 \left\{ u^{(1)} + \epsilon u^{(2)} + \dots \right\}$$

and then use criteria like

$$|\epsilon u^{(2)}/u^{(1)}|_{\max} = 1/2 \quad \text{or} \quad 1/10$$

to indicate whether nonlinear steepening may have led to shock formation or not. This procedure leads to a bifurcation curve in a two-dimensional $(\omega \tau, M/\epsilon)$ space, with a U -shaped form (see Davidson & Scott [1], Figure 11). Our condition (4.2) gives good agreement with the right-hand branch of the U -curve, for high frequencies. The left hand branch cannot be correct at low $\omega \tau$, because we know that shocks can never be formed, for any M, ϵ , as $\omega \tau \rightarrow 0$. Analytical prediction of the "bifurcation surface" in $(M, \epsilon, \omega \tau)$ space, on one side of which shocks form in finite time and on the other side of which shocks never form, remains a formidable problem (and, of course, a different nonlinear problem for every different initial condition). Recently we have made some analytical progress by functional analysis methods (Hammerton & Crighton [8]) but the sufficient conditions obtained there, under which a shock will definitely form in finite time, seem to be very conservative compared with those under which shocks are observed in computation to form. Computation is itself far from straightforward for this problem, because finite-difference and spectral methods have inherent numerical viscosity that always prevents infinite gradients from occurring even when they certainly would in the absence of genuine fluid viscosity. To get round this problem we have devised a computational procedure (Hammerton & Crighton [9]) based on the use of intrinsic coordinates to describe the wave profile at any

instant. Checks with known exact solutions (e.g. that of (4.1)) indicate that the method can be reliably used to diagnose shock formation in the absence of genuine fluid viscosity. The method is used, together with asymptotic and exact results, in Hammerton & Crighton [8] to take the discussion of shock formation in relaxing gases much further than can be done here.

5. FULLY AND PARTLY DISPERSED SHOCK WAVES

The relaxing gas equation (in the form (3.11), for example) has a travelling wave solution of fixed form, $u = f(\xi)$, $\xi = x - Vt$, which describes a transition from one uniform state ahead of the wave to another uniform state behind, as ξ decreases from $+\infty$ to $-\infty$. Such a transition, in the present weakly nonlinear model, is a weak relaxing shock wave, and in the case of the aerosol or dusty gas, as in other relaxing media have the possibility of *fully dispersed* and *partly dispersed shocks* (cf. [3]).

Put $u = f(\xi)$, $\xi = x - Vt$, in (3.11), integrate once, and suppose (by choice of axes) that $u \rightarrow 0$ as $\xi \rightarrow +\infty$, $u \rightarrow U$ (constant) as $\xi \rightarrow -\infty$. These conditions determine the shock propagation velocity as

$$V = a_0 + \frac{\gamma+1}{2} \frac{U}{2} \quad (5.1)$$

i.e. as the *mean of the excess wavelet speeds* ahead of and behind the wave, relative to a reference frame translating with the *equilibrium sound speed* a_0 . Note that this result holds generally, for all $\delta \neq 0$; for then it is believed that the wave profile is infinitely differentiable. However, a number of interesting features arise in the limit $\delta \rightarrow 0$. Setting $\delta = 0$ one finds that the first integral is

$$\begin{aligned} (1 - V\tau \frac{\partial}{\partial\xi}) \left[-Vf + a_\infty f + \frac{\gamma+1}{2} \frac{f^2}{2} \right] \\ = (a_\infty - a_0)f \quad , \end{aligned}$$

from which we get

$$V\tau \frac{df}{d\xi} = \frac{\gamma+1}{4} \frac{f(U-f)}{(V-a_\infty - \frac{\gamma+1}{2}f)} .$$

It follows from this that there will be an internal singularity within the shock (at which $df/d\xi = \infty$, invalidating the neglect of the thermoviscous term) unless

$$V < a_\infty \quad (5.2)$$

i.e. the shock propagation speed (5.2) must not exceed the frozen sound speed a_∞ (which is the highest value of either the phase or group velocity for waves $\exp(ikx -$

$i\omega t$) in the linear model). When condition (5.2) for a *fully dispersed shock* is satisfied, we write $V = a_\infty - \frac{\gamma+1}{2}W$, say, and complete the integration to give

$$\frac{W}{U} \ln f - (1 + \frac{W}{U}) \ln(U - f) = -\frac{1}{2V\tau}(\xi - \xi_0) \quad (5.3)$$

where ξ_0 is an arbitrary constant.

This describes a smooth monotonic rise from 0 to U , with exponential decay into the limiting values as $\xi \rightarrow \pm\infty$. However, the transition is only symmetrical (actually anti-symmetrical) in the case when the wave strength U is small compared with the dispersion ($a_\infty - a_0$). Then

$$\frac{W}{U} = \left(\frac{2}{\gamma+1} \right) \left(\frac{a_\infty - a_0}{U} \right) - \frac{1}{2} >> 1 \quad , \quad (5.4)$$

and (5.3) gives

$$f(\xi) = \frac{U}{2} \left\{ 1 - \tanh \left(\frac{U(\xi - \xi_0)}{4\tau V W} \right) \right\} \quad . \quad (5.5)$$

This profile is antisymmetric about the shock centre $\xi = \xi_0$ (where $f = U/2$), and it is in fact just the famous hyperbolic tangent profile of a shock wave in a thermoviscous gas, found by G.I. Taylor [10]. Moreover, the viscosity or diffusivity which controls (5.5) is just the bulk diffusivity that emerges in the low-frequency (near-equilibrium) analysis of (3.11). That analysis, for $\delta = 0$, gives

$$\begin{aligned} & \frac{\partial u}{\partial t} + (a_\infty + \frac{\gamma+1}{2}u) \frac{\partial u}{\partial x} \\ & \simeq (1 - \tau \frac{\partial}{\partial t})(a_\infty - a_0) \frac{\partial u}{\partial x} \simeq (1 + \tau a_\infty \frac{\partial}{\partial x})(a_\infty - a_0) \frac{\partial u}{\partial x} \end{aligned}$$

i.e.

$$\frac{\partial u}{\partial t} + (a_0 + \frac{\gamma+1}{2}u) \frac{\partial u}{\partial x} - \frac{1}{2}\delta_B \frac{\partial^2 u}{\partial x^2} = 0 \quad , \quad (5.6)$$

where the *bulk diffusivity* is

$$\delta_B = 2\tau a_\infty (a_\infty - a_0) \quad . \quad (5.7)$$

Seeking a travelling wave solution to (5.6), $u = g(\xi)$, $\xi = x - V_0 t$, we find

$$V_0 = a_0 + \frac{\gamma+1}{2} \frac{U}{2} = V \quad , \quad (5.8)$$

and

$$g(\xi) = \frac{U}{2} \left\{ 1 - \tanh \left(\frac{(\gamma+1)U(\xi - \xi_0)}{4\delta_B} \right) \right\} \quad . \quad (5.9)$$

Now from (5.4)

$$\begin{aligned}\tau V W(\gamma + 1) &\simeq 2\tau V(a_\infty - a_0) \\ &\simeq 2\tau a_0(a_\infty - a_0) \\ &\simeq 2\tau a_\infty(a_\infty - a_0)\end{aligned}$$

since the dispersion $(a_\infty - a_0)/a_\infty \ll 1$. Therefore (5.5) and (5.9) coincide, and a weak shock, in the sense $U \ll a_\infty - a_0$, is governed by the Taylor profile with the bulk diffusivity of (5.7).

Stronger waves have noticeably asymmetric profiles, as in the sketch below.



Figure 1
Structure of a fully-dispersed shock in a relaxing medium.

As the wave strength increases, W decreases, and at the condition $W = 0$, (5.3) gives

$$f(\xi) = U - \exp\left(\frac{\xi - \xi_0}{2V\tau}\right)$$

and the condition as $\xi \rightarrow +\infty$ cannot be satisfied. In the limit $W \rightarrow 0$ the profile consists of the exponential curve, plus the axis $f \equiv 0$ to the right of the point where the exponential meets the axis. For $W < 0$ the curve turns back on itself, and in the absence of thermoviscosity there is no continuous single-valued shock profile: the shock is *partly-dispersed* when (5.2) is not satisfied.

To complete the shock structure in this case one has to insert into the relaxing shock profile a discontinuity whose fine structure is resolved by thermoviscous diffusion. A consistent description can be obtained by using the fully-dispersed shock profile (5.3) from $\xi = -\infty(u = U)$ to the point $\xi = \xi_*$ at which $u = u_*$ and u_* is determined by the following argument. For a fully-dispersed transition between u_* and U the propagation speed is given by the argument leading to (5.1) as

$$V - u_* = a_0 + \frac{\gamma + 1}{2} \frac{U - u_*}{2}$$

and the propagation speed *relative to the fluid ahead* is

$$V - u_* = a_0 + \frac{\gamma + 1}{2} \left(\frac{U - u_*}{2} \right) .$$

We determine u_* by the requirement

$$V - u_* = a_\infty . \quad (5.10)$$

Then for all ξ in the range $-\infty < \xi < \xi_*$, we have $u_* < u < U$ and the relaxing shock velocity relative to the fluid ahead is less than a_∞ , allowing the use of the fully-dispersed profile. At $\xi = \xi_*$ there is a discontinuous jump from $u = u_*$ down to $u = 0$, a jump which propagates into the still medium ahead with speed

$$V_* = a_\infty + \frac{\gamma + 1}{2} \frac{u_*}{2} , \quad (5.11)$$

and has internal structure given by the Taylor solution $u = g(\xi)$ of (5.9), provided that we take $\xi = x - V_* t$, replace U by u_* and replace the bulk diffusivity δ_B by the molecular diffusivity δ . This follows formally by introducing a Taylor shock variable $X = (x - V_* t)/\delta$ into (3.11) and taking the limit $\delta \rightarrow 0$ with $u = O(1)$. Integrating and using $u \rightarrow 0$ as $X \rightarrow +\infty$, $u \rightarrow u_*$ as $X \rightarrow -\infty$ (matching of the inner diffusive sub-shock to the rest state ahead and to the relaxing shock behind) determines V_* as in (5.11), and then further integration leads to the Taylor profile (5.9) with the replacements noted.

In many cases (both of the aerosol or dusty gas and of a gas with molecular relaxation) the scale of the relaxing outer shock is very large compared with that of the inner Taylor sub-shock. See Figure 2. The speed of propagation of the whole wave into the fluid at rest ahead is given by the Taylor shock speed (5.11), with u_* given by (5.10) as

$U - 4(a_\infty - a_0)/(\gamma + 1)$. Thus we find

$$V_* = a_0 + \frac{\gamma + 1}{2} \frac{U}{2}$$

as required by (5.1) for all $\delta \neq 0$.

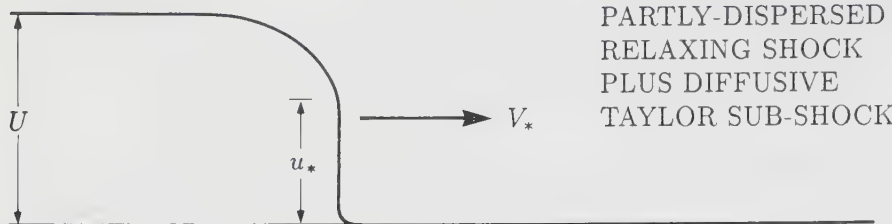


Figure 2

Structure of a partly-dispersed shock in a relaxing medium, showing the presence of an internal diffusive Taylor sub-shock.

REFERENCES

1. Davidson, G.A. & Scott, D.S. 1973 "Finite-amplitude acoustics of aerosols", *J. Acoust. Soc. Am.* **53**, 1717-1729.
2. Davidson, G.A. & Scott, D.S. 1973 "Finite-amplitude acoustic phenomena in aerosols from a single governing equation", *J. Acoust. Soc. Am.* **54**, 1331-1342.
3. Lighthill, M.J. 1956 "Viscosity effects in sound waves of finite amplitude". In "Surveys in Mechanics", eds. G.K. Batchelor & R.M. Davies, pp.250-351, Cambridge University Press.
4. Polyakova, A.L., Soluyan, S.I. & Khokhlov, R.V. 1962 "Propagation of finite disturbances in a relaxing medium", *Sov. Phys.-Acoust.* **8**, pp.78-82.
5. Blythe, P.A. 1969 "Nonlinear wave propagation in a relaxing gas", *J. Fluid Mech.* **37**, 31-50.
6. Ockendon, H. & Spence, D.A. 1969 "Nonlinear wave propagation in a relaxing gas", *J. Fluid Mech.* **39**, 329-345.
7. Johannessen, N.H. & Hodgson, J.P. 1979 "The physics of weak waves in gases", *Rep. Progress Phys.* **42**, 629-676.
8. Hammerton, P.W. & Crighton, D.G. 1991 "Nonlinear acoustic propagation through relaxing gases", to be submitted to *J. Fluid Mech.*
9. Hammerton, P.W. & Crighton, D.G. 1991 "Overturning of nonlinear acoustic waves", submitted to *J. Fluid Mech.*
10. Taylor, G.I. 1910 "The conditions necessary for discontinuous motion in gases", *Proc. R. Soc. Lond. A.* **84**, 371-377.

NONLINEAR WAVES IN FLUIDIZED BEDS

D. G. Crighton

University of Cambridge, Cambridge, UK

ABSTRACT

This chapter deals briefly with the modelling, via nonlinear wave analysis, of voidage disturbances in fluidized beds. It is shown that, after an initial stage of linear instability, a first nonlinear stage arises in which the voidage perturbation is governed by a Burgers-Korteweg-de Vries equation with negative viscosity. Accordingly, the linear stage of instability of a fluidized bed is replaced by a nonlinear stage in which the voidage disturbances are represented by slowly amplifying KdV soliton pulses.

1. INTRODUCTION

In the process of fluidization, gas or liquid is forced upward, under pressure, through a bed of fine particles (diameters in the range 1mm – 10^{-2} mm, typically). When the flow velocity exceeds a threshold, the drag force on the particles exceeds the gravitational force, the bed of particles becomes fluidized and large-scale wave-like phenomena become possible, and are observed. Similar phenomena are observed in the process of hindered settling, in which a cloud of fine particles falls under gravity towards a fixed surface on which the sedimenting particles form a bed. The general description should be identical for the two systems, although detailed constitutive laws may differ because fluidization and sedimentation often involve rather different parameter ranges.

Modelling of these processes is still a very controversial matter, and so are many predictions derived from earlier models, while the latest models have not yet been developed to the point at which critical qualitative predictions can be made. In these Notes we give a brief discussion of some of the current issues and their implications for nonlinear waves, with reference to several recent papers.

2. PROPAGATION OF A VOIDAGE DISTURBANCE IN A FLUIDIZED BED

A fine-particle bed becomes fluidized when the flow rate exceeds a threshold, and usually remains uniformly fluidized (on the macroscopic scale) until the flow rate reaches some higher value, beyond which “bubbling” in wide beds and “slugging” in narrow beds takes place. These phenomena, undesirable in practical applications in chemical engineering, involve the propagation upward of voids, or regions of essentially particle-free fluid, in roughly spherical form in the wide containers where bubbling takes place and in the form of horizontal bands or slugs in narrow containers. It is natural to approach these problems from linear and nonlinear instability wave analysis of the uniformly fluidized state.

Take a one-dimensional model, x vertically upwards, and a two-phase continuum model, writing u for fluid velocity, v for particulate phase velocity and ϕ for “voidage” (volume of fluid in unit volume of the two-phase mixture). Since the particles do not move with the fluid, we have to write separate mass conservation equations for the two phases. That for the fluid (taken to have uniform density ρ_f) is

$$\frac{\partial \phi}{\partial t} + \frac{\partial}{\partial x}(\phi u) = 0 \quad (2.1)$$

and that for the particulate phase (uniform density ρ_s) is

$$-\frac{\partial \phi}{\partial t} + \frac{\partial}{\partial x}[(1 - \phi)v] = 0 \quad . \quad (2.2)$$

These equations have an integral

$$\phi u + (1 - \phi)v = Q \quad (2.3)$$

with $Q = Q(t)$ only, which states that the net volume flux of mixture is the same across all horizontal planes at any given t ; (2.3) is used to eliminate u from later equations.

The particulate momentum equation is taken to be

$$\begin{aligned} \rho_s(1 - \phi) \left(\frac{\partial v}{\partial t} + v \frac{\partial v}{\partial x} \right) &= B(\phi)(u - v) \\ -\rho_s(1 - \phi)g + \frac{\partial S}{\partial x} &\quad , \end{aligned} \quad (2.4)$$

where the fluid-particle drag force is associated with a drag coefficient $B(\phi)$ (per unit volume of the mixture) multiplied by the relative velocity, and where inter-particle effects are explicitly represented as the gradient of a stress S (and these effects also contribute indirectly to the dependence of $B(\phi)$ on ϕ). Batchelor [1] discusses these inter-particle effects in some detail; they arise from short-range forces, among which are those barrier forces which prevent one particle occupying a site already occupied by another particle. Here we assume, following many others, that the stress can be written as the sum of an isotropic “particle-pressure” and a deviatoric stress which depends on the strain rate of the v -field through a “particle-viscosity”, just as in a single phase Newtonian fluid. Thus

$$S = -p + \mu \frac{\partial v}{\partial x} \quad , \quad (2.5)$$

and

$$\begin{aligned} \rho_s(1 - \phi) \left(\frac{\partial v}{\partial t} + v \frac{\partial v}{\partial x} \right) \\ = B(\phi)(u - v) - \rho_s(1 - \phi)g - \frac{\partial p}{\partial x} + \mu \frac{\partial^2 v}{\partial x^2} \quad , \end{aligned} \quad (2.6)$$

where we use no special symbols but emphasise that p and μ refer to the particle phase.

If u, v, p are calculated from (2.2), (2.3) and (2.6), and if fluid inertia is neglected (and also fluid viscosity effects except in the drag force) then the fluid pressure p_f follows from

$$\frac{\partial p_f}{\partial x} = -B(\phi)(u - v) \quad . \quad (2.7)$$

To close the system and determine ϕ also, we need to specify $B(\phi)$ and to relate p to ϕ . Write $B(\phi) = (1 - \phi)D(\phi)/V_p\phi$, where V_p is the volume of a single particle; then D is the drag coefficient of one particle, a function of ϕ and of the particle Reynolds number. This is commonly modelled by an empirical form

$$D(\phi) = D_0\phi^{-(n-1)} \quad (2.8)$$

where D_0 is the isolated particle Stokes drag coefficient, and for typical gas-fluidized beds $n \simeq 3$ (but see Batchelor [1], p.94, for discussion). Experiments also suggest that p can be taken as a function of ϕ , vanishing as $\phi \rightarrow 1$, and in the simplest model one would try

$$p(\phi) = P_0(1 - \phi) \quad (2.9)$$

with a constant P_0 , apparently of order 10 dyn/cm^2 .

Equations (2.2, 2.3, 2.6, 2.8, 2.9) are now a closed set for (u, v, ϕ, p, D) .

The simplest solution corresponds to uniform fluidization, $u = U_0$, $v = 0$, $\phi = \phi_0$, where

$$Q = U_0\phi_0, \quad B(\phi_0)U_0 = (1 - \phi_0)\rho_s g, \quad \text{and}$$

$$U_0 = U_t\phi_0^n$$

where U_t is the terminal free-fall velocity of an isolated particle in static fluid. The last of these is essentially an experimental correlation from which (2.8) is derived.

Now introduce a (localised) voidage disturbance of length scale h , and use U_0, h to make u, v, x, t dimensionless, $\rho_s U_0^2$ to make p dimensionless and $\rho_s U_0/h$ to make $B(\phi)$ dimensionless. Then

$$\phi u + (1 - \phi)v = Q, \quad (2.10)$$

$$-\frac{\partial \phi}{\partial t} + \frac{\partial}{\partial x}[(1 - \phi)v] = 0, \quad (2.11)$$

$$(1 - \phi)\left(\frac{\partial v}{\partial t} + v\frac{\partial v}{\partial x}\right) = B(\phi)(u - v) - \frac{(1 - \phi)}{F^2} + P_0\frac{\partial \phi}{\partial x} + \frac{1}{R}\frac{\partial^2 v}{\partial x^2}, \quad (2.12)$$

with $B(\phi) = [(1 - \phi)/F^2](\phi_0/\phi)^n$, $F = U_0/(gh)^{1/2}$ (Froude number), $R = \rho_s U_0 h / \mu$ (particle-phase Reynolds number).

3. LINEAR INSTABILITY

Writing $u = 1 + u'$, $v = v'$, $\phi = \phi_0 + \phi'$, leads, on dropping the prime and linearising, to

$$F^2 \frac{\partial^2 \phi}{\partial t^2} = -A \frac{\partial \phi}{\partial x} - B \frac{\partial \phi}{\partial t} + F^2 P_0 \frac{\partial^2 \phi}{\partial x^2} + F^2 C \frac{\partial^3 \phi}{\partial x^2 \partial t} , \quad (3.1)$$

with

$$A = \frac{(n+1)(1-\phi_0)}{\phi_0} , \quad B = \frac{1}{\phi_0} , \quad C = \frac{1}{R(1-\phi_0)} .$$

In many applications $F \ll 1$ is appropriate, and then (cf. Needham & Merkin [2]), analysis of the dispersion relation for (3.1), or use of singular perturbation methods, indicates the following:

(a) Over scales $x, t = O(1)$,

$$\frac{\partial \phi}{\partial t} + \frac{A}{B} \frac{\partial \phi}{\partial x} = 0$$

and an initial voidage disturbance $\phi(x, 0) = g(x)$ simply propagates upwards at speed A/B ,

$$\phi(x, t) = g(x - \frac{A}{B}t) ; \quad (3.2)$$

(b) imposition of a second initial condition $\partial\phi/\partial t = 0$ at $t = 0$ requires a boundary layer $t = O(F^2)$ in which the adjustment of $\partial\phi/\partial t$ is made; in the boundary layer ($\bar{t} = t/F^2 = O(1)$),

$$\phi = g(x) + \left[\frac{Ag'(x)}{B^2} (1 - e^{-B\bar{t}}) - \frac{A}{B} g'(x)\bar{t} \right] F^2 + O(F^4) , \quad (3.3)$$

which matches with the solution in (a);

(c) on a long time scale, $\tau = F^2 t = O(1)$

$$B \frac{\partial \phi}{\partial \tau} = (P_0 - \frac{A^2}{B^2}) \frac{\partial^2 \phi}{\partial z^2} - \frac{AC}{B} \frac{\partial^3 \phi}{\partial z^3} \quad (3.4)$$

with $z = x - (A/B)t$.

Thus on long scales, particle-phase viscosity is *dispersive* (not diffusive), while particle pressure effects are diffusive and *stabilising* if $P_0 > A^2/B^2$. Previous work, using models of this kind, but omitting particulate-phase pressures, had predicted instability for all flow rates (see the discussion in [2]).

4. NONLINEAR INSTABILITY

Equation (3.4) indicates instability to disturbances of all wavenumbers unless $P_0 > A^2/B^2$ in the limit $F \ll 1$ (and Needham & Merkin [2] show that this is in fact the stability condition for *all* F). If $P_0 < A^2/B^2$, disturbances will grow, slowly

if $F \ll 1$, and one might hope that a small-but-finite-amplitude wave analysis would lead to some long time behaviour that might correspond to the observed “*slugging*”. Needham & Merkin [2] attempt to do this, and derive a nonlinear wave equation

$$\begin{aligned} \frac{\partial \phi}{\partial t} + C(\phi) \frac{\partial \phi}{\partial x} \\ = \tilde{F}^2 \frac{\partial}{\partial x} \left\{ \psi(\phi) \frac{\partial \phi}{\partial x} + \frac{\phi^{n+1}}{\tilde{R}} \frac{\partial^2 \eta(\phi)}{\partial x^2} \right\} \quad , \end{aligned} \quad (4.1)$$

in which \tilde{F}, \tilde{R} are F, R with the terminal free fall velocity U_t as velocity scale instead of U_0 , and

$$\begin{aligned} C(\phi) &= \tilde{Q} + (n+1)\phi^n - (n+2)\phi^{n+1} \quad , \\ \psi(\phi) &= \phi^{n+1} \left\{ \tilde{P}_0 - (n+1)^2(1-\phi)^2\phi^{2n} \right\} \\ \eta(\phi) &= \tilde{Q} - \phi^{n+1} \quad . \end{aligned}$$

They examine, analytically and numerically, the phase plane for travelling wave solutions of this equation, and show that a shock solution is possible, with monotonic transition between two states of uniform voidage, but that at higher amplitudes the transition behind the shock becomes oscillatory. They suggest that this new stable quasi-steady oscillatory state is a model for the slugging phenomenon.

It seems to me that the basis for the derivation of (4.1) is not clear, as regards which terms are retained and which neglected, and I now propose a simpler nonlinear wave model. The method to be used is exactly that of my other contributions to these Notes, and is based on the prediction of (3.2); in the limit $F \rightarrow 0$, with $P_0 = O(1)$, $R = O(1)$, linear waves in a fluidized bed are non-dispersive, non-dissipative and propagate upwards at speed A/B . We attempt to balance quadratically nonlinear perturbations to such waves against small linear dispersive and dissipative (or amplifying) effects $O(F^2)$ which are represented by the right side of (3.4).

Write $\phi = \phi_0 + \phi'$, $u = 1 + u'$, $v = v'$ in (2.10) – (2.12), with the specific form for $B(\phi)$, and retain quadratically nonlinear terms independent of F and linear terms $O(F^2)$. (Note that F^2 is the natural parameter for the long-scale linear processes.) We get

$$\phi' + \phi_0 u' + (1 - \phi_0)v' + W_1 = 0 \quad , \quad (4.2)$$

$$\begin{aligned} W_1 &= \phi'(u' - v') \quad , \\ -\frac{\partial \phi'}{\partial t} + (1 - \phi_0) \frac{\partial v'}{\partial x} + W_2 &= 0 \quad , \\ W_2 &= -\frac{\partial}{\partial x}(\phi' v') \quad , \end{aligned} \quad (4.3)$$

and

$$\begin{aligned} u' - v' - n \frac{\phi'}{\phi_0} + W_3 &= 0 \quad , \tag{4.4} \\ W_3 &= \frac{F^2}{(1 - \phi_0)} P_0 \frac{\partial \phi'}{\partial x} + \frac{F^2}{R(1 - \phi_0)} \frac{\partial^2 v'}{\partial x^2} - F^2 \frac{\partial v'}{\partial t} \\ &\quad + \left\{ -n \frac{\phi'}{\phi_0} (u' - v') + \frac{n(n+1)}{2} \left(\frac{\phi'}{\phi_0} \right)^2 \right. \\ &\quad \left. - \frac{\phi'}{(1 - \phi_0)} (u' - v' - \frac{n\phi'}{\phi_0}) \right\} . \end{aligned}$$

Eliminating u', v' from the linear terms we get

$$\begin{aligned} \frac{\partial \phi'}{\partial t} + (n+1)(1-\phi_0) \frac{\partial \phi'}{\partial x} \\ = W_2 + (1-\phi_0) \frac{\partial}{\partial x} (\phi_0 W_3 - W_1) . \end{aligned} \tag{4.5}$$

Now the linear contributions to the right side give (when use is made of the $O(1)$ approximations

$$v' + (n+1)\phi' = 0 \quad , \quad u' - v' = \frac{n}{\phi_0}\phi' \tag{4.6}$$

which follow from (4.2) – (4.4) with the W_i neglected), precisely the higher order derivatives necessary to make the linear form of (4.5) agree with (3.1); for the nonlinear elements of (4.5) we again use (4.6) and finally obtain

$$\begin{aligned} \frac{\partial \phi'}{\partial t} + (n+1)(1-\phi_0) \frac{\partial \phi'}{\partial x} - (n+1)(2+n - \frac{n}{\phi_0})\phi' \frac{\partial \phi'}{\partial x} \\ = \phi_0 F^2 (P_0 - (n+1)^2 (1-\phi_0)^2) \frac{\partial^2 \phi'}{\partial x^2} - \frac{(n+1)\phi_0 F^2}{R} \frac{\partial^3 \phi'}{\partial x^3} . \end{aligned} \tag{4.7}$$

Equation (4.7) is formally the Burgers-Korteweg de Vries equation, except that if $P_0 < A^2/B^2$ it is the *unstable BKdV*, with negative viscosity. I do not know of any previous occurrence of the UBKdV. If ϕ_0 is near the critical value for which $2+n-n/\phi_0 = 0$, then one must retain quadratically and cubically nonlinear terms, and the resulting equation is an (unstable) Burgers-Gardner equation, Gardner's equation being the mixed KdV-modified KdV equation (see Drazin & Johnson [3]).

One immediate prediction is that near the instability threshold, $P_0 \simeq A^2/B^2$, localised *KdV soliton pulses of voidage* ϕ' should appear. On the unstable side,

$P_0 < A^2/B^2$, these solitons will slowly amplify until higher-order nonlinear effects in the set (2.10-2.12), but neglected in (4.7), become important. On the stable side we have the standard dissipative BKdV equation, and the possibility (as in bubbly liquids) of monotonic or oscillatory shock wave solutions. The analysis of (4.7) will be taken up elsewhere (Harris & Crighton [4]), where we shall also show how the soliton pulses develop when their amplitude has become so large as to invalidate use of (4.7).

REFERENCES

1. Batchelor, G.K. 1988 "A new theory of the instability of a uniform fluidized bed", *J. Fluid Mech.* **193**, 75-110.
2. Needham, D.J. & Merkin, J.H. 1983 "The propagation of a voidage disturbance in a uniformly fluidized bed", *J. Fluid Mech.* **131**, 427-454.
3. Drazin, P.G. & Johnson, R.S. 1989 "Solitons: an introduction", Cambridge University Press.
4. Harris, S.E. & Crighton, D.G. 1991 "Solitons and other finite-amplitude wave effects in fluidized beds", to be submitted to *J. Fluid Mech.*

NONCLASSICAL DYNAMICS OF CLASSICAL GASES

M. S. Cramer

Virginia Polytechnic Inst. and State University,
Blacksburg, VA, USA

Abstract

In the present article we examine the dynamics of single-phase, equilibrium, i.e., classical, fluids in the dense gas regime. The behavior of fluids of moderately large molecular weight is seen to differ significantly from that of air and water under normal conditions. New phenomena include the formation and propagation of expansion shocks, sonic shocks, double sonic shocks, and shock-splitting. The more complicated existence conditions for shock waves are described and related to the dissipative structure. We also give a brief description of transonic flows and show that the critical Mach number for conventional blade shapes can be increased by a factor of 30-50% for these fluids.

1. Introduction

The dynamics of compressible flows and shock waves plays a critical role in the design of aircraft and turbomachinery. As a result, some form of gasdynamics is presented at all stages of a fluid mechanics education. Most of these presentations and much of our intuition are based on the theory of perfect gases. The choice of this fluid model is due to its simplicity and, when applied to many gases at atmospheric conditions, its accuracy. This standard gasdynamic theory, known to most undergraduates in the mechanical sciences, states that the only type of shocks possible are compression

shocks. By compression shocks we mean shocks which result in an increase in the pressure of a fluid particle as it passes through the shock. A discontinuity for which the pressure decreases will spread to form a centered expansion fan. However, if the scope is extended beyond the domain of validity of the perfect gas theory, the situation can be more complex. Ultimately, the type of shock capable of propagating in any particular fluid is determined by the sign of the thermodynamic parameter

$$\Gamma \equiv \frac{V^4}{2a} \left. \frac{\partial^2 p}{\partial V^2} \right|_S , \quad (1.1)$$

where $p = p(V, s)$ is the thermodynamic pressure, V is the specific volume, s is the entropy and

$$a \equiv \left(-V^2 \left. \frac{\partial p}{\partial V} \right|_S \right)^{1/2} \quad (1.2)$$

is the thermodynamic sound speed. Because the sign of Γ also determines the qualitative behavior of virtually all other gasdynamic behavior, we follow Thompson [1] in referring to (1.1) as the fundamental derivative of gasdynamics. Furthermore, we will refer to the case where $\Gamma > 0$ as positive nonlinearity and the case where $\Gamma < 0$ as negative nonlinearity. Liquids and many dense gases have $\Gamma > 0$. Thus, the resultant gasdynamic behavior is qualitatively the same as that of perfect gases. In fluids having $\Gamma < 0$ most of the standard inequalities need to be reversed [1]. As an example, in $\Gamma < 0$ fluids, compression shocks are seen to violate the entropy inequality and therefore disintegrate to form a centered compression fan. In these fluids, the expansion shock, forbidden in the perfect gas theory, is the only discontinuity capable of remaining intact.

The basic behavior and existence issues involved in the study of negative nonlinearity are really no different than those encountered in the study of positive nonlinearity, provided one takes into account the various sign changes. However, when Γ changes sign within a flow, the situation becomes more complex by an order of magnitude. We refer to this case as that of mixed nonlinearity. The basic existence issues, while at root are necessarily the same as those for perfect gases, must be applied more carefully when Γ changes sign across the shock wave of interest. Furthermore, new phenomena having no counterpart in the classical theory can arise. Examples include sonic shocks, the partial disintegration of both compression and expansion shocks, collisions between compression and expansion shocks and shock-splitting. By sonic shock we mean a shock having a speed identically

equal^{*} to the convected sound speed just upstream or downstream of the shock.

The types of fluids and conditions under which this anti-intuitive behavior becomes manifest were first given by H. A. Bethe, Ya. B. Zel'dovich and P. A. Thompson and co-workers; their results are summarized in Section 3 of the present article. Because of the significance of each of these studies to the early development of this work, we refer to fluids having negative nonlinearity of the type described in Section 3, as Bethe-Zel'dovich-Thompson (BZT) fluids.

Although the results described here are, at best, anti-intuitive, the scope of our discussion is restricted to precisely the same class of fluids ordinarily treated in classical gasdynamics and fluid mechanics. That is, we restrict our attention to single-phase gases in which relaxation, chemical reactions, dissociation, ionization, etc., play no role. A more mathematical statement of the fluid model is given later in Section 2. The idea of developing a more complete understanding of classical fluids is, of course, part of the motivation for the study of BZT fluids. Another important motivation comes from the potential for applications. After all, many of the most important technological advances are due to the exploitation of new materials. Through use of BZT fluids new dynamical processes are possible completely within the context of ordinary single-phase gases.

The idea of negative and mixed nonlinearity is by no means restricted to the single-phase gases treated here. In fact, the past 10-15 years has shown a remarkable surge in the interest in these nonclassical phenomena. Perhaps the work having the closest relation to ours is that of Borisov, et al. [2] who generated expansion shocks in Freon-13 through use of a shock tube configuration. The region of negative nonlinearity^{**} was generated by the near-critical singularity in the specific heat^{***}. The flow also appears to enter the two-phase regime. These authors also gave a brief discussion of mixed nonlinearity. Due to similar effects, ordinary steam also appears to admit negative and mixed nonlinearity in the two-phase regime just

* An alternate definition is that the Mach number measured in a frame in which the shock appears as a normal stationary shock is unity either upstream or downstream of the shock. In the case of oblique waves we could state that the Mach lines immediately upstream or downstream of the shock are parallel to the shock surface.

** We formally exclude near-critical effects here. However, if nonequilibrium effects can be avoided in the single-phase region, there is no reason why the near-critical effects cannot be included in our definition of BZT fluids.

below the critical point; see, e.g., Novikov [3] and Kahl and Mylin [4]. Negative and mixed nonlinearity are also known to occur in temperature shocks in superfluid helium ^4He [5] - [10]. The calculations of Torczynski [11] clearly shows that fourth sound in ^4He will exhibit mixed nonlinearity. Garrett [12] has described mixed nonlinearity in $^3\text{He-B}$. Expansion shocks in two-fluid plasmas were described by Bezzerides, et al. [13] and mixed nonlinearity was shown by Nariboli and Lin [14] to occur in MHD start-up shocks. Two-phase flows are a rich source of mixed nonlinearity. The well-known fact that negative and mixed nonlinearity occurs in suspensions has been described in References [15] - [18]. In the context of liquid-vapor phase changes, the equilibrium isentropes have a slope discontinuity at the saturated vapor line. In retrograde fluids, i.e., those which dry on adiabatic expansion, the kink in the isentropes is such that expansion shocks are possible across which a vapor-liquid mixture can undergo a complete vaporization [19]. Shock-splitting has also been observed by Dettleff et al. [20] and Thompson and Kim [21]. For a complete review of these and related issues, the articles by Thompson, Carofano and Kim [19] and Thompson et al. [22] are recommended as are the articles in the present series by Professors Thompson and Meier. Similar kinks in the shock adiabats of solids are also known to occur during solid-solid phase changes. General discussions of this point have provided by Zel'dovich and Raizer [23]. Discussions in the context of graphite-diamond transition may be found in references [24] - [25]. Transitions for iron and steel were first discussed by Ivanov and Novikov [26] and Erkman [27]. Single-phase solids also give rise to negative nonlinearity. Kolsky [28] has demonstrated the existence of tensile shocks in rubber and negative nonlinearity in fused silica was reported in [29] - [30]. Evidence suggesting mixed nonlinearity in fused silica has also been given by Conner [31]. Nariboli and Lin [14] and Lee-Bapti [32] have demonstrated that viscoelastic solids of the Kelvin-Voigt type admit mixed nonlinearity. Morris and Nariboli [33] have shown similar results for elastic dielectrics. Perhaps the simplest model of mixed nonlinearity is the propagation of electromagnetic waves in a nonlinear isotropic dielectric. If we approximate the constitutive relation for the relative dielectric constant by $\epsilon(1 + \alpha|E|^2)$, where ϵ and α are positive constants and E is the electric field strength, we find that speed of light in one-dimensional right-moving waves is given by $c_L(1 + 3\alpha E^2)^{-\frac{1}{2}}$, where c_L is the linear speed of light, which yields positive nonlinearity for $E < 0$ and negative nonlinearity for $E > 0$. Negative and mixed nonlinearity may also occur in dispersive systems. Here we simply refer to the recent work on internal gravity waves by Kakutani and Yamasaki [34] and Helfrich, Melville and Miles [35].

In the following, we first give the basic equations used (Section 2) followed by a discussion of the types of fluids and conditions under which negative nonlinearity is expected (Section 3). As an introduction to the nonclassical dynamics, nonlinear steepening and shock formation are described in Section 4. The properties of the

shock adiabat are given in Section 5 and the fundamental existence criteria are given in Section 6. In the remainder of this article we provide a partial survey of the nonclassical dynamics expected in BZT fluids.

2. Governing Equations

Throughout we will consider conventional single-phase Navier-Stokes-Fourier fluids. The differential conservation laws are written

$$\frac{D\rho}{Dt} + \rho \nabla \cdot \tilde{v} = 0 \quad (2.1)$$

$$\rho \frac{D\tilde{v}}{Dt} + \nabla p = \nabla \cdot \hat{\underline{T}} + \rho \tilde{f} \quad (2.2)$$

$$\rho \frac{De}{Dt} = \frac{p}{\rho} \frac{D\rho}{Dt} + \phi - \nabla \cdot \tilde{q} + \rho r, \quad (2.3)$$

where ρ , v , f , and r are the fluid density, velocity, body force density and volumetric energy supply, respectively. The quantity $e = e(\rho, T)$ is the internal energy and $p = p(\rho, T)$ is the thermodynamic pressure defined in Section 1. As usual, the symbol T denotes the absolute temperature. The operator

$$\frac{D}{Dt} \equiv \frac{\partial}{\partial t} + \tilde{v} \cdot \nabla$$

is recognized as the material derivative and $\phi \equiv \hat{\underline{T}} : \nabla \tilde{v}$ is the usual dissipation function. In accord with our constitutive assumption we take the viscous part of the stress tensor $\hat{\underline{T}}$ and the heat flux vector \tilde{q} to be given by

$$\hat{\underline{T}} \equiv \lambda (\nabla \cdot \tilde{v}) \underline{I} + \mu (\nabla \tilde{v} + (\nabla \tilde{v})^T) \quad (2.4)$$

$$\tilde{q} \equiv -k \nabla T, \quad (2.5)$$

where \underline{I} is the identity tensor and the superscript T denotes the transpose. The coefficients $\mu(\rho, T)$, $\lambda(\rho, T)$ and $k(\rho, T)$ are the shear viscosity, second (or dilatational) viscosity, and thermal conductivity, respectively. The fluid entropy $s = s(\rho, T)$ introduced in the previous section is related to the other thermodynamic parameters through Gibbs' relation

$$Tds = de - \frac{p}{\rho} d\rho. \quad (2.6)$$

The fluids treated here will be required to satisfy the following inequalities

$$\mu \geq 0, \quad \mu_b \equiv \lambda + \frac{2}{3}\mu \geq 0, \quad k \geq 0 \quad (2.7)$$

$$c_v \equiv T \left. \frac{\partial s}{\partial T} \right|_{\rho} \geq 0, \quad \left. \frac{\partial p}{\partial \rho} \right|_T \geq 0 \quad (2.8)$$

$$\beta \equiv - \left. \frac{1}{\rho} \frac{\partial \rho}{\partial T} \right|_{\rho} \geq 0, \quad (2.9)$$

where $c_v = c_v(\rho, T)$ is referred to as the specific heat at constant volume; $\beta(\rho, T)$ is the coefficient of thermal expansion and $\mu_b = \mu_b(\rho, T)$ is the bulk viscosity. The first set guarantee that the second law of thermodynamics is satisfied by all motions consistent with (2.1) - (2.5) and second set arises from the requirement of thermodynamic equilibrium. The usual manipulations of thermodynamics yields the well-known relations

$$c_p \geq c_v \geq 0, \quad (2.10)$$

where

$$c_p(\rho, T) \equiv T \left. \frac{\partial s}{\partial T} \right|_p \quad (2.11)$$

is the specific heat at constant pressure. The following relation between the isothermal and isentropic compressibilities is also well-known in thermodynamics:

$$\left. \frac{\partial p}{\partial V} \right|_S = \gamma \left. \frac{\partial p}{\partial V} \right|_T, \quad (2.12a)$$

or, if we note that $V \equiv \rho^{-1}$,

$$\left. \frac{\partial p}{\partial \rho} \right|_S = \gamma \left. \frac{\partial p}{\partial \rho} \right|_T. \quad (2.12b)$$

Here $\gamma \equiv c_p/c_v$ is the ratio of specific heats; (2.10) may be used to demonstrate that $\gamma \geq 1$. By combining (2.12) with (1.2), we see that the sound speed is always real.

The condition that the coefficient of thermal expansion be positive is not mandated by any general principle but is assumed here for convenience. Most vapors are expected to satisfy (2.9) although it is known that $\beta < 0$ for some substances, e.g., water near its freezing point. By combining (2.9) with (2.8) it can be shown that the Grüneisen parameter is positive for fluids considered here. Furthermore, (2.9) can be shown to be considerably stronger than the corresponding conditions on β imposed by Bethe [36] and Hayes [37].

Shock waves are required to satisfy the Rankine-Hugoniot jump conditions

$$[\rho U] = 0 \quad (2.13)$$

$$[v_t] = 0 \quad (2.14)$$

$$\frac{[p]}{[V]} = -m^2 \quad (2.15)$$

$$[h] = [p] \frac{v_2 + v_1}{2}, \quad (2.16a)$$

where $U \equiv v_n - u$ is the normal component of the relative velocity between the fluid and the shock, $u(x,t)$ is the shock speed, v_t is the component of fluid velocity parallel to the shock surface, and $h = h(\rho, T) \equiv e + p/\rho = e + pV$ is the fluid enthalpy. The square brackets will always denote jumps in indicated quantity, i.e.,

$$[A] \equiv A_2 - A_1,$$

where A is any quantity and the subscripts 1 and 2 denote conditions on either side of the shock. The quantity m is mass flux through the shock which, by virtue of (2.13), can be written as

$$m = \rho_2 U_2 = \rho_1 U_1. \quad (2.17)$$

If we use the definition of the enthalpy, (2.16a) may be recast in terms of the internal energy to yield:

$$[e] = -[V] \frac{p_2 + p_1}{2}. \quad (2.16b)$$

Equation (2.13) or (2.17) is recognized as the principle of mass conservation whereas (2.14) and (2.15) represent the tangential and normal components of the momentum jump condition. Equation (2.16) is the well-known Hugoniot relation representing the energy equation.

The relative direction of most of the jumps is found by a direct analysis of (2.13)-(2.16). As is well-known, the sign of the jump of the density, enthalpy and internal energy is the same as that of the pressure. The change in the relative flow velocity is in a sense opposite of the pressure. That is, the flow is decelerated through a stationary normal compression shock and is accelerated if the shock is of the expansion type. In stationary oblique shocks, the change in direction of the flow velocity can also be determined by a direct analysis. If the oblique shock is of the compression type, the flow is turned away from the normal while expansion shocks turn the flow toward the normal. The direction of the temperature jump requires somewhat more effort. Under the conditions assumed in this section and in Section 5, it may be shown that all acceptable shocks will always have temperature jump of the same sign as the pressure jump, i.e., compression shocks heat the flow, whereas expansion shocks result in a cooler fluid.

Finally, we note that the jump conditions (2.13)-(2.16) are invariant with respect to time reversals, i.e., interchanges of the upstream and downstream conditions. However, when it is recognized that the dissipative effects dominate the flow in the interior of the shock layer, it is natural to require the usual form of the entropy inequality

$$s_2 \geq s_1 \quad (2.18)$$

be satisfied for all admissible shock waves. Here it is clear that s_1 is the upstream entropy and s_2 is the downstream value.

3. Conditions for $\Gamma < 0$ in Single-Phase Gases

The definition (1.1) shows that the sign of Γ will give the direction of the curvature of the isentrope in the p-V plane. Regions where $\Gamma > 0$ will correspond to an upward curvature and regions where $\Gamma < 0$ will correspond to downward curvature. Alternate versions of (1.1) may be derived by standard thermodynamic manipulations. These include

$$\Gamma = \frac{a}{\rho} + \left. \frac{\partial a}{\partial \rho} \right|_s = \frac{1}{\rho} \left. \frac{\partial(\rho a)}{\partial \rho} \right|_s \quad (3.1)$$

$$= \frac{V^4}{2a} \left\{ \frac{\partial^2 p}{\partial V^2} - \frac{3T}{c_v} \frac{\partial p}{\partial T} \frac{\partial^2 p}{\partial V \partial T} + \left(\frac{T}{c_v} \frac{\partial p}{\partial T} \right)^2 \left[3 \frac{\partial^2 p}{\partial T^2} + \frac{1}{T} \frac{\partial p}{\partial T} \left(1 - \frac{T}{c_v} \frac{\partial c_v}{\partial T} \right) \right] \right\} \quad (3.2)$$

The first tends to occur naturally in derivations. The second was first given by H. A. Bethe [36] and is derived directly from (1.1) by taking p to depend on V, T rather than V, s . The expression (3.2) is particularly useful for the computation of Γ from equations of state of the form $p = p(V, T)$. For other versions of (1.1) we refer the reader to Thompson [1]. To avoid confusion, it should be noted that many authors reserve the symbol Γ for the nondimensional version of (1.1) given by $\rho\Gamma/a$.

Bethe [36] was the first to explore the possibility that Γ can be negative in normal fluids. The two extremes of liquids and dilute gases appear to be ruled out immediately. Under normal conditions liquids tend to have values of $\rho\Gamma/a$ on the order of 3-10, see, for example, Beyer [38] or Thompson [1], [39]. The value of Γ corresponding to perfect gases is

$$\Gamma = \frac{a}{\rho} \frac{\gamma+1}{2}$$

which is clearly always positive. Bethe also examined the effect of variable specific heat and found that $\Gamma < 0$ only if

$$\frac{\gamma-1}{\gamma+1} \frac{T}{\gamma} \frac{d\gamma}{dT} < -1,$$

where γ is the ratio of specific heats in the dilute gas limit. However, fluids having rapid variations of γ also tend to have $\gamma \approx 1$ and it would not seem likely that this mechanism will give rise to negative nonlinearity. Both Bethe and Zel'dovich [40] recognized that fluids having large specific heats could give rise to negative nonlinearity in the dense gas region. This is seen by noting that (3.2) can be approximated by

$$\Gamma \approx \frac{V^4}{2a} \left. \frac{\partial^2 p}{\partial V^2} \right|_T + O(c_v^{-1}) \quad (3.3)$$

if c_v is large. A useful interpretation of this result is that the isentropes approach the isotherms in the large c_v limit. It is well-known that the isotherms of all fluids have downward curvature, i.e.,

$$\left. \frac{\partial^2 p}{\partial V^2} \right|_T < 0$$

in the general vicinity of the thermodynamic critical point. If the specific heat is large enough the isentropes will also have negative curvature, i.e., $\Gamma < 0$. To illustrate the region of negative nonlinearity we have plotted constant $p\Gamma/a$ contours in Figure 3.1 and isentropes in Figure 3.2 for a van der Waals gas with $c_{v_\infty}(T_c) = 50 R$, where R is the gas constant, T_c is the critical temperature and c_{v_∞} is the dilute gas (or zero-pressure) specific heat defined by

$$c_{v_\infty}(T) \equiv \lim_{V \rightarrow \infty} c_v(V, T). \quad (3.4)$$

The numerical value of $c_{v_\infty}(T_c)$ roughly corresponds to that of normal decane ($n-C_{10}H_{22}$). The downward curvature indicating $\Gamma < 0$ is clearly evident in Figure 3.2.

The region of negative nonlinearity is always of the general form indicated in Figures 3.1 and 3.2. That is, it is a finite region partially bounded on the left by the saturated vapor curve. The fact that the negative Γ region is embedded in the $\Gamma > 0$ region should not be surprising. After all, all fluids become ideal gases in the zero pressure limit. On the left, the values of Γ must approach those of liquids. The number of times an isentrope or shock adiabat crosses a $\Gamma = 0$ locus will have a strong influence on the dynamics. In both Figure 3.1 and 3.2, it can be seen that there are at most two such crossings possible.

At this stage, it is useful to reiterate the conditions for negative Γ . The first is that the specific heats should be relatively large. Although not entirely reliable, it appears that inspection of the ratio $c_{v_\infty}(T_c)/R$ gives a reasonable first estimate of the likelihood of regions of negative nonlinearity (see, also, the

discussion of Section 2 of Thompson and Lambrakis [41]). This large c_v requirement immediately eliminates air and water from consideration. Furthermore, the phenomena of interest tends to occur at moderately high pressures and temperatures. Although the pressures and temperatures involved are frequently found in power cycles and a number of industrial processes, they tend to be out of the range of daily human experience.

To provide further evidence for negative nonlinearity, Lambrakis and Thompson [42], Thompson and Lambrakis [41], and Cramer [43] have employed relatively sophisticated equations of state to compute Γ for a number of fluorocarbons and hydrocarbons of practical interest. A partial list of fluids found to exhibit negative nonlinearity within the single-phase vapor region is given in Table 3.1. The computation of Γ and estimate for the saturation boundary is identical to that of Cramer [43]. The equation of state employed is that of Martin and Hou [44], which is expected to be one of the most conservative models for this purpose and the ideal gas specific heat (3.4) is represented by a power law $c_v^\infty(T) = c_v^\infty(T_c)(T/T_c)^n$. To illustrate the strength of the nonlinearity we have also listed the minimum value of $\rho\Gamma/a$ on the critical isotherm. The input data is drawn from a number of sources. The sources of the data for PP10, PP11, PP24, PP25, FC-43, FC-70, and FC-71 are described by Cramer [43]. The data for PP5 and PP9 are taken directly from the manufacturer's (ISC Chemicals, Avonmouth, England) data. In particular, the values of $c_v^\infty(T_c)$ and n were estimated by interpolations of superheated vapor tables. The data for the fluorinated ethers were taken directly from Thompson and Lambrakis' Table 1. The boiling temperatures were chosen to reproduce their Reidel parameters. The value of n was chosen to be 0.5 even though Thompson and Lambrakis suggest 0.45; however, tests indicate that this seems to make little difference. The same basic approach was used for perfluorodecane although the specific heat was estimated using the technique of Rihani and Doraiswamy [45].

In order to see the variation of Γ with temperature and density we have also plotted $\rho\Gamma/a$ for FC-70 in Figure 3.3. As pointed out by Thompson and Lambrakis [41], the value of $\rho\Gamma/a$ can become quite small at subcritical temperatures. Inspection of the variation on subcritical isotherms clearly shows that even smaller values will be attained at metastable conditions between the Wilson line and saturated vapor curve.

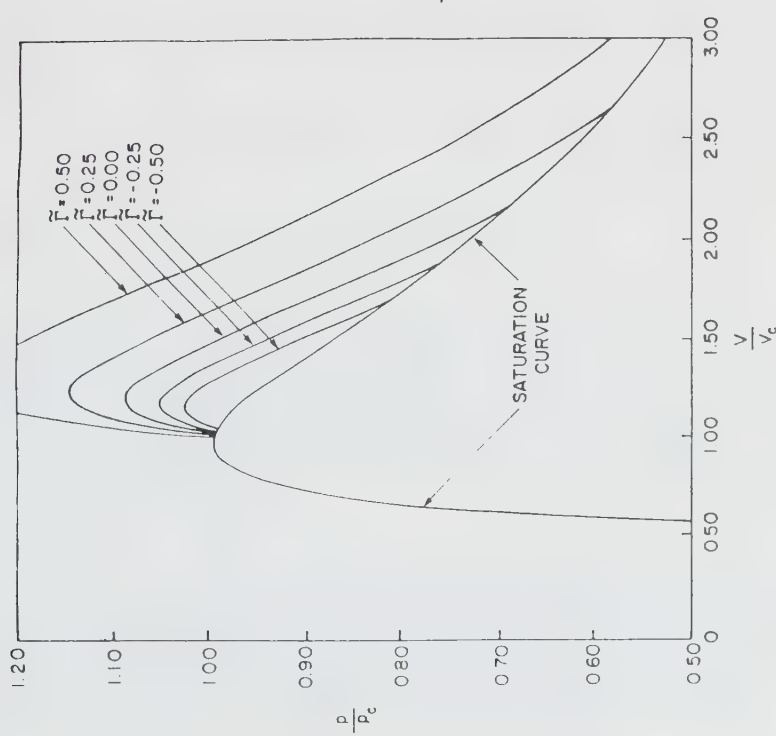


Figure 3.1: Constant $\bar{\gamma}$ contours for a van der Waals gas with $C_v = 50$. The subscript c denotes conditions at the thermodynamic critical point.

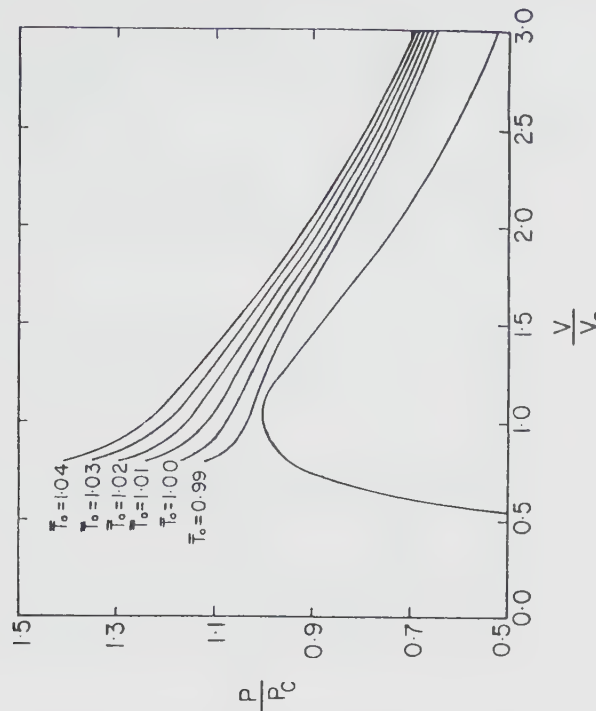


Figure 3.2: Isentropes for a van der Waals gas. $C_v = 50$. Each isentrope goes through the point $T = \frac{P}{V}^{\frac{1}{\gamma}} c^{\gamma}$, $V = 2.0V_c$.

FLUID	T_c	p_c atm	ζ_c	T_b	$\frac{c_{v_\infty}(T_c)}{R}$	n	$\left.\frac{\rho\Gamma}{a}\right _c$
C ₁₀ F ₂₂	pf-decane	578	12.9	0.255	436	74.8	0.5
C ₁₀ F ₁₈ (PP5)	pf-decalin	565.2	17.3	0.262	415.2	64.5	0.4081
C ₁₁ F ₂₀ (PP9)	pf-methyldecalin	586.6	16.4	0.261	433.2	72.8	0.2081
C ₁₃ F ₂₂ (PP10)	pf-perhydrofluorene	632.2	16.0	0.283	463.2	78.4	0.5255
C ₁₄ F ₂₄ (PP11)	pf-perhydrophenanthrene	650.2	14.4	0.269	488.2	97.3	-0.15
C ₁₆ F ₂₆ (PP24)	pf-fluoranthene	701.2	15.1	0.289	517.2	112.0	0.5113
C ₁₇ F ₃₀ (PP25)	pf-benzyltetralin	687.3	10.9	0.239	533.2	123.0	-0.22
C ₁₂ F ₂₇ N(FC-43)	pf-tributylamine	567.2	11.2	0.260	447.2	93.0	-0.03
C ₁₅ F ₃₃ N(FC-70)	pf-tripentylamine	608.2	10.2	0.270	488.2	118.7	0.4930
C ₁₈ F ₃₉ N(FC-71)	pf-triheptylamine	646.2	9.3	0.275	526.2	145.0	0.4273
C ₁₁ F ₂₃ H ₃	fluorinated ether E3	536	10.7	0.254	430.4	82.9	-0.17
C ₁₄ F ₂₉ H ₄	fluorinated ether E4	568	8.3	0.245	470.0	109.0	-0.29
C ₁₇ F ₃₅ H ₅	fluorinated ether E5	595	7.6	0.239	500.0	135.7	-0.11

Table 3.1: Negative Γ Fluids. Each fluid was found to have a region of negative nonlinearity in the pure single-phase region. Calculation procedure employs the Mart n-Hou equation [44]; full details are found in Cramer [43]. The last column gives the minimum value of ρ/α on the critical isotherm.

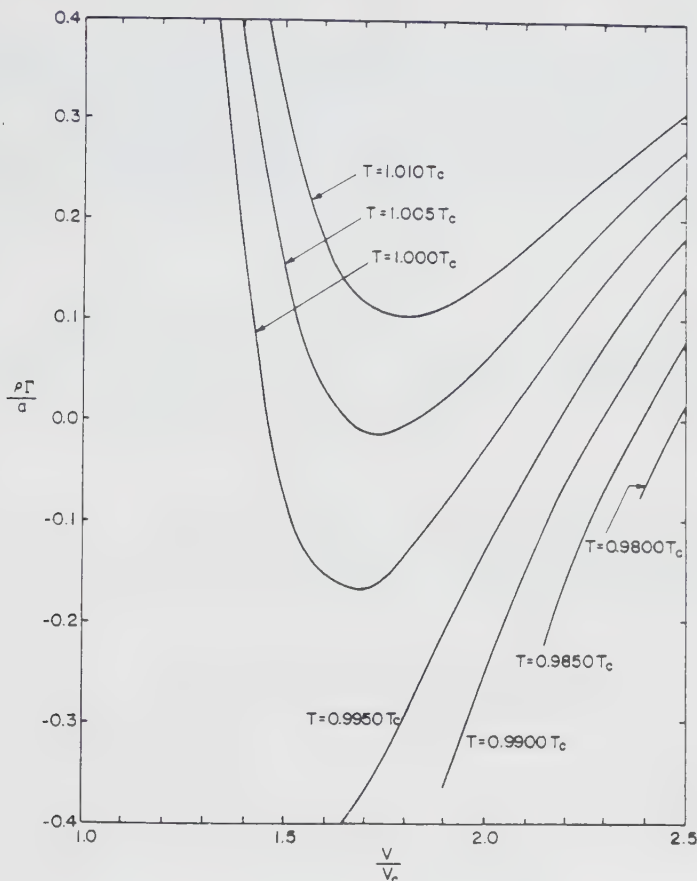


Figure 3.3: Variation of $\rho\Gamma/a$ on isentropes. Fluid is FC-70 and is modeled by the Martin-Hou equation with a power law $c_{y,\infty}(T)$. Complete details are found in Cramer [43].

For a further discussion of the Martin-Hou equation in the context of the fundamental derivative we refer the reader to Lambrakis and Thompson [42], Thompson and Lambrakis [41] and Cramer [43]. Both articles by Thompson and Lambrakis also discuss the use of other gas models. The use of the Martin-Hou equation to compute properties of dense, heavy fluorocarbons has also been described by Burnside [46] and Richter and Burnside [47].

As a result of the discussion provided here and by previous investigators we conclude that the existence of negative Γ fluids is reasonably well established, at least from the theoretical/numerical side. An important milestone in fluid mechanics or for that matter, classical physics, is the experimental confirmation of negative nonlinearity in single-phase gases. Unfortunately such evidence is not yet available and further work is clearly needed.

4. Shock Formation

Perhaps the simplest demonstration of the effects of nonlinearity is by considering the classical shock formation problem. If we assume the flow to be one-dimensional ($v = (v(x,t), 0, 0)$), unsteady, inviscid ($\mu, \lambda, k = 0$) and isentropic with negligible body force and energy supply r , we find that (2.1)-(2.3) may be reduced to the usual equations:

$$\frac{\partial \rho}{\partial t} + v \frac{\partial \rho}{\partial x} + \rho \frac{\partial v}{\partial x} = 0 \quad (4.1)$$

$$\frac{\partial v}{\partial t} + v \frac{\partial v}{\partial x} + \frac{a^2}{\rho} \frac{\partial \rho}{\partial x} = 0, \quad (4.2)$$

which are recognized as a 2×2 system for (v, ρ) . Because a is real, (4.1)-(4.2) are hyperbolic and general solutions may be obtained by the method of characteristics. If we confine our attention to simple right-moving waves, we find that the convected sound speed may be written:

$$\sigma(\rho) = v_* + a_* + \int_{\rho_*}^{\rho} \Gamma(\xi, s_*) d\xi, \quad (4.3)$$

where s_* , v_* , ρ_* and a_* are the entropy, particle velocity, density and thermodynamic sound speed at a reference state. Similar expressions for the convected sound speed are found in [41] and [48].

The usual viewpoint is to recognize that each portion of the initial waveform will shift forward with the speed (4.3). The dependence of σ on ρ gives rise to the well-known distortion leading to the formation of shock waves. The form of (4.3) is particularly convenient because the distortion and wave steepening may be related directly to the area under a Γ vs. ρ curve for the isentrope in question. A second form of (4.3) is obtained by differentiation; this reads

$$\frac{d\sigma}{d\rho} = \Gamma(\rho, s_*). \quad (4.4)$$

Thus, in regions where $\Gamma > 0$, σ increases with density and the steepening is forward to form compression shocks. By the same reasoning σ decreases with the density when $\Gamma < 0$ and the steepening is then backward to form expansion shocks. As in a perfect gas, the value of Γ changes from point to point within the wave. Pulses or wavetrains having sufficiently large variations of ρ may result in a change in sign of Γ ; this fact is probably most easily seen by inspection of Figure 3.3 (recall that $V = \rho^{-1}$). In such cases, part of the wave will steepen backwards while the other part steepens forward.

An example of the steepening of a triangle wave propagating to the right into a fluid which is uniform and at rest is illustrated in Figure 4.1. The gas model is again that of van der Waals with $c = 50 R$ and the isentrope is that marked $\bar{T} = 1.0$ in Figure 3.2. In this figure, Γ changes sign twice between ρ_0 and the maximum

density $\rho_0(1+A)$. As a result, three shocks, two compression and one expansion, will be formed. The compression shocks form near the peak and at the front at scaled times 0.97 and 0.66, respectively. The expansion shock forms at the rear at a scaled time of 3.24. Early comments on the shock formation process were given by Thompson [1] and Thompson and Lambrakis [41]. The formation of weak shocks with mixed nonlinearity has been given by Cramer and Kluwick [49] and a relatively complete description of finite amplitude waves was given by Cramer and Sen [48].

Shock formation in steady flows may also be considered. The most extensive discussion may be found in the article by Thompson [1]. The main result with respect to shock formation is Thompson's equation (19) which can be written

$$\frac{d\psi}{d\theta} = \frac{M^2}{M^2 - 1} \frac{\rho \Gamma}{a}, \quad (4.5)$$

where M is the local Mach number, θ is the flow deflection angle as measured counterclockwise from the freestream direction and the angle made by the Mach line is given by $\mu_\infty + \psi(\theta)$, where μ_∞ is the Mach angle of the freestream. As expected, the Mach lines diverge rather

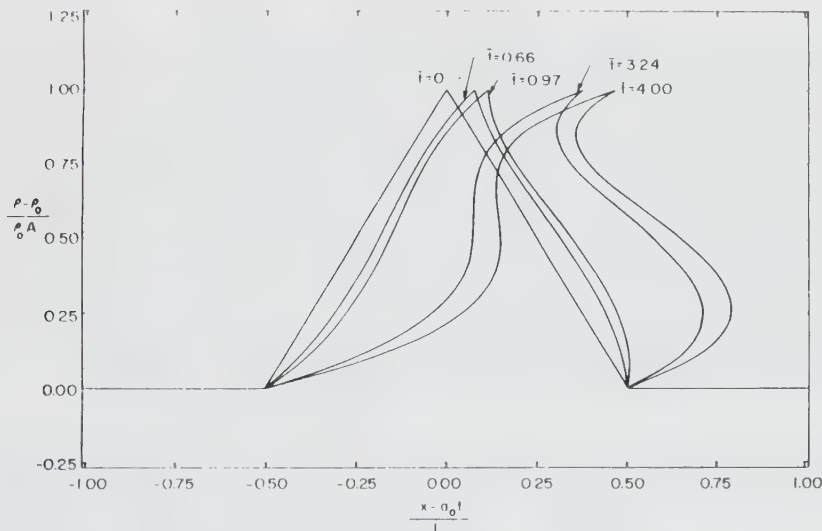


Figure 4.1: Evolution of a right moving triangle pulse. Times are scaled with $x_0 t$ and the initial length.

than converge in a compression corner when $\Gamma < 0$ everywhere in the fluid. Furthermore, when $\Gamma < 0$ the Mach lines tend to converge in regions of expansion thus generating expansion shocks. The Mach line pattern over a standard airfoil shape has been sketched in Figure 4.2.

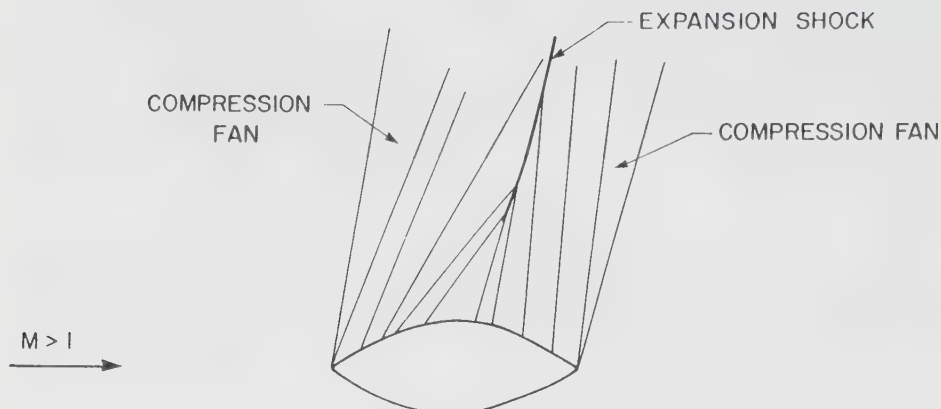


Figure 4.2: Shock formation over a conventional airfoil. $\Gamma < 0$ everywhere in the flow.

From (2.10) it is clear that the minimum value of the ratio of specific heats of any fluid is unity. In Section 2, we have already pointed out that $\rho\Gamma/a$ for perfect gases is given by $(\gamma+1)/2$. Thus, $\rho\Gamma/a \geq 1$ for perfect gases, that is, there is always a lower bound on the strength of the nonlinearity of perfect gases. However, it is clear from Figures 3.1 and 3.3 that arbitrarily small values of the basic nonlinearity parameter $\rho\Gamma/a$ can be attained simply by choosing the undisturbed state judiciously. The fact that nonlinear effects may be suppressed is likely to have advantages in applications. For example, air at atmospheric conditions has $\rho\Gamma/a \approx 1.2$. From Figure 3.3 it is clear that values of 0.12 are easily attained over a wide range of temperatures and pressures. Because shock formation distances and times tend to be inversely proportional to the nonlinearity parameter, the onset of shock waves and harmonic generation can be delayed by a factor of ten in this example. On the other hand, the use of FC-70 (or other BZT fluids) permit disturbance amplitudes which are ten times larger than air for the same likelihood of shock formation or harmonic generation. Applications which may realize significant benefits are processes which involve acoustically enhanced solubility, diffusion, heat transfer and agglomeration. It should also be noted that the nonlinearity of gasdynamic springs and shock absorbers is also proportional to the fundamental derivative. Again, the elimination of harmonic generation, nonlinear resonances and, in some cases, chaos can be accomplished simply by taking advantage of the natural dynamics of BZT fluids.

An intriguing possibility related to the shock formation process is that of isentropic supersonic flows through cascade configurations;

this has been illustrated in Figure 4.3. In ordinary cascade configurations, supersonic flows with $\Gamma > 0$ will generate compression shocks which represent a strong adverse pressure gradient. If these shock waves strike a neighboring blade, shock-induced separation may give rise to major losses and vibration. The latter can have significant impact on the fatigue life. However, if a BZT fluid is

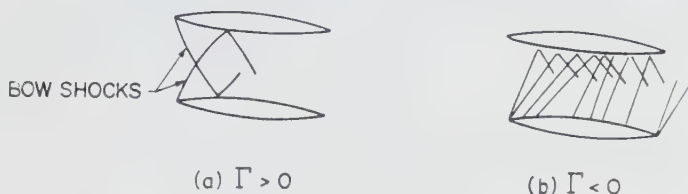


Figure 4.3: Steady flows in cascade configurations.
In (b) only Mach lines emanating from
the lower surface are sketched.

employed with an upstream state corresponding to $\Gamma < 0$, the compression shocks are inadmissible and disintegrate to form centered fans. As a result, the adverse pressure gradients are significantly reduced and it is expected that the boundary layers will remain attached. As indicated in Figure 4.2, the Mach lines in the expansion section will converge and ultimately form an expansion shock if the interblade spacing is large enough. However, if $\rho\Gamma/a$ is relatively small the formation process will be interrupted by the neighboring blade as illustrated in Figure 4.3(b). It therefore appears that we can exploit the natural dynamics of BZT fluids to simultaneously eliminate shock-induced separation and stagnation pressure loss due to the shock irreversibility in a supersonic lifting cascade. Thus, both form and wave drag are eliminated and the flow is entirely isentropic, i.e., lossless, with no modification to the hardware.

We note that the reduction of the adverse pressure gradients and the formation of the expansion shock are both due to the same physical effects and therefore nominally occur at the same rate. Validation of the scenario proposed here will require further numerical and experimental work; the former is now underway at VPI & SU and will be reported in future publications.

5. Shock Adiabat

We note that the material velocities do not appear explicitly in the Hugoniot relation (2.16). Thus, (2.16) can interpreted as the locus of thermodynamic states which can be connected through a shock wave. Because the thermodynamic variables are invariant, conclusions

based solely on a consideration of (2.16) therefore hold for all shock surfaces, including oblique and moving shocks. We will refer to solutions to (2.16), and in particular those represented in the p-V plane, as shock adiabats.

The general shape of the shock adiabat will always appear similar to the isentropes in its neighborhood. In fact, the first and second derivatives of the shock adiabat are identical to those of the isentropes at the same point. As a result, the shock adiabat must have a negative slope in the p-V plane and, in addition, the curvature is downward in regions of negative nonlinearity and upward in regions of positive nonlinearity. A typical shock adiabat going through the region of negative Γ is sketched in Figure 5.1. It is useful to note that these results may be recognized as a manifestation of Bethe's relation for the entropy jump [s] across weak shock waves:

$$[s] = - \frac{\Gamma_1}{6T_1 V_1} \left(\frac{[V]}{V_1} \right)^3 + O\left(\frac{[V]}{V_1} \right)^4. \quad (5.1)$$

Thus, in the neighborhood of a given point V_1, s_1 , the pressures along an isentrope and shock adiabat will be matched to second order. This, of course, is only possible if the slope and curvature are also equal.

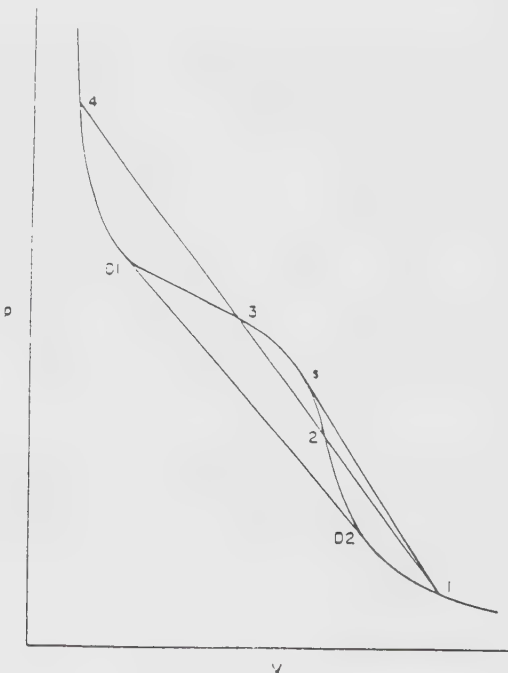


Figure 5.1: Sketch of a shock adiabat going through the $\Gamma < 0$ region.

A Rayleigh line is defined to be the straight line connecting any two points in the p-V plane. Here we will be concerned with Rayleigh lines connecting two points on a shock adiabat. The slope of the Rayleigh line is just $[p]/[V] < 0$, which may be related to the mass flux (2.17) through the momentum equation (2.15). Because of the well-known equivalence between stationary normal shocks and arbitrarily moving and oriented shock waves and the fact that (2.16) contains only thermodynamic quantities, we may restrict our attention to stationary, normal shocks with no loss in generality. In this case, the Mach number can be defined

$$M \equiv \frac{V}{a} , \quad (5.2)$$

where V is the flow velocity. Thus, the slope of the Rayleigh line can be written

$$\frac{[p]}{[V]} = -m^2 = -(\alpha_1 \rho_1)^2 M_1^2 = -(\alpha_2 \rho_2)^2 M_2^2 . \quad (5.3)$$

A useful relation between the slope of the shock adiabat and that of the Rayleigh line is

$$M_i < 1 \text{ whenever } \left. \frac{dp}{dV} \right|_i < \frac{[p]}{[V]} , \quad (5.4)$$

where $i = 1$ or 2 and $(dp/dV)|_i$ is the slope of the shock adiabat $p = p(V)$ evaluated at $V = V_i$. Thus, we may determine whether the flow is subsonic or supersonic through a straightforward comparison of the slopes of the shock adiabat and Rayleigh line. For example, point 3 in Figure 5.1 corresponds to a supersonic flow ($M_3 > 1$) because the slope of the adiabat at 3 is greater (less negative) than that of the Rayleigh line 1-3 or 3-4. Of particular interest here are shocks having a Rayleigh line which is tangent to the adiabat. In this case, the Mach number at point i is identically one and, for this reason, we refer to these shocks as sonic. (The earlier studies of P. A. Thompson refer to these as Chapman-Jouguet shocks after the related phenomena in detonation wave theory.) One such example is the shock represented by 1-s in Figure 5.1; the sonic point is at s. It is clear that sonic shocks can only occur in problems of mixed nonlinearity. If we set $M_2 = 1$ in (5.3) we also find

$$\left. \frac{dp}{dV} \right|_2 = \frac{[p]}{[V]} = -\left(\frac{\alpha_2}{V_2} \right)^2 = \left. \frac{\partial p}{\partial V} \right|_s (V_2, s_2) . \quad (5.5)$$

Thus, at a sonic point, the shock adiabat, Rayleigh line and isentrope are all tangent.

Shock adiabats of the form shown in Figure 5.1, i.e., those having two inflection points, can have two tangency points. These are the double sonic shocks described in Section 4 of Thompson and Lambrakis [41] and are represented by D1-D2 in Figure 5.1.

Further solutions for weak sonic shocks have been given by Cramer and Kluwick [49]. Exact solutions for finite amplitude sonic shocks in van der Waals gases have been provided by Cramer and Sen [50]. We should also refer the reader to Section 5 of the article by Thompson and Lambrakis [41] for an alternate derivation of relations (5.4).

The variation of the entropy may be derived by differentiating (2.16), holding state 1 constant. Direct use of Gibbs' equation (2.6) yields

$$T_2 \frac{ds_2}{dV_2} = -\frac{[V]}{2} \left\{ \frac{dp_2}{dV_2} - \frac{[p]}{[V]} \right\} = \frac{[V]^2}{2} \frac{dm^2}{dV_2}. \quad (5.6)$$

Relations equivalent to (5.6) were given by Bethe [36]. From the first of (5.6), it is clear that the entropy has an extremum at sonic points. Clearly, Bethe's monotone increase of entropy is not guaranteed if mixed nonlinearity is present.

Before moving on, we summarize our results for sonic shocks. At the sonic point, say point 2,

- (i) $M_2 = 1$ (by definition).
- (ii) The Rayleigh line is tangent to the shock adiabat at 2 as well as the isentrope $s = s_2$.
- (iii) The entropy has a local maximum or minimum.
- (iv) The mass flux, and from (5.3), M_1 has a local maximum or minimum.

Here point 2 may refer to either the upstream or downstream state. Results (i), (iii) and (iv) are illustrated in Figure 5.2. Here the Hugoniot relation (2.16b) was solved iteratively for PP10. The gas model is that used by Cramer [43], i.e., the Martin-Hou equation combined with a power law c_{∞} . As discussed in Section 6, shocks having supersonic downstream Mach numbers are inadmissible. However, to illustrate the variation of the entropy and Mach numbers we have continued these curves into the inadmissible region.

The sign of the entropy jump may be deduced from the following identity

$$\int_{s_1}^{s_2} T ds = A_H - A_R \quad (5.7)$$

where

$$A_H \equiv \int_{V_1}^{V_2} p dV$$

is the area under the shock adiabat from state 1 to 2 and

$$A_R = \frac{p_2 + p_1}{2} [V]$$

is the area under the Rayleigh line connecting states 1 and 2. Its derivation combines (2.16b) with a straightforward integration of Gibbs' relation (2.6). Because $T > 0$, the sign of $[s]$ is the sign of the integral on the left of (5.7). To illustrate the application of this result we consider shock 2-3 and the double sonic shock D1-D2 in Figure 5.1. From (5.7) it is clear that both shocks must be expansion shocks in order to satisfy the entropy inequality.

At this stage we may recover the classical theory. The shock adiabats of fluids having $\Gamma > 0$ at all temperatures and pressures are always concave up. Thus, the Rayleigh line always lies above the adiabat. From (5.7) we conclude that the only shocks satisfying the entropy inequality (2.18) are compression shocks. Application of (5.4) shows that such shocks necessarily have supersonic upstream conditions and subsonic downstream conditions. In like manner, if we consider a range of temperatures and pressures such that $\Gamma < 0$ everywhere, then (5.7) implies that compression shocks always violate the entropy inequality and expansion shocks are the only type possible. As in the case of positive Γ , these expansion shocks also result in a supersonic-subsonic transition.

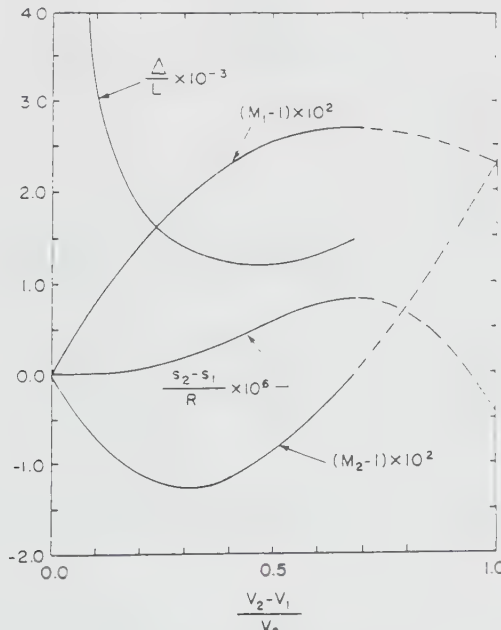


Figure 5.2: Variation of Mach numbers, entropy jump and thickness along a shock adiabat. Fluid is PP10 with $V_1 = 1.75 V_c$, $T_1 = 0.99 T_c$, $p_1 = 0.9194 p_c$, $c_1/a_1 = -0.298$.

6. Dissipative Structure and Existence Criteria

The usual model for the dissipative structure takes the flow to be steady, one-dimensional and governed by the Navier-Stokes equations. The resultant system is a set of three equations expressing conservation of mass, momentum and energy. It is well-known that the first integral of these equations may be written

$$\rho v = m \quad (6.1)$$

$$(\lambda + 2\mu)v' = F(v, T) \equiv p - p_i + m(v - v_i) \quad (6.2)$$

$$kT' = G(v, T) \equiv m(e - e_i) + p_i(v - v_i) + \frac{m}{2} (v - v_i)^2. \quad (6.3)$$

where primes denote differentiation with respect to the distance in the flow direction x and the subscripts i denote either the upstream ($i=1$) or downstream ($i=2$) state. The constant m is the mass flux (identical to (2.17) for the case considered here) and inequalities (2.7) may be employed to show that $\lambda + 2\mu > 0$. The solutions to (6.1)-(6.3) are required to approach constants as $x \rightarrow \pm \infty$. In particular

$$\begin{aligned} T, v &\rightarrow T_1, v_1 \text{ as } x \rightarrow -\infty \\ T, v &\rightarrow T_2, v_2 \text{ as } x \rightarrow \infty. \end{aligned} \quad (6.4)$$

When (6.4) are applied to (6.1)-(6.3) we find that the Rankine-Hugoniot conditions (2.13)-(2.16) are recovered. In particular, it may be shown that an alternate expression for (2.13)-(2.16) simplified for the present case may be taken to be

$$m = \text{constant}, \quad F(v_j, T_j) = 0, \quad G(v_j, T_j) = 0, \quad (6.5)$$

where j can also be either 1 or 2 but is not necessarily equal to i . The case where $j=i$ is, of course, the trivial solution of a shock of zero strength.

In addition to the recovery of the Rankine-Hugoniot conditions, the well-known identity

$$m[s] = \int_{-\infty}^{\infty} \left\{ \frac{\lambda + 2\mu}{T} \left(\frac{dv}{dx} \right)^2 + \frac{k}{T^2} \left(\frac{dT}{dx} \right)^2 \right\} dx,$$

(derived by combining (2.3) with (2.6) and then integrating through the shock layer) combined with the inequalities $k > 0$, $\lambda + 2\mu > 0$ may be used

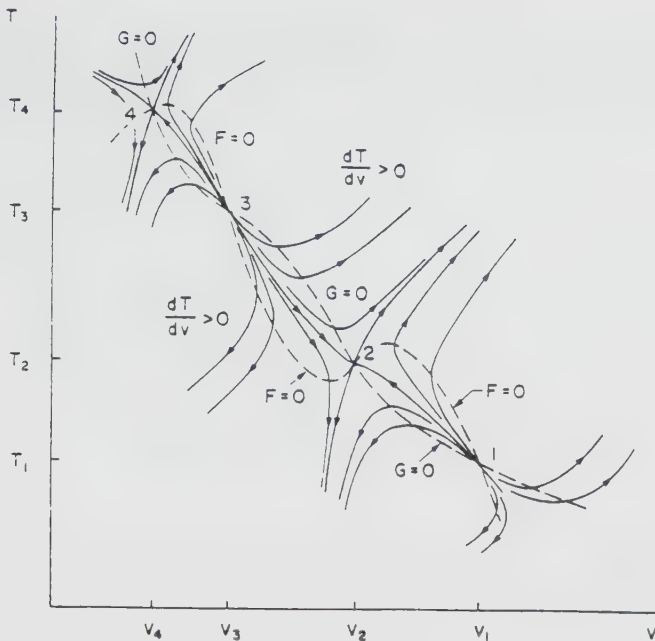


Figure 6.1: T - v phase-plane with mixed nonlinearity. Points 1, 2, 3, 4 correspond to those of Figure 5.1.

to derive the entropy inequality (2.18) for the shock wave. That is, every shock having an acceptable structure satisfying (6.1)-(6.4) results in an increase in entropy. This should hardly be surprising as the imposition of (2.7) guarantees that all motions of the Navier-Stokes-Fourier equations satisfy the second law of thermodynamics in the form of the Clausius-Duhem inequality. Furthermore, an analysis of (6.1)-(6.3) in the neighborhood of the asymptotes (which are singular points in the T - v phase plane), shows that upstream conditions are necessarily supersonic whereas downstream conditions are necessarily subsonic. Thus, both the principle of increasing entropy and the supersonic-subsonic transition are implied by the existence of a dissipative structure. Although application of either condition is sufficient to guarantee the existence of a shock where Γ is strictly positive or strictly negative, a more general sufficiency condition is required when mixed nonlinearity is present. This condition is given in the following development.

When Γ is strictly positive the shock adiabat is concave up and there are only two roots to (6.5). The existence and uniqueness of a solution curve to (6.1)-(6.3) which satisfies (6.4) was first given by Gilbarg [51]. When Γ is strictly negative, the adiabat is concave down and there are again only two points at which the Rayleigh line

intersects the adiabat. It is a straightforward exercise to extend Gilbarg's arguments to this case. Thus, if Γ is either strictly positive or strictly negative, the existence of a transition between the inviscid states is guaranteed. If $\Gamma > 0$, it can be shown that the shock will be a compression shock and if $\Gamma < 0$ it will be an expansion shock.

The Rankine-Hugoniot conditions (2.13)-(2.16) or (6.5) have more than two solutions when problems involving mixed nonlinearity are considered, see, e.g., Figure 5.1. The analysis of Gilbarg may be applied to pairs of neighboring roots to demonstrate the existence and uniqueness of solution curves between neighboring pairs. However, the new issue raised by the existence of additional roots is whether solution curves exist between non-neighboring roots. The fact that such solutions are impossible is most easily seen by an inspection of the T-v phase plane. The correct form for the phase plane has been sketched in Figure 6.1 and the relevant arguments justifying the sketch have been provided by Cramer [52] and Menikoff and Plohr [53].

Because no solution connecting non-neighboring points may be constructed we conclude that solution curves are only possible between neighboring roots. A solution starting at any root will inevitably be attracted to the appropriate neighboring root and will arrive at that root only as $x \rightarrow +\infty$. Thus, if the Rayleigh line connecting two shock states p_1, V_1 and p_2, V_2 on an adiabat intersects the adiabat at an intermediate point p', V' , then no dissipative structure may be constructed and the corresponding shock between states 1 and 2 is inadmissible. This is recognized as equivalent to Lax's generalized entropy condition [54] which states that the straight line connecting acceptable upstream and downstream states lies entirely above or entirely below the adiabat connecting these points.

It is of interest to note that we can construct discontinuities which satisfy all the conventional requirements placed on the upstream and downstream states, that is, they satisfy the Rankine-Hugoniot jump conditions (2.13)-(2.16), the entropy inequality (2.18) and result in a supersonic-subsonic transition of the flow, but do not have an acceptable internal structure due to the existence of intermediate intersections. Such a discontinuity is therefore inadmissible and will not remain intact as a pure discontinuity. An example is the discontinuity represented by 1-4 in Figure 5.1. A numerical example is the case of a van der Waals gas with $c_v = 50R$ and upstream pressure, density and Mach number given by $0.85 p_c$, $0.5 \rho_c$ and 1.0124 , where the subscripts c denote quantities evaluated at the thermodynamic critical point. The downstream pressure, Mach number and the entropy jump are then computed to be $1.1 p_c$, 0.696 and $0.9 \times 10^{-3} R$, approximately. It may be verified that this proposed shock is of the same type as 1-4 in Figure 5.1, i.e., the Rayleigh line intersects the adiabat at two points between the proposed upstream and downstream states.

To summarize, the basic existence issues are clearly more complicated when the scope is extended to include BZT fluids. The existence of a shock of some type is guaranteed if the Rayleigh line lies entirely above or below the shock adiabat. (Cases having intermediate intersections will not have a physically realizable dissipative structure and are not admissible.) Application of the entropy inequality then determines the correct direction of the jump. The final result may be stated:

A compression shock between two states satisfying (2.13)-(2.16) exists if and only if the Rayleigh line lies entirely above the shock adiabat and is of the expansion type if the Rayleigh line lies entirely below the shock adiabat.

The inequalities (5.4) may be used to show that acceptable shocks of both types will always take the flow from supersonic to subsonic conditions.

Clearly, this principle can be simplified further for fluids having $\gamma > 0$ at all temperatures and pressures. Under the conditions assumed here, the shock adiabat is necessarily concave up and the Rayleigh line will always lie above the adiabat. Thus, the only types of shocks occurring for $\gamma > 0$ fluids are compression shocks. This, of course, is in complete agreement with the results of the perfect gas theory.

7. Evolution - Unsteady Flows

In the theory of perfect gases, an expansion discontinuity, once inserted in the flow, will spread to form a centered expansion fan. Here it is also useful to ask what happens to an inadmissible discontinuity if inserted in a BZT fluid. The simplest case is where the sign of Γ does not change anywhere in the flow, including inside the shock. If the discontinuity is inadmissible, the result is again a centered expansion ($\Gamma > 0$) or compression ($\Gamma < 0$) fan. If Γ only changes sign once across the inadmissible shock, it will undergo a partial disintegration into a centered fan and sonic shock. An example

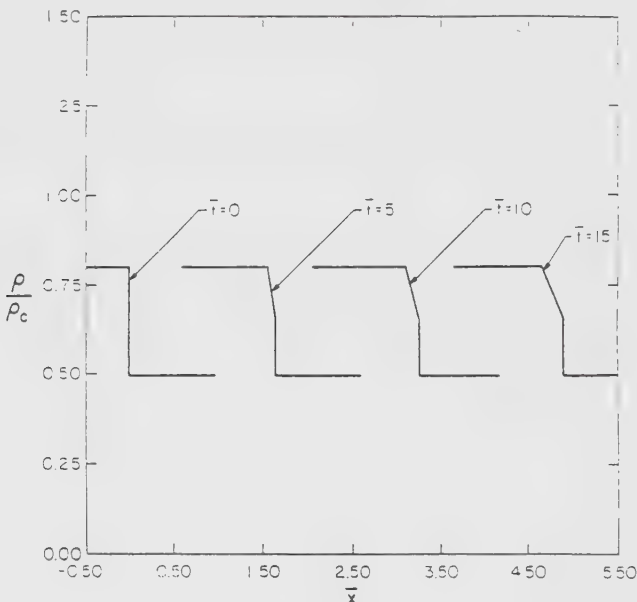


Figure 7.1: Computed evolution of step function initial condition with mixed nonlinearity. The undisturbed state is at rest at $\rho_0 = 0.497\rho_c$. \bar{x} and \bar{t} are scaled position and time.

of the partial disintegration of compression shocks is plotted in Figure 7.1. The latter was computed using the exact solutions of Cramer and Sen [50]. Further exact solutions for the partial breakup of expansion discontinuities, including the generation of double sonic shocks, have also been given by Cramer and Sen [50]. A p-V diagram corresponding to a breakup of the type depicted in Figure 7.1 is found in Figure 7.2.

The evolution depicted in Figures 7.1-7.2 corresponds to cases where Γ changes sign once across the proposed discontinuity. As one might expect, new features arise when we relax our condition that Γ can only change sign once in the flow of interest. Expansive discontinuities

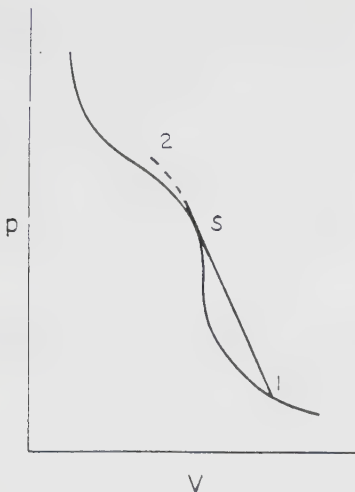


Figure 7.2: p-V diagram corresponding to Figure 7.1. Sonic shock is represented by 1-s and isentropic compression is the dotted line from s to 2.

nuities of the type 4-1 in Figure 5.1 will break up into a double sonic shock embedded between two centered expansion fans. Compressive discontinuities of the type 1-4 will result in shock-splitting, i.e., the discontinuity will break up into two sonic compression shocks separated by a centered compression fan. This fact is most easily motivated by reconsidering the compression shock-fan depicted in Figures 7.1 and 7.2. If we continue to increase the density or pressure following the shock-fan combination, the isentrope necessarily passes out of the negative Γ region. If this occurs, the convected sound speed will have a local minimum at the density corresponding to $\Gamma = 0$ and overturned, triple-valued solutions will appear in the compression fans, necessitating the insertion of a second shock at the trailing edge of the fan. The resultant p-V diagram is sketched in Figure 7.3. A discussion of the formation of the split-shock configuration from smooth initial conditions may be found in the article by Cramer [52].

In Figure 7.4, the result of a continuous increase in the downstream density of the proposed discontinuity is depicted. These plots have been taken from Cramer [52] which were computed by the exact solutions of Cramer and Sen [50]. Each case is plotted at identical times for purposes of comparison. If the strength of the discontinuity is relatively small, it remains intact as a classical compression shock. The partial disintegration occurs at larger amplitudes. This is

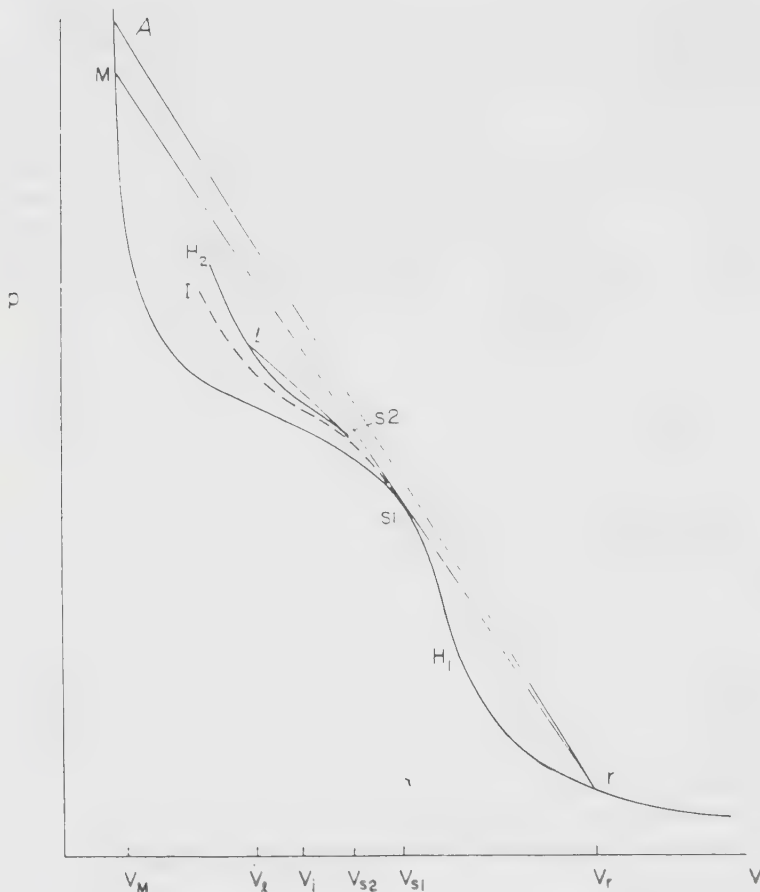


Figure 7.3: p-V diagram for shock-splitting. Shock adiabats are marked H_1 , H_2 , and the isentropic compression is represented by I . Forerunner shock is represented by $r - s_1$. and second shock is represented by $s_2 - \ell$.

the case having a density of approximately $0.75 \rho_c$ at the far left. At larger amplitudes a second shock forms resulting in the split-shock configuration. As the density after the initial discontinuity is increased, the second shock increases in strength and moves forward through the compression fan. At the point where the Rayleigh line is exactly tangent to the negative Γ hump in the shock adiabat, the second sonic shock merges with the leading shock. Further increases in the downstream density result in an admissible discontinuity (the Rayleigh line no longer intersects the adiabat) which therefore remains intact as a classical compression shock. This is the large amplitude shock having a downstream density of $1.4 \rho_c$, approximately, in Figure 7.4.

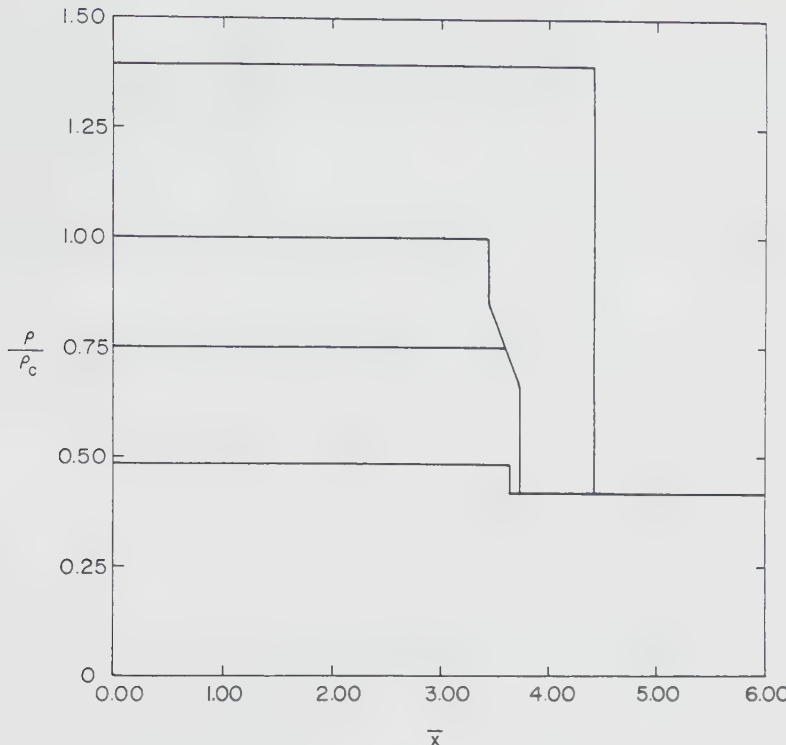


Figure 7.4: Computed waveforms for four step function initial conditions. Initial discontinuity was originally at $x=0$ and each distribution is plotted at the same time. Fluid is van der Waals with $c_v = 50R$ and the computational technique is described by Cramer [52]. Undisturbed state is at rest with $c_0 = 0.42c_c$ and $p_0 = 0.75 p_c$.

In conclusion, we note that the significance of sonic shocks is that they are always generated by the partial disintegration of inadmissible discontinuities. Further discussion of the role of sonic shocks in the disintegration of weak gasdynamic shocks is found in the articles by Cramer and Kluwick [49] and Cramer, Kluwick, Watson and Pelz [55]. Developments involving finite strength waves include those of Thompson and Lambrakis [41], Cramer and Sen [50], Cramer [52] and Menikoff and Plohr [53].

8. Dissipative Structure - Nonclassical Details

In this section we give an overview of the nonclassical features of the dissipative structure of shock waves in BZT fluids. We begin by summarizing the weak shock theory of Cramer and Kluwick [49] and Cramer [56]. This is seen to be the natural extension of Taylor's [57] theory. Cramer and Kluwick's theory incorporates mixed nonlinearity by assuming that the undisturbed state is in the vicinity of the $r = 0$ locus, i.e.,

$$\frac{\rho_0 \Gamma_0}{a_0} = O\left(\frac{\rho - \rho_0}{\rho_0}\right) = o(1), \quad (8.1)$$

where the subscripts 0 denote quantities evaluated at the undisturbed state. As a result, the local value of the fundamental derivative

$$\Gamma \approx \Gamma_0 + \left. \frac{\partial \Gamma}{\partial \rho} \right|_S (\rho - \rho_0) + \dots$$

can change sign even though the disturbances are small. The results of these two studies can be summarized as follows:

- i) The solution in a sonic shock approaches the asymptote corresponding to the sonic condition algebraically rather than exponentially.
- ii) This algebraic approach is considerably slower than the exponential approach and gives rise to a thickening of the shock as the sonic condition is approached.
- iii) The Mach number has an extremum where the local value of Γ changes sign.
- iv) All expansion shocks in both the $\rho\Gamma/a = O(1)$ theory as well as in the Cramer-Kluwick approximation correspond to an entropy deficit. That is, $s(x) < s_1$ over most of the shock layer although the entropy ultimately exceeds the upstream value as the downstream conditions are approached.

Remarks similar to (i) have also been made by Lee-Baptist and Crighton [58]. With respect to point (ii), we note that the thickening can lead to an increase in thickness with strength rather than the well-known decrease of the classical weak shock theory. This will occur when the sonic shock is the shock of maximum strength. In the Cramer-Kluwick theory such shocks are only possible if

$$\left. \frac{\partial \Gamma}{\partial \rho} \right|_S (\rho_0, s_0) < 0.$$

We have computed and plotted the thickness based on the maximum slope criterion for the Cramer-Kluwick theory and the conventional Taylor ($\rho\Gamma/a = O(1)$) theory; the results are found in Figure 8.1. As pointed out by Cramer [56], this thickening could easily be misinterpreted as a manifestation of relaxation or the well-known increase in thickness due to temperature-dependent viscosities. However, the viscosities are held constant in either type of weak shock theory. Thus, the thickening is due to the weakening of the internal nonlinear effects as the sonic condition is approached inside the shock layer.

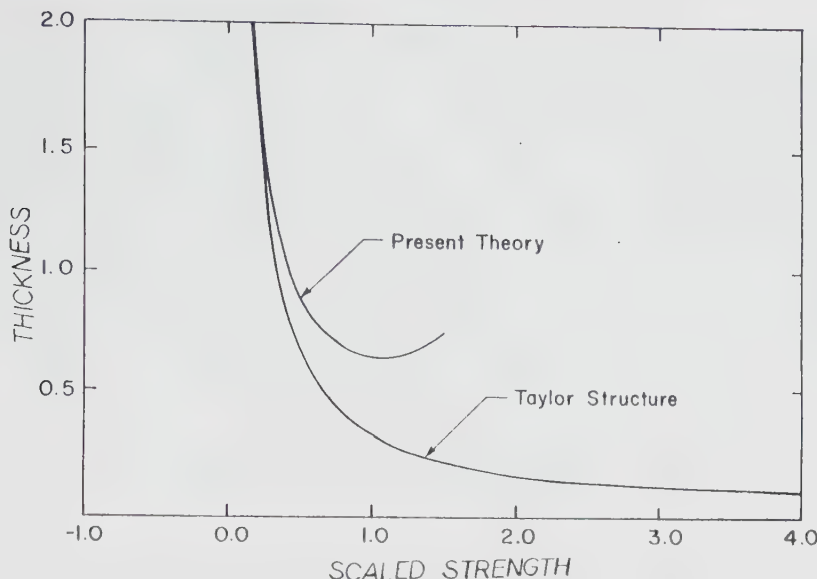


Figure 8.1: Variation of scaled thickness with scaled strength for $(\alpha/\alpha_0)|_{\Gamma} < 0$. Present theory denotes that of Cramer and Kluwick [49] and Cramer [56]. Curve is terminated at sonic state.

Result (iii) also contrasts with the perfect gas theory where the Mach number normally decreases monotonically through a weak shock from supersonic to subsonic conditions. Result (iv) also contrasts with the standard perfect gas theory where the entropy remains greater than the upstream value at every point within the shock layer.

The weak shock approximation of Cramer and Kluwick [49] is limited to shocks having no more than one sign change of Γ in the interior of the shock layer. In order to verify these approximate results and extend the scope to include shocks which take the fluid from one side of the negative Γ region to the other (resulting in two sign changes of Γ) the author, along with A. B. Crickenberger, has developed a numerical scheme capable of integrating the exact structure equations (6.1)-(6.3) for arbitrary gas models. The full details of our results will appear in future publications. Here we will simply outline the approach and summarize some of the more interesting findings.

$\frac{V_2}{V_c}$	$\frac{P_2}{P_c}$	$\frac{T_2}{T_c}$	$\frac{r_2 \rho_2}{a_2}$	M_1	M_2	$\frac{s_2 - s_1}{R} \times 10^5$	$\frac{\Delta}{L}$
1.95	0.8896	0.9876	-0.1633	1.014	0.989	0.72	1768
2.15	0.8589	0.9855	-0.0222	1.023	0.988	3.93	1231
2.35	0.8279	0.9836	0.1002	1.027	0.995	7.63	1290

Table 8.1: Numerical Data for Figures 8.2-8.4. Fluid is PP10 with $V_1 = 1.75V_c$, $T_1 = 0.99T_c$, $P_1 = 0.9194P_c$, $r_1 r_1/a_1 = -0.298$, $\mu_b/\mu = 0.5$.

$\frac{V_2}{V_c}$	$\frac{P_2}{P_c}$	$\frac{T_2}{T_c}$	$\frac{r_2 \rho_2}{a_2}$	M_1	M_2	$\frac{s_2 - s_1}{R} \times 10^5$
1.3000	1.0528	1.0088	0.8330	1.017	0.949	13.94
1.2875	1.0551	1.0089	0.8979	1.017	0.942	18.04
1.2750	1.0575	1.0091	0.9644	1.018	0.934	22.82
1.2625	1.0599	1.0092	1.0322	1.019	0.926	28.36
1.2500	1.0624	1.0094	1.1011	1.020	0.917	34.76
1.2375	1.0649	1.0096	1.1707	1.021	0.907	42.10
1.2250	1.0675	1.0097	1.2408	1.022	0.897	50.50

Table 8.2: Numerical Data for Figures 8.5-8.7. Fluid is FC-71 with $V_1 = 2.5 V_c$, $T_1 = T_c$, $P_1 = 0.8523 P_c$, $r_1 r_1/a_1 = 0.2160$ and $\mu_b/\mu = 0$.

The general scheme was to regard the problem as that of an initial value problem. Because of the well-known numerical instabilities associated with the approach to the saddle point at the downstream side of the shock, the integration was started in the vicinity of this saddle point and then marched upstream. For each of the examples given below the Martin-Hou equation and the power law model for $c_v(T)$ discussed in Section 3 were employed. The shear viscosity and thermal conductivity were estimated by the dense gas models of Chung, Ajlan, Lee and Starling as described in Reid, Prausnitz and Poling [59]. Due to a lack of data, the ratio μ_b/μ , where μ_b is the bulk viscosity introduced in (2.7) and μ is the shear viscosity, was assumed to be constant with both temperature and pressure. Again, due to lack of data, the value of this ratio was chosen rather arbitrarily although different choices appear to make no difference in the qualitative features observed.

In all figures, the distance is scaled with

$$L \equiv \mu_* \left(\frac{V}{p_c} \right)^{\frac{1}{2}},$$

where μ_* is the shear viscosity computed at a reference state, typically the critical temperature and one atmosphere. In each set of cases the reference state is fixed. Thus, no rescaling is required to account for different shock strengths. In Tables 8.1-8.2 we have also listed estimates for the thickness Δ . These were again computed on the basis of the maximum slope of the $(V-V_1)/(V_2-V_1)$ vs. x/L curves.

The first example is a series of expansion shocks in PP10. The upstream state was taken to be

$$V_1 = 1.75V_c, T_1 = 0.99T_c, p_1 = 0.9194p_c, \Gamma_1 \rho_1 / a_1 = -0.298.$$

At this temperature, the saturation pressure is estimated to be $0.924p_c$; thus, the upstream state is just to the right of the saturated vapor curve in the p - V diagram. The downstream conditions, Mach numbers and scaled thickness are listed in Table 8.1 and the nondimensional variations of specific volume, entropy and Mach number are plotted in Figures 8.2-8.4. The entropy jump, Mach numbers and thickness for this fluid and upstream conditions have also been plotted in Figure 5.2. In Figure 5.2, it can be seen that the sonic condition is attained at $V_2 \approx 2.44 V_c$. Even though the strongest shock in Figures 8.2-8.4 is not yet sonic, the relatively slow approach to the downstream conditions can already be seen. This series of shocks also has a local minimum in the thickness at about $V_2 = 2.2V_c$. The minimum is clearly evident in both Figure 5.2 and Table 8.1, thus providing some verification of result (ii) of the weak shock theory. The entropy variation also verifies the predictions of Cramer [56]. Although $s < s_1$ over most of the shock layer, the nondimensional entropy becomes positive as the downstream conditions are approached. In Table 8.1 it can be seen that the strongest shock crosses the $r = 0$ locus ($r_2 > 0$). As predicted by

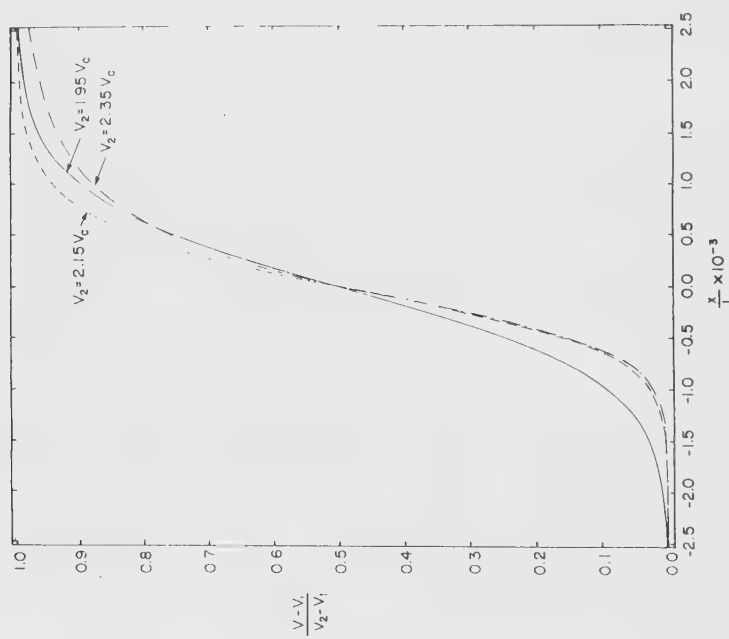


Figure 8.2: Variation of specific volume vs. x . Fluid is PP10 with upstream state $V_1 = 1.75V_c$, $T_1 = 0.99T_c$, $P_1 = 0.9194P_c$, $\rho_1/a_1 = -0.298$ and $u_b/u_a = 0.5$.

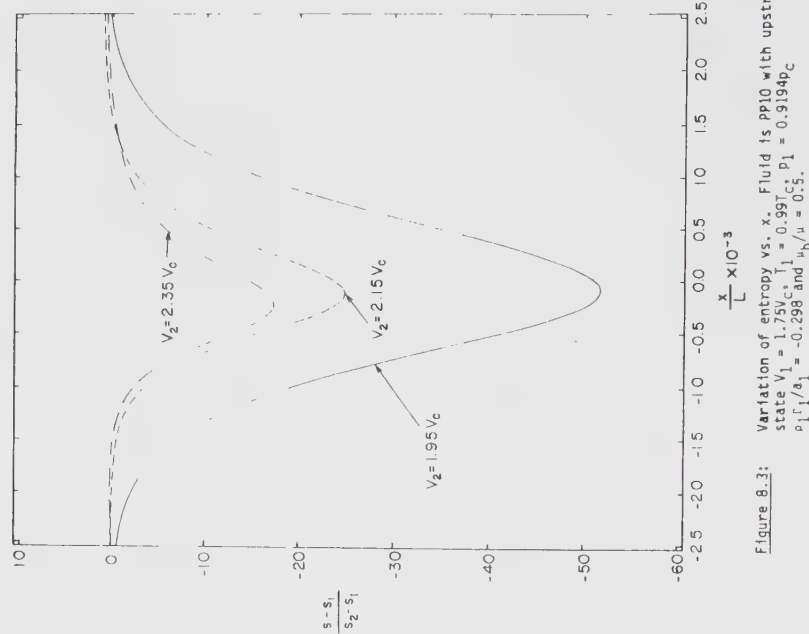


Figure 8.3: Variation of entropy vs. x . Fluid is PP10 with upstream state $V_1 = 1.75V_c$, $T_1 = 0.99T_c$, $P_1 = 0.9194P_c$, $\rho_1/a_1 = -0.298$ and $u_b/u_a = 0.5$.

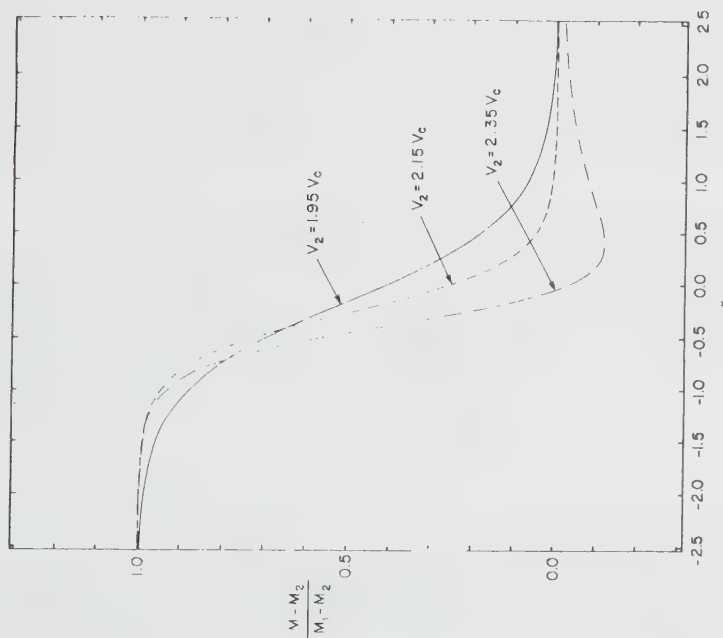


Figure 8.4:
Variation of Mach number vs. x . Fluid is PP10 with upstream state $V_1 = 1.75V_c$, $T_1 = 0.99T_c$, $p_1 = 0.9194p_c$, $\rho_1/a_1 = -0.298$ and $u_b/a_1 = -0.216$ and $u_b = 0$.

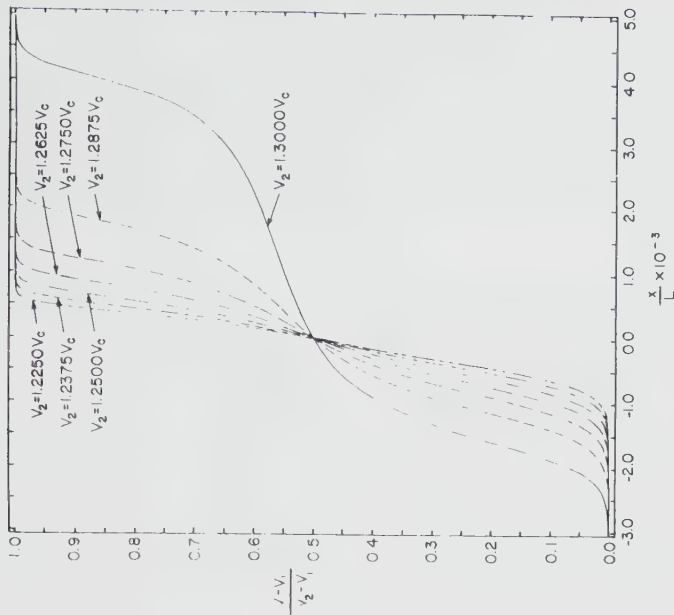


Figure 8.5:
Variation of specific volume vs. x . Fluid is FC-71 with upstream state $V_1 = 2.5V_c$, $T_1 = T_c$, $p_1 = 0.853p_c$, $\rho_1/a_1 = 0.216$ and $u_b = 0$.

Figure 8.5:
Variation of specific volume vs. x . Fluid is FC-71 with upstream state $V_1 = 2.5V_c$, $T_1 = T_c$, $p_1 = 0.853p_c$, $\rho_1/a_1 = 0.216$ and $u_b = 0$.

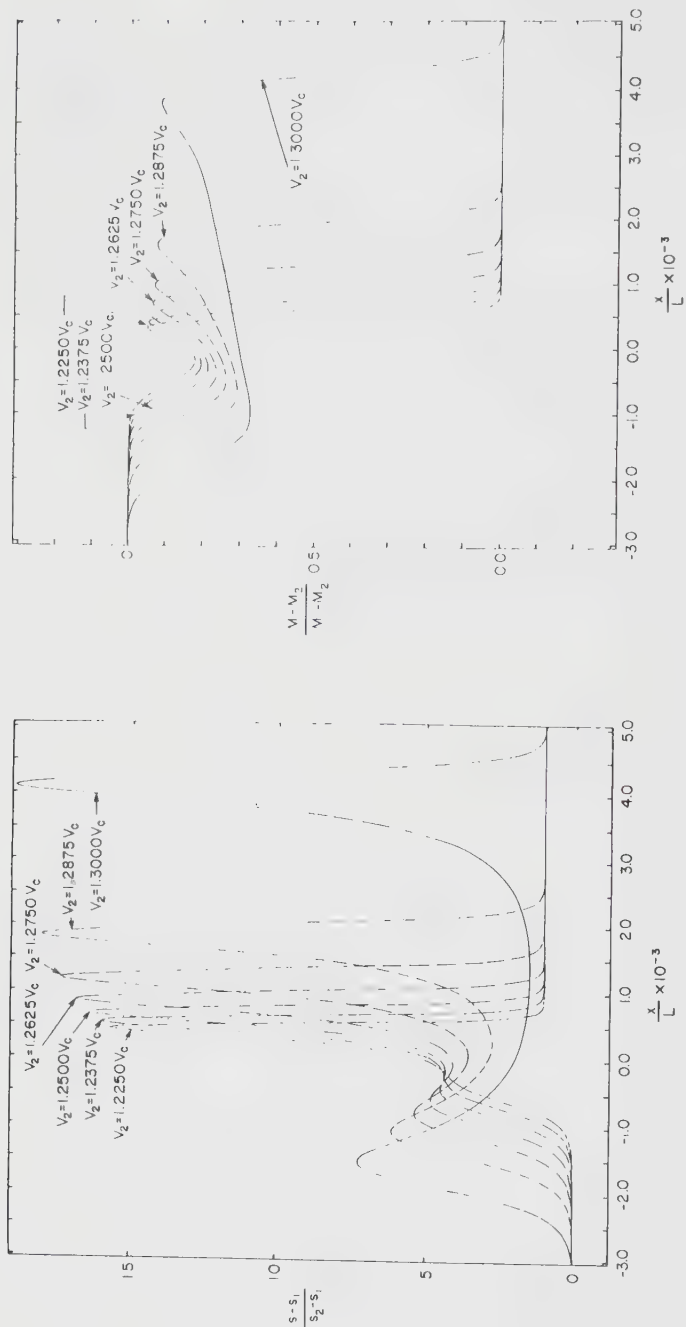


Figure 8.6: Variation of entropy vs. x . Fluid is FC-71 with upstream state $V_1 = 2.5V_c$, $T_1 = T_c$, $P_1 = 0.8523P_c$, $\rho_1/a_1 = 0.216$ and $\gamma_b = 0$.

Figure 8.7: Variation of Mach number vs. x . Fluid is FC-71 with upstream state $V_1 = 2.5V_c$, $T_1 = T_c$, $P_1 = 0.8523P_c$, $\rho_1/a_1 = 0.216$ and $\gamma_b = 0$.

the weak shock theory, the Mach number variation in Figure 8.4 has a local minimum.

At this stage, it is useful to give dimensional results for the thermodynamic variables. From Tables 3.1 and 8.1 we find that the $V_2 = 2.35V_C$ shock results in dimensional pressure and temperature jumps of $p_2 - p_1 = -1.5$ atmosphere and $T_2 - T_1 = -4.0^\circ\text{C}$. The relatively small temperature drop is to be expected in light of the large specific heats involved.

Results which were completely unanticipated are represented in the next series of shocks. The fluid chosen was FC-71 and the upstream state was taken to be to the right of the negative r region in the p-V diagram. The upstream state is given in the captions to Figures 8.5-8.7 and Table 8.2. The shocks then take the flow all the way through the region of negative nonlinearity. These shocks are therefore similar to the strongest shock seen in Figure 7.4 and r-A of Figure 7.3. The most dramatic new features are seen in Figure 8.5. As the shocks become weaker (the weakest shock is that having $V_2 = 1.3V_C$) two additional inflection points in the V vs. x curves become evident. Both the classical weak shock theory and that of Cramer and Kluwick [49] can only admit one inflection point in the V vs. x curve. The entropy distribution plotted in Figure 8.6 gives further clues as to the process. The weakening of the shock leads to a splitting of the single hump ordinarily associated with the entropy variation. In fact, the weakest shocks appear to have undergone an internal splitting reminiscent of the shock-splitting described in Section 7. The explanation for this phenomenon is that we are approaching the shock-splitting condition (where the middle of the Rayleigh line first makes contact with the negative r hump of the shock adiabat) as the shock is weakened. The internal structure is simply anticipating the inviscid splitting. For this reason we refer to this phenomenon as impending shock-splitting.

A second new result is seen in the Mach number distributions plotted in Figure 8.7. In each case, the local maximum corresponds to a Mach number of 1.01 or larger. It appears that this class of shock can have an internal layer of supersonic flow, i.e., after first decelerating to subsonic conditions, the flow accelerates to supersonic conditions before again decelerating to the subsonic downstream state.

* We have, of course, checked the admissibility of this shock. The Rayleigh line was found to lie entirely above the adiabat. Thus, in terms of the inviscid theory, the shock appears as a single discontinuity.

As the shock strength increases, the additional inflection points in the V vs. x curves vanish and the entropy distribution returns to the classical single-hump configuration. The latter can already be seen in Figure 8.6 although the extra inflection points still appear in Figure 8.5.

The author has further analyzed impending shock-splitting through use of an extension of the Cramer-Kluwick approximation. Condition (8.1) is replaced by

$$\frac{\rho_0 \Gamma_0}{a_0} = 0 \left(\frac{\rho - \rho_0}{\rho_0} \right)^2, \quad \left. \frac{\rho_0}{a_0} \frac{\partial \Gamma}{\partial \rho} \right|_S (\rho_0, s_0) = 0 \left(\frac{\rho - \rho_0}{\rho_0} \right) \text{ and } \left. \frac{\rho_0}{a_0} \frac{\partial^2 \Gamma}{\partial \rho^2} \right|_S (\rho_0, s_0) = 0 \quad (1)$$

which is appropriate in the vicinity of the peak of the negative Γ locus depicted in Figure 3.1. When applied to the shock structure, the main result of interest is that the V vs. x curve will have an inflection point at each V where the Rayleigh line is parallel to the shock adiabat. The reader can easily verify that three such parallel points will always occur as the shock strength is decreased toward the shock-splitting condition. In the context of this approximation, the condition for impending shock-splitting can be shown to be

$$V_1 > V_{ir}, \quad \left. \frac{dp}{dV} \right|_{ir} < \frac{[p]}{[V]},$$

where V_{ir} is the specific volume at the right-most inflection point on the shock adiabat and $(dp/dV)_{ir}$ is the slope of the shock adiabat there. Furthermore, it can be shown that the entropy distribution has an extremum at each inflection point in the V vs. x curve (see, e.g., (87.5) of Landau and Lifshitz [60]). As in the Cramer-Kluwick approximation, extrema in the Mach number are also expected whenever $r = 0$. Each of these results appear to be consistent with the numerical results illustrated in Figures 8.2-8.7 and provide some guidance as to when each phenomenon is to be expected. Further details of this approximate theory along with explicit solutions will be presented in future publications.

9. Steady Isentropic Flow - Variable Area Ducts

We now consider the flow of BZT fluids through variable area ducts or streamtubes. The usual assumptions of quasi one-dimensional, isentropic, inviscid ($\lambda, \mu, k = 0$) flow are made. The body forces and volumetric energy supply are also taken to be zero. The governing equations are typically derived by a control volume technique or the equivalent method of integrating (2.1) and (2.3) over a typical volume. The resultant equations read:

$$\rho v A = \hat{m} = \text{constant} \quad (9.1)$$

$$h + \frac{v^2}{2} = \text{constant}, \quad (9.2a)$$

$$s = \text{constant}, \quad (9.3)$$

where $A = A(x)$ is the area of the duct or streamtube and \hat{m} is a version of the mass flux which accounts for gradual area changes. Equation (9.2a) is recognized as the Bernoulli equation and equation (9.3) expresses the assumption of isentropic flow. The relations between the changes in density, temperature, pressure, velocity, enthalpy and area are obtained by differentiation of (9.1)-(9.3), use of Gibbs' equation (2.6), standard thermodynamic identities and the definition of the sound speed. These read

$$\frac{dp}{\rho} = \frac{dp}{\rho a^2} = \frac{c_p}{\beta a^2} \frac{dT}{T} = \frac{dh}{a^2} = - M^2 \frac{dv}{v} = \frac{M^2}{1-M^2} \frac{dA}{A}.$$

where M is the local Mach number defined by (5.2). Thus, p , T , h all increase monotonically with ρ while the flow velocity decreases with ρ . As in the classical theory, the variation of area with ρ depends on the local Mach number. Our intuition from the perfect gas theory leads us to expect that the Mach number will decrease monotonically as the density increases. However, inspection of (3.1) shows that the sound speed a could also decrease with ρ if $\rho\Gamma/a < 1$. Thus, the ratio (5.2) may or may not decrease and the actual Mach number variation must be obtained from the Bernoulli equation (9.2a) combined with the definition (5.2), i.e.,

$$h + \frac{a^2 M^2}{2} = H_0 \text{ or } M^2 = \frac{2}{a^2} (H_0 - h(\rho, s)). \quad (9.2b)$$

Here the constant in (9.2a) has been written H_0 . By the results derived below, it can be shown that M^2 is a single-valued function of ρ for this isentropic flow. To determine whether M increases or decreases we differentiate (9.2b) to obtain

$$\frac{dM}{d\rho} = \frac{M}{\rho} J(\rho, M), \quad (9.4)$$

where we have made use of the definition of J and (9.3) and have defined

$$J \equiv 1 - \frac{\rho\Gamma}{a} - \frac{1}{M^2}. \quad (9.5)$$

A result similar to (9.4)-(9.5) was obtained by Thompson [1]. From (9.4) we see that M decreases with ρ only if $J < 0$ but may increase if $J > 0$. Perfect gases have $\rho\Gamma/a = (\gamma+1)/2$ which yields

$$J = -\left\{1 + M^2 \frac{\gamma-1}{2}\right\} \frac{1}{M^2} < 0.$$

In fact, $J < 0$ for any fluid having $\rho\Gamma/a > 1$. Fluids in which $\rho\Gamma/a$ can become less than one will have $J = 0$ for values of $M = M(\rho)$ given by

$$M = \left(1 - \frac{\rho \Gamma}{a}\right)^{-\frac{1}{2}}. \quad (9.6)$$

The general form of this curve has been analyzed and is sketched in Figure 9.1 for the case of a BZT fluid, i.e.,

$$\frac{\rho \Gamma}{a} \Big|_{\min} < 0.$$

We note that (9.6) becomes singular where $\rho \Gamma/a = 1$; the two densities at which this occurs are denoted by ρ_r^I , ρ_r^0 , where $\rho_r^I > \rho_r^0$. The shape of the $J = 0$ curve is similar if $1 > (\rho \Gamma/a)_{\min} > 0$ but

$$M_{\min} = \left(1 - \frac{\rho \Gamma}{a} \Big|_{\min}\right)^{-\frac{1}{2}}. \quad (9.7)$$

will be greater than one. Inside the $J = 0$ curve is the nonclassical $J > 0$ region where $dM/d\rho > 0$.

The Mach number variation has been sketched for various stagnation densities* (given by the $M = 0$ intercept). All curves corresponding to

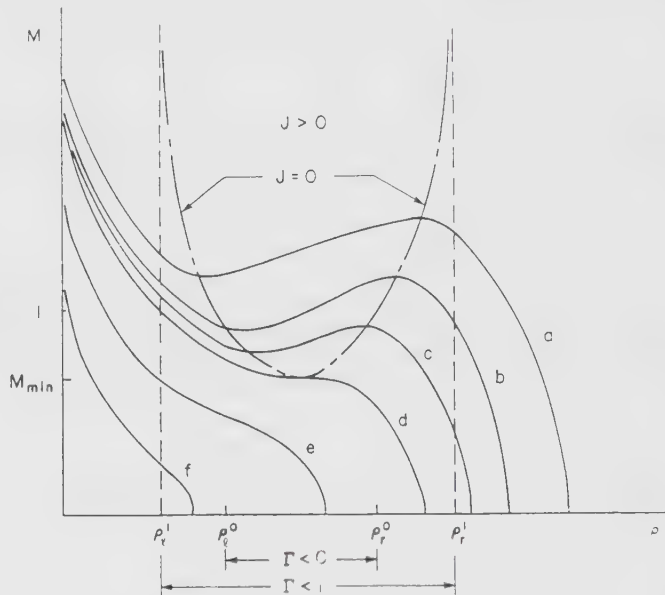


Figure 9.1: Solutions to the Bernoulli equation (9.2).

* It is useful to recall that the analysis presented here is based on the assumption of a fixed entropy. Thus, the stagnation states in Fig. 9.1 correspond to different T_0, p_0 pairs on the same isentrope.

sufficiently large stagnation densities must enter the $J > 0$ region and such curves will therefore have a local maximum and minimum. Curves such as a marked a remain supersonic after passing through the sonic point indicated at the right of the $J > 0$ region. Curves such as b will go subsonic in the $J > 0$ region and therefore have three sonic points during a full expansion from stagnation conditions to the full expanded state $\rho = 0$, $M = \infty$. At lower stagnation densities, the isentrope will appear similar to that marked c and will enter the positive J region but remain subsonic. Although not indicated by the sketch, curves originating in the $r < 0$ portions of the ρ axis to the right of the minimum of the $J = 0$ curve may also exhibit this behavior. Finally, curve d is the limiting case separating flows which enter the $J > 0$ region and those which do not.

A detailed analysis of isentropic flows governed by (9.1) - (9.4) has been provided by Cramer [61]. The main results may be summarized as follows:

- (i) Full isentropic expansions from stagnation states ($\rho = \rho_0$, $M = 0$) to arbitrarily small density and pressure and arbitrarily large Mach numbers are always possible.
- (ii) Supersonic states corresponding to $r < 0$ are also always attainable through isentropic expansion from a stagnation state.

Clearly, if a $r < 0$, $M > 1$ state cannot be achieved by some conventional process, e.g., a wind tunnel or set of turbine blades, the practical interest in the nonclassical supersonic dynamics is limited. Further motivation for the study of this question is provided by the conclusions of Thompson [1] who showed that a fluid with a constant, but negative, $\rho r/a$ cannot be accelerated supersonically. In fact, it can be shown that a flow can be accelerated from rest to supersonic conditions only if it enters a region of positive r . Thus, a fluid having $r < 0$ everywhere can never be accelerated supersonically from rest, even though we allow for variable $\rho r/a$. The proof relies on the easily verified fact that any sonic points in the $J < 0$ region necessarily occur where $r > 0$. By inspection, all curves in the M vs. ρ plane must go through at least one such sonic point in order to become supersonic.

Application of the well-known identity

$$\frac{1}{A} \frac{dA}{dx} = \frac{1-M^2}{M^2} \frac{1}{\rho} \frac{d\rho}{dx} \quad (9.8)$$

reveals the nozzle contours required for the flows described in (i) and (ii). It is easily verified that the expansion to supersonic $r < 0$ states is always attainable through a conventional converging-diverging nozzle of the type found in all introductory treatments of gasdynamics. The full expansion to arbitrarily large Mach numbers is

somewhat more complicated in that isentropes of the type b in Figure 9.1 result in three sonic points. The required area variation is sketched in Figure 9.2 and is seen to consist of a throat followed by an anti-throat which then is necessarily followed by a second conventional throat. For stagnation densities other than those of type b, only one sonic state is encountered and the full expansion is through a conventional single throat.

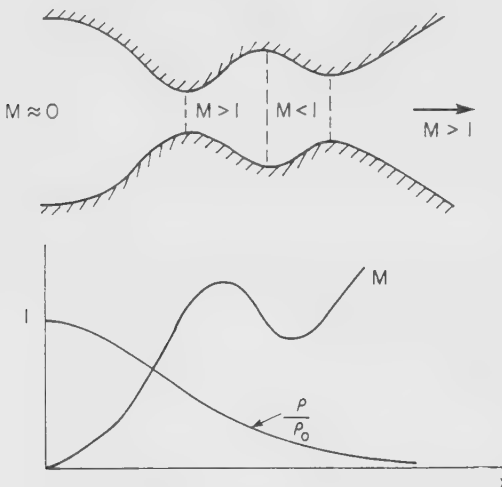


Figure 9.2: Area variation for full isentropic expansion. Isentrope is of the type b in Figure 9.1.

The anti-throat seen in Figure 9.2 was first described by Thompson [1] on the basis of the now well-known formula

$$\left(\frac{dM}{dx}\right)^2 = \frac{1}{2} \left(\frac{\rho f}{A} \frac{1}{A} \frac{dA}{dx} \right) \Big|_{M=1} \quad (9.9)$$

Although our results are completely consistent with Thompson's result, we have not made explicit use of it here.

10. Steady Isentropic Flows - External Flows

In this section, we examine fully two-dimensional flows similar to those generated by wings, bodies, or turbine blades. We begin by estimating the critical Mach number for flow over a two-dimensional wing. Recall that the critical Mach number is the freestream Mach number at which the flow first becomes sonic at some point on the wing. The simplest approach combines the Prandtl-Glauert rule

$$C_p = \frac{C_{p\text{inc}}}{(1-M^2)^{\frac{1}{2}}}, \quad (10.1)$$

where C_p is the pressure coefficient and $C_{p\text{inc}}$ is the minimum value of the pressure coefficient at incompressible conditions, i.e., $M = 0$, with the Bernoulli equation (9.2) evaluated at sonic conditions, i.e.,

$$\begin{aligned} M_\infty^2 &= \frac{2}{a_\infty^2} (h_s - h_\infty) + \left(\frac{a_s}{a_\infty}\right)^2 \\ C_p &= \frac{2}{M_\infty^2 \rho_\infty a_\infty^2} (p_s - p_\infty), \end{aligned} \quad (10.2)$$

where ρ_s = density at which the local Mach number becomes one. In (10.2) the pressure, enthalpy and sound speed must be given by an equation of state, i.e.,

$$p_s = p(\rho_s, s_\infty), \quad h_s = h(\rho_s, s_\infty), \quad a_s = a(\rho_s, s_\infty).$$

Thus, (10.2) gives a parametric relation between C_p and M_∞ (here the parameter is ρ_s). Once the wing shape is specified $C_{p\text{inc}}$ will be known and (10.1) then gives a second $C_p = C_p(M_\infty)$ relation. The intersection of these two curves yields the critical Mach number. We have evaluated (10.2) exactly using a van der Waals gas with $c_v = 50$ R and plotted the results along with those for (10.1) in Figure 10.1. The freestream pressure was taken to be the critical pressure p_c . The various freestream specific volumes are indicated on the plot. These range from perfect gas values, $V = \infty$, to dense gas values, $V \approx V_c$. In plotting (10.1) we have chosen typical values of $C_{p\text{inc}}$. For example, the case $C_{p\text{inc}} \approx -0.77$ corresponds to the value obtained for a NACA 0012 at small ($\approx 2^\circ$) angle of attack. For fixed wing shape, i.e., fixed $C_{p\text{inc}}$, it is clear that the critical Mach number is significantly increased as we approach the dense gas region. For example, if the $C_{p\text{inc}} = -0.77$ case is considered we see that the critical Mach number for the perfect gas is approximately 0.67. If the freestream specific volume is decreased to $1.3V_c$, the critical Mach number becomes 0.91, approximately. This is an increase of approximately 36%. A similar trend is shown in Figure 10.2. Here the freestream pressure was again taken to be the critical value and the $C_{p\text{inc}}$ was taken to be -0.75. The critical Mach number computed by iteration is plotted against the value of $c_v(T)/R$ used. This shows the effects of changing fluids, e.g., $c_v(T) \approx 2.5$ R for air whereas it is ≈ 48 R for normal decane. Critical Mach numbers over 0.9 are easily attained.

The physical reason behind this dramatic increase appears to be related to Thompson's formula, our equation (9.9). It is impossible to accelerate a flow supersonically through a minimum in the streamtube area if $r < 0$ there. At the maximum thickness of the airfoil, the streamtube area is constricted which normally is sufficient to render the flow

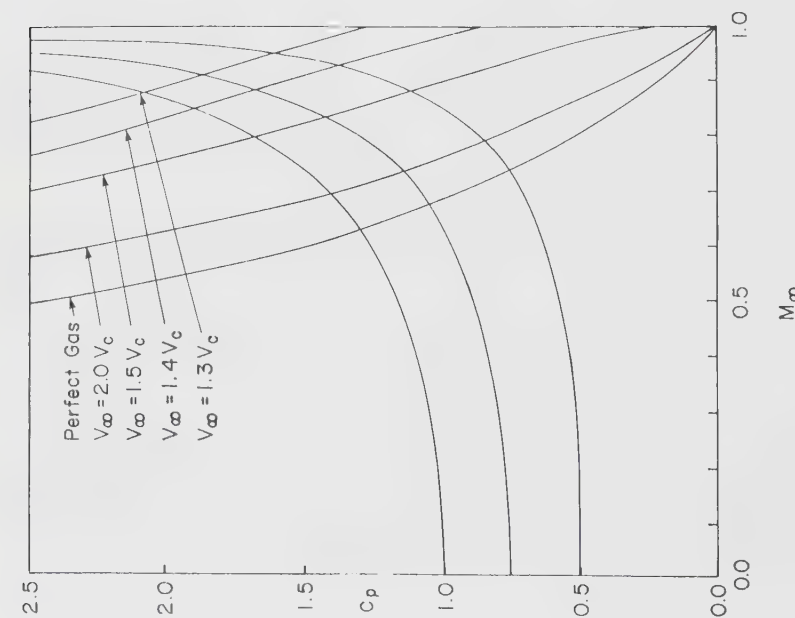


Figure 10.1: Determination of critical Mach number. Various solutions to the Bernoulli equation (10.2) are marked by their respective value of V_∞/V_c . Gas model used for Bernoulli equation is a van der Waals with $C_v = 50R$.

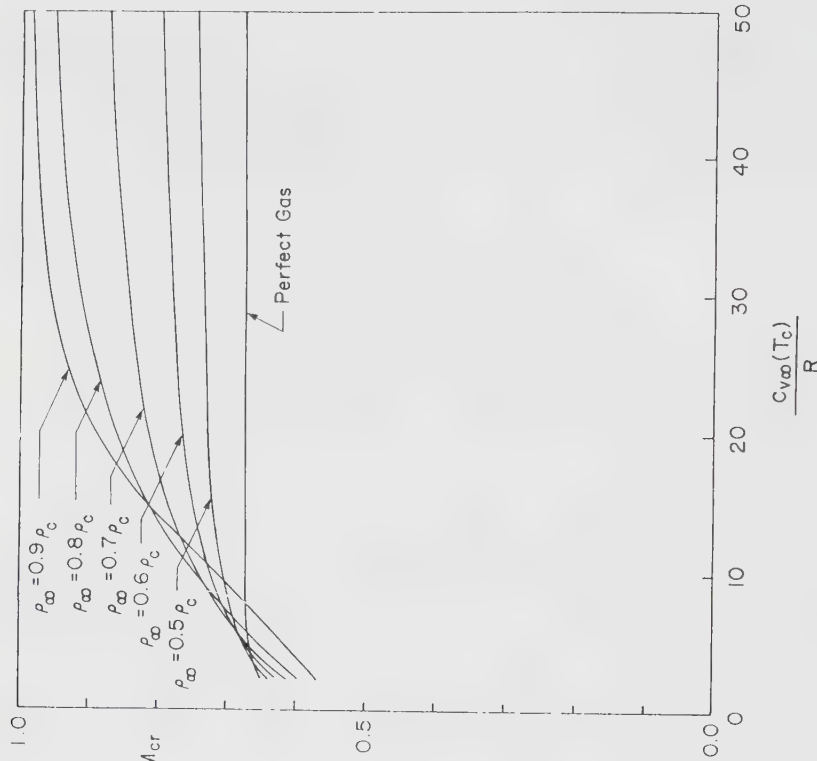


Figure 10.2: Computed critical Mach number by technique of Figure 10.1. $C_v = 50R$, $\rho_\infty = 1.75$, $\rho_c = \rho_\infty$.

sonic. However, if $\Gamma < 0$ there, the flow cannot become sonic and the onset of transonic flow is delayed.

This clearly has technological advantages. Turbomachinery employing BZT fluids as working fluids can operate at considerably higher speeds before transonic losses set in. The use of BZT fluids as working fluids in power systems is by no means far-fetched. After all, the same class of fluids have been used to great advantage in organic Rankine cycles (ORC). We also note that the fluid leaves the boiler and enters the main gasdynamic stage (the turbine) exactly where the negative Γ region lies, i.e., at near-critical pressures at the saturated vapor line.

Once the critical Mach number is exceeded, isolated regions of supersonic flow appear. Thus, the problem is of a mixed hyperbolic-elliptic type. Furthermore, even in the limit of thin airfoils, the equations of motion are necessarily nonlinear in order to facilitate the change in type. When Γ is strictly positive or strictly negative everywhere in the flow the well-known transonic small disturbance equation gives a reasonable lowest-order approximation if the airfoil or blade is thin. The extension of this equation capable of describing mixed nonlinearity in transonic flows has been derived by the author and is given below. The advantages of this small disturbance equation are similar to those of the classical equation. That is, the dependence on the physical parameters and any self-similarity can be obtained explicitly. Furthermore, numerical solutions depicting the main flow features may be obtained with relative ease.

We make the usual assumptions for thin airfoils in transonic flow. We take the freestream to be uniform with speed U_∞ , density ρ_∞ and sound speed a_∞ . The small disturbances caused by the two-dimensional wing are assumed to be inviscid, isentropic and irrotational. In addition, we make the assumption of Cramer and Kluwick [49] given here by (8.1). That is, the undisturbed state is near the $\Gamma = 0$ locus depicted in Figure 3.1. As a result, even small disturbances will result in a change in sign of Γ . Because the freestream is uniform and the flow is inviscid, the only sources of vorticity are shock waves. The analysis of Cramer and Kluwick [49] shows that the jump in entropy is of the fourth order in the shock strength under the conditions stipulated here. Thus, the vorticity generated will be relatively weak and the assumption of irrotationality seems as reasonable as in the conventional theory. As in this latter theory, the freestream Mach number $M_\infty = U_\infty/a_\infty$ is taken to be near one. In order to conserve space, we will not relate the derivation here; this will appear in future publications. If we align the positive x direction with that of the freestream, it can be shown that the boundary value problem governing the flow is

$$(M^2 - 1) \phi_{xx} = \phi_{yy} \quad (10.3)$$

$$\phi_y = \epsilon U_\infty F'(\frac{x}{\ell}) \quad \text{on } y \approx 0 \quad (10.4)$$

$$\phi_x, \phi_y \rightarrow 0 \text{ as } x^2 + y^2 \rightarrow \infty, \quad (10.5)$$

where ϕ is the perturbation velocity potential such that the velocity is $U \hat{i} + \nabla \phi$ (\hat{i} is the unit vector in the positive x direction), ℓ is the chord, ϵ is a small nondimensional thickness parameter, the wing shape is given by $y = \epsilon \ell F(x/\ell)$ and $dF'(\xi) \equiv F(\xi)/d\xi$. The quantity M is the local Mach number given by

$$M^2 - 1 \approx M_\infty^2 - 1 + 2 \frac{\rho_\infty \Gamma_\infty}{a_\infty} \frac{\phi_x}{U_\infty} - \Lambda \left(\frac{\phi_x}{U_\infty} \right)^2 \quad (10.6)$$

and

$$\Lambda \equiv \frac{\rho_\infty^2}{a_\infty^2} \frac{\partial \Gamma}{\partial \rho} \Big|_S (\rho_\infty, s_\infty) = O(1) \quad (10.7)$$

is the second nonlinearity coefficient found in the weak shock theory of Cramer and Kluwick [49]. The pressure coefficient can be shown to be

$$C_p \approx 2 \frac{\rho - \rho_\infty}{\rho_\infty} \approx -2 \frac{\phi_x}{U_\infty}. \quad (10.8)$$

The various small quantities were found to be related to the thickness parameter ϵ by

$$\begin{aligned} \frac{\rho_\infty \Gamma_\infty}{a_\infty}, \frac{\rho - \rho_\infty}{\rho_\infty}, \frac{\phi_x}{U_\infty} &= O(\epsilon^{1/2}) \\ \frac{\phi_y}{U_\infty}, M_\infty^2 - 1 &= O(\epsilon) \end{aligned} \quad (10.9)$$

If we compare this to the result of the classical transonic theory, i.e.,

$$M_\infty^2 - 1 = O(\epsilon^{1/3}), \quad C_p = O(\epsilon^{2/3}),$$

we see that the range of Mach numbers at which the transonic effects become important is smaller than that of the classical theory by a factor of $\epsilon^{1/3}$ and the pressure coefficient is larger by a factor of $\epsilon^{-1/3}$. This appears to support the previous finding of significant increases in the critical Mach number. The general trend appears to be that the range of flow speeds at which the deleterious effects of transonic flow become noticeable is considerably smaller than that for perfect fluids. The increase in the C_p is due to the Prandtl-Glauert increase as we approach the singularity at $M_\infty = 1$. Because the subsonic

range is extended, the lift (and therefore power output of a turbine) increases with no significant increase in drag.

To conclude this section, we consider fully supersonic flow around thin wings or blades. We assume the airfoil or blade is of the type described in the previous discussion of transonic flows, i.e., two-dimensional and thin. The freestream is aligned with the positive x

axis, is taken to be uniform and, as already indicated, in the neighborhood of the $r = 0$ locus. In order to develop a weak shock theory we must first prove that the

- (i) entropy is negligible, even over integrations over distances of the order of the nonlinear interaction time and that
- (ii) reflected waves are negligible, i.e., the simple wave approximation can be made.

The results of Cramer and Kluwick [49] show that the entropy jump is of fourth order in the pressure jump when (8.1) is assumed. The author has shown, by a technique similar to the unsteady analysis of Cramer and Kluwick [49], that the accumulated error in integrations over distances of the order of $((\rho - \rho_\infty)/\rho_\infty)^{-2}$ is also negligible. Thus, (i) is satisfied. We have also shown that

$$[R^-] = O\left(\frac{\rho - \rho_\infty}{\rho_\infty}\right)^3 = o(1)$$

which, in the present theory, is sufficient for the neglect of reflected waves everywhere. Here R^- is the Riemann invariant associated with left-running waves. Thus, all waves may be regarded as simple right-running waves. The lowest-order solution which is valid to distances on the order of the shock formation distance can be written

$$C_p \approx \frac{2}{M^2} \frac{\rho - \rho_\infty}{\rho_\infty} \approx \frac{2\theta}{(M^2 - 1)^{1/2}} = \text{constant}, \quad (10.10)$$

where C_p is the pressure coefficient and θ is the flow deflection angle as measured counterclockwise from the freestream, on Mach lines $y = y(x; \theta)$ given by

$$\frac{dy}{dx} = \frac{1}{(M_\infty^2 - 1)^{1/2}} + \frac{M_\infty^4}{(M_\infty^2 - 1)^2} \left\{ \frac{\rho_\infty \Gamma_\infty}{a_\infty} \theta + \frac{M_\infty^2}{(M_\infty^2 - 1)^{1/2}} \frac{\Lambda}{2} \theta^2 \right\} + o(\theta^3) \quad (10.11)$$

where Λ is defined by (10.7). Cramer [61] has also found the slope of the two-dimensional shock surface to be

$$\frac{dy}{dx} = \frac{1}{(M_{\infty}^2 - 1)^{\frac{1}{2}}} + \frac{M_{\infty}^2}{(M_{\infty}^2 - 1)^2} \left\{ \frac{1}{2} \frac{\rho_{\infty} \Gamma_{\infty}}{a_{\infty}} (\theta_2 + \theta_1) \right. \\ \left. + \frac{\Lambda}{6} \frac{M_{\infty}^2}{(M_{\infty}^2 - 1)^{\frac{1}{2}}} (\theta_2^2 + \theta_2 \theta_1 + \theta_1^2) \right\} + O(\theta^3), \quad (10.12)$$

where θ_1, θ_2 are the values of the flow deflection angle immediately before and after the shock. From (10.10) - (10.11) it is clear that the Mach lines are straight although the slope depends on the strength of the signal carried. This, of course, is consistent with the classical weak shock theory as well as the unsteady analog of (10.10)-(10.11) developed by Cramer and Kluwick [49]. It is also easily verified that the shock slope (10.12) is

$$\frac{|Q|}{|\theta|}$$

where

$$Q = \int_0^\theta \frac{dy}{dx} (\theta) d\theta$$

and the integrand is just the slope of the Mach lines (10.11).

Because there is only one inflection point in the isentropes and shock adiabat, the admissibility conditions can be derived by a speed-ordering relation. In particular, we require that the normal components of the Mach number

$$M_n \equiv M \sin (\Sigma - \theta), \quad (10.13)$$

where Σ is the shock angle measured in the same manner as θ , satisfy the supersonic-subsonic condition:

$$M_{n1} \geq 1 \geq M_{n2}, \quad (10.14)$$

where the subscripts 1 and 2 denote the upstream and downstream conditions, respectively. Cramer [61] has shown that the admissibility conditions corresponding to (10.10)-(10.12) are

$$\frac{dy}{dx} \Big|_1 \leq \frac{dy}{dx} \Big|_{shock} < \frac{dy}{dx} \Big|_2 \quad \text{if } \Lambda > 0 \\ (10.15)$$

$$\frac{dy}{dx} \Big|_1 < \frac{dy}{dx} \Big|_{shock} \leq \frac{dy}{dx} \Big|_2 \quad \text{if } \Lambda < 0.$$

Furthermore, the sonic shock is the lower limit on the strength $|[\theta]|$ if $\Lambda > 0$ and is the shock of maximum strength (again measured by $|[\theta]|$) if $\Lambda < 0$. The strength of the sonic shocks is given by

$$\begin{aligned} [\theta] &= \frac{3}{2} \left\{ \theta_2 + \frac{\rho_\infty \Gamma_\infty}{a_\infty} \frac{(M_\infty^2 - 1)^{1/2}}{\Delta M_\infty^2} \right\} \text{ if } \Lambda > 0, \\ [\theta] &= -\frac{3}{2} \left\{ \theta_1 + \frac{\rho_\infty \Gamma_\infty}{a_\infty} \frac{(M_\infty^2 - 1)^{1/2}}{\Delta M_\infty^2} \right\} \text{ if } \Lambda < 0. \end{aligned} \quad (10.16)$$

Various flow patterns can be constructed as in Cramer and Kluwick [49] and Cramer, Kluwick, Watson and Pelz [55]. As in the unsteady theory, there will be a large number of subcases corresponding to positive and negative values of Γ and Λ . In blade-or wing-like configurations at nonzero angles of attack, the flow patterns on the compression and expansion sides can be different even in the classical

case. With mixed nonlinearity the resultant number of subcases is enormous. Here we simply describe a thickness problem (zero angle of attack) having

$$\Gamma_\infty < 0, \Lambda > 0, \theta_n > 3 \left| \frac{\rho_\infty \Gamma_\infty}{a_\infty} \right| \frac{(M_\infty^2 - 1)^{1/2}}{\Delta M_\infty^2},$$

where θ is the flow deflection angle at the nose, i.e., it is the nose half-angle. The flow pattern and pressure distributions at various distances from the wing are depicted in Figure 10.3. The shock at the nose is relatively strong and can be shown to be admissible. Near the trailing edge the flow has been expanded below p_∞ . Thus, $\Gamma < 0$ there and a pure compression fan emanates from the trailing edge. Near the point of maximum thickness the local value of Γ is also negative and the Mach lines converge to form an expansion shock at a finite distance from the wing. As the compression shock is weakened it becomes sonic at s and is thereafter inadmissible. The inadmissible shock breaks up into the smooth compression precursor followed by a sonic compression shock. The precursor and expansion shock are shown in the third pressure distribution. Ultimately, the expansion shock collides with the sonic compression shock resulting in a single expansion shock. In the far-field the expansion shock interacts with the precursor at the front and the centered compression fan from behind. The pressure distribution therefore is comprised of a smooth compression (which is the far-field remnant of the precursor) followed by an expansion shock which in turn is followed by a second smooth compression which takes the flow back to p_∞ .

In this example, we see the nonclassical dependence of the far-field flow on the initial ($y \approx 0$) conditions similar to that described in references [32], [49], [55] and [58]. The ultimate decay of the expansion shock is due in part to the Mach lines originating between the nose and maximum thickness. However, these Mach lines have first been refracted through the nose shock (the refracted wave is the precursor).

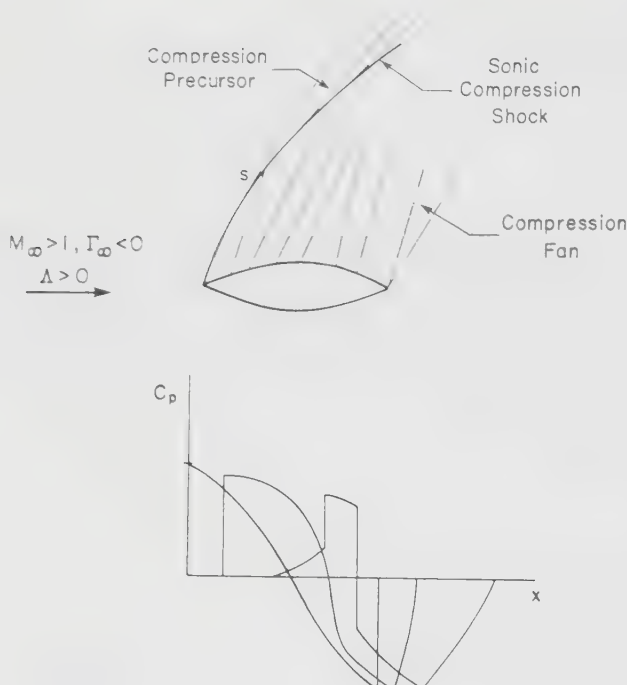


Figure 10.3: Mach lines and variation of pressure coefficient for typical airfoil/blade configuration. At s the nose shock becomes sonic. The first pressure distribution is on the airfoil surface, the second is on a streamline between s and the airfoil, and the last is on a streamline lying above the formation point for the expansion shock but below the point at which the compression and expansion shock collide.

The elimination of the compression shock at finite distances is to be expected. The undisturbed state corresponds to $r < 0$. We naturally expect the disturbance to decay asymptotically to zero at large distances from the wing. Thus, in the far-field $r < 0$ everywhere and compression shocks of any kind are clearly inadmissible there. With mixed nonlinearity the compression shock is frequently eliminated by both a partial disintegration and a collision with an expansion shock. Similar remarks hold for the $r_\infty > 0$ case with the terms compression and expansion interchanged.

Although the present weak shock theory is not valid at such large amplitudes, nose shocks which take the flow all the way across the region of negative nonlinearity, similar to the strongest shock seen in Figure 7.4 and shock r -A in Figure 7.3, are expected to undergo shock-splitting due to the weakening effect of the Mach lines behind it. In such cases, the expansion shock will usually evolve into a double sonic shock.

12. Conclusions

We have restricted our attention to single-phase fluids in local equilibrium. In this sense, they are indistinguishable from those found in classical gasdynamics. Even with this very simple model, fluids can be found which exhibit behavior which differs dramatically from that of perfect gases. This appears to occur in virtually all aspects of compressible flow. As a result, we feel that the study of BZT fluids is a major step toward completing our understanding of the dynamics of single-phase fluids. Furthermore, this study helps to place the well-known rules associated with perfect gases in a broader context by identifying results which are fundamental and universal rather than dependent on the particular gas model. This work is also important because of the potential for applications. Because our intuition and design strategies are based on the dynamics of perfect gases, the relaxation of any constraints associated with perfect gases is likely to give rise to a number of new and exciting technologies.

REFERENCES

1. Thompson, P. A.: A fundamental derivative in gasdynamics, *Phys. Fluids*, 14 (1971), 1843-1849.
2. Borisov, A. A., AL. A. Borisov, S. S. Kutateladze and V. E. Nakorykov: Rarefaction shock wave near the critical-liquid-vapour point, *J. Fluid Mech.*, 126 (1983), 59-73.
3. Novikov, I. I.: Existence of shock waves rarefaction, *Dokl. Akad. Nauk SSSR*, 59 (1948), 1545-1546.
4. Kahl, G. D. and D. C. Mylin: Rarefaction shock possibility in a van der Waals-Maxwell fluid, *Phys. Fluids*, 12 (1969), 2283-2291.
5. Temperley, H. N. V.: The theory of propagation in liquid helium II of 'temperature waves' of finite amplitude, *Proc. Phys. Soc. Lond.*, A 64 (1951), 105-114.
6. Osborne, D. V.: Second sound in liquid helium II, *Proc. Phys. Soc. Lond.*, A 64 (1951), 114-123.
7. Dessler, A. J. and W. M. Fairbank: Amplitude dependence of the velocity of second sound, *Phys. Rev.*, 104 (1956), 6-10.

8. Turner, T. N. Second-sound shock waves and critical velocities in liquid helium II, Ph.D. Dissertation, California Institute of Technology, Pasadena, CA 1979.
9. Turner, T. N.: New experimental results obtained with second-sound shock waves, *Physica*, 107B (1981), 701-702.
10. Atkin, R. J., and N. Fox: The dependence of thermal shock wave velocity on heat flux in Helium II, *J. Phys. C: Solid State Phys.*, 17 (1984), 1191-1198.
11. Torczynski, J. R. Nonlinear fourth sound, *Wave Motion*, 7 (1985), 487-501.
12. Garrett, S. Nonlinear distortion of 4th sound in superfluid $^3\text{He-B}$, *J. Acoust. Am.*, 60 (1981), 139-144.
13. Bezzerides, B., D. W. Forslund, and E. L. Lindman: Existence of rarefaction shocks in a laser-plasma corona, *Phys. Fluids*, 21 (1978), 2179-2185.
14. Nariboli, G. A. and W. C. Lin: A new type of Burgers' equation, *ZAMM*, 53 (1973), 505-510.
15. Kynch, G. J.: A theory of sedimentation, *Trans. Faraday Soc.*, 48 (1952), 166-176.
16. Shannon, P. T. and E. M. Tory: Settling of slurries, *Ind. Engng Chem.*, 57 (1965), 18-25.
17. Amberg, G., A. A. Dahlkild, F. H. Bark, and D. S. Henningson: On time-dependent settling of a dilute suspension in a rotating conical channel, *J. Fluid Mech.*, 166 (1986), 473-502.
18. Auzerais, F. M., R. Jackson, and W. B. Russel: The resolution of shocks and the effects of compressible sediments in transient settling, *J. Fluid Mech.*, 195 (1988), 437-462.
19. Thompson, P. A., G. C. Carafano, and Y. G. Kim: Shock waves and phase changes in a large-heat-capacity fluid emerging from a tube, *J. Fluid Mech.*, 166 (1986), 57-92.
20. Dettleff, G., G. E. A. Meier, H. D. Speckmann, P. A. Thompson, and C. Yoon: Experiments in shock liquefaction, In Proc. 13th Intl. Symp. on Shock Tubes and Waves (ed. C. E. Trainor & J. G. Hall), (1982), 716-723.
21. Thompson, P. A. and Y. G. Kim: Direct observation of shock splitting in a vapor-liquid system, *Phys. Fluids*, 26 (1986), 3211-3215.

22. Thompson, P. A., H. Chaves, G. E. A. Meier, Y. G. Kim, and H. D. Speckmann: Wave splitting in a fluid of large heat capacity, *J. Fluid Mech.*, 185 (1987), 385-414.
23. Zel'dovich, Ya. B. and Yu. P. Raizer: Physics of Shock Waves and High Temperature Hydrodynamic Phenomena, Vol. 2, Academic 1967.
24. McQueen, R. G. and S. P. Marsh: Hugoniots of graphites of various initial densities and the equation of state of carbon, in: Behavior of Dense Media Under High Dynamic Pressures, Gordon and Breach 1968, 207-216.
25. Gust, W. H. and D. A. Young: High Pressure Science and Technology, Vol. I, Plenum 1979.
26. Ivanov, A. G. and S. A. Novikov: Shock rarefaction waves in iron and steel, *Zh. Eksp. Teor. Fiz.*, 40 (1961), 1880-1882.
27. Erkman, J. O. Smooth spalls and the polymorphism in iron, *J. Appl. Phys.*, 32 (1961), 939-944.
28. Kolsky, H. Production of tensile shock waves in stretched natural rubber, *Nature*, 224 (1969), 1301.
29. Barker, L. M. and R. E. Hollenbach: Shock wave studies of PMMA, fused silica, and sapphire, *J. Appl. Phys.*, 42 (1970), 4208-4226.
30. Bains, J. A. and M. A. Breazeale: Nonlinear distortion of ultrasonic waves in solids: approach of a stable backward sawtooth, *J. Acoustic Soc. Amer.*, 57 (1975), 745-746.
31. Conner, M. P. Shear Wave Measurements to Determine Nonlinear Elastic Response of Fused Silica Under Shock Loading, MS Thesis, Washington State University, Pullman, Washington.
32. Lee-Bapty, I. P. Nonlinear wave propagation in stratified and viscoelastic media, Ph.D. dissertation, Leeds University, England, 1981.
33. Morris, F. E. and G. A. Nariboli: Photoelastic waves, *Int. J. Engng. Sci.*, 10 (1972), 765-774.
34. Kakutani, T. and N. Yamasaki: Solitary waves on a two-layer fluid, *J. Phys. Soc. Japan*, 45 (1978), 674-679.

35. Helfrich, K. R., W. K. Melville, and J. W. Miles: On interfacial waves over slowly varying topography, *J. Fluid Mech.*, 149 (1984), 305-317.
36. Bethe, H. A. The theory of shock waves for an arbitrary equation of state, *Office Sci. Res. & Dev. Rep. 545*, Washington, D.C. 1942.
37. Hayes, W. D.: Gasdynamic discontinuities, in: *Princeton Series on High Speed Aerodynamics and Jet Propulsion*, Princeton University Press 1960.
38. Beyer, R. T.: *Nonlinear Acoustics*, Naval Ship Systems Command, Dept. of the Navy, Washington, D. C. 1974.
39. Thompson, P. A.: *Compressible Fluid Dynamics*, McGraw-Hill, New York 1972.
40. Zel'dovich, Ya. B.: On the possibility of rarefaction shock waves, *Zh. Eksp. Teor. Fiz.*, 4 (1946), 363-364.
41. Thompson, P. A. and K. Lambrakis: Negative shock waves, *J. Fluid Mech.*, 60 (1973), 187-208.
42. Lambrakis, K. and P. A. Thompson: Existence of real fluids with a negative fundamental derivative Γ , *Phys. Fluids*, 5 (1972), 933-935.
43. Cramer, M. S.: Negative nonlinearity in selected fluorocarbons, *Phys. Fluids*, A. 1 (1989), 1894-1897.
44. Martin, J. J. and Y. C. Hou: Development of an equation of state for gases, *AIChE J.*, 1 (1955), 142-151.
45. Rihani, D. N. and L. K. Doraiswamy: Estimation of heat capacity of organic compounds from group contributions, *Ind. Engr. Chem. Fund.*, 4 (1965), 17-21.
46. Burnside, B. M.: Thermodynamic properties of five halogenated hydrocarbon vapour power cycle working fluids, *J. Mechanical Engineering Science*, 15 (1973), 132-143.
47. Richter, H. R. D. and B. M. Burnside: A general programme for producing pressure-enthalpy diagram, *J. Mechanical Engineering Science*, 17 (1975), 31-39.
48. Cramer, M. S. and R. Sen: Shock formation in fluids having embedded regions of negative nonlinearity, *Phys. Fluids*, 29 (1986), 2181-2191.

49. Cramer, M. S. and A. Kluwick: On the propagation of waves exhibiting both positive and negative nonlinearity, *J. Fluid Mech.*, 142 (1984), 9-37.
50. Cramer, M. S. and R. Sen: Exact solutions for sonic shocks in van der Waals gases, *Phys. Fluids*, 30 (1987), 377-385.
51. Gilbarg, D.: The existence and limit behavior of the one-dimensional shock layer, *Am. J. Maths*, 73 (1951), 256-274.
52. Cramer, M. S.: Shock splitting in single-phase gases, *J. Fluid Mech.*, 199 (1989), 281-296.
53. Menikoff, R. and B. Plohr: Riemann problem for fluid flow of real materials, *Reviews of Modern Physics*, 61 (1989), 75-130.
54. Lax, P. D.: Shock waves and entropy, in: *Contributions to Nonlinear Functional Analysis* (ed. E. H. Zarantonello), Academic 1971.
55. Cramer, M. S., A. Kluwick, L . T. Watson, and W. Pelz: Dissipative waves in fluids having both positive and negative nonlinearity, *J. Fluid Mech.*, 169 (1986), 323-336.
56. Cramer, M. S.: Structure of weak shocks in fluids having embedded regions of negative nonlinearity, *Phys. Fluids*, 30 (1987), 3034-3044.
57. Taylor, G. I.: The conditions necessary for discontinuous motion in gases, *Proc. R. Soc. Lond.*, A 84 (1910), 371-377.
58. Lee-Bapty, I. P. and D. G. Crighton: Nonlinear wave motion governed by the modified Burger's equation, *Phil. Trans. R. Soc. Lond.*, A 323 (1987), 173-209.
59. Reid, R. C. J. M. Prausnitz, and B. E. Poling: *The Properties of Gases and Liquids*, 4th Edition, Wiley 1987.
60. Landau, L. D. and E. M. Lifshitz: *Fluid Mechanics*, Addison-Wesley 1959.
61. Cramer, M. S. Nonclassical Dynamics of Classical Gases, Virginia Polytechnic Institute and State University Engineering Report #VPI-E-89-20, Blacksburg, VA 1989.

LIQUID-VAPOR ADIABATIC PHASE CHANGES AND RELATED PHENOMENA

P. A. Thompson
Rensselaer Polytechnic Institute, Troy, NY, USA

ABSTRACT

Adiabatic phase changes in liquid-vapor systems are described experimentally and theoretically. The emphasis is on real systems, with departures from equilibrium (metastability). The phase changes are driven by pressure differences and tend to be rapid. Typically, the phase changes occur across shockfronts. Analog systems are also described. In the liquid-vapor systems, at least five distinct phase changes have been discovered within recent years. Several of the phenomena were not predicted in advance. The discoveries reported here were made by various researchers, including co-authors of this book.

1. INTRODUCTION

This article describes phase changes which originate from a metastable state. Depending on the degree of departure from equilibrium, the transition to a new equilibrium state may be quite rapid. Consistent with the title, the phase changes are driven by forces other than heat transfer, that is, they are *adiabatic*. Typically, the transitions are driven by pressure changes, sudden acceleration, impact, or in the special case of explosive boiling, by the metastability itself.

Common examples of adiabatic phase changes include condensation of CO₂ from a fire extinguisher, producing the solid phase, opening a bottle of champagne, the explosion of a nuclear reactor, cavitation in a hydraulic turbine, ice skating (involving adiabatic melting under the pressure of the skate blade) and finally, the condensation of water vapor in the atmosphere to form clouds, with subsequent precipitation as rain or snow.

The main purpose, however, is to describe *new* forms of adiabatic phase changes which have been discovered within the last fifteen years, although their roots extend back to antiquity (see Section 3, Table 1) and are based on contributions of many scientists, including Max Planck, J.D. van der Waals, Hans Bethe, and Ya. B. Zel'dovich, among others.

The new phenomena are the following:

Liquefaction shock. A transition from vapor to liquid takes place across a compression shock wave (Thompson & Sullivan 1975; Dettleff 1978; Dettleff *et al.* 1979, 1982). If the phase transition is complete across the wave, it is called a *complete* liquefaction shock; otherwise, it is called a *partial* liquefaction shock.

Shock splitting. A single, partial liquefaction shock splits into two discrete waves, which then diverge from each other (Thompson & Kim 1983; Speckmann 1984; Thompson, Kim & Meier 1984). The first wave of the split-shock system is called the *forerunner shock*, the following wave the *condensation discontinuity* or condensation front. The forerunner shock and condensation discontinuity propagate approximately at the single-phase vapor soundspeed and the mixture soundspeed, respectively, for the case of waves of small amplitude. The finite amplitude case will be described in Section 3.

Rarefaction shock. A rarefaction wave steepens to form a rarefaction-shock discontinuity. In the single-phase case, this will occur in the neighborhood of regions of negative nonlinearity, as discussed by Thompson & Lambrakis (1973) and by Cramer & Kluwick (1984). In the two-phase case, the rarefaction shock will bridge two points on each side of the saturated-vapor boundary, the upstream state lying in the mixture region and the downstream state lying in the superheated-vapor region (Thompson, Carofano & Kim, 1986). The near-critical rarefaction shock recently reported by Borisov, Borisov & Kutateladze (1983) differs in that the requisite large value of c_v is associated with near-critical power laws [$c_v \rightarrow \infty$ as $(T - T_c)^{-\alpha}$]. The upstream state must, apparently, be very near the critical point and the downstream state is in the mixture region. The measured thickness of the shockfront is relatively large (≈ 5 cm) and is believed to be related to the large, near-critical correlation length.

Complete evaporation shock. A liquid is evaporated completely across a rarefaction shock. Solutions of this type exist for van der Waals fluids (Slemrod 1990). Solutions for non-equilibrium upstream states near the liquid spinodal show a double Chapman-Jouguet structure. No experimental results corresponding to these models are known to the author.

Liquid-evaporation waves. Sudden reduction of the pressure of a liquid produces a superheated metastable state, followed by evaporation. In the experiments of Chaves (1984), the initial reduction of pressure takes place across a sharp forerunner expansion wave propagating into the liquid; this is followed by an evaporation discontinuity which propagates more slowly and is analogous to a Chapman-Jouguet deflagration. The two-wave system is thus another example of wave splitting. This topic will be addressed by Dr. Meier.

Unstable Liquefaction Shockfronts. Under certain conditions, the liquefaction shockfront becomes unstable in shock-tube experiments. Depending on the shock Mach number, the shockfront displays regular patterns; at higher Mach numbers, the shockfront may become chaotic.

Related Phenomena: Analog solid-solid systems and dissolved gas in liquid (champagne effect), analogs in combustion, Cheerio instability.

The structure of partial liquefaction shocks could be addressed in analogy to the Zel'dovich-von Neumann-Döring structure of laminar detonation waves, but is not treated here.

Most of the phenomena discussed require that the test fluid have a large molar heat capacity, the so-called 'retrograde' property, which effectively divides fluids into two different categories, the 'regular' and the 'retrograde' fluids.

The following pages enlarge on the subject of metastability, using the example of explosive boiling. The distinction between regular and retrograde fluids is discussed, as are the two basic forms of shockwave — the rarefaction shock and the compression shock.

Stable, metastable and unstable states. In the experiments of interest here, a fluid often originally exists in a stable, static state. When the system is disturbed, for example, by bursting a diaphragm to release the pressure, the fluid state will often become metastable for a short time before a new equilibrium state is reached. In some cases, the metastable state may become absolutely unstable and undergo a drastic change before reaching a new equilibrium state. A schematic representation of stable, metastable and unstable states is shown in Figure 1.

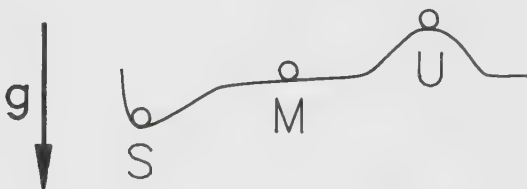


Figure 1. Stable, metastable and unstable states. g is the gravity force.

Creation of a metastable state. A metastable state may be created by heating or cooling the fluid, by adding fuel to an oxidant to form a combustible mixture, by altering the pressure suddenly or shocking the fluid. In mixtures of co-existing vapor/liquid/solid phases, the metastable states have special names as follows.

Supercooled liquid. If a liquid phase below the equilibrium freezing temperature is disturbed, the liquid may suddenly undergo partial freezing accompanied by an audible sound.

Superheated liquid. A liquid phase at a temperature above the equilibrium boiling point $T_B(P)$. We will discuss this case in a following section.

Supersaturated vapor. Vapor can exist at a pressure above the equilibrium saturation vapor pressure $P_\sigma(T)$. Supersaturation exists if $P > P_\sigma(T)$, as illustrated in Figure 2.

Various co-existing solid phases, such as graphite/diamond and quartz/stishovite often display marked metastability.

For a liquid-vapor system, metastable supersaturated-vapor states can be displayed on a conventional vapor-pressure diagram. For convenience, we assume that the equilibrium state is initially in the superheated-vapor region and that the vapor becomes supersaturated by an isentropic process — as shown in Figure 2.

There are two cases. In case 1, the regular fluid, the vapor becomes supersaturated by isentropic *expansion* and cools rapidly, ultimately condensing. This is just the process which leads to rainfall from a cloud, for example, where adiabatic cooling in the atmosphere produces condensation. It is typical of substances with relatively few atoms per molecule, i.e., $n < 7$, where n is the number of atoms in the molecule. The expansion isentrope in case 1 extends from A to B. At state B, the vapor is supersaturated but has not yet condensed, although further supersaturation will eventually produce condensation.

In case 2, the retrograde fluid, the vapor becomes supersaturated by isentropic *compression*. In this case, the vapor is heated in the compression process, but the increase in pressure dominates over temperature rise, so that

$$\left[\frac{\partial P}{\partial T} \right]_s > \left[\frac{dP}{dT} \right]_\sigma$$

and the path from A to B crosses the vapor-pressure curve σ . State B is again supersaturated and further compression may lead to condensation. The distinction between regular fluids and retrograde fluids will be elaborated in Section 2.

The leap from a metastable state to a new equilibrium state may occur when the metastable state is so far from the initial equilibrium state that it cannot be sustained, or when the system is strongly disturbed. We give two examples here.

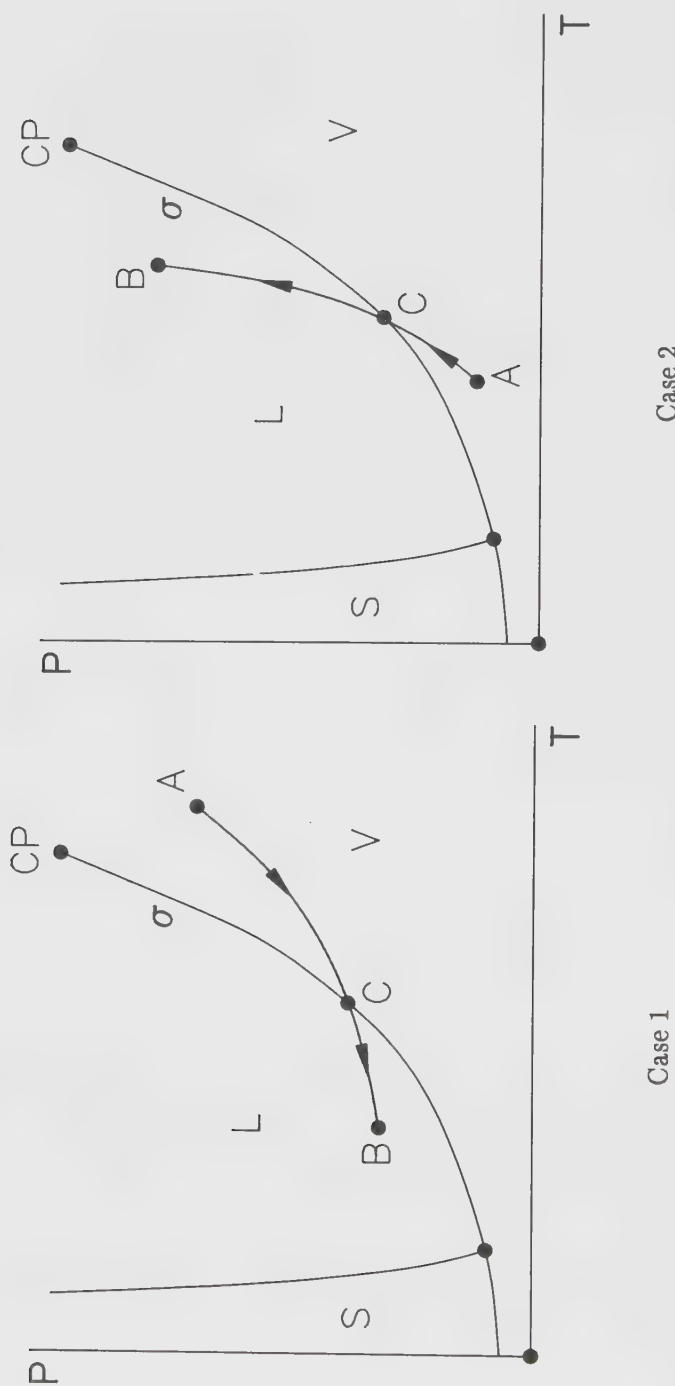


Figure 2. Supersaturated vapor states on a Pressure-Temperature diagram. Case 1 shows a regular fluid, which condenses on isentropic expansion and Case 2 shows a retrograde fluid, which condenses on isentropic compression. In both cases, state A is superheated vapor and state B is supersaturated vapor. Equilibrium phase transitions would take place at point C in each case, where the isentrope passes the vapor-pressure curve σ .

As the first example, consider the heating of pure water at a constant pressure of one atmosphere in an extremely clean and very smooth vessel (in practice, the smooth walls are formed by a stable host liquid). With care, the water can be heated to a temperature on the order of 300°C , nearly 200° above the equilibrium boiling point! Further heating will inevitably result in explosive boiling, sometimes called a vapor explosion. Experiments show that there is a reproducible limit (the superheat limit) for the temperature which may be reached before explosive boiling occurs (Skripov and Pavlov 1989; Skripov 1974).

This comes about as follows. As the water is heated at constant pressure, the volume expands and the temperature increases. The intermolecular forces which hold the water together become weaker because of the expansion (the intermolecular distance increases). At the same time, the molecular agitation is increased by the rising temperature, resulting in an increase in the momentum forces tending to push the molecules apart. At some point, a nearly exact balance is reached between the intermolecular forces tending to hold the water together and the momentum forces tending to push the fluid apart (Lighthill 1956). This equilibrium corresponds closely to the limit of superheat and exactly to the state E in Figure 3, where $(\partial P / \partial v)_T = 0$.

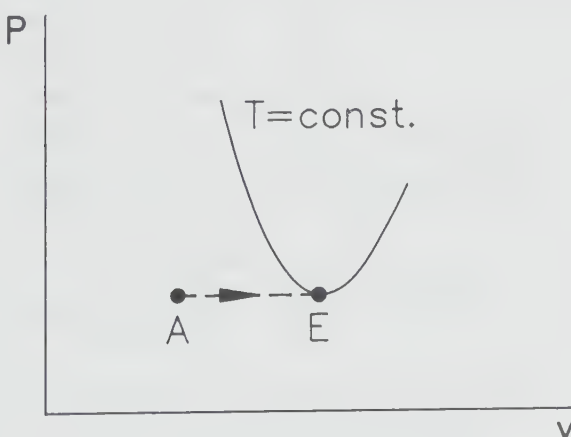


Figure 3. The spinodal limit at state E corresponds to the maximum possible superheat. State A is the initial equilibrium state.

Note that the states to the right of state E are absolutely unstable, in agreement with the stability condition $(\partial P / \partial v)_T < 0$.

A comprehensive discussion of explosive boiling would include the concept of *nucleation*, which plays an essential role in triggering the explosive boiling.

A second and familiar example of the leap from a metastable state is provided by a chemical explosion. Suppose that a room is filled with a stoichiometric mixture of hydrogen and oxygen, i.e., in the proportions $H_2 + 1/2 O_2$. Such a mixture is very stable, in the absence of high temperature, sparks, flames and the like, which could serve as triggers. In short, the mixture is in a metastable state and can leap to a new, stable equilibrium state, consisting of hot, gaseous H_2O . If the mixture is far from stoichiometric (e.g., $H_2 + 15 O_2$), the mixture will be outside the flammability limits and no leap will take place.

As a rule of thumb, the further a state is from equilibrium, the more violent and/or rapid will be the uncontrolled leap to a new equilibrium state. Technical devices, such as a fuel cell or automobile, however, are designed to control and tame the transition for purposes such as doing work.

Possible and impossible phase transitions. We consider that the phase transition takes place across a front, such as a shockwave. This front will have a finite thickness which will incorporate in its structure both the phase change and the pressure-density change. The front may or may not be stable. If there is instability, it may take the form of splitting into two separate fronts, or the appearance of a chaotic, unsteady surface, among other possibilities. We will treat the wave fronts as discontinuities in most cases, and require that energy, momentum and mass be conserved across the front, and that the entropy creation be positive or zero, but not negative. These requirements constitute the Rankine-Hugoniot equations, that is, the shock jump conditions.

Some of the recently discovered transitions have been described in the past as "impossible". Among them are the *liquefaction shock* and the *rarefaction shock*. Perhaps the most celebrated of these "impossible" phenomena is the rarefaction shockwave, at least in what might be called the popular press. It was believed that such a rarefaction discontinuity violated the Second Law of thermodynamics by destroying entropy. It might be interesting to see if this is the case!

As it turns out, there are at least two forms of rarefaction shocks in fluids. Let us consider the simpler, single-phase version in which the fluid is a homogeneous vapor. I wish to calculate the entropy jump $s_2 - s_1 \equiv [s]$ across a shock, where s_1 is the specific entropy upstream of the shock and s_2 the specific entropy downstream of the shock, and show that it can be positive for a rarefaction (expansion) shock, so that the second law is satisfied. By using the Rankine-Hugoniot equation,

$$[h] = v_1 [P] + \frac{1}{2} [v] [P], \quad (1.1)$$

where h is the specific enthalpy, v specific volume, P the pressure and the jump notation follows that for the entropy, i.e., $[P] = P_2 - P_1$ and so on. If the enthalpy $h(s, P)$ is expanded in a Taylor series (Thompson 1972, p. 318), the entropy jump is found to be

$$[s] = \frac{1}{12} T_1 \left[\frac{\partial^2 v}{\partial P^2} \right]_s [P]^3 + 0 ([P])^4. \quad (1.2)$$

For ordinary compression shocks, the pressure increases across the shock and $[P] > 0$. The second derivative $(\partial^2 v / \partial P^2)_s$ is normally positive: For example, the isentrope of an ideal gas in the pressure-volume plane curves upward, as shown in Figure 4.

Thus, for a compression shock, all of the terms through $[P]^3$ are positive and normal compression shocks may be expected to satisfy the Second Law, at least for small amplitudes (more powerful arguments prove the validity for all amplitudes).

Now consider applying Equation (1.2) to a rarefaction shock, for which $[P] < 0$. The density jump $[\rho]$ will also be negative, as shown by the shock condition

$$[w]^2 = - [P] [v] \quad (1.3)$$

where $[w]$ is the change in velocity across the shockfront. Thus, both the pressure and the density will decrease across the shockfront, while the velocity increases.

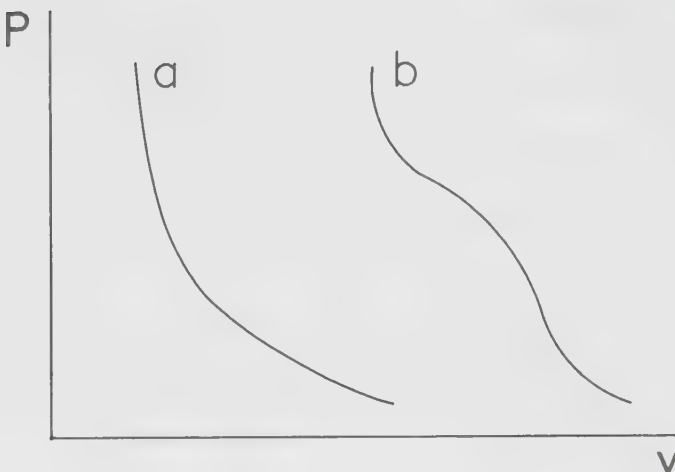


Figure 4:
 a) Positive curvature of an ideal-gas isentrope.
 b) Negative curvature required for a rarefaction shock.

A glance at Equation (1.2) shows that a rarefaction shock can satisfy the condition of increasing entropy only if the partial second derivative is negative, as shown in Figure 3.

Rarefaction shocks have now been found in many materials, including fluids, glass, rubber, quartz and iron. In the case of rarefaction shocks in a single-phase vapor, Dr. Cramer will describe their peculiar behavior quite thoroughly.

Finally, the second derivative $\left[\frac{\partial^2 v}{\partial P^2} \right]_s$ will be written in the coming sections in the more convenient nondimensional form

$$\Gamma \equiv -v \frac{\left(\frac{\partial^2 P}{\partial v^2} \right)_s}{2 \left(\frac{\partial P}{\partial v} \right)_s}.$$

This form retains the property that a negative value of Γ corresponds to a rarefaction shock satisfying the Second Law and a positive value of Γ corresponds to a compression shock satisfying the Second Law. The parameter Γ is usually called the *fundamental derivative*, because it plays an ubiquitous role in gas dynamics (Thompson 1971). It is sometimes suggestively called the *nonlinearity parameter*.

2. REGULAR AND RETROGRADE FLUIDS

The idea of a distinction between a *regular* and a *retrograde* fluid was introduced in Section 1. A regular fluid was defined as a fluid such as water which condenses on isentropic expansion. A retrograde fluid such as octane was defined as a fluid which condenses on isentropic compression. Now we wish to put these definitions on a formal and physical basis.

Temperature-entropy diagrams. Consider the saturated-liquid boundary and the saturated-vapor boundary for a liquid-vapor system on a temperature-entropy diagram, as shown on Figure 5 (note that both saturation boundaries are labeled σ). This diagram is typical of substances such as water or carbon dioxide, among many others. For an arbitrary point A on the saturated vapor boundary, it is clear that equilibrium condensation along an isentropic path corresponds to the arrow $A \rightarrow B$. The pressure is decreasing along this path, along with temperature, because $(dP/dT)_\sigma$, i.e. the slope of the vapor-pressure curve, is always positive. Thus, we are dealing here with condensation in an isentropic rarefaction: By definition, the fluid is *regular*. All fluids which have a saturated-vapor boundary with $(ds/dT)_\sigma < 0$ are regular. By analogous reasoning, all fluids which have a saturated-vapor boundary with $(ds/dT)_\sigma > 0$ are *retrograde*. In Figure 6, the fluid is strictly retrograde over temperatures between X and Y, and regular above X and below Y. It has become conventional, however, to describe a fluid as retrograde if $(ds/dT)_\sigma$ is positive over any portion of the saturated-vapor boundary.

Relation of regular and retrograde behavior to the heat capacity. Starting from the Gibbs equation,

$$Td\sigma = du + Pdv \quad (2.1)$$

and using thermodynamics identities, it is easy to derive the equation

$$T \left[\frac{ds}{dT} \right]_\sigma = c_v + T \left[\frac{\partial P}{\partial T} \right]_v \left[\frac{dv}{dT} \right]_\sigma \quad (2.2)$$

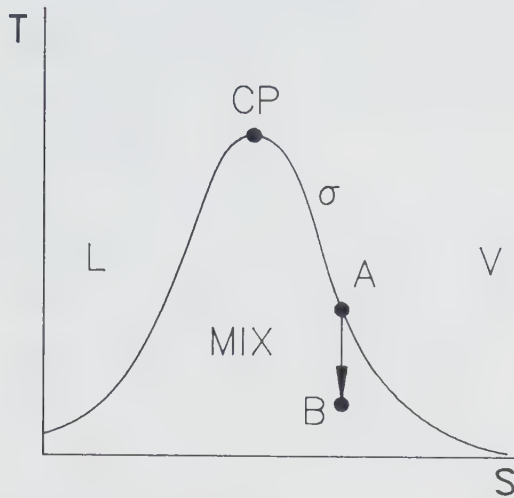


Figure 5. Saturated-liquid and saturated-vapor boundaries for a regular fluid.
L = liquid, MIX = mixture, V = vapor

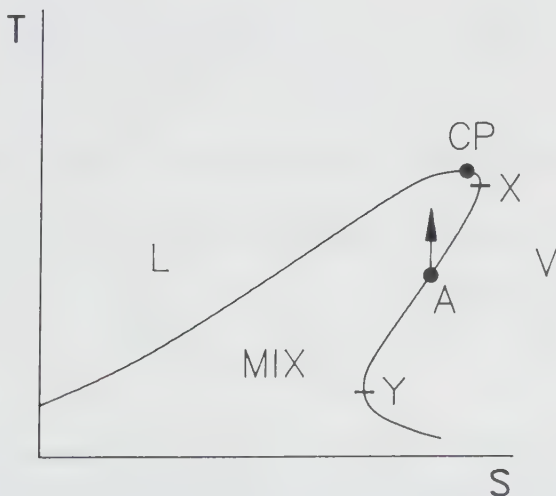


Figure 6. Saturated-liquid and saturated-vapor boundaries for a retrograde fluid.

which relates the slope $(ds/dT)_\sigma$ of the saturation boundary to the heat capacity c_v . The equation applies to both the saturated-liquid and saturated-vapor boundaries, but our interest is focused on the latter. The partial derivatives and heat capacities correspond to single-phase values in the region immediately adjacent to the saturation boundary σ (i.e. liquid or vapor) and the subscript σ refers to saturation properties. On the liquid side, both of the right-hand terms are positive right up to the critical point and the slope given by (2.2) is positive. On the vapor side, the first right-hand term, c_v , is always positive and the second term is always negative. For sufficiently large values of the vapor c_v , the slope given by (2.2) can become positive, corresponding to retrograde behavior. Near the critical point on the vapor side, however, the slope $(ds/dT)_\sigma$ will always be negative, because the value of $\left[\frac{dv}{dT}\right]_\sigma$ approaches $-\infty$ much more rapidly than c_v approaches $+\infty$, as described by the respective critical exponents (the above statement also holds for a classical van der Waals description, in which c_v remains finite).

The work discussed here deals chiefly with shock-induced vapor-liquid phase changes in fluids with large molar heat capacities, i.e. fluids with many molecular degrees of freedom, octane for example. As we have seen, the vapor of such fluids tends to condense on adiabatic compression (retrograde behavior), as distinct from the vapor of fluids of lower heat capacity, such as water, which tends to condense on adiabatic expansion (regular behavior). For liquid-vapor systems showing retrograde behavior, many of the accepted rules of gas-dynamics are inverted and new phenomena appear, e.g. the liquefaction shock wave described by Dettleff *et al.* (1979).

It is convenient to assign each substance a *characteristic heat capacity*

$$\tilde{c}_v \equiv \frac{c_v^0(T_c)}{R}, \quad (2.3)$$

i.e., the ideal-gas heat capacity at the thermodynamic critical temperature T_c , normalized by the gas constant R (in general, the non-dimensional heat capacity c_v/R will be denoted \hat{c}_v). Compression of the vapor will lead to condensation for sufficiently large values of \tilde{c}_v , because the work of compression produces a

correspondingly small increase in temperature: In this case, the behavior is retrograde, as typified by octane in Figure 7. For smaller values of \tilde{c}_v , compression of the vapor will lead to such a large temperature rise that no condensation is possible: The behavior is regular as typified by ethene and other common substances such as air and steam.

Retrograde phase changes, in the general sense of an adiabatic transition to a denser phase under increasing pressure, are often found in solids in association with shock waves. The synthesis of industrial-grade diamond from graphite is one specific example. The "ice-skating" transition from ice to water when the ice is subjected to increasing pressure is a solid-liquid example.

A brief inspection of a temperature-entropy diagram such as the one shown below suggests the possibility of various adiabatic phase changes in retrograde liquid-vapor systems. Several forms of wave-induced phase changes have recently been studied and observed.

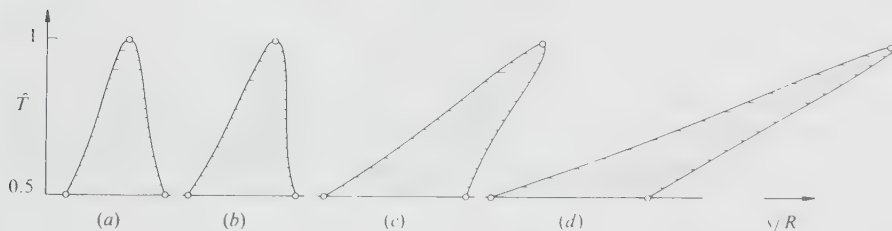


Figure 7. Temperature-entropy diagrams of substances with increasing characteristic heat capacities \tilde{c}_v . The reduced temperature \hat{T} ranges from 0.5 to the critical-point value 1.0. Only the liquid and vapor-saturation boundaries are shown. (a) Ethene C_2H_4 , $\tilde{c}_v = 4.03$; (b) Propane C_3H_8 , $\tilde{c}_v = 9.64$; (c) n-Octane C_8H_{18} , $\tilde{c}_v = 36.82$; (d) Pf-methyldecaline $C_{11}F_{20}$, $\tilde{c}_v = 73.4$.

Definitions and identities. From corresponding-states calculations (Lambrakis 1972), it is found that the saturated vapor boundary just reaches the vertical ($(ds/dT)_\sigma$ has a value of zero) for $\tilde{c}_v = 11.2$, a value which happens to correspond to sulfur hexafluoride SF_6 and falls between propane and butane in the alkane-series hydrocarbons. Benzene, with a characteristic heat capacity

$\tilde{c}_v = 17.1$, thus shows a limited degree of retrograde behavior. In order to quantify the retrogradicity, it is convenient to introduce the non-dimensional parameter $r(T)$,

$$r(T) \equiv \left[\frac{\partial T}{\partial v} \right]_p \left[\frac{ds}{dP} \right]_\sigma , \quad (2.4)$$

where the partial derivative refers to the value in the single-phase region (vapor in the present case) adjacent to the saturation boundary σ and the total derivative refers to the variation along the saturation boundary, as in (2.2). Because the slope $(dP/dT)_\sigma$ of the vapor-pressure curve is positive, $r(T)$ will necessarily have the same sign as $(ds/dT)_\sigma$. Thus, retrograde behavior is normally associated with $r > 0$ and regular behavior with $r < 0$ on the vapor boundary. The dependence of such behavior on the single-phase heat capacity can be shown by writing (2.4) in the form

$$r(T) = \frac{c_p}{T} \left[\frac{\partial T}{\partial v} \right]_p \left[\frac{dT}{dP} \right]_\sigma - 1 , \quad (2.5)$$

in which the coefficient c_p plays the dominant role in fixing the magnitude of the product on the right-hand side. Using the Clapeyron equation, (2.5) can be rewritten as

$$r(T) = c_p \left[\frac{\partial T}{\partial v} \right]_p \left[\frac{v_{lv}}{L} \right] - 1 , \quad (2.6)$$

where $v_{lv}(T)$ is the volume change of evaporation and $L(T)$ is the latent heat (enthalpy of vaporization). In the low-pressure approximation, corresponding to an ideal-gas vapor and the Clausius-Clapeyron equation, this reduces to

$$r(T) = -\frac{c_p^0 T}{L} - 1 . \quad (2.7)$$

The parameter in this form often occurs in heat-transfer problems with phase change.

Regular and retrograde behavior can be conveniently represented in the pressure-temperature plane, as shown in Figure 2. The retrogradicity $r(T)$ defined in (2.4) can be expressed in the appropriate form

$$r(T) = \frac{(\partial P/\partial T)_s - (dP/dT)_\sigma}{(dP/dT)_\sigma}, \quad (2.8)$$

which describes the difference in slopes between isentropes and the vapor-pressure curve σ . For $r > 0$, isentropes are steeper than the vapor-pressure curve and condensation occurs on compression; for $r < 0$, isentropes are less steep than the vapor-pressure curve and condensation occurs on expansion.

For more detail on retrograde/regular behavior, especially the physical aspects, the reader is referred to the paper of Thompson, Carofano and Kim (1986).

Both Max Planck (1903) and van der Waals (1908) were aware of the unusual properties of fluids with large molar heat capacities, that is, with many internal (vibrational) degrees of freedom. Bethe, however, dismissed the possibility of such fluids in his celebrated report (Bethe 1942) and thus reached formally incorrect conclusions about phenomena such as shock splitting. Of the known fluids, however, the great majority are retrograde. Of the known solid and solid-liquid systems, the majority are retrograde, including the minerals of which the Earth is made.

The kink: discontinuity in the equilibrium soundspeed at the saturation boundary. In the liquid-vapor region adjacent to a saturation boundary, the isentropic compressibility of the mixture is increased over that of the single-phase fluid, i.e. the mixture is "softer".

The soundspeed C , given by $C^2 = -v^2 (\partial P/\partial v)_s$, is thus discontinuous at the saturation boundary. A measure of the jump magnitude is provided by the "kink" k ,

$$k(T) = \frac{(\partial P/\partial v)_s - (dP/dv)_{sm}}{(dP/dv)_\sigma} = -\frac{T}{c_v} \left[\frac{\partial P}{\partial v} \right]_T \left[\frac{ds}{dP} \right]_\sigma^2 \geq 0 , \quad (2.9)$$

where the subscript m refers to the equilibrium derivative on the mixture side of the saturation boundary σ and the other derivative corresponds to the single-phase value; thus, making use of the continuity of v at σ , k gives the difference between soundspeeds at the saturation boundary in the form

$$k(T) = \frac{C^2 - C_m^2}{C_m^2} \geq 0 , \quad (2.10)$$

where C is the equilibrium soundspeed. In Figure 8(a), k is a measure of the difference in slopes of the equilibrium isentropes at point g on the saturated-vapor boundary. The equilibrium soundspeed of the mixture is thus always smaller than or equal to that in the adjacent single-phase region. (The special case of equal soundspeeds, corresponding to $k = 0$, occurs at points where the isentrope is tangential to the saturation boundary, where $\Gamma = 0$.)

The "kink" k and "retrogradicity" r are related by

$$\frac{k}{r^2} = \frac{T}{c_v} \left[\frac{\partial P}{\partial T} \right]_v \left[\frac{\partial v}{\partial T} \right]_p = \gamma - 1 \geq 0 , \quad (2.11)$$

where γ is the ratio of specific heats in the single phase. For $r > 0$, the equilibrium isentrope bends downward at the phase boundary, as shown in Figure 8(a). This situation is associated with equilibrium-state shock splitting (Bethe 1942). For small-amplitude waves, it can be understood as a splitting into two compression discontinuities, a forerunner shock and a condensation shock, which propagate with velocities C and C_m respectively.

For sufficiently large \tilde{c}_v the kink at the saturation boundary will be mimicked at higher pressures in the single-phase vapor region, as shown in Figure 8(b), this behavior being analogous to that of isotherms. The curvature of the isentrope is represented by the non-dimensional parameter Γ ,

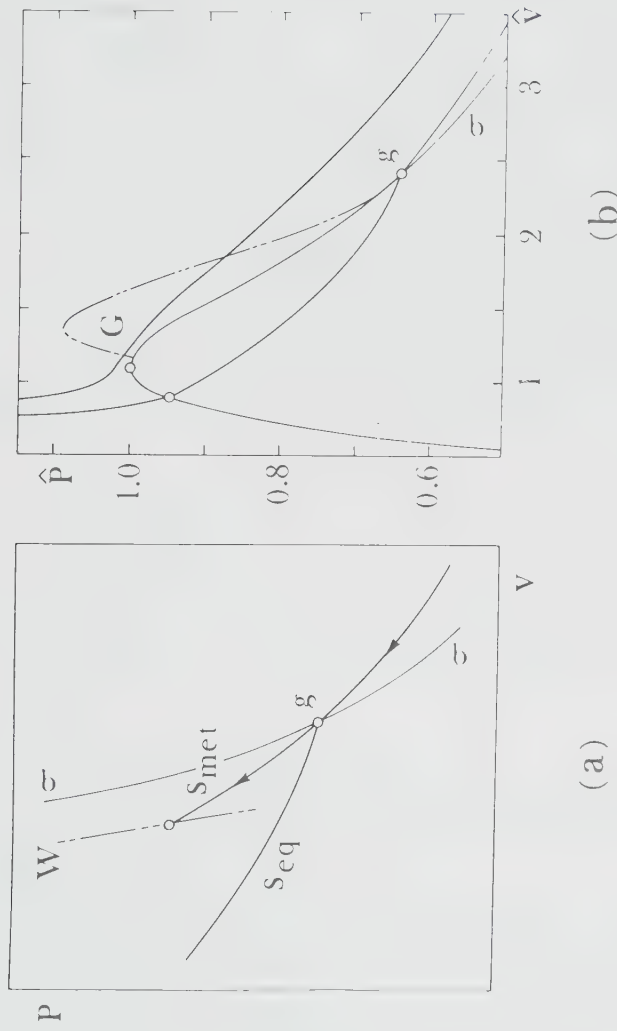


Figure 8. (a) Equilibrium and metastable isentropes at the saturated-vapor boundary for the case of retrograde behavior ($r > 0$). W = Wilson line (super-saturation limit), σ = saturation boundary; (b) Analogy of a retrograde kink ($r > 0$) at g to $\Gamma < 0$ behavior (in region G) at higher pressure in the single-phase vapor region. The isentropes shown are not to scale.

$$\Gamma \equiv \frac{-v(\partial^2 P / \partial v^2)_s}{2(\partial P / \partial v)_s}, \quad (2.12)$$

sometimes referred to as the fundamental gasdynamic derivative or non-linearity parameter. For a perfect gas, $\Gamma = \frac{1}{2}(\gamma + 1)$. For the special case in Figure 8(b), $\Gamma < 0$ over a limited region G , analogous to $\Gamma = -\infty$ at the kink g on the saturated-vapor boundary. The condition $\Gamma < 0$ is necessary and sufficient for the existence of rarefaction shock waves (Bethe 1942; Zel'dovich 1946; Thompson & Lambrakis 1973). A familiar material for which $\Gamma < 0$ is the ordinary stretched rubber band, where v in (2.12) is replaced by length ℓ and P by the negative of tension. Indeed, rarefaction shocks are observed in this case and in other common materials, such as quartz and glass.

In the experiments reported in the following section, rarefaction shocks are associated with the kink at point g in Figure 8(b): the upstream states lie in the mixture region and the downstream states in the (dry) vapor region, so that the shockfront is coincident with a phase discontinuity. The flow thus experiences sudden evaporation.

3. LIQUEFACTION, SPLITTING AND RAREFACTION SHOCKS

As we have discussed, a variety of phase changes proceed spontaneously and often quite rapidly from a metastable state without the need for significant heat transfer. Several examples were given in Section 1 and a partial listing is provided in Table 1. We cannot pursue all of these fascinating phenomena; rather, we concentrate on the *liquefaction shock* and its two companions, the *split shock* and the *rarefaction-evaporation shock*.

The liquefaction shock was first proposed as a possible form of retrograde behavior by Thompson and Sullivan (1975) in a paper titled "On the Possibility of Complete Condensation Shock Waves in Retrograde Substances" (the term *condensation* in this sense was later replaced by *liquefaction*). Definitive laboratory experiments showing the existence of partial and complete liquefaction shocks were later published by Dettleff, Thompson, Meier and Speckmann (1979).

As it turned out, the liquefaction shock belonged to the family of "impossible" events. Landau and Lifshitz (1959) wrote in their excellent book on fluid mechanics the following:

It should be emphasized that condensation discontinuities are a distinct physical phenomena and do not result from the compression of gas in an ordinary shock wave; the latter effect cannot lead to condensation, since the increase of pressure in the shock wave has less effect on the degree of supersaturation than the increase of temperature...

This argument is, of course, correct only for a regular fluid and is thus incomplete. For a more complete historical description, see Dettleff, Thompson, Meier and Speckmann (1979).

The liquefaction shock and associated discontinuities. Liquefaction shocks are possible for fluids with a large characteristic heat capacity \tilde{c}_v , with correspondingly large values of the retrogradicity r . According to the calculations of Thompson and Sullivan (1975), the minimum value of \tilde{c}_v , permitting a complete phase transition from saturated vapor to saturated liquid

Table 1
ADIABATIC PHASE TRANSITIONS IN LIQUID-VAPOR SYSTEMS
(Partial List)

TRANSITION PHENOMENON	AUTHOR	YEAR
Rain and Snow	G Old Testament (Genesis)	900 BC
Turbine Expansion/Condensation	G Heron of Alexandria	120 BC
Negative Liquid Pressure	B Berthelot	1850
Vapor Explosion	B Dufour	1861
Supersaturation of a Vapor Jet	B Helmholtz	1886
Cavitation in Water	G Reynolds	1894
Condensation-Induced Shock ("moisture shock")	T Prandtl/Wieselsberger	1935
Vapor-Phase Rarefaction Shock (not yet demonstrated)	T Zel'dovich	1946
Liquid-Evaporation Wave	B Grolmes/Fauske	1974
Cavitation-Wave Splitting(?)	T Yamaguchi/Ichikawa	1977
Complete and Partial Liquefaction Shocks	T Dettleff/Thompson/Meier	1979
Rarefaction Shock from a Critical State	B Borisov <i>et al.</i>	1983
Shock Splitting	T Speckmann/Thompson/Kim	1983
Chapman-Jouguet Liquid-Evaporation Wave	T Chaves	1984
Mixture-Evaporation Rarefaction Shock	T Thompson/Carofano/Kim	1986

G = Regular

T = Retrograde

B = Both

(complete liquefaction) is 24.1. In most experiments approaching complete liquefaction of a vapor, fluids with $\tilde{c}_v \sim 50$ have been used. Properties of typical test fluids are shown in Table 2. The substances FC-75, PP3 and PP1 are proprietary heat-transfer fluids. PP3 is mainly perfluoro-dimethylcyclohexane and iso-octane is 2,2,4-trimethylpentane, equivalent to 100-octane gasoline.

Table 2
Properties of Some Retrograde Substances

Property	Substance			
	FC-75	PP3	Iso-Octane	PP1
Formula	C ₈ F ₁₆ O	C ₈ F ₁₆	C ₈ H ₁₈	n-C ₆ F ₁₄
Molecular Weight M	416.06	400.060	114.230	338.040
Boiling Point (K)	375.80	374.650	398.820	330.310
Critical Temperature T _c (K)	500.21	514.650	568.760	448.000
Critical Pressure P _c (bar)	16.07	18.810	24.870	18.680
Critical Volume v _c (cm ³ /g)	1.70	1.520	4.310	1.790
Acentric Factor ω	0.55	0.472	0.394	0.483
$\tilde{c}_v = c_v^0 (T_c)/R$	53.40	53.900	36.800	40.500
Purity of Sample	—	—	99.98%	98.80%

Extensive shock-tube experiments with liquefaction shocks have been carried out at the Max-Planck-Institut für Strömungsforschung in Göttingen (MPI) and at Rensselaer Polytechnic Institute in Troy (RPI). Results from both places will be shown.

In the *RPI experiments*, the closed end of the shock tube test section is replaced by an open end, followed by a large-diameter, closed observation chamber, shown in Figure 9. The observed flow is a discharge emerging from a tube, headed by a shock wave. This arrangement yields a rich variety of phase-change phenomena which can be observed photographically.

The shock tube at RPI has been described by Thompson *et al.* (1986). It is heated to an initial test temperature T_0 in the range 80–170°C: For the test fluids used, this allows an initial test pressure $P_0 > P_\sigma(T_0)$ in the range from 0.1 bars to well over 10 bars.

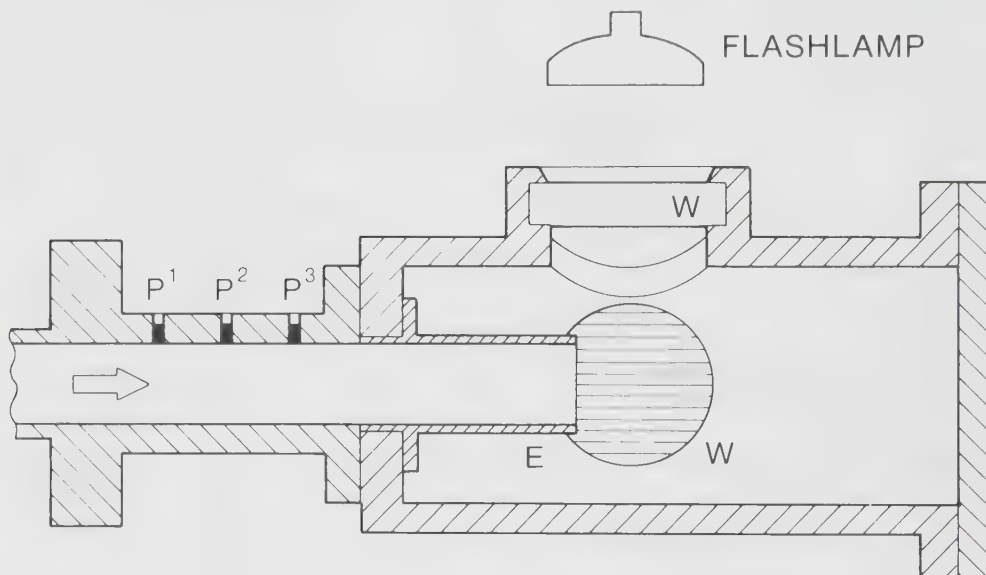


Figure 9. Observation chamber mounted at the end of the test section of the Rensselaer shock tube. Pressure transducers are P^1 , P^2 and P^3 . W = window (with background grid shown in the vertical window). E = end of the constant-diameter test section. The arrow indicates both the shock propagation and the flow direction.

The shock tube inside diameter is 57.6 mm, the driver section is 3.50 m long and the test section is 1.67 m long, measured from the diaphragm to the open end. In shock-tube experiments from the year 1990 and beyond, the test section is 2.8 meters in length and additional modifications have been made.

Three Kistler pressure transducers are located 306, 256, and 206 mm from the open end of the test section. The shock tube, including the observation chamber, is wound with electrical resistance heating and covered with ceramic-fiber insulation. With this arrangement, initial test temperatures can be maintained to within $\pm 2^\circ\text{C}$. Pressure burst of the diaphragms is achieved by releasing nitrogen driver gas from the gas bottle. Burst pressures ΔP between 1 and 40 bars can be selected, using various combinations of diaphragm films. Transient data from the three pressure transducers and from a photodiode registering the flashlamp discharge time are stored in a digital transient recorder. The shock signal at the first pressure transducer is used as an initiating signal.

Experimental results. Photographs are taken through the side window W shown in Figure 9. For partial liquefaction shocks, the shockfront is clearly visible as a two-phase mixture, somewhat similar to a cloud in the atmosphere. Figure 10 shows a partial liquefaction shock in iso-octane in two different views.

The liquefaction shockfront LS remains planar until it is overtaken by expansion waves originating at the end E of the shock tube, producing a curved and weakening shockfront. Splitting occurs at the triple point TP: It is assumed that the pressure amplitude of the forerunner shock at this point is just sufficient to produce critical supersaturation S_c , i.e., that splitting occurs at the *Wilson line*. Enlarged photographs of the triple point TP show that the three discontinuities propagate at the same normal velocity (see Figure 11). Measurement of this velocity yields a unique value for the critical supersaturation. We define the local supersaturation $S(P,T)$ in the conventional way as

$$S \equiv \frac{P}{P_\sigma(T)} \quad (3.1)$$

and affix the subscript c to indicate the critical value S_c . A large number of measurements of S_c will determine the Wilson line.

For smaller driving pressures, splitting will occur in the shock tube test section and the wave system will be globally split on emergence (Thompson *et al.* 1984).

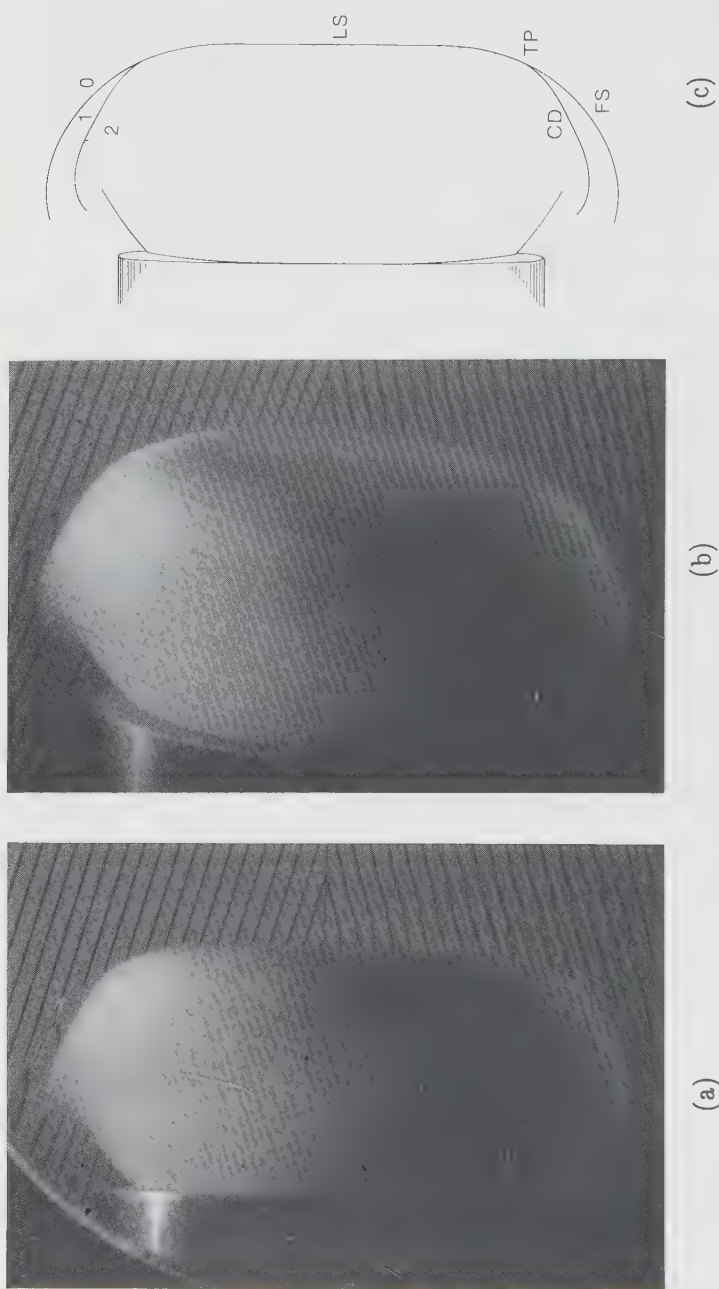


Figure 10. Emergence of a liquefaction shock wave in iso-octane into the observation chamber. Flow is from left to right. At the triple point, i.e. TP, the main liquefaction shock LS has split into a curved, vapor-phase forerunner shock FS and a condensation discontinuity CD. Initial conditions $P_0 = 1.10 \text{ bar}$, $T_0 = 110^\circ\text{C}$. Plane liquefaction-shock Mach number $M_0 = 2.79$. (a) Side view. (b) Oblique view, showing the plane liquefaction shockfront. CD = condensation discontinuity, FS = forerunner shock, TP = triple point, LS = liquefaction shockfront. (c) Nomenclature and splitting sketch.



Figure 11. Closeup of the triple point in FC-75.

Initial conditions $P_0 = 0.95$ bar, $T = 110^\circ\text{C}$.

Plane liquefaction shock Mach number $M_0 = 2.04$.

Each of the three discontinuities (liquefaction shock, forerunner shock and condensation discontinuity) is described by a Rankine-Hugoniot equation,

$$[h] = \bar{V} [P], \quad (3.2)$$

where the square brackets denote a jump, i.e., the downstream value minus the upstream value, and \bar{V} denotes the arithmetic average of the upstream and downstream values. The successive thermodynamic states will be denoted 0, 1, 2:

- 0 equilibrium superheated vapor: initial state
- 1 supersaturated vapor (metastable): intermediate state
- 2 equilibrium mixture: final state.

The possible sequences of state are then $0 \rightarrow 1$ (forerunner shock), $1 \rightarrow 2$ (condensation discontinuity) and $0 \rightarrow 2$ (liquefaction shock). In the case of a strong liquefaction shock, the downstream state 2 could be compressed liquid, but such a case does not occur in the results reported in this section.

One-dimensional wave splitting for vapor-condensation is shown schematically for one-dimensional flow in Figure 12. The wave and fluid motion is initiated by a driving piston, as in conventional one-dimensional gasdynamics. For uniform initial states, the waves may be considered to be simple with all waves travelling to the right.

In the most elementary form, wave splitting shown in Figures 8 and 12 can be explained simply by the difference between the single-phase soundspeed C_f and the mixture soundspeed C_m . $C_f > C_m$ at both the saturated-liquid boundary and the saturated-vapor boundary. Under the assumption of equilibrium states and small-amplitude (acoustic) waves, the forerunner shock wave FS propagates with the single-phase soundspeed and the phase-discontinuity wave CD propagates with the mixture soundspeed. Because the single-phase soundspeed is greater, the forerunner wave will run ahead of the phase-discontinuity wave, i.e., shock splitting will occur.

The difference between the single-phase soundspeed C_f and the mixture soundspeed C_m is expressed at the saturation boundary by the "kink" k by

$$k(T) \equiv \frac{C_f^2 - C_m^2}{C_m^2} = \frac{-T}{c_v} \left[\frac{\partial P}{\partial v} \right]_T \left[\frac{ds}{dP} \right]_\sigma^2. \quad (3.3)$$

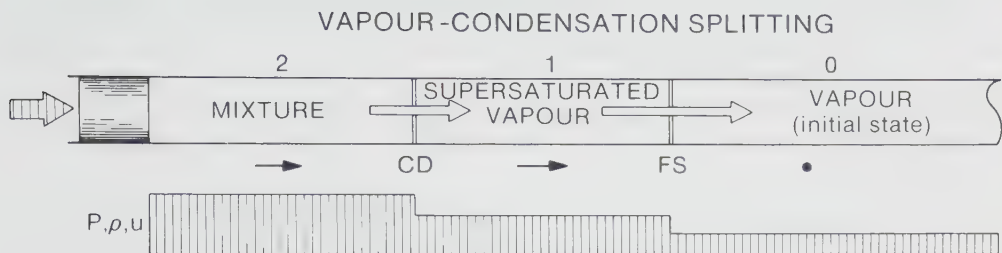


Figure 12. Conceptual representation of one-dimensional wave splitting in a liquid-vapor system. All waves are travelling to the right. Direction of the impulsive piston motion is indicated by the broad-banded arrow, fluid motion by the thin black arrows. The compression wave leads to vapor-condensation wave splitting. FS = forerunner shock, CD = condensation discontinuity.

A realistic set of shock adiabats is shown in Figure 13, using the somewhat unconventional coordinates volume and entropy. The initial state is at 0. The path taken from the initial state depends on the *amplitude* of the shock, which is measured here by the entropy jump $s - s_0$.

Consider the path $0 \rightarrow e$ along the dry adiabat DA. Although the saturated-vapor boundary σ has been crossed at g, no condensation has occurred, because the supersaturation is too small: The downstream state is metastable vapor. The shock is a "dry" shock. If the shock amplitude is increased to point 1, crossing the Wilson line W, the critical supersaturation will be reached (very large nucleation rate) and condensation will occur. The state will jump from the metastable state 1 to a new, dynamically permissible state satisfying the Rankine-Hugoniot equations. Depending on the shock amplitude, these permissible states may lie on the condensation adiabat CA or the equilibrium adiabat EA. A jump from 1 to a certain point on CA represents a condensation discontinuity travelling at a speed fixed by the slope of the

corresponding Rayleigh line. At state 2, the equilibrium adiabat EA and the condensation adiabat cross and a further increase in amplitude will apparently produce a joined, continuous liquefaction shock.

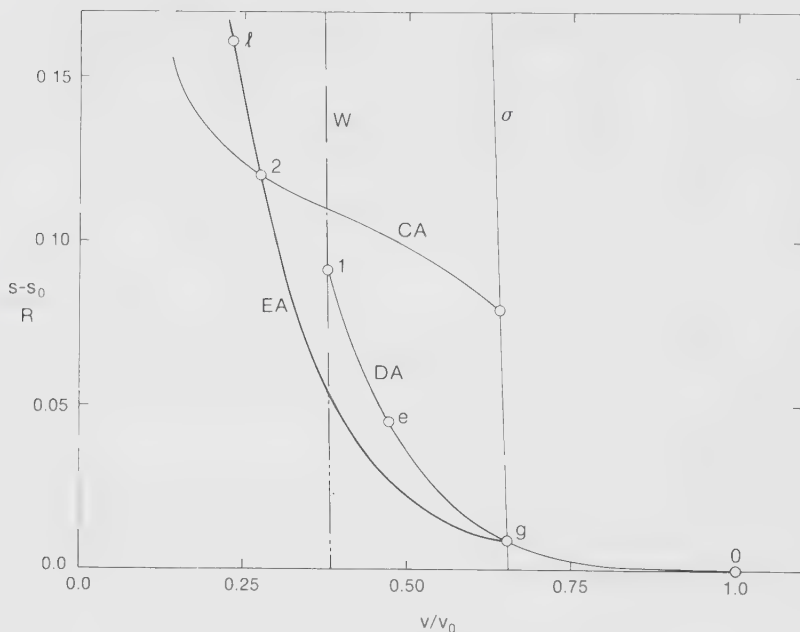


Figure 13. The system of shock adiabats for shock splitting in the fluorocarbon FC-75, calculated from the Hobbs equation of state. Forerunner shock Mach number $M_{FS} = 1.497$. Initial conditions $P_0 = 1.80$ bar, $T_0 = 135^\circ\text{C}$, $v_0 = 40.85 \text{ cm}^3/\text{g}$, $C_0 = 82.3 \text{ m/s}$. EA = equilibrium adiabat, CA = condensation adiabat, DA = dry adiabat (metastable), σ = saturated vapor boundary, W = Wilson line. Adiabats are in the entropy-volume plane (\hat{v} is the specific volume normalized by the initial volume v_0).

A remarkable feature of the condensation discontinuity is that it travels subsonically with respect to the fluid ahead. It can be shown (Thompson, Chaves, *et al.*, 1987) that

$$M_{CD} \approx M_{FS}^{-1}. \quad (3.4)$$

That is, the Mach number of the condensation discontinuity CD is approximately the inverse of the Mach number of the forerunner shock.

The inner structure of a diffracted shock wave. Figure 10 shows the typical structure of a liquefaction shockfront as it undergoes diffraction while expanding from the end E of the shock tube into the large-diameter observation chamber. This expansion structure is surprisingly similar to that of a perfect gas, shown in Figure 14. The strong vortex (marked with a cross +) and the Prandtl-Meyer expansion characteristics are notable features of the axisymmetric, unsteady flow. An internal shock originates near the vortex center. Note that the extreme characteristic in the expansion fan has not yet reached the shock tube center-line, so that the uniform state below this fan is identical to that in the shock tube. For the case shown, this region extends right up to the small planar portion of the shockfront. All of these features of the perfect gas diffraction structure carry over to the liquefaction shock, see Figure 10.

We refer to the structure of the extreme expansion fan as the "Mach trumpet", as shown in Figure 15.

The "trumpet" is actually a Mach construction based on the supersonic flow in the two-phase fluid downstream of the main shock. In Figure 15, the wavefront follows the path C-MC-E-B. It is quite useful in measuring the soundspeed in the mixture (Chen, *et al.* 1986). In addition, the Mach trumpet will, under certain conditions, form the approximate boundary of the rarefaction-evaporation shock.

The rarefaction-evaporation shock (mixture-evaporation shock). The rarefaction shocks found in our experiments are of the mixture-evaporation type. Their formation is associated with the discontinuity in equilibrium soundspeed at the saturated-vapor boundary, i.e. the "kink" k of (3.3), illustrated in Figure 8. The upstream state for these shocks is a liquid-vapor mixture, typically of low

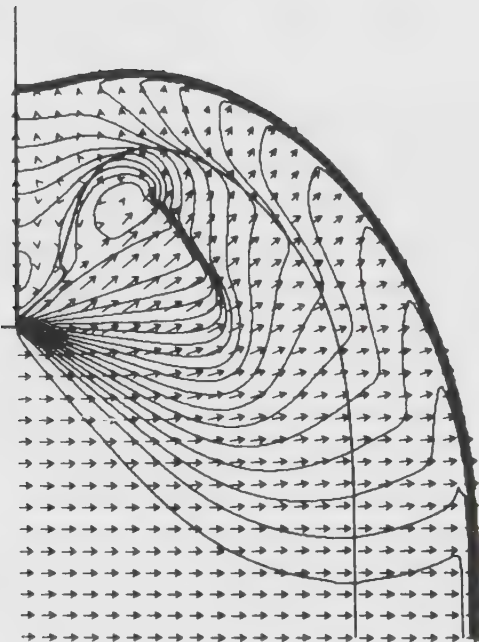


Figure 14. Emerging flow of a perfect gas ($\gamma = \frac{7}{5}$) from a tube, with shock Mach number $M_0 = 3$ and non-dimensional time $c_0 t / R = 0.49$, where R is the tube radius. Velocity vectors and contours of constant pressure are shown. CS = contact surface. The bottom row of arrows is on the shock tube centerline.

moisture, and the downstream state is superheated vapor. The calculated shock-front shown in Figure 16 has a typical "Mach-trumpet" shape similar to that in Figure 15 ($\tilde{c}_v = 25$). The rarefaction shock forming the sides of the trumpet has developed by the nonlinear ($\Gamma < 0$) concentration of the distributed expansion waves. The main compression shock forms the front of the trumpet. Two experimentally observed rarefaction shockfronts are shown in Figure 17.

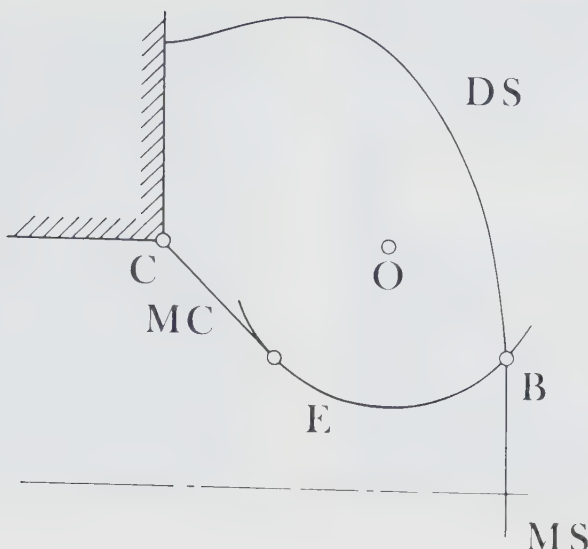


Figure 15. Mach construction, showing the first-signal expansion front E which originates when the plane main shock MS reaches the tube corner C . The diffracted shockfront is labelled DS . The expansion front E is centered on point O , originating at the corner C and convected with the (undisturbed) flow behind the shockfront MS . Supersonic flow in the laboratory frame results in a "Mach-trumpet" configuration: $MC = \text{Mach cone}$.

The pressure range of the expansion at the shock tube exit is on the order of $P_2 - P_0$ and is typically large compared with the maximum possible pressure amplitude of the evaporation shock. In this situation, the evaporation shock discontinuity is imbedded in an isentropic expansion and will evolve toward a double Chapman-Jouguet wave, or sonic-sonic shock, as discussed by Thompson & Lambrakis (1973) for the case of one-dimensional unsteady flow. The sonic-sonic solution is thus the natural limiting form, determined by the characteristic wave velocities, with the normal components of both the inflow and outflow being sonic, e.g. $M = M_{1n} = M_{2n} = 1$. The amplitude of the evaporation-shock is a

maximum in this case, as illustrated in the pressure-volume diagram of Figure 18(a). The evolution of the limiting sonic-sonic solution is shown in Figure 18(b).

For sonic-sonic evaporation shocks, both the entropy jump [s] and the pressure jump [P] (which is negative!) are very small, as illustrated for n-octane in Figure 19. Extensive details are given in Thompson, Carofano & Kim (1986).

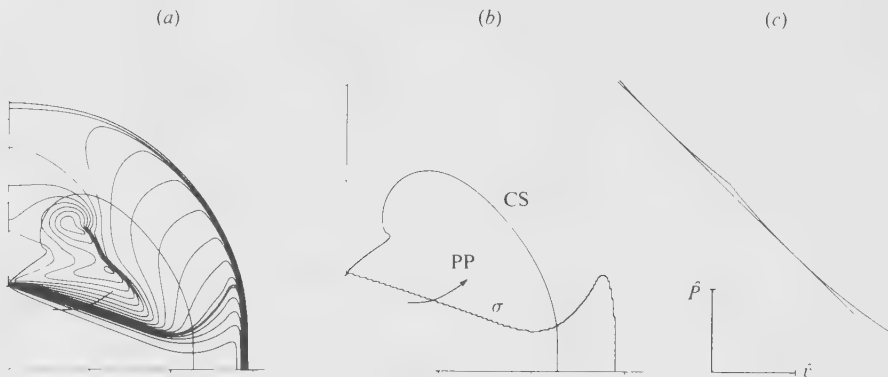
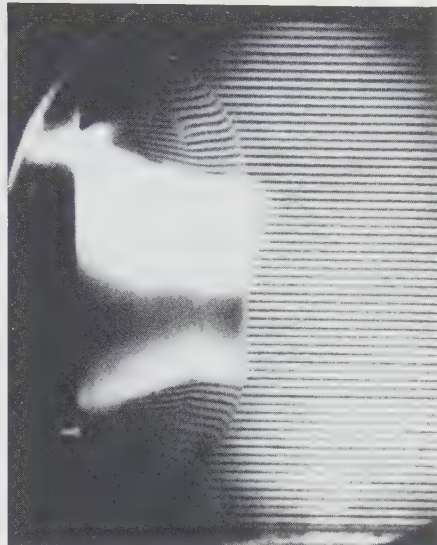


Figure 16. Computed evaporation-rarefaction shock with initial conditions $\hat{P}_0 = 0.275$, $\hat{v}_0 = 6.90$. The liquefaction-shock Mach number $M_0 = 1.45$ and $c_{0t}/R = 1.43$. (a) Pressure contours showing the rarefaction with a form similar to the "Mach trumpet" in Figures 14 and 15. (b) Contact surface CS, vapor saturation boundary σ and particle path PP. (c) Computed adiabat $P(v)$ along the particle path. The pressure bar corresponds to a reduced pressure change of 0.1; the volume bar corresponds to a reduced volume change of 1.



(a)



(b)

Figure 17. Experimental photographs of evaporation-rarefaction shocks. (a) Rarefaction shock with a low-moisture ($y \approx 6\%$) upstream state. Initial conditions $P_0 = 1.30$ bar, $T_0 = 160^\circ\text{C}$. Liquefaction-shock Mach number $M_0 = 2.31$ ($C_0 = 88.68$ m/s). (b) Rarefaction shock with a high-moisture ($y \approx 20\%$) upstream state. Initial conditions $P_0 = 1.50$ bar, $T_0 = 160^\circ\text{C}$. Liquefaction-shock Mach number $M_0 = 2.26$ ($C_0 = 87.99$ m/s).

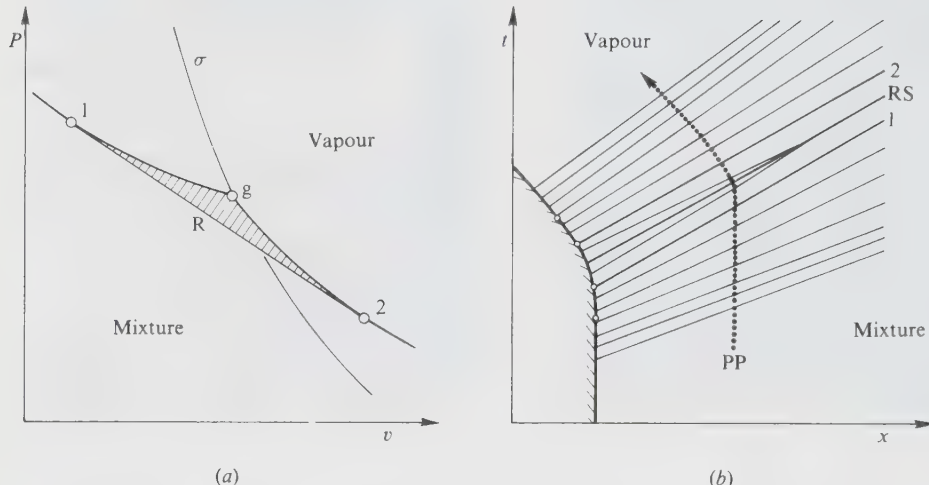


Figure 18. Double Chapman-Jouguet (sonic-sonic) evaporation shocks.
 (a) Construction of the sonic-sonic solution in the pressure-volume plane. The shaded area corresponds to the entropy jump $[s]$. R = Rayleigh line.
 (b) Development of the sonic-sonic shock in one-dimensional flow in an x - t wave diagram, corresponding to piston withdrawal (shaded line). The (Chapman-Jouguet characteristics (1) and (2) are parallel, yielding the asymptotic sonic-sonic solution at $x = \infty$. PP = particle path, RS = rarefaction shock.

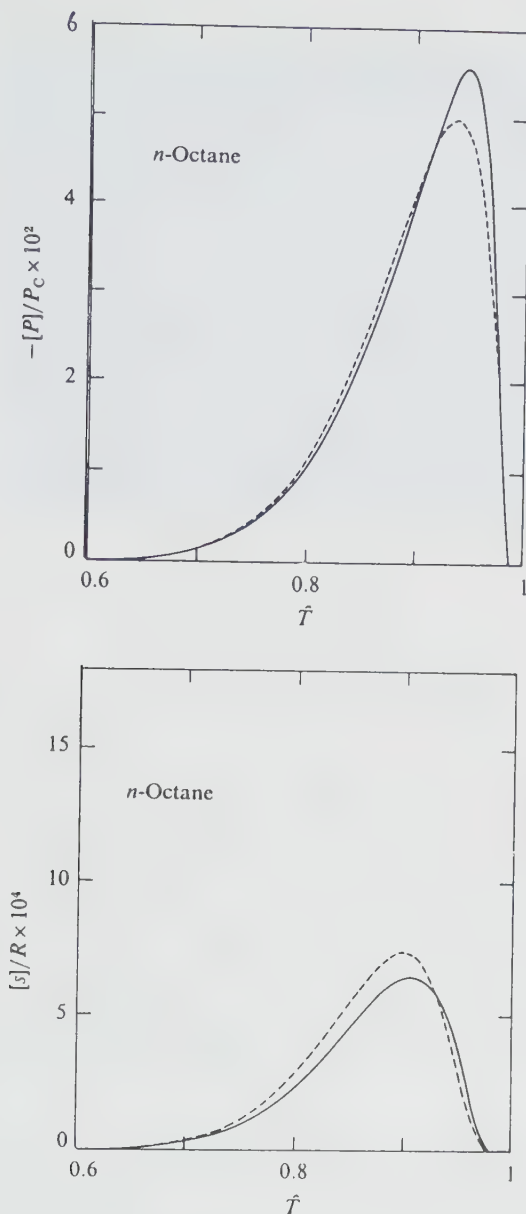


Figure 19. Pressure amplitude $[P]$ and entropy jump $[s]$ for sonic-sonic shocks as functions of reduced temperature \hat{T} . The continuous curves represent "exact" calculations using the Hobbs equation of state, the dashed curves represent closed-form solutions. (a) Pressure jump. (b) Entropy jump.

4. NEAR-CRITICAL STATES

The topic is the *flow of fluids with a state near the thermodynamic liquid-vapor critical point*, including shock-induced and steady flows, which may, or may not be, in a state of thermodynamic equilibrium. This topic is quite new and involves many puzzles.

The rarefaction shock waves of Borisov, Borisov, Kutateladze & Nakoryakov (1983). In a series of careful experiments in Novosibirsk, extending over several years, these workers have demonstrated the existence of rarefaction shock waves originating from a state very near the equilibrium critical point. The measured critical properties of the test fluid CF_3Cl trifluorochloromethane (Freon-13) were as follows:

$$P_c = 39.68 \text{ bar} \quad T_c = 302.02 \text{ K} \quad V_c = 1.72 \text{ cm}^3/\text{g.}$$

Extreme care was taken to achieve a nearly-equilibrium close-to-critical state, including settling times of more than 20 hours and temperature regulation to $\pm 10^{-3} \text{ K}$. The average time for one experiment was about three days. Upon diaphragm burst, a rarefaction wave propagated into the high-pressure side of the shock tube and steepened into a rarefaction shock, as shown in Figure 20.

In Section 1, it was shown that rarefaction shocks can exist *only* if the fundamental derivative $\Gamma < 0$ (see Equation 2.12). The possibility of a negative value of Γ is, in turn, associated with large values of the molar heat capacity c_v/R (See Thompson & Lambrakis 1973 and Zel'dovich 1946). In the case of near-critical states, the heat capacity c_v increases as the critical point is approached according to

$$c_v \propto \epsilon^{-\alpha} \tag{4.1}$$

where α is the critical exponent ≈ 0.1 and $\epsilon \equiv \left| \frac{T - T_c}{T_c} \right|$ is a measure of the distance from the critical point, e.g., along the critical isochore. For example, a few values are given in Table 3.

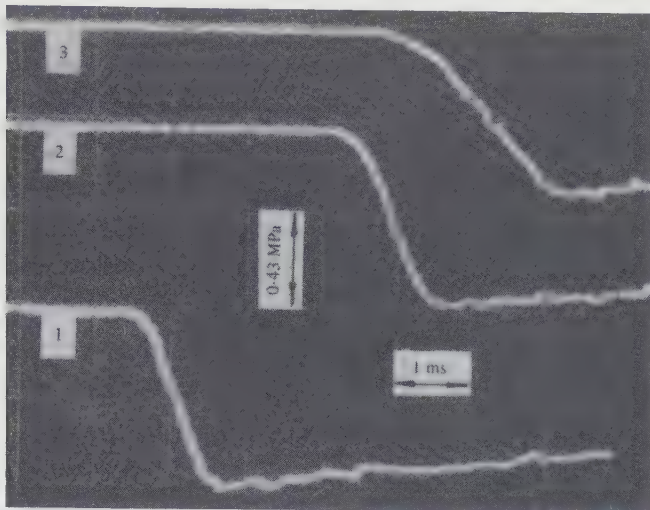


Figure 20. Structure of a rarefaction shock wave in F-13. $P_0 = 3.30 \text{ MPa}$, $\rho_0 = 270 \text{ kg/m}^3$. $T_0 = 295.15 \text{ K}$. Lines 1,2,3 correspond to transducer distances from the diaphragm of 0.15, 0.45, 2.35 m respectively.

ϵ	10^{-2}	10^{-3}	10^{-4}	10^{-5}	10^{-6}	10^{-7}
c_v Factor	1.58	2.00	2.51	3.16	3.98	5.01

Table 3. Amplification of the heat capacity c_v near the critical point.

Remark: In the work of Borisov, Borisov, *et al.* (1983), the symbol α is used for the fundamental derivative Γ . This symbol is independent of the critical exponent α . We also note that the fundamental derivative is written in the alternate form,

$$\Gamma = 1 + \rho c \left[\frac{\partial c}{\partial P} \right]_S . \quad (4.2)$$

Further information on this and related experiments is given by Kutateladze, Nakoryakov and Borisov (1987). A peculiar feature of the rarefaction shock is that it propagates almost unchanged, although the pressure level has dropped well below the critical value. According to the authors, the state downstream of the rarefaction shock is in the single-phase region.

The transcritical expansion flows of Zauner. These experiments were performed at the Max-Planck-Institut für Strömungsforschung in Göttingen in the period 1985-1988 (Zauner & Meier 1990). In the theoretical part, Laval-nozzle flows under near-critical conditions, using retrograde fluids were investigated. Assuming phase equilibrium, both compression and expansion shocks were found.

The experiments and corresponding high-speed films are, perhaps, the most interesting aspects of this study. Figure 21 shows a cross-section through the expansion tube, which serves both as a fluid reservoir and, in the lower part, as a Laval nozzle. The flow discharge is upward into the vacuum vessel. The sidewalls of the vessel are made of glass, so that high-speed photos can be taken of the flow in the cross section shown.

The test section is 115 mm long with a cross section of $20 \times 15 \text{ mm}^2$ at the bottom and an opening angle of 11° . The throat of the arc nozzle has a cross section of $20 \times 4.5 \text{ mm}^2$. Pressure transducers or fast-acting iron-constantan thermocouples can be mounted in the sidewalls.

To prepare the experiment, the expansion tube is evacuated and then partially filled with degassed test liquid and heated to the desired initial temperature. The test section is heated with hot air circulating within an enclosing shroud. Temperatures up to 200°C can be achieved.

The experiment is initiated when the diaphragm ("Capton" polyamide or aluminum in thicknesses up to 0.22 mm) is ruptured by an arrowhead plunger falling under gravity. The expansion tube is thus connected with a large vacuum vessel (0.090 m^3). Measured experimental quantities are the temperature $T(t)$ in the reservoir and the pressure $P(t)$ at several transducer locations. To minimize disturbing effects due to temperature transients, the transducers were protected by a layer of silicon rubber.

High-speed photography which uses parallel light from an LED-stroboscope is applied to visualize the flow in the nozzle. The test substance used in our experiments is PP1 (C_8F_{14}), with critical properties as shown in Table 2.

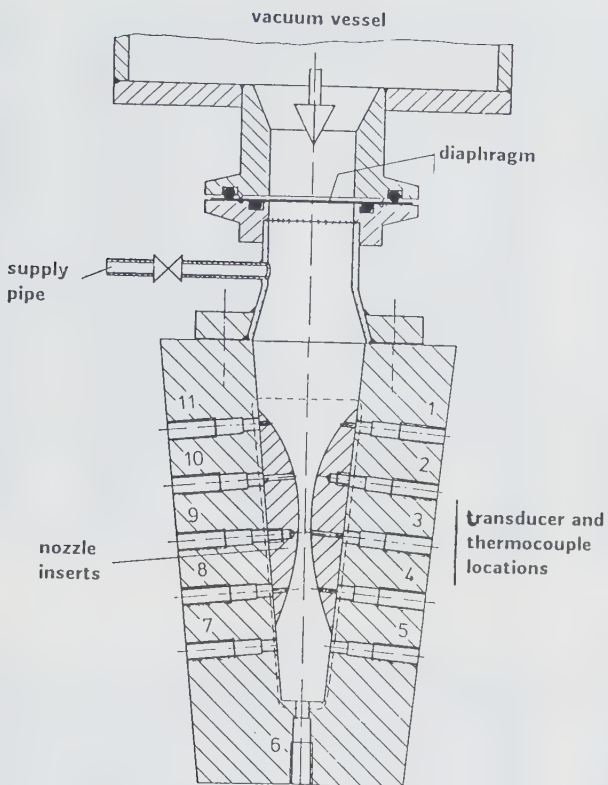


Figure 21. Axial cut through the expansion tube.

Blowdown from supercritical temperatures in the Zauner expansion tube.

Initial conditions were chosen such that the state in the nozzle and in the reservoir pass the critical region during blowdown both left and right of the critical point. Figure 22 shows a typical blowdown transient from an initial state of 1.90 P_c on a supercritical isentrope ($s - s_c > 0$). At the beginning, the pressure drops very fast. At about 2.5 ms , the throat pressure reaches the phase boundary. It is arrested at this value for the time in which the throat velocity decreases from the value of the single-phase soundspeed to that of the mixture soundspeed. The unusual plateau in the throat pressure gives rise to an acoustic wave propagating

upstream. About 1 ms later, the condensation front follows. An evaporation shock, as predicted by the equilibrium model, is not observed.

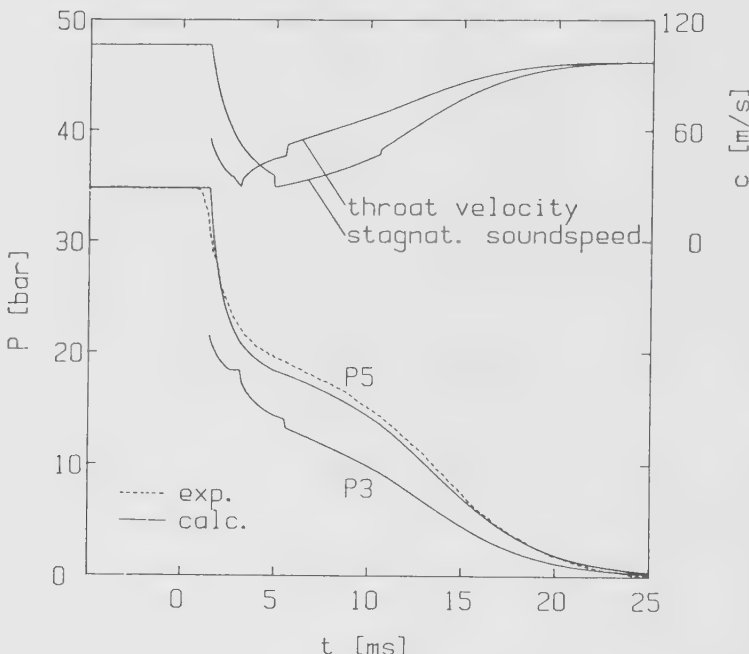


Figure 22. Blowdown transient for PP1 along a supercritical isentrope $(s-s_c)/R = 0.06$: $P_0 = 34.8$ bar, $T_0 = 192^\circ\text{C}$.

The selected photographic frames in Figure 23 correspond to the supercritical blowdown experiment of Figure 22. The framing rate is 6000 frames per seconds, so that the time interval between frames is $\frac{1}{6}$ ms. The flow direction is upward and the frames proceed in time from right to left and downward, i.e., set (16) is approximately 7 ms later than set (4). In set (4), fast-growing, wedge-shaped perturbations are seen in the shear layers at the windows. Much later, Mach lines are observed, followed by a shock structure and turbulence.

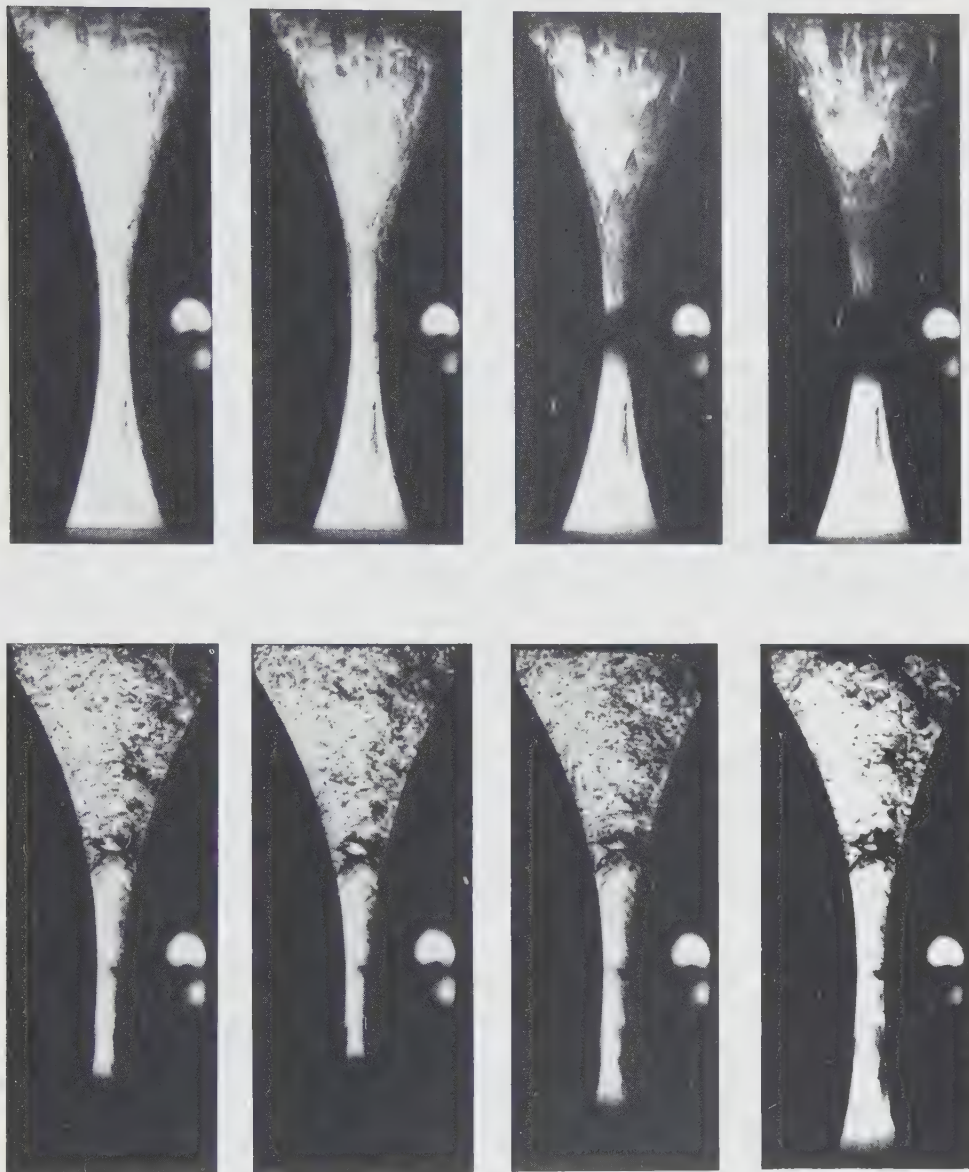


Figure 23. Photographs taken from the high-speed film of Zauner (see text).

Near-critical states reached behind a shock wave. Although it is likely to prove to be an elusive target, it is possible to reach a near-critical state from an initial state far from the critical point. For a precisely-known critical state, this could be done, in principle, by drawing the inverse shock adiabat through the critical point and selecting an initial state on the inverse critical adiabat. If such a procedure were successful, it would amount to the creation of a critical state in a very short time, on the order of the shock thickness divided by the average of the upstream and downstream velocities, leading to a value of perhaps 5 ms. It is then questionable whether these 5 ms would be long enough to allow the state downstream of the shock to reach equilibrium, bearing in mind that, in the experiments of Borisov, Borisov, *et al.* (1983), more than twenty hours were allowed to reach equilibrium!

A fundamental question in this connection is: Are there nonequilibrium critical points? That is, are there non-equilibrium states which show nearly infinite compressibility, satisfying conditions such as

$$\left[\frac{\partial P}{\partial v} \right]_T = \left[\frac{\partial^2 P}{\partial v^2} \right]_T = 0. \quad (4.3)$$

It appears that there is a general belief in the idea of a critical point which is displaced by departures from equilibrium, such that the critical pressure, volume and temperature take on new and transient values. Although this kind of behavior could be tested by *molecular dynamics*, these authors are not aware of any relevant studies.

Preliminary near-critical experiments at RPI. The experiments of Thompson, Kim, Yoon and Chan (1988) dealt with liquefaction shocks intended to produce a near-critical downstream state in the test fluid PP1 (See Table 2). Among the interesting results were the following:

1. A minimum soundspeed behind the shock of 10 m/s, measured by using Skew's construction.
2. The region of minimum soundspeed was found at a reduced pressure of about 1.3, i.e., not at the nominal critical point.
3. The flow behind the shock had a Mach number of 30 in the laboratory frame, a consequence of the very low soundspeed.

4. In the frame of the shockfront, the outflow satisfied the Chapman-Jouguet condition $u = c$ at the state of minimum soundspeed.

Photographs of near-critical shockfronts are shown in Figures 24 and 25. See Thompson, Kim *et al.* (1988) for a more complete description of these experiments.



Figure 24. Oblique photograph showing shockfront vortex rings with downstream states in the general neighborhood of the thermodynamic critical point, but nearer to the liquid side. Test fluid $n\text{-C}_6\text{F}_{14}$. $P_0 = 2.78$ bars, $T_0 = 110^\circ\text{C}$, $M_0 = 3.12$.



(a)



(b)

Figure 25. Photographs of the near-critical shockfront structure emerging from the end of the shock tube test section into the observation chamber. Test fluid $n\text{-C}_6\text{F}_{14}$. Shock Mach number $M_0 = 2.95$, reduced pressure $P_2 = 1.30$, soundspeed $C_2 = 10.1 \text{ m/s}$. (a) Oblique view. (b) Profile view.

5. INSTABILITIES AND ANALOG SYSTEMS

In the course of our experiments, diverse phenomena were discovered. Notable among these are two forms of instability. The first instability found was the small *ring vortex* imbedded in large numbers within and behind a complete liquefaction shock. The second instability was the development of patterned and even *chaotic shockfronts*, found under certain conditions in partial liquefaction shocks. The unstable shockfront appears to be analogous to unstable detonation fronts. Finally, we will discuss in this section diverse phase changes related to the liquefaction shock.

Ring vortices in the shockfront. In Figure 24, numerous ring vortices with two-phase cores can be observed. These vortices were already found in the experiments of Dettleff, Thompson, *et al.* (1979) and, to some extent, qualitatively analyzed. A further study was made by Dettleff, *et al.* (1982).

In the earlier studies of Dettleff, complete liquefaction shocks were produced by shock reflection from the closed end of the Göttingen shock tube. The end wall was formed by a cylindrical glass window, so that the shock-liquefaction process could be observed photographically. One such photograph is shown in Figure 26(a). It shows the vortices at time $t = 0.03$ ms after reflection, while Figure 26(b) shows them 0.3 ms after reflection from the endwall window. In the brief time interval between the photographs, the vortices have enlarged considerably and many have disappeared entirely. The smallest vortex ring which can be measured from photographs is about 50 microns in diameter.

A reasonable hypothesis for the origin of the vortex rings is that each primitive ring is created at a homogeneous-nucleation event, the vorticity being created by the gradient in density around the nucleating droplet, as discussed in Dettleff, Thompson, *et al.* (1979).

Stable and unstable liquefaction shockfronts. Plane shockfronts are typically very stable. When disturbed, they tend to return to the planar form (Menikoff & Plohr 1989). It came as a surprise when plane shockfronts produced in a shock tube were observed photographically to distort into chaotic, irregular forms in the experiments of Thompson, Carofano & Kim (1986). It is notable that shockfront instability has been observed in all of the test fluids that have been investigated,

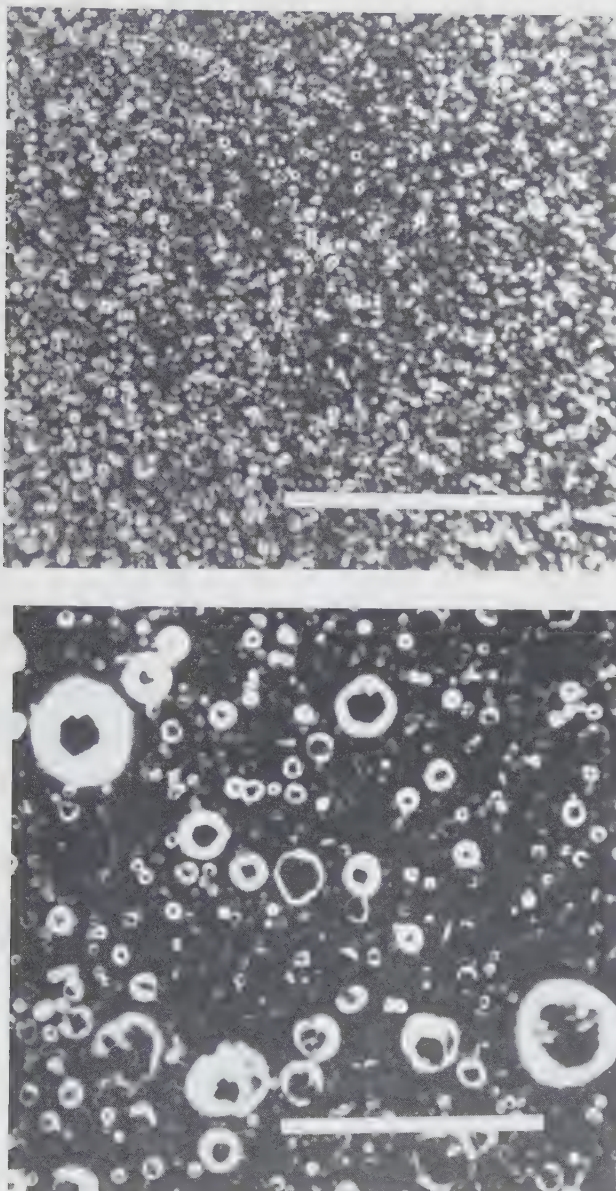


Figure 26. Ring objects at short and intermediate times after reflection. The test fluid is PP3 with $T_0 = 130^\circ\text{C}$, $P_0 = 0.67 \text{ bar}$; $M_I = 2.4$. Arrangement B.
(a) $t_R = 0.03 \text{ ms}$, reference line length 5 mm. (b) $t_R = 0.3 \text{ ms}$, reference line length 10 mm.

i.e., those shown in Table 2. Thus, there is reason to expect that shockfront instability may be found in fluids with more than about twenty atoms per molecule, over certain ranges of shock Mach number and initial conditions.

The experimental observations were made in the test chamber shown in Figure 9. The incident liquefaction shock emerges from the end of the shock tube at E and undergoes shockfront diffraction. For comparison, two shockfronts are shown in Figure 27 with the test fluid FC-75 : Shock (a) is considered to be stable and (b) to be in an intermediate state of instability. In the experiments, shock velocity, pressure and the initial conditions are measured; the soundspeed behind the shock is also measured using a Mach construction for the expansion wave in the diffracted shockfront. Derived measurements, such as the density ratio ρ_2/ρ_0 across the shock are calculated using the Rankine-Hugoniot equations and the equation of state of Hobbs (1983).

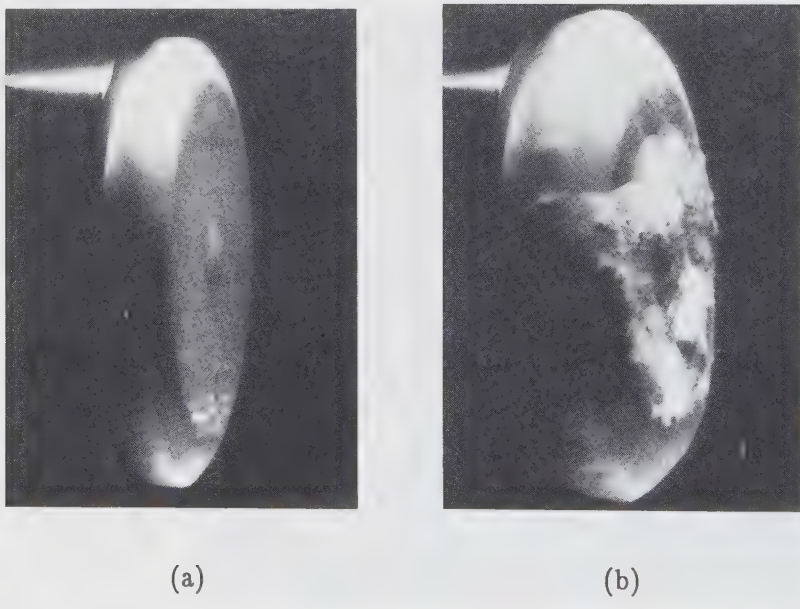


Figure 27. Shockfronts in FC-75 emerging from the shock tube test section into the observation chamber. (a) Initial conditions $T_0 = 120^\circ\text{C}$, $P_0 = 1.4$ bars, $c_0 = 84.6 \text{ m/s}$; shock Mach number $M_0 = 2.10$, moisture fraction behind the shock $y = 0.7$. (b) Conditions as in (a), with $M_0 = 2.20$, moisture fraction $y = 0.8$.

In the FC-75 experiments, the onset of instability was compared with the stability limit proposed by Kontorovich (1957) and discussed by Fowles & Houwing (1984) as well as Teshukov (1990). According to this theory, spontaneous acoustic emission can lead to the amplification of transverse waves along the shockfront for values of the Kontorovich parameter $K > 1$, where

$$K \equiv (G + 1)(r - 1)M^2, \quad (5.1)$$

with G the Grüneisen parameter downstream of the shock, $r = \rho_2/\rho_0$ the density ratio across the shock and M the downstream shock Mach number ≤ 1 . For fixed initial conditions ($T_0 = 120^\circ\text{C}$, $P_0 = 1.4$ bars) and increasing shock Mach number M_0 , the instability was first observed at $M_0 \approx 2.2$. In these experiments, the onset of instability appeared to be consistent with the Kontorovich model.

In the FC-75 experiments, several runs were made with a balsa wood piston separating the driver gas from the driven fluid. No influence on the presence or absence of shockfront instability was found.

Recent experiments with 2,2,4-trimethylpentane (iso-octane) with initial conditions $T_0 = 110^\circ\text{C}$ and $P_0 = 1.10$ bars shows a surprising alternation between stable and unstable shockfronts with increasing M_0 . A series of 22 photographs over a Mach-number range between 2.23 and 3.34 illustrates the sequential states stable \rightarrow unstable \rightarrow stable \rightarrow unstable. The Kontorovich parameter has been calculated for these experiments using both the experimental soundspeed and the calculated equilibrium isentropic soundspeed in the mixture. For both models, K increases with increasing M_0 and $K > 1$ is reached at about $M_0 = 2$. The parameter K appears to increase monotonically thereafter, with no suggestion of oscillating stability in the Kontorovich model.

For more information on liquefaction shock instabilities and a discussion of the analogy to detonation instability, see Shepherd, Thompson & Cho (1989).

Among the diverse adiabatic phase changes related to the liquefaction shock, several have to do with atmospheric or wind-tunnel phenomena. The usual fluid is then moist air, a regular substance which condenses on adiabatic expansion. We will mention four phase changes of this kind, as follows.

The first is the *moisture shock*, sudden condensation of metastable vapor in high-speed flow, for example in the flow of moist air through a Laval nozzle. It represents a practical problem in turbines and wind tunnels, in that the liquid condensate (droplets) may destroy the turbine blades or other surfaces, by virtue of their large relative velocities. According to Schneer (1989), the steady or oscillating shockwaves induced by the sudden condensation may lead to a crash (and destruction?) of the blade rows in a turbine. It has been estimated that moisture shocks can result in an increase of 1% in the fuel consumption of a jet airplane (Hobbs 1982). Actually, the moisture shock is not a shock wave at all, but a region of sudden condensation triggered by the onset of critical supersaturation corresponding to the "Wilson line" and homogeneous nucleation. In practice, almost all moisture shock discontinuities are supersonic, as illustrated for a moist-air system in Figure 28. The supersonic flow velocities are required to produce the necessary degree of supersaturation. At the formation of the moisture shock, latent heat is released, accompanied by a rise in temperature and pressure. This perturbation in the flow typically produces an ordinary gas-dynamic shock downstream of the "moisture shock". This true shock is sometimes called a *condensation shock*, even though there is no condensation in the shock!

The discovery of the moisture shock resulted from an "unsuccessful" experiment performed by Ludwig Prandtl in 1935 and reported to the Volta Congress in that year (Prandtl 1936). The experiment concerned supersonic flow through a two-dimensional Laval nozzle, which would normally be shock-free. In spite of careful experimentation, the shock persisted. The culprit, of course, was a moisture shock which triggered the unwanted gasdynamic shock. Two relevant Schlieren photos are shown in Figures 29(a) and 29(b). Figure 29(a) shows the modern experiment of Schneer (1989), with a sensitive Schlieren system. The moisture-shock region corresponds to the crescent-shaped regions just upstream of the plane gasdynamic shock wave. Figure 29(b) shows the Prandtl experiment with the unwanted shock system, roughly in the shape of an X — the moisture-shock discontinuity is not visible.

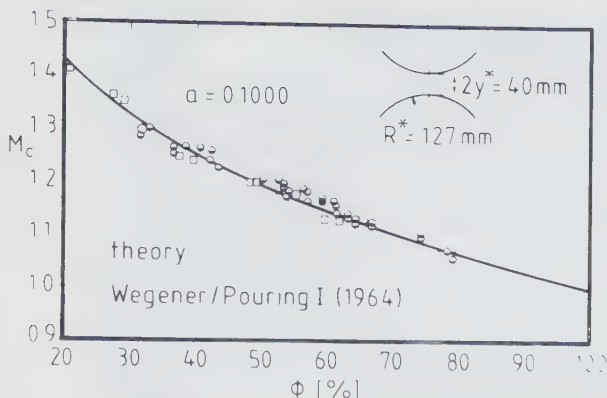
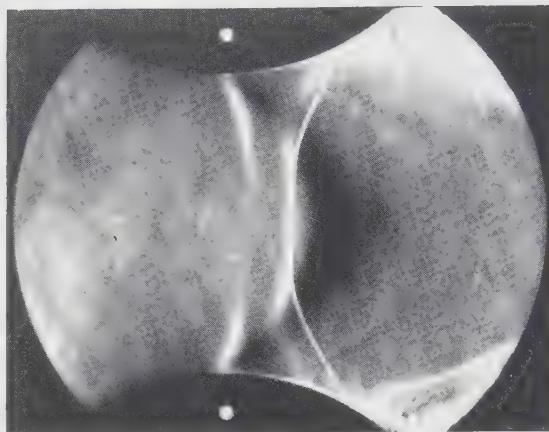


Figure 28. Mach number M_c at the onset of condensation in moist air for a particular two-dimensional nozzle geometry, as a function of the relative humidity Φ . Taken from Schneer (1989).

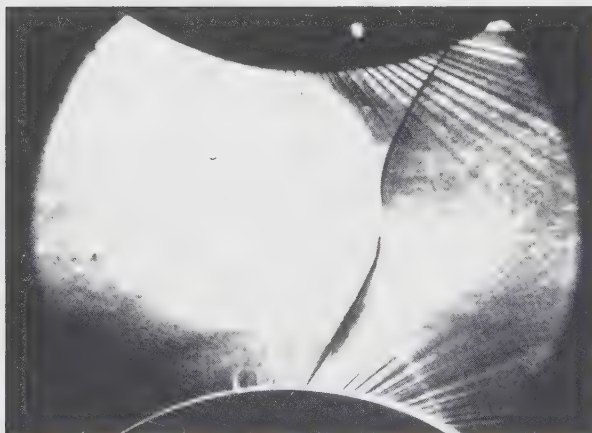
Prandtl's comment on the mysteriously persistent shock was as follows:

Ich zeige nun noch ein letztes Bild, das Ihnen eine Erscheinung zeigt, die wir bisher noch nicht zu erklären imstande waren. Obwohl die beiden Backen auf der Drehbank hergestellt sind, und also eine sehr regelmässige Expansion ergeben sollten, ergibt sich hier ein sich kreuzendes System von Verdichtungsstößen. (Die Aufnahme stammt von Dr. Busemann, Beleuchtung von unten). Derartige Vorgänge haben uns bei der Herstellung von parallelen Strömungen schon manche Sorge gemacht. Wir fanden bisher kein Mittel zu ihrer Vermeidung.

The cause of the persistent shock was suggested by Wieselsberger to be moisture in the supply air: this was a comment at the same Volta Congress (Hermann 1942). Humidity effects can be avoided in modern blowdown tunnels by using silica-gel desiccators at the inlet.



(a)



(b)

Figure 29. Plane Laval-nozzle flow of moist air with moisture shock induced gasdynamic shocks. (a) Experiment of Schneer, with $\Phi_0 = 71.3\%$, $x = 7 \text{ g/kg}$, $T_0 = 286.8 \text{ K}$. Flow is from left to right. (b) Prandtl experiment, schlieren photo by A. Busemann, flow is from left to right, the conditions are unknown.

The second phase change in air-water vapor fluid is the *condensation discontinuity at a stable cloud base*. Under steady heating from below, upwelling moist air will condense moisture adiabatically, often forming a stable cloud base, a kind of moisture shock with an upward throughflow. Temperature and velocity are discontinuous at the cloud-base plane (Traugott 1988). The heterogeneous nucleation takes place at supersaturations on the order of 1.04.

A third form of atmospheric phase change is associated with the *downburst* (Fujita 1985), a strong downdraft in the atmosphere which is especially dangerous to aviation. One form of downburst is produced by high altitude rainfall descending into dry air at lower altitude, such that strong evaporative cooling takes place. This creates a cold, dense air mass which falls to the earth as a high-speed downburst (Emanuel 1981, Srivastava 1985).

Our final example of atmospheric phase change is *condensation produced in low-pressure regions* of flying aircraft, a phenomenon which can be quite striking if the relative humidity is large (Campbell, *et al.* 1989). See also Schneer and Dohrmann (1989, 1990).

Two forms of retrograde phase changes, somewhat analogous to the liquefaction shock, will be described in closing. Metastability plays an important role in both cases.

The *phase transition Quartz → Stishovite* is associated with the impact of meteorites, asteroids and similar extraterrestrial bodies against the earth. The transition occurs at a pressure above 8.5 GPa (85 kilo bars), which is comparable to the pressure required for the Graphite → Diamond phase transition. Once formed, the Stishovite is metastable up to a few hundred kelvins at atmospheric pressure. Again, this is similar to the behavior of Diamond, which is metastable at room temperature and pressure. The high-pressure (impact) conversion of Quartz to Stishovite is a transition to a more dense phase, analogous to a liquefaction shock. The phases of Quartz-family minerals are shown in the following table, together with their densities (expressed as specific gravity).

Stishovite	4.28
Coesite	2.93
Quartz	2.65
Cristobalite	2.32
Tridymite	2.26
Lechatelierite	2.20

Various other minerals undergo phase transitions under asteroid impact. At sufficiently high pressures, minerals such as Feldspar and Quartz melt to produce diaplectic glass (pressures of 30 to 40 gigapascals). See the article of Grieve (1990). Recent interest in such phenomena has been stimulated by the *Impact Hypothesis* for the massive extinctions of species at the Cretaceous-Tertiary geological boundary 65 million years ago (Silver *et al.*)

Our final retrograde phase change is the *Champagne Effect*. This terminology derives from the spouting of a bottle of too-warm Champagne or carbonated water. In current usage, it refers to the uncontrolled (and occasionally catastrophic) release of dissolved gas from a host liquid, which is typically water. It is a technical problem in the underground storage of compressed air (Sneck, *et al.* 1985) and in reactor emergency core cooling (Simoneau 1981). The application to be described here is the natural catastrophe which occurred on the 21st of August 1986 at Lake Nyos, in Cameroon, West Africa. The brief account given here is largely based on the paper of Kling, Clark, *et al.* (1987). On the day of the catastrophe, the lake was saturated (probably supersaturated) with carbon dioxide of magmatic origin. Lake Nyos lies in the crater of an extinct volcano. The carbon dioxide, along with other gases in lesser concentrations, emanated from the volcanic rock.

The physical basis for the disaster is in Henry's Law, which states that the solubility of a gas in a liquid is proportional to pressure:

$$\Phi = A(T) P \quad (5.2)$$

where Φ is the mol fraction of dissolved gas per mol of liquid, $A(T)$ is Henry's constant (which is temperature-dependent) and P is the absolute pressure. In the case of a lake saturated with gas, this means that the concentration of dissolved gas will be approximately proportional to the depth in the lake, i.e., the concentration of CO_2 in Lake Nyos would normally be greatest at the bottom. The depth of the lake is about 200 m, based on a hydrostatic pressure gradient of about one atmosphere per 10 meters change in depth. Thus, the concentration at depth would be about twenty times the concentration at the surface. The total dissolved CO_2 in Lake Nyos prior to the disaster is estimated to be equivalent to a CO_2 cloud of about 1.5 cubic kilometers at one atmosphere.

A liquid column or a lake containing large amounts of dissolved gas can be unstable. Consider a small packet of liquid which is disturbed and carried upward by convection to a point where the local hydrostatic pressure is smaller: then the small bubbles in the packet will expand, the packet acquires buoyancy and the upward motion is accelerated. The packet then expands further, and so on. In the case of Lake Nyos, a plausible disturbance for the initiation of this chain could be a small landslide, or even a strong gust of wind.



Figure 30. Tranquil Lake Nyos before the release of gas. Photos by Anthony Suau.

Figure 30 shows an aerial view of Lake Nyos before the disaster (Stager 1987) and Figure 31 shows almost the same view after the sudden and catastrophic release of gas on the summer evening of August 21, 1986.



Figure 31. Lake Nyos after the release of gas.

The instability, once started, produced spectacular effects, including a two-phase fountain that produced a high wash against the cliffs of the lake, about 80 m high at its maximum. The enormous cloud of released CO₂ was more dense than the surrounding air (in the ratio of 44/29) and rapidly overflowed the volcanic basin of Lake Nyos into the low-lying areas. 1700 human beings and 3000 cattle died of CO₂ asphyxiation. Other lakes in Africa have the potential for a dangerous champagne effect, including Lake Kivu, near Lake Victoria.

Finally, the principal motif of this work — which is metastability — is brought back in the form shown in Figure 32(a) and (b). Pressure-Volume and Pressure-Temperature diagrams are shown for the test fluid C₆F₁₄, and in the

inset for Argon. Three kinds of lines are shown: The equilibrium Pressure-Volume saturation boundaries as thin lines, including the critical point CP, the equilibrium isentropes I shown as heavy lines (and identical with the vapor-pressure curve between g and h) and the non-equilibrium isentropes shown as thin lines. By following the non-equilibrium isentropes from their point of departure from the equilibrium isentrope, one can find the correct extrapolations into the metastable states. For example, if one starts an isentropic expansion from point h and continues along the non-equilibrium isentrope downwards, the process represents a realistic version of isentropic expansion into a metastable state which must, in turn, break down with a jump to a new, stable state.

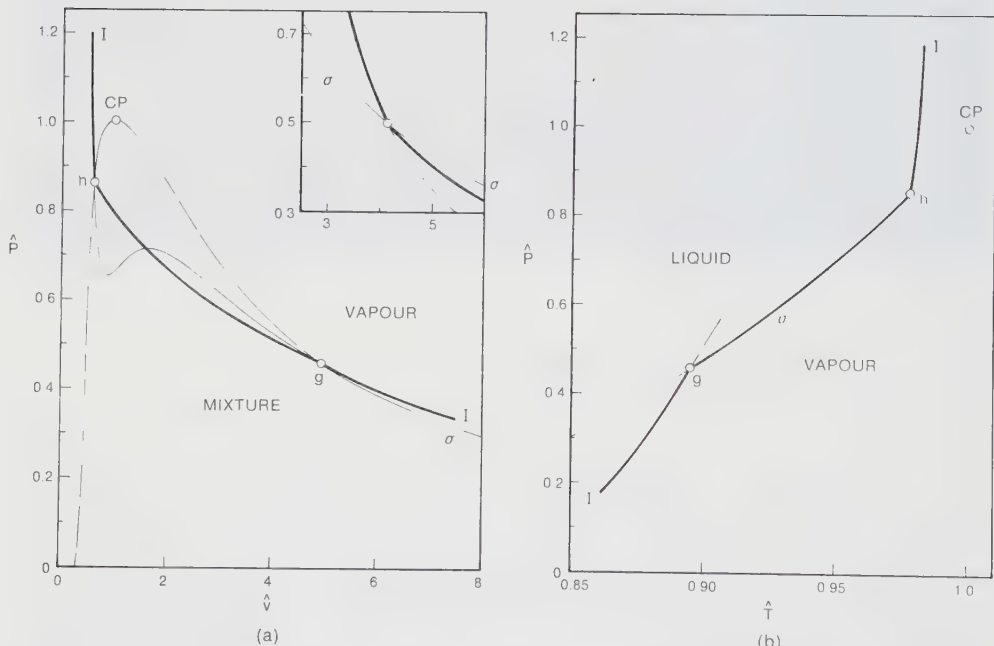


Figure 32. Equilibrium isentropes (heavy lines) and non-equilibrium isentropes (lighter lines) for perfluoro-n-hexane C_6F_{14} ($\tilde{C}_v = 40.5$). σ = saturation boundary. The single isentrope shown has an entropy $(S - S_c)/R = -2.07$, where S_c is the critical value. (a) Pressure-Volume diagram in reduced coordinates. (Inset: Isentrope for argon, with $C_v = 1.5$, near the saturated-vapor boundary.) (b) Pressure-Temperature diagram in reduced coordinates.

ACKNOWLEDGEMENTS

Many individuals have contributed to this work over the years. In many cases, the contributors have been essential to the advancement of the research. We would particularly like to mention the following persons.

At the Max-Planck Institut für Strömungsforschung

Professor E.-A. Müller
G.E.A. Meier
Willi Möhring
Georg Dettleff

Humberto Chaves
Irwin Zauner
H.-D. Speckmann
Françoise Gossieaux

At Rensselaer

Paul Harteck[†]
Frederick Ling
Garry Carofano
Hendrick van Ness
Michael Abbott
Konstantine Lambrakis
Daniel Sullivan

David Hobbs
Yoon-Gon Kim
Susan McCahan
Joseph Bursik
Chong Yoon
Joseph Shepherd
Esther Parslow Rendano

At Other Places

Ernst Becker[†] — Darmstadt
Ya.B. Zel'dovich[†] — Moscow
Bradford Sturtevant — Caltech
B.W. Skews — Troy

G.H. Schneer — Udine
J. Serrin — Minneapolis
Amyn Teja — Atlanta
Wolfgang Wagner — Bochum

REFERENCES

1. Thompson, P.A. and D.A. Sullivan: On the possibility of complete condensation shock waves in retrograde fluids, *J. Fluid Mech.*, **70**, 4 (1975), 639-649.
2. Dettleff, G., P.A. Thompson, G.E.A. Meier and H.-D. Speckmann: An experimental study of liquefaction shock waves, *J. Fluid Mech.*, **95**, 2 (1979), 279-304.
3. Dettleff, G., G.E.A. Meier, H.-D. Speckmann, P.A. Thompson and C. Yoon: Experiments in shock liquefaction, in: *Proc. 13th Int'l Symp. on Shock Tubes and Waves*, (Ed. C.E. Trainor and J.G. Hall), State Univ. of New York Press, 1982.
4. Thompson, P.A. and Y.-G. Kim: Direct observation of shock splitting in a vapor-liquid system, *Phys. Fluids* **26**, 11 (1983), 3211-3215.
5. Speckmann, H.-D.: Aufspaltung von kondensationsstößen in fluiden hoher spezifischer Wärme, *Mitteilungen aus dem Max-Planck-Institut für Strömungsforschung* (Herausgegeben von E.-A. Müller) **76** (1984).
6. Thompson, P.A., Y.-G. Kim and G.E.A. Meier: Flow visualization of a shock wave by simple refraction of a ruled background grid, in: *Optical Methods in Dynamics* (Ed. M. Pichal), Springer-Verlag, Berlin 1984, 225-231.
7. Thompson, P.A. and K.C. Lambrakis: Negative shock waves, *J. Fluid Mech.*, **60**, 1 (1973), 187-208.
8. Cramer, M.S. and A. Kluwick: On the propagation of waves exhibiting both positive and negative nonlinearity, *J. Fluid Mech.*, **142** (1984), 9-37.

9. Thompson, P.A., G.C. Carofano and Y.-G. Kim: Shock waves and phase changes in a large-heat-capacity fluid emerging from a tube, *J. Fluid Mech.*, 166 (1986), 57-92.
10. Borisov, A.A., Al.A. Borisov, S.S. Kutateladze and V.E. Nakoryakov: Rarefaction shock wave near the critical liquid vapour point, *J. Fluid Mech.*, 126 (1983), 59-73.
11. Slemrod, M.: Korteweg theory and van der Waals fluids, in: *Adiabatic Waves in Liquid-Vapor Systems* (Ed. G.E.A. Meier and P.A. Thompson) Springer-Verlag, Berlin 1990. To appear.
12. Chaves, H.: Phasenübergänge und Wellen bei der Entspannung von Fluiden hoher spezifischer Wärme, Dissertation, Georg-August-Universität, Göttingen, 1980.
13. Skripov, V.P. and P.A. Pavlov: Superheating and explosive boiling of liquids, *Sov. Tech. Rev. B. Thermal Physics*, 2, (1989).
14. Skripov, V.P.: Metastable Liquids, John Wiley, New York 1974.
15. Lighthill, M.J.: Viscosity effects in waves of finite amplitude, *Surveys in Mechanics* (Ed. G.K. Batchelor & R.M. Davies), Cambridge University Press 1956.
16. Thompson, P.A.: Compressible Fluid Dynamics, Rosewood Press, Troy, New York 1972.
17. Thompson, P.A.: A Fundamental derivative in gasdynamics, *Phys. Fluids*, 14, (1971), 1843-1849.
18. Lambrakis, K.C.: Negative- Γ fluids, Dissertation, Rensselaer Polytechnic Institute 1972.

19. Thompson, P.A., G.C. Carofano, and Y.-G. Kim: Shock waves and phase changes in a large-heat-capacity fluid emerging from a tube, *J. Fluid Mech.*, 166 (1986), 57-92.
20. Planck, M.: *Treatise on Thermodynamics*, Longmans-Green, 1903, 150-152.
21. Van der Waals, J.D.: *Lehrbuch der Thermodynamik*, Bearbeitet von Ph. Kohnstamm, Maas und Van Suchtelen, Leipzig 1908.
22. Bethe, H.A.: The theory of shock waves for an arbitrary equation of state, Office of Scientific Research and Development, Washington, Report No. 575 (1942), 57.
23. Zel'dovich, Ya.B.: On the possibility of rarefaction shock waves, *Zh. Eksp. Teor. Fiz.*, 4 (1946), 363-364.
24. Landau, L.D. and E.M. Lifshitz: *Fluid Mechanics* (1959) Pergamon, 496.
25. Thompson, P.A., Y.-G. Kim and G.E.A. Meier: Shock-tube studies with incident liquefaction shocks, in: *Proceedings of the 14th Int'l. Symp. Shock Tubes and Waves*, University of Sydney, Australia 1984, 413-420.
26. Thompson, P.A., H. Chaves, G.E.A. Meier, Y.-G. Kim and H.-D. Speckmann: Wave splitting in a fluid of large heat capacity, *J. Fluid Mech.*, 185 (1987), 385-414.
27. Chen, G., P.A. Thompson and J.W. Bursik: Soundspeed measurements in vapor-liquid mixtures behind shock waves, *Exp. in Fluids*, 4 (1986), 279-282.
28. Borisov, A.A., Al.A. Borisov, S.S. Kutateladze and V.E. Nakoryakov: Rarefaction shock wave near the critical liquid vapour point, *J. Fluid Mech.*, 126 (1983), 59-73.

29. Kutateladze, S.S., V.E. Nakoryakov and A.A. Borisov: Rarefaction waves in liquid and gas-liquid media, *Ann. Rev. of Fluid Mech.*, 19 (1987), 577-600.
30. Zauner, E. and G.E.A. Meier: Phase changes of a large-heat-capacity fluid in transcritical expansion flows, in: *Adiabatic Waves in Liquid-Vapor Systems* (Ed. G.E.A. Meier and P.A. Thompson) Springer-Verlag, Berlin 1990. To appear.
31. Thompson, P.A., Y.-G. Kim, C.J. Yoon and Y. Chan: Nonequilibrium, near-critical states in shock-tube experiments, in: *Proceedings 16th Int'l. Symp. on Shock Tubes and Waves* (Ed. H. Grönig), VCH, Weinheim, Federal Republic of Germany, 1988, 342-349.
32. Menikoff, R. and B.J. Plohr: Riemann problem for fluid flow of real materials, *Rev. Mod. Phys.*, 61, 1989, 75.
33. Hobbs, D.E.: A virial equation of state utilizing the principle of corresponding states. Dissertation, Rensselaer Polytechnic Institute 1983.
34. Kontorovich, V.M.: Concerning the stability of shock waves, *Sov. Phys. Tech. Phys.*, 6 (1957), 1179-1181.
35. Fowles, G.R. and A.F.P. Houwing: Instability of shock and detonation waves, *Phys. Fluids*, 27, (1984), 1982-1990.
36. Teshukov, V.M.: Stability of shock waves and general equations of state, in: *Adiabatic Waves in Liquid-Vapor Systems* (Ed. G.E.A. Meier and P.A. Thompson) Springer-Verlag, Berlin 1990. To appear.
37. Shepherd, J.E., P.A. Thompson and H.-J. Cho: Alternating stability and instability of liquefaction shockfronts in 2,2,4-Trimethylpentane, To appear in: *Proceedings 17th Int'l Symp. on Shock Waves and Shock Tubes*, held July 17-21, Lehigh University, Bethlehem, Pennsylvania 1989.

38. Schneer, G.: 2-D transonic flow with energy supply by homogeneous condensation: Onset condition and 2-D structure of steady Laval nozzle flow, *Exp. in Fluids*, 7 (1989), 145-156.
39. Hobbs, David E.: Private communication 1982.
40. Prandtl, L.: Remarks, *Atti del V Convengno Volta, Reale Accademia d'Italia*, Roma 558 (1936), 196-197.
41. Hermann, R.: Der Kondensationstoß in Überschall-Windkanaldüsen, *Luftahrtforschung*, 19 (1942), 201-209.
42. Traugott, S.: Private communication 1988.
43. Fujita, T. Theodore: The Downburst, Satellite and Mesometorology Research Project, Univ. of Chicago 1985.
44. Emanuel, Kerry A.: A similarity theory for unsaturated downdrafts within clouds, *J. of Atmos. Sci.*, 38 (1981), 1541-1557.
45. Srivastava, R.C.: A simple model of evaporatively driven downdraft: Application to microburst downdraft, *J. of Atmos. Sci.*, 42 (1985), 1004-1023.
46. Campbell, James F., Joseph R. Chambers and Christopher L. Rumsey: Observation of airplane flowfields by natural condensation effects, *J. Aircraft*, 26, 7 (1989).
47. Schneer, G.H. and U. Dohrmann: Transonic flow around airfoils with relaxation and energy supply by homogeneous condensation, *AIAA Journal* (1989), 89-1834.

48. Schneer, G.H. and U. Dohrmann: Numerical investigation of nitrogen condensation in 2-D Transonic flows in cryogenic wind tunnels, in: IUTAM Symposium, Adiabatic Waves in Liquid-Vapor Systems, Göttingen, F.R. Germany 1990.
49. Grieve, Richard A.F.: Impact cratering on the Earth, *Scientific American*, 262, 4 (1990), 66-73.
50. Silver, L.T. and P.H. Schultz: Geological implications of impacts of large asteroids and comets on the Earth, *Geolog. Soc. Amer.*, special paper 190 (1982).
51. Sneed, H. James, P.A. Thompson, B.E. Hand, B.R. Meyer, Chen Ping: Modeling of the champagne effect, in: Fundamental Aspects of Gas-Liquid Flows, *Amer. Soc. Mech. Engrs. FED-29*, 1985.
52. Simoneau, R.J.: Depressurization and two-phase flow of water containing high levels of dissolved nitrogen gas. NASA Technical Paper 1839, Lewis Research Center, Cleveland, Ohio 1981.
53. Kling, G.W., M.A. Clark, H.R. Compton, J.D. Devine, W.C. Evans, A.M. Humphrey, E.J. Koenigsberg, J.P. Lockwood, M.L. Tuttle, and G.N. Wagner: The 1986 Lake Nyos gas disaster in Cameroon, West Africa, *Science* 236, (1987) 169-175.
54. Stager, C.: Killer Lake, *National Geographic*, September Issue (1987) 404-420.

NUCLEATION, CONDENSATION AND EVAPORATION IN WAVES AND JETS

G. E. A. Meier

Max-Planck-Institut, Göttingen, Germany

I. Introduction

In waves and jets of real fluids at states below the critical point phase transitions often occur. These processes are called condensation and evaporation depending on a growth or diminishing of the liquid phase (phase transition of the solid phase is not considered here). In a pressure- volume- temperature-diagram of states of such a fluid (see Fig 1) the considered changes take place in the so-called two phase regime. When crossing the border of this regime, the phase boundary, nucleation occurs either on the liquid or the gas side. In the first case the bubble formation is called cavitation, in the second case the droplet formation is referred to as condensation. In both cases the initial process of nucleation up to a critical cluster of atoms or molecules is somewhat different from the later growth beyond the critical size to larger bubbles or droplets. For substances with high molar specific heat some general differences exist in the adiabatic flow process with rapid and large state changes. Because of the different shape of the phase boundary (see Fig 2), surprising phenomena become possible. An expansion flow in a nozzle starting from a superheated liquid state can lead to pure gas flow with supersonic velocities. Otherwise a shock wave in a gas like octane can liquefy this gas completely and the shock wave becomes the surface of a liquid. The instantaneous formation of a liquid surface by circumvention of the normal nucleation process is not yet understood. Thus, it is especially interesting to investigate waves and jets in fluids of high specific heat.

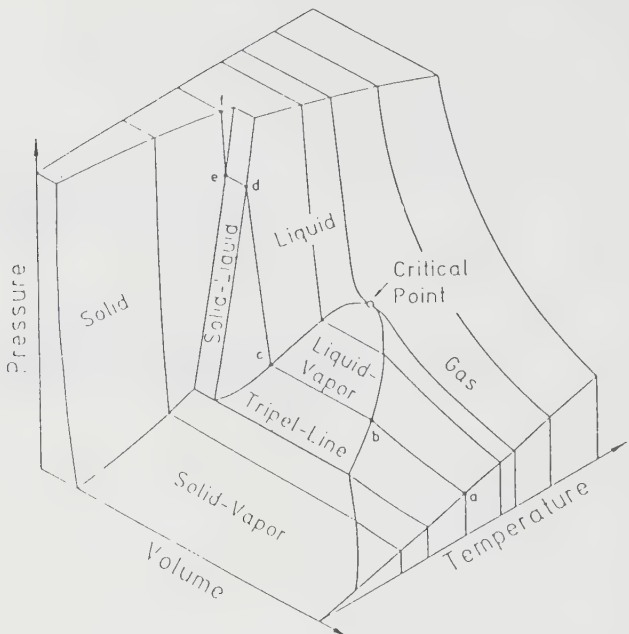


Fig. 1:
Diagram of state
of a real fluid

I.1 Thermodynamics, Equation of State

Thermodynamics used in fluid dynamics are usually restricted to the use of the ideal-gas-equation $pV = RT$ to describe the gas-behavior. As this method is not adequate for our problem, the use of at least the van-der-Waals equation (in a revised form) or a kind of virial equation is necessary. The thermodynamic state of a simple single component system is defined by only two quantities of state like pressure p and volume V , the others being fixed by the equation of state. On a line of constant temperature, the behavior of the gas is defined as long as the variations of state are quasistatic. The existence of two phases in equilibrium requires - in addition to the equality of pressure and temperature of the phases - the equality of the chemical potentials. Fortunately, this reduces the number of free variables via the Gibb's law of phases. Therefore, the state of the two phases and also the phase-boundary in equilibrium are fixed, as soon as the temperature is additionally fixed. Calculation of the phase-boundary is done by the Maxwell-criterium.

In the decay of metastable states, time is a ruling factor. To treat gas dynamics including phase transitions with a time-independent equation of state, it is necessary to neglect all effects due to relaxation and molecular kinetics. Sometimes this can be done by very quick variations of the states of equilibrium, to avoid the interference of relaxations. For example, if the expansion of a metastable state is too quick for any gas nuclei to develop, the liquid state can be "frozen" and be in equilibrium like a single-phase-state. The following state of equilibrium, obtained from this superheated state by phase-transition, can be described properly, but not the phase-transition itself.

The thermal equation of state is a modified van-der-Waals equation (Abbot and Chaves):

$$p_r = \frac{T_r}{Z_c(V_r - 1) - (\Omega_c - 1)} = \frac{\Omega_c^3 + [\alpha_c \Omega_c^2 (\Omega_c - 1) + \Omega_c^2] * (T_r - 1)}{Z_c^2 (V_r - 1)^2 + \Omega_c Z_c (V_r - 1) - \Omega_c^2 (\Omega_c - 1)} \quad (1)$$

being written in reduced variables, $p_r := p/p_c$, $V_r := V/V_c$ and $T_r := T/T_c$, c denoting the critical point. Three parameters in equation (1) are specific to the substance (e.g. PP1 [$C_6 F_{14}$]):

$$Z_c = p_c V_c / R T_c = 0.267$$

$$\alpha_c = 8.18$$

$$\Omega_c = 0.838$$

the critical compressibility,

the Riedel-parameter, and

the critical value of the dimensionless temperature function Ω :

$$\Omega := \Omega_c^3 + [\alpha_c \Omega_c^2 (\Omega_c - 1) + \Omega_c^2] * (T_r - 1)$$

The advantages of this relation consist in the description of the liquid and the gaseous phase in a single relation, and the ability to describe metastable states. Thus, it is possible to treat flows with phase transitions in a way similar to normal ideal-gas-dynamics. On the other hand, its accuracy is inferior compared to more complex equations, which are specialized on single phase states. Since however the differences in pressure and volume are in the order of some percent, basic physical qualities can be shown properly.

The calorical equation used here was developed by *Thompson et al.* [0.2], and is an algebraic relation for the specific heat at constant volume c_v , normalized with the gas constant R :

$$c_v = \frac{Y}{(1 + Y^2)} c_w + c_\alpha \quad \text{for } Y \geq 0,$$

$$c_v = c_\alpha \quad \text{for } Y < 0, \quad (2)$$

with

$$Y = \beta (T_r - t).$$

The above relation models the excitation of the vibrational degrees of freedom in dependence of temperature. c_w (= 54) is the specific heat of the translational, vibrational and rotational degrees of freedom at full excitation, respectively c_α (= 3) is the specific heat when the vibrational degrees of freedom are not excited. β (= 1.08) and t (= 0.389) are matter-specific values ruling the temperature dependence of the excitation for a certain substance (PP1).

Some of these integrations can be done analytically, others have to be done numerically. However, it is impossible to calculate time-dependent phenomena like nucleation rates and metastable states by such a model.

I.1.1 Retrograde Behavior of Real Gases

Figure 2 is showing the phase-boundaries of two characteristic substances in a temperature-entropy-diagram. The main difference is found in the inclination of the saturation borderline at the gas side, which is inclined backwards (retrograde) for

PP1. An isentropic compression of a gas, beginning at point 1, is able to cross fully through the two phase region to the liquid state 0. If the inclination of the saturation borderline is not retrograde, a compression always leads away from a phase-boundary. Additionally in the retrograde case a complete evaporation by expansion is possible, for a normal substance only a partial one (0 to 1') is.

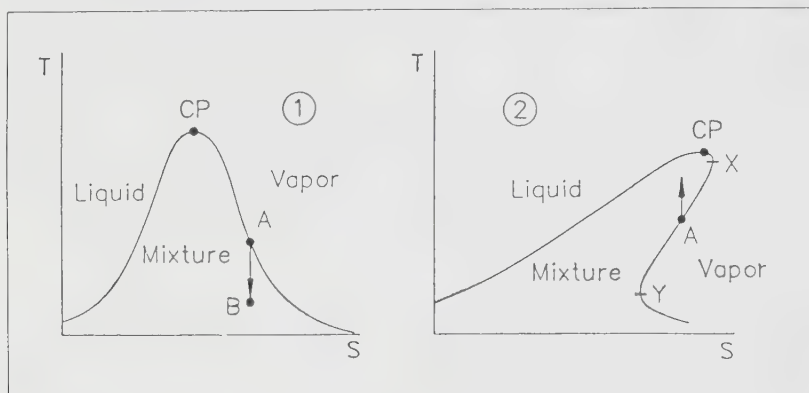


Fig 2: T-S diagram with normal (1) and retrograde behavior (2, between X and Y)

The characteristic parameter for this behavior, is the ideal-gas specific molar heat c_v^* at the critical point c introduced by *Thompson and Sullivan*. For values greater than $c_v^* = 11.2$ retrograde behavior can be observed. For substances with $c_v^* > 24.1$, complete condensation of the gas by a shockwave with increasing entropy is possible.

Isentropic expansion of superheated liquids seems to be the same procedure for normal and retrograde substances at a first glance. In both cases evaporation will take place, but it would lead to a strong reduction of temperature for normal liquids. Evaporation is "frozen" and in the end a mixture of the two phases would be left. In the case of a retrograde substance the enthalpy of evaporation can be taken completely from its internal energy, due to its high molar specific heat. The decrease of temperature of the substance during evaporation is smaller. So, if the temperature of the retrograde substance is sufficiently high, it is possible to completely evaporate the liquid by isentropic expansion.

In a microscopic view, evaporation of a substance with retrograde behavior is an energy transfer from vibrational degrees of freedom to translational or rotational degrees of freedom of the molecules by molecular collisions. As has been shown for substances with high specific heat, only a single stroke between two molecules is necessary to transmit the characteristic energy for phase transition. Thus, retrograde evaporation is possible without diffusion or heat conduction and has therefore very high transition-rates. For that reason it is justified to take states of nonequilibrium into account, but to neglect effects of relaxations containing the growth of a new phase. These high transition-rates directly lead to the question of shock-like evaporation waves (see chapter III.3.3).

I.1.2. Mechanical Laws of Conservation

In addition to the thermodynamic equations of state and energy, mechanical equations and some boundary conditions are necessary to fix the problem of two-phase flows and waves with phase transition properly. The steady-state, one-dimensional continuity and momentum equations for one-component, two-phase flow can be written as [Henry, Fauske, 1971]:

continuity

$$\text{liquid: } W_l V_l = A_l u_l \quad \text{vapor: } W_g V_g = A_g u_g \quad (3)$$

momentum

$$- A dp = d(W_g u_g + W_l u_l) + dF_w \quad (4)$$

with

and the indices

W := flow rate

l := liquid phase

A := cross-sectional area

g := vapor phase

p := pressure

w := wall

F := viscous forces

V := specific volume

u := velocity

The equation of conservation of momentum is given in general form by the Euler-equation (neglecting friction):

$$\frac{\partial}{\partial t} u + (u \nabla) u = - \frac{1}{\rho} \nabla p \quad (5)$$

with u the velocity,

or, with respect to friction by the Navier-Stokes-equation in the incompressible case.

$$\frac{\partial}{\partial t} u + (u \nabla) u = - \frac{1}{\rho} \nabla p + \frac{\eta}{\rho} \Delta u \quad (5')$$

with ρ : density and η : viscosity.

Due to the complexity of the Navier-Stokes- or Euler-equation, we will turn to two special cases relevant for our further work, jets and shocks, in more detail.

A. Jets

Because of the cylindric symmetry of a jet, the Euler-equation is much simpler than in the universal case. We will use cylindric co-ordinates:

$$\frac{\partial w}{\partial t} + w \frac{\partial w}{\partial z} = \frac{z}{\rho} + \frac{\sigma}{\rho} \left(\frac{1}{r^2} \frac{\partial r}{\partial z} + \frac{\partial^2 r}{\partial z^2} \right) \quad (6)$$

with z : main flow direction, r : radius, σ : surface tension, w : velocity in z -direction. If $A = A(z, t)$ is a function of the cross section area, with $A = \pi r^2$, the continuity-equation follows as:

$$\frac{\partial r}{\partial t} + w \frac{\partial z}{\partial r} + \frac{r}{2} \frac{\partial w}{\partial z} = 0 \quad (7)$$

and Ohnesorge-number:

$$\text{Re} := \frac{u d \rho}{\mu} \quad \text{Oh} := \frac{\mu}{\sqrt{\rho \sigma d}} \quad (8)$$

with μ : dynamic viscosity, ρ : density, σ : surface tension, u : velocity of the liquid, and d : nozzle diameter.

Three regions are distinguished:

1. Small Reynolds- and Ohnesorge-numbers lead to the well-known Rayleigh-instability: growing surface-waves divide the jet into nearly uniform droplets.
2. In the second region the decay is initiated by wave-like deformations of the jet axis. The intact jet is shorter than in the first case.
3. In the last region, with the greatest Reynolds- and Ohnesorge-numbers, friction of the surrounding atmosphere leads to fast disintegration of the jet.

B. Shocks

To simplify the problem, only perpendicular shocks will be treated. Consider a system of coordinates with the plane of unsteadiness being at rest. The flow is steady in this system and one obtains from mass-, momentum-, and energy-conservation [e.g. Landau, Lifschitz]:

$$\frac{u_1^2}{V_1} = \frac{u_2^2}{V_2} = j \quad (9)$$

$$\frac{u_1^2}{V_1} + p_1 = \frac{u_2^2}{V_2} + p_2 \quad (10)$$

$$\frac{u_1^2}{2} + h_1 = \frac{u_2^2}{2} + h_2 \quad (11)$$

with h : enthalpy, indices 1 and 2 indicating the states before and after the shock respectively and j : the massflux-density. Combining (6) and (7), one obtains:

$$-j^2 = \frac{p_2 - p_1}{V_2 - V_1} \quad (12)$$

and with (8):

$$h_1 - h_2 = \frac{(V_1 + V_2) * (p_1 - p_2)}{2} \quad (13)$$

Equation (10) is the Rankine-Hugoniot-relation, which is a function of the shock-adiabates. As entropy is not constant along this dynamical adiabate; It only fixes the initial- and end-state, while nothing is said about the way of variation or about transition states. The line, connecting initial- and end-state, is called Rayleigh-line and its steepness is given by the massflux-density j .

One obtains the variation of the entropy S by an expansion for small $S_2 - S_1$ and $p_2 - p_1$ to the third order: As the system is closed, entropy must increase.

$$S_2 - S_1 = \frac{1}{12 T_1} \left[\frac{\partial^2 V}{\partial p_1^2} \right]_S (p_2 - p_1)^3 \quad (14)$$

Therefore the derivative in (14), describing the curvature of the isentrope in a normal p - V -diagram, is a ruling criterium for the existence of unsteady variations of

state and their direction. For ideal gases one only finds compression-shocks, as can be shown easily with the help of the equation of the isentropes $pV^\gamma = \text{const}$. Only for high-molecular substances near the critical point, can regions with negatively curved isentropes be found, which means stability of expansion-shocks.

II Nucleation

II.I Homogeneous Nucleation

II.I.1 Introduction

The process of formation of microscopic bubbles in liquids or droplets in vapor is called nucleation. It is called homogeneous if the nuclei are formed only by thermal fluctuations and interactions of the molecules of the supersaturated medium. It has been shown that a critical number of molecules exists in a cluster i^* below which the cluster is tending to shrink. For overcritical clusters the probability of catching another molecule is greater than losing one. Collisions between two or more clusters are fully neglected in most models. In the following part we will treat homogeneous nucleation in the way suggested by Dillmann (1989) and Dillmann and Meier (1989), using the Fisher droplet model expressing the Gibbs free energy ΔG by real gas properties.. which is different to the classical approximation mainly developed by Volmer, Weber etc.

II.I.2 Basic Relations

Following the statistical mechanical treatment of real gases below the critical point, the equilibrium concentration of clusters containing i molecules in a system with volume V is given by

$$\rho_{i,\text{eq}} = \frac{1}{V} \exp \left(-\frac{\Delta G_i}{kT} \right) \quad (1)$$

where k is Boltzmann's constant, T is the temperature and G_i represents the Gibbs free energy of formation of the i -mer. When the system is supersaturated and the transition to the liquid phase begins, the process of nucleation is mainly determined by the clusters of "critical" size i^* defined by

$$\frac{\partial \Delta G_i}{\partial i} \Big|_{i=i^*} = 0 \quad (2)$$

which can be regarded as condensation nuclei. The rate of formation of these critical clusters is consequently given in the following generalized form:

$$I = \sqrt{-\frac{1}{2\pi kT} \frac{\partial^2 \Delta G_i}{\partial i^2}} \cdot c_{i^*} \cdot \frac{1}{V} \exp \left(-\frac{\Delta G_{i^*}}{kT} \right) \quad (3)$$

where the factor c_{i^*} is the rate of monomer impact on the surface s_{i^*} of the critical cluster:

$$c_{i^*} = \frac{ps_{i^*}}{\sqrt{2\pi m_i kT}} \quad (4)$$

In this relation p is the total pressure in the system and m_i is the mass of a single molecule. In the case of a spherical cluster s_{i*} is given by:

$$s_{i*} = s_i i^{2/3} \quad (5)$$

with s_i being the mean surface of a single molecule in the bulk liquid phase. If we follow these general considerations so far, then the nucleation rate (3) is mainly governed by the Gibbs free energy of formation ΔG_{i*} of the critical cluster. The exact determination of ΔG_{i*} seems to be the real problem of nucleation theory and therefore the following attempt is made.

II.I.3 A new Droplet Model for the Gibbs Free Enthalpy of a Cluster

We use a semiphenomenological droplet model for the Gibbs free energy of formation of an i -mer, which is similar to a form originally proposed by Fisher:

$$\Delta G_i = x_i \gamma s_i i^{2/3} + \tau kT \ln i - kT \ln (q_0 V) - ikT \ln S \quad (6)$$

where γ is the bulk surface tension, $s_i^{2/3}$ is the surface of a spherical cluster containing i molecules, and the new quantity x_i describes deviations of the surface free energy of an i -mer compared to a macroscopic spherical liquid droplet. In the limiting case for an infinite number of molecules this factor of course approaches unity. The second and the third term arise according to Kiang *et al.* from translational, rotational, vibrational and configurational contributions to the droplet free energy. The last term represents the change in chemical potential caused by supersaturation. For an ideal gas the supersaturation S is given by the ratio of the actual pressure p to the vapor pressure p_{sat} at the actual temperature T :

$$S = \frac{p}{p_{sat}}. \quad (7)$$

With the ansatz (6), the equilibrium distribution (1) can be used to construct a thermal equation of state for real gases by simply applying the definition of the number density ρ :

$$\rho = \frac{n}{V} = \sum_{i=1}^{\infty} i \rho_{i,eq} = q \sum_{i=1}^{\infty} \exp(-x \Theta i^{2/3} - (\tau - 1) \ln i + i \ln S) \quad (8)$$

where n is the total number of molecules in V , and Θ is an abbreviation for $\gamma s_i / kT$. It is easily noticed that the density ρ is thus given as a power series in p with its coefficients depending on temperature.

By comparison with other equations of state, we now have the possibility to determine the free parameters of the droplet model (6). Following Fisher and Staufer and Kiang, τ and q_0 are constant in a wide range of state and can thus be calculated from the experimentally known variables of states at the critical point (denoted by the index "c"), where the surface tension γ vanishes:

$$\rho_c = q_0 \zeta(\tau - 1) \quad (9a)$$

$$p_c = q_0 k T_c \zeta(\tau) \quad (9b)$$

with $\zeta(x)$ being the well-known Riemann zeta function of x :

$$\zeta(x) = \sum_{i=1}^{\infty} i^{-x} \quad (10)$$

The new quantity x_i can be found by forcing the identity of (8) with another experimentally verified equation of state. Comparison of the coefficients of (8) with those of an ordinary Taylor expansion of φ yields:

$$x_i = -\frac{1}{\Theta i^{2/3}} \ln \left[\frac{p_{sat}}{q_0} i^{\tau-1} \frac{1}{i!} \lim_{T \rightarrow 0} \left(\frac{\partial \varphi}{\partial p} \right)_T \right]. \quad (11)$$

Since no equation of state exists which provides the derivatives of density with respect to pressure correctly for all i , the direct computation of the higher x_i from (11) is not yet feasible. However, it is possible to consider a dependence on x from cluster radius r of the following form:

$$x_i = f\left(\frac{\delta}{r_i}\right) \quad (12)$$

with δ being a submolecular characteristical length much smaller than the radius of a monomer r_i . Therefore, we can expand the function (12) into a power series around $\delta/r_i = 0$ (i.e. $i \rightarrow \infty$) and truncate the series after the quadratic term. With the assumption of spherical clusters (i.e. $r_i \sim i^{1/3}$) we obtain in powers of i :

$$x_i = 1 + \alpha_1 i^{-1/3} + \alpha_2 i^{-2/3}. \quad (13)$$

If now x_1 and x_2 are known, the unknown parameters α_1 and α_2 in (13) can be expressed as:

$$\begin{aligned} \alpha_1 &= \frac{(x_1 - 1) - (x_2 - 1) \cdot 2^{-2/3}}{2^{-1/3} - 2^{-2/3}} \\ \alpha_2 &= \frac{(x_2 - 1) - (x_1 - 1) \cdot 2^{-1/3}}{2^{-1/3} - 2^{-2/3}} \end{aligned} \quad (14)$$

so that finally x_i can be computed for all i from an equation of state which provides at least the first two derivatees of density with respect to pressure correctly. From the well-known virial equation of state,

$$\frac{p}{\varphi} = kT + Bp + Cp^2 + \dots \quad (15)$$

with its virial coefficients B, C, \dots depending on temperature, one obtains for example:

$$\begin{aligned} x_1 &= -\frac{1}{\Theta} \ln \frac{p_{sat}}{q_0 k T} \\ x_2 &= -\frac{1}{\Theta 2^{2/3}} \ln \left[-\left(\frac{p_{sat}}{q_0 k T} \right)^2 2^{\tau-1} q_0 B \right]. \end{aligned} \quad (16)$$

By means of the equations (9), (13), (14) and (16) all model parameters are finally given only in terms of well-known macroscopic quantities. Tab. 1 gives some values for the constants τ and q_0 and the correction factor x_i . In consequence of the determination of the equation of state, x_i is not only a function of cluster size i , but also of temperature T .

Substance	τ	q_0	χ_1	χ_{100}
Water	2.166	0.151	0.986	1.033
n-Nonane	2.190	0.171	0.640	0.926
Methanol	2.162	0.148	1.297	1.109
Ethanol	2.175	0.159	1.132	1.042

Tab. 1: model constants τ and q_0 and correction factors χ_1 and χ_{100} (at $T=273.15$ K) for some substances.

II.I.4 Final Results

Since all unknown quantities are now determined, the nucleation rate I can be calculated from equation (3) for the droplet model (6):

$$I = \frac{1}{3} \sqrt{\frac{\Theta}{\pi}} \left(1 + \alpha_1 i^{*-1/3} + \frac{9\tau}{2\Theta} i^{*-2/3} \right) \frac{ps_1}{\sqrt{2\pi m_i kT}} \rho_{i^*} \quad (17a)$$

with

$$\rho_{i^*} = q_0 \exp(-\chi_1 \Theta i^{*2/3} - \tau \ln i^* + i^* \ln S) \quad (17b)$$

where the size of the critical i^* is given by the real root of the cubic equation

$$\tau x^3 + \frac{1}{3} \alpha_1 \Theta x^2 + \frac{2}{3} \Theta x - \ln S = 0 \quad , \quad x := i^{*-1/3} \quad (17c)$$

Fig. 3:

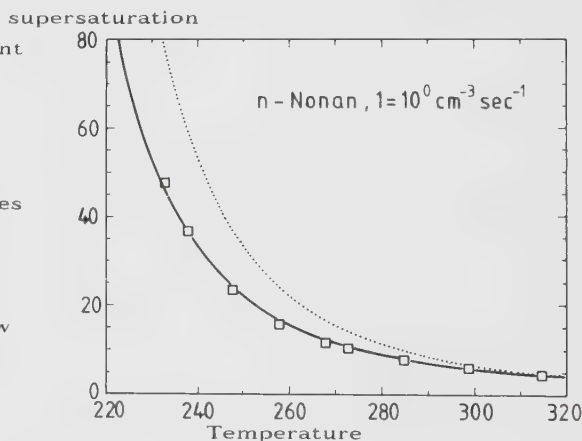
Comparison of theory and experiment for n-Nonane ($\tau = 2.190$, $q_0 = 0.171 \rho_0$, $\chi = f(T, i)$)

..... classical, — new theory

[] Katz et al.

Comparable results for all substances for which

- macroscopic fluid parameters are sufficiently accurately known
 - nucleation rate measurement allow for comparison
- (Water, Methanol, Ethanol, etc.)



For $\tau = 0$ (no additional degrees of freedom) and $\chi = 1$ (Cluster is a macroscopic droplet) this is a linear equation and with $q_0 = p/kT$ we obtain the expression for the classical Becker-Döring-Zel'dovich nucleation rate I_{class} , which therefore is a special case of the improved theory:

$$I_{\text{class}} = \frac{1}{3} \sqrt{\frac{\Theta}{\pi}} \frac{ps_1}{\sqrt{2\pi m_i kT}} \frac{p}{kT} \exp\left(-\frac{4}{27} \frac{\Theta^3}{\ln S^2}\right) \quad (18)$$

II.II Heterogeneous Nucleation

II.II.1 Introduction

Nucleation is called heterogeneous if external effects, e.g. walls (little caves) or dust in liquids or vapors, are involved in nucleation. The heterogeneous nucleation rate I will be treated, following [Sigsbee, 1969], in terms of an equilibrium reaction occurring on the substrate. A description of the properties of the parent phase, which is the absorbed vapor, will be attempted first, followed by some approaches which have been used for the calculation of the free energy change for this equilibrium reaction. The resulting form of the critical embryo distribution will also be discussed.

II.II.2 The heterogeneous Equilibrium in Unary Systems

The distinguishing feature of nucleation models, which are based upon the attainment of an equilibrium distribution of monomer and clusters in the supersaturated parent phase, is the existence of a maximum in the quantity ΔG . Since an embryo of the critical size can grow beyond the critical size with a monotonic decrease in free energy and the total system free energy will also decrease, a formal kinetic barrier can be considered to exist at the critical size. It has been observed experimentally throughout many nucleation rate studies that relatively small changes in supersaturation cause large changes in the nucleation rate. The high sensitivity to supersaturation, coupled with the observed high growth rates of the nucleating phase, makes a nucleation rate approach, based on the attainment of a metastable equilibrium distribution of subcritical and critical sized clusters, seem reasonable. The nucleation rate is then the rate of "leakage" of a small number of critical clusters past the critical size, which is followed by growth to observable nuclei.

A: A macroscopic Approach to ΔG .

Because of its simplicity and mathematical tractability, the most often used approach to calculate ΔG for the formation of an embryo is based upon the assignment of macroscopic properties, such as surface free energy and a volume free energy of condensation, to the embryo. As an example we will discuss the approach via a cap-shaped embryo:

For a cap-shaped embryo "wetting" the substrate with a contact angle Θ , the free energy of embryo formation, taking into account the net interfacial free energy terms and the volume free energy change, is:

$$\Delta G = \frac{4}{3} \pi r^3 \Delta G_v \left(\frac{2 - 3 \cos \Theta + \cos^3 \Theta}{4} \right) + 4\pi r^2 \left(\frac{1 - \cos \Theta}{2} \right) \sigma_{vv} + \pi r^2 \sin^2 \Theta (\sigma_{sx} - \sigma_{sv}) \quad (1)$$

with:

$$\Delta G_v = \frac{-kT}{v} \ln \frac{P(1)}{P(1)_e}$$

where r : embryo size, ΔG_v : Gibbs free energy of condensation per unit volume, Θ : embryo-to-substrate contact angle, σ : surface free energy per unit area, v : condensed monomer volume, $P(1)$: partial pressure of monomer and $P(1)_e$: equilibrium vapor pressure of bulk material.

The above form of ΔG , which uses macroscopic concepts for the free energies involved, is subject to question because of the small embryos but has the advantage of referring to often known quantities and of yielding mathematically tractable results. The maximum in ΔG again occurs at the point determined by

$$\frac{\partial \Delta G}{\partial r} = 0 = 4\pi r^2 \Delta G_v \left(\frac{2 - \cos \Theta + \cos^3 \Theta}{4} \right) + 8\pi r \left(\frac{1 - \cos \Theta}{2} \right) \sigma_{sv} + 2\pi r \sin \Theta (\sigma_{sx} - \sigma_{sv}). \quad (2)$$

Upon using the Young equation for the contact angle Θ ,

$$\sigma_{sv} = \sigma_{sx} + \sigma_{vx} \cos \Theta \quad (3)$$

one finds that $r = -2\sigma_{vx}/\Delta G^*$ and ΔG^* is 1/3 of the surface energy

$$\Delta G^* = \frac{16}{3} \pi \frac{\sigma_{vx}^3 \Phi(\Theta)}{\Delta G_v^2}. \quad (4)$$

Here

$$\Phi(\Theta) = \left(\frac{2 - 3 \cos \Theta + \cos^3 \Theta}{4} \right) \quad (5)$$

varies between 0 for $\Theta = 0$ and 1 for $\Theta = 180^\circ$, and expresses the total energetic interaction between the embryo and the substrate, excluding configurational entropy effects. In terms of cluster size i the free energy of formation can be briefly written as

$$\Delta G(i) = -ikT \ln \frac{P(1)}{P(i)} + [36\pi\Phi(\Theta)]^{1/3} (iv)^{2/3} \sigma_{vx} \quad (6)$$

and the maximum ΔG^* occurs at

$$i^* = \frac{32\pi\sigma_{vx}\Phi(\Theta)}{3v\Delta G_v^3}. \quad (7)$$

The concentration of embryos of critical size is then found as

$$n(i) = n_s \exp(-\Delta G^*/kT) \quad (8)$$

with n_s being the concentration of absorption sites.

A line tension contribution to the free energy of embryo formation may also require consideration. It was noted that this could be done by a periphery energy term, $2\pi r(\sin \Theta)\gamma_{sv}$, γ being the line tension (energy per length), which should be included in ΔG , analogous to the edge free energy for a faceted crystalline embryo. Considering this additional term, the free energy of embryo formation becomes

$$\Delta G = \frac{4}{3} \pi r^3 \Delta G_v \Phi(\Theta) + 4\pi r^2 \left(\frac{1 - \cos \Theta}{2} \right) \sigma_{vx} + \pi r^2 \sin^2 \Theta (\sigma_{sx} - \sigma_{sv}) + 2\pi r(\sin \Theta)\gamma_{sv}. \quad (9)$$

This expression can be maximized with respect to r to determine the critical embryo size, analogously to the treatment for equation (1). The contact angle Θ will then be a function of embryo size.

B: Calculating the Nucleation rate I

The nucleation rate is approximately the rate at which the critical-sized clusters, whose concentrations are given by equation (8), grow beyond the critical

size. Actual nucleation rates will be reduced below the calculated value because of the re-evaporation of some embryos into absorbed monomer and a reduction in the calculated critical embryo population below the equilibrium population given by equation (8). Three other effects which could reduce the calculated nucleation rate are the time τ required to attain a steady state population of monomer, the time τ_1 required to attain the embryo population from the monomer given by equation (8) and the parent phase depletion by growing nuclei. The calculations have been done by Becker, Döring and Zel'dovich, who considered the stationary state nucleation rate at the inception of nucleation ($\partial I/\partial t = 0$). The nucleation rate at the beginning of nuclei appearance is then

$$I = \left[\frac{\Delta G^*}{3\pi k T_i^{*2}} \right]^{1/2} 2\pi r \sin \Theta a_0 n(1) n_s v \exp [(-\Delta G^* - \Delta G_{sd})/kT] \quad (10)$$

with a_0 : adatom jump distance or lattice parameter, $n(1)$: concentration of monomer, v : adatom vibrational frequency and ΔG_{sd} : surface diffusion free energy; for cap-shaped embryos.

II.III Condensation

II.III.1 Introduction

As an example we will treat shockwave induced condensation of retrograde fluids. It could be produced by shock waves reflected from the rigid end-wall of a shock tube. The flow is treated as one-dimensional, the influence of walls being neglected. The effect of conductivity of the vapor is taken into account only in the vicinity of the macroscopic droplets. The vapor phase behaves like an ideal gas, that is, it obeys the thermal equation for the ideal gas, and the internal energy and the enthalpy are functions of temperature only.

The liquid phase is assumed to be incompressible. It is present in the form of spherical droplets which do not interact with each other; hence the coagulation effects are neglected. The droplets have the same velocity as the vapor and the temperature at the surface of the droplet is the same as inside.

II.III.2 Basic Relations

The droplets appear just behind the shock wave in the process of spontaneous homogeneous nucleation. The homogeneous nucleation is described by the Frenkel-Zel'dovich steady-state nucleation model. A well-known approach was used here to show how nucleation was treated in the elder nucleation models. Therefore the nucleation rate is given in the following classical form (compare eqn. (18), p. 10):

$$I = \left(\frac{P}{k_B T} \right) V_{mc} \sqrt{\frac{2\sigma}{\pi \tilde{m}}} \exp \left(-\frac{4\pi\sigma r^*{}^2}{3k_B T} \right) \quad (1)$$

with

$$r^* = \frac{2\sigma}{\rho_L RT \ln(p/p_\infty)}, \quad R = \frac{R}{M}, \quad p = \text{vapor pressure} \quad (2)$$

V_{mc} = volume of one vapor molecule, σ = surface tension

\tilde{m} = mass of one vapor molecule

The nucleation rate strongly depends on the supersaturation and on the surface tension. As regards surface tension, for the retrograde liquid the bulk value of the surface tension σ_∞ depends on the temperature as follows:

$$\sigma_\infty(T) = \sigma_\infty(T_c) \left[\frac{(1 - T/T_c)}{(1 - T_c/T_c)} \right]^{1.2} \quad (3)$$

This is the *Gambill* formula. The exponent 1.2 is strictly applicable to nonpolar gases; T_c is the critical temperature. The critical temperature of a pure material may be defined as the maximum temperature at which liquid and vapor phases can coexist in equilibrium; above this temperature no liquid phase is then possible. The vapor pressure at this temperature is called the critical pressure (p_c) and the volume per unit mass, the critical volume (V_c).

From a mathematical point of view the definition of the critical point is

$$\left(\frac{dp}{dV} \right)_{T_c} = \left(\frac{d^2p}{dV^2} \right)_{T_c} = 0 \quad (4)$$

If for a certain temperature the value of the interfacial tension (for the flat surface between two phases) is known, then formula (3) makes it possible to get the values of surface tension for any other temperature.

The influence of the radius on the droplet surface tension is given by the *Tolman* relation:

$$\sigma_r = \sigma_\infty \left(1 - \frac{2}{kr} + \frac{2}{k^2 r^2} \right) \quad (5)$$

where $1/k \approx (2...5) \cdot 10^{-8}$ cm and r the droplet radius. Tolman suggests that the surface tension for a droplet lies below its bulk value. We also admit this correction. It should be noted that for the critical radius r^* and nucleation rate, the value of supersaturation $S = p/p_\infty$ is required, where p_∞ is the equilibrium pressure of a vapor coexisting with its liquid phase. The equilibrium pressure is given by the *Clausius-Clapeyron* equation for retrograde fluids. It is the so-called *Riedel* equation for retrograde fluids:

$$p_{\infty r} = f(T_r, \alpha_c)$$

as follows:

$$\begin{aligned} \log p_{\infty r} &= -\Phi(T_r) - (\alpha_c - 7)\Psi(T_r), \\ \Phi(T_r) &= 0.118\varphi(T_r) - 7 \log T_r \\ \Psi(T_r) &= 0.0364\varphi(T_r) - \log T_r \\ \varphi(T_r) &= 36/T_r + 42 \ln T_r - 35 - T_r^6 \end{aligned} \quad (6)$$

where $T_r = T/T_c$ and $p_r = p/p_c$ and where $p_{\infty r} = 1$ when $T_r = 1$. α_c is the so-called Riedel parameter which could be estimated from the properties of normal boiling point and critical ones. We use it in the form of the *Thompson* correlation formula:

$$\alpha_c = 5.7 + 0.34 \left(\tilde{c}_v - \frac{3}{2} \right)^{1/2}, \text{ where } \tilde{c}_v = c_v / R \quad (7)$$

where c_v is the specific heat.

The size of the droplet just behind the shock wave is very small, less than the mean molecular free path in the gas. Therefore the *Hertz-Knudsen* model for the mass and energy exchange between two phases is applicable here. Due to condensation, the droplets grow and at a certain distance from the shock wave they become larger than the mean molecular free path. At this stage we may use the following equations:

$$\frac{dm}{dt} = 4\pi r D(\rho - \rho_d), \quad \text{where } r = \bar{r} \quad (8)$$

with m : droplet mass, D : self-diffusion coefficient, ρ : vapor density at infinity from the droplet, ρ_d : vapor density at droplet surface and \bar{r} : "surface-averaged" droplet radius. This describes the flux of vapor mass towards the droplet in the form of *Fick's law* of diffusion for a spherical droplet, though nowadays a flow model is used for the mass transport [Gyarmathy 1982].

To describe the energy exchange between two phases the equation for conduction of heat away from the droplet surface may be written in the form of the Fourier equation:

$$h_{fg} \cdot \frac{dm}{dt} = h_{fg} 4\pi r^2 \rho_L \frac{dr}{dt} = -4\pi k r (T_d - T) \quad (9)$$

where $r = \bar{r}$, $dr/dt = d\bar{r}/dt$ and ρ_L : liquid density. These two equations are needed to compute the droplet temperature T_d and then the rate of droplet growth dr/dt . Here T is the temperature of the vapor at a certain distance from the droplet (temperature of a vapor environment).

There is a number of physical quantities entering these equations. First: h_{fg} is the specific heat of phase transition, k is the thermal conductivity of the retrograde vapor. For the estimation of the thermal conductivity coefficient we use the semiempirical *Eucken* correlation. This correlation was introduced for polyatomic gases at low pressures.

We also must have a value for the dynamic viscosity η and to this end the *Bromley and Wilke* empirical formula is applied. This formula is an empirical correlation of the viscosity values obtained in the *Chapman-Enskog* theory with the critical properties:

$$\eta = \frac{0.00333 \cdot (M T_c)^{1/2} f_1(1.33 T_r)}{V_c^{2/3}}. \quad (10)$$

The self-diffusion coefficient values are also taken from the semi-empirical formula obtained in the *Chapman-Enskog* theory:

$$D = 1.2(R T/M p)(1.1)\eta \quad (11)$$

where R : the universal gas constant, T , p : vapor temperature and pressure M : mole mass, and where η is expressed in poises, p in atmospheres, D in square centimetres per second. ρ_d is the vapor density at the droplet surface with

$$\rho_d = P_d / RT_d. \quad (12)$$

P_d is the ambient pressure which would be necessary to keep the droplet in equilibrium, both droplet and vapor having the temperature T_d . Using the *Helmholtz* equation this pressure is:

$$p_d = p_\infty(T_d) \exp\left(2\sigma/\rho_L RT_d r\right) \quad (13)$$

In each cross section of the shock tube the radii of all droplets are the same and equal to the so-called "surface-averaged" droplet radius. It has been shown that a more realistic model with the radii distribution function of droplets gives almost the same results (in one-dimensional flow) as a model of a surface-averaged droplet radius adopted from Hill. We also assume that a behavior of this artificial droplet with a surface-averaged droplet radius is the same as the physical one and its growth is described by Fick's law of diffusion and the Fourier equation of conduction.

It is obvious to take as the initial condition for the droplet radius its critical value: $r_0 = \bar{r} = r^*$. This implies its temperature being equal to the gas temperature $T_0 = T$. One-dimensional, two phase flow is described by the mass, momentum and energy conservation equations for a vapor-liquid mixture:

$$\frac{1}{\rho_m} \frac{d\rho_m}{dx} + \frac{1}{u} \frac{du}{dx} = 0 \quad (14)$$

$$\frac{dp}{dx} + \rho_m u \frac{du}{dx} = 0 \quad (15)$$

$$\frac{d}{dx} \left(h_m + \frac{u^2}{2} \right) = 0 \quad (16)$$

where

$$\rho_m = \frac{\rho \rho_L}{(1 - \mu) \rho_L + \mu \rho} \quad (17)$$

$$h_m = (1 - \mu) h_v + \mu h_L. \quad (18)$$

To complete the system of equations the thermal and calorical equations of state are required. In the considered condensation model the relative rate of formation of a new phase is given by one integrodifferential equation:

$$u \frac{du}{dx} = \left(\frac{\rho_L}{\rho_m} \right) \left[\frac{4}{3} \pi r_0^3 I^*(x) + \left\{ \int_0^x 4 \pi \left(r_0 + \int_{x_1}^x \frac{dr}{dt} \frac{dx_2}{u} \right)^2 \frac{I^*(x_1)}{\rho_m(x_1)} \frac{dx_1}{u} \right\} \rho_m \frac{dr}{dt} \right]. \quad (19)$$

The first term on the right-hand side is the condensation rate due to the formation of new droplets in a fluid element at x . The second term describes the condensation rate due to the growth of all droplets which have been created somewhere before a fluid element at x along the streamline.

II.III.3 Results

Attention should be paid to the fact that, in retrograde fluids, condensation causes the increase of both temperature and pressure in the subsonic flow. One can compare the condensation process in the regular fluid, for example water vapor, to the heat addition. When condensation takes place either in regular or retrograde fluids, it causes a removal of a part of the vapor phase (because of phase transition) and the increase of temperature of vapor due to the energy released in the process of condensation. In the case of a regular fluid, heating

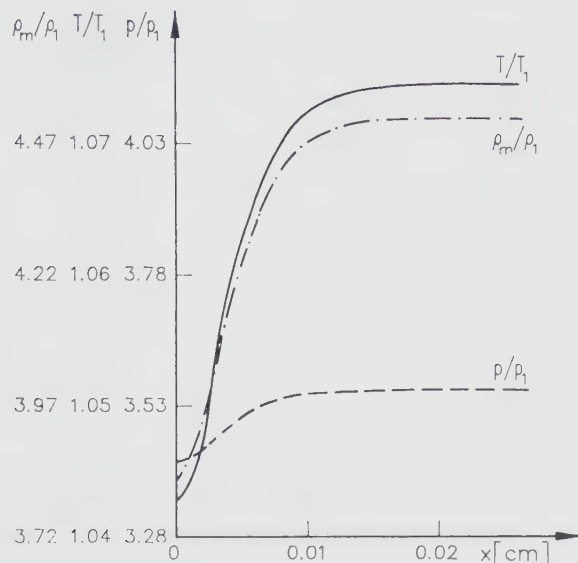


Fig. 4:
Profiles of different
quantities of state in
the condensation zone
behind the shock wave
($V_1 = 79 \text{ cm}^3/\text{g}$).
 $T_1 = 393 \text{ K}$, $M_1 = 1.91$)

has a larger effect on the stream properties than the vapor removal, whereas for retrograde fluid the effect of a removal of a part of the vapor seems to be dominant. As a result of this, we observe the rise of pressure and temperature in the subsonic flow.

Experiments with partial and complete shock liquefaction of a substance with retrograde behavior have been performed in a shock tube [Dettleff et al.]. In a p - V diagram (Fig 5), transitions from an initial state 0 to an end state A', for partial, or, to an end state A, for complete liquefaction are possible. The experiments mainly use the reflected wave at the end of the shock tube to perform the phase transition (Fig 6).

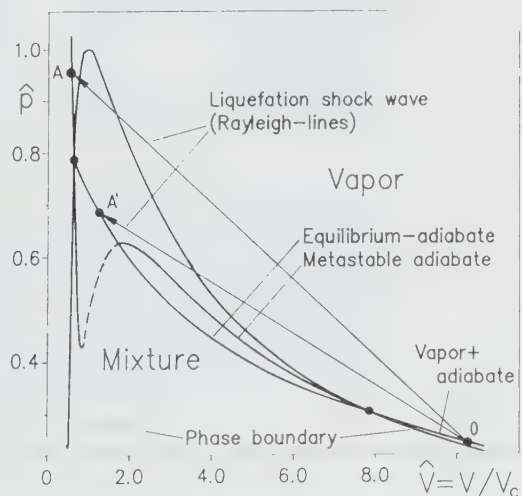
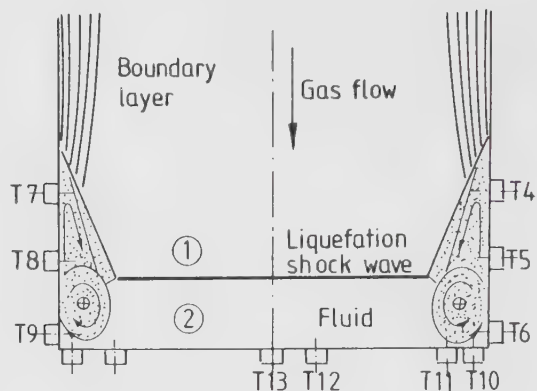


Fig. 5:
Shock waves with partial (A') and
complete (A) liquefaction of the gas

Fig 6:
Model of the shock-
boundary layer- relation
at complete shock wave
induced liquefaction



With the help of the transducers T4 to T13, pressure and temperature changes can be recorded and compared with the calculated values. In Fig 7 and Fig 8 numerous experiments for different initial conditions and shock Machnumbers are plotted and show a fairly good agreement of the expected and measured pressures and temperatures. This indicates that the equilibrium conditions are finally achieved independently of the complicated processes of nucleation and condensation.

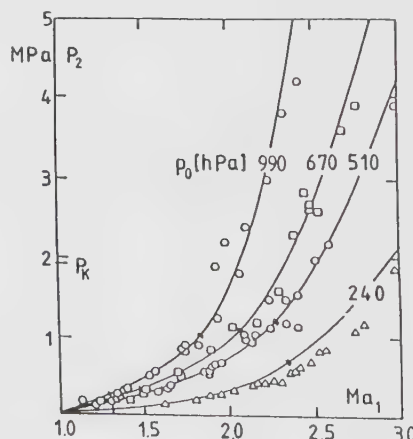
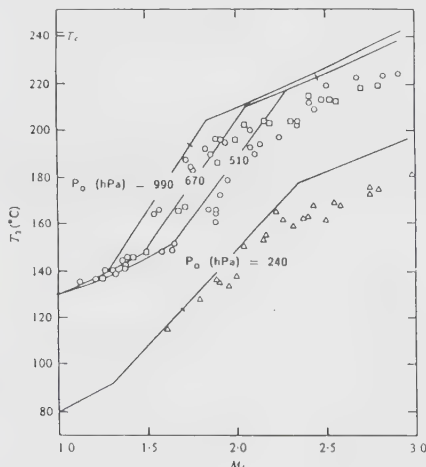


Fig 7, 8: Calculated and measured pressure P_2 (A) and temperature T_2 (B) behind liquefaction-shock waves in relation to the shock-Machnumber Ma_1 . (substance PP3/ C_8F_{16})

One effect in the case of partial condensation of a substance with retrograde behavior is so spectacular that it has to be mentioned here. The so-called shock splitting occurs if by the end state B of a shock, liquefaction cannot be reached by a straight Rayleigh line without intersecting with the shock adiabate (see Fig 9).

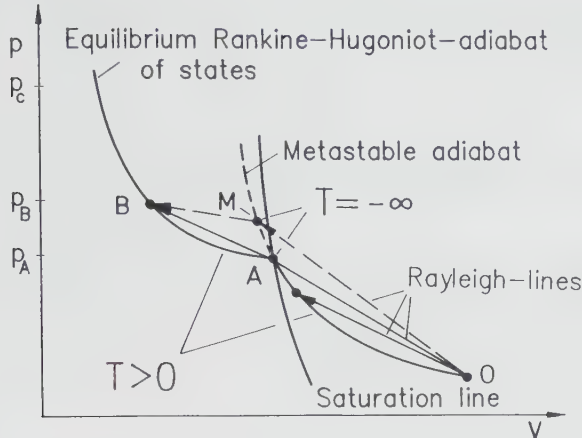


Fig. 9:

Shock-splitting at partial condensation in nucleation and condensation waves

In this case a precursor wave is formed (0 to A), which introduces the super-saturation and nucleation. A slowly propagating condensation wave is following behind. By this splitting in a fast nucleation wave and a slower condensation wave, the crossing of the Hugoniot-adiabates is avoided. Fig 10 shows experimental results for shock motion and pressure, which confirm the effect of shock splitting [Speckmann et al.]

Another spectacular case of retrograde behavior is the condensation of a retrograde gas in the bow shocks of projectiles moving with supersonic Mach-numbers [Fig. 11].

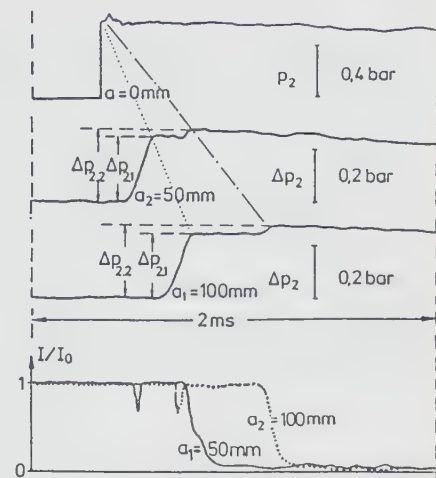


Fig. 10:

Pressure runs (1-3) and light-barrier response in the shock tube

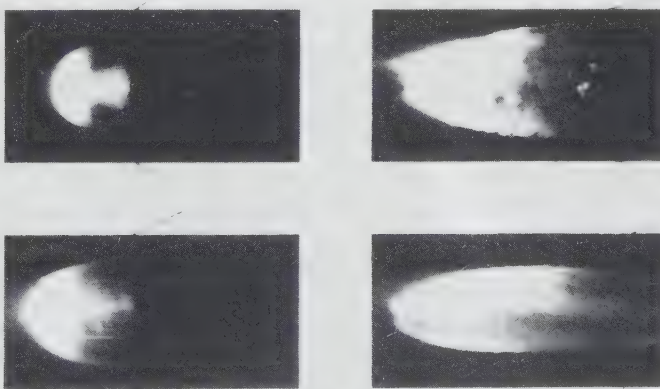


Fig. 11: Transsonic flight of projectiles in a gas of high molar heat (PP1/C₆F₁₆, T = 313 K, Ma₁ = 1.76, Ma₂ = 2.3, Ma₃ = 4.4, Ma₄ = 4.9)

The strongest condensation occurs in the stagnation area. At the shoulder of the projectiles a reevaporation takes place. At the higher Mach-numbers the condensation shock waves show a frontal instability which is not very well understood up to now.

III Metastable States in the Beginning of Nucleation

III.0 Stable and Metastable States

The equilibrium of liquid and vapor of a single phase system with planar boundary surface between the phases is generally described by assuming the equality of pressure and temperature of the phases. This is possible only for quasistatic changes of state which are expressed by the *Maxwell-criterion*:

$$\int_{V_i}^{V_v} p(V, T) dV = p(T) (V_v - V_i). \quad (1)$$

The necessity of this criterion is formed by the triplicity of the specific volume at constant pressure and temperature in the regime of two phases of the *van-der-Waals* equation:

$$\hat{p} = \frac{p}{p_c} = \frac{8\hat{T}}{3\hat{V} - 1} - \frac{3}{\hat{V}^2}, \quad \hat{T} = \frac{T}{T_c}, \quad \hat{V} = \frac{V}{V_c}. \quad (2)$$

States of single phase between the maxima and minima of the isothermals, the so-called spinodals, are generally unstable. The only possible states are mixtures of the two phases. However, assuming non-quasistatic changes of state, single phase states between spinodal and saturation line are possible. It is possible to enter the regime of saturation by rapid changes of state without causing a condensation of the vapor. These states are single phased and, because the temperature is higher than the temperature associated with the pressure of saturation, are called superheated or supersaturated. For liquids, which are treated the same way, this holds also. These states are described by an extrapolation of the qualities of the pure phase in the regime of saturation.

This is the reason why the p-V-plane is divided into five regions, the first being the thermal stable regime with specific volumes smaller than the saturation-volumina at equal pressure and the second one being the supersaturated liquid with states between the saturation line and spinodal in the regime of fluids. The third region, where the pure phases cannot exist, is settled between the spinodals. The fourth regime of superheated vapor is located between the vapor spinodal and the saturation line, and lastly the stable region of gases with specific volumina higher than the saturation line at the same pressure.

Supersaturated states of a phase are called metastable. The reason is found in the chemical potential of these states being higher than the potential of the phase present in the other case. This is an unstable equilibrium, because the presence of an embryo causes a rapid phase transition which reduces the supersaturation. An example of a metastable fluid is glass, which has a very high viscosity, preventing nucleation, and thus stabilizing the fluid.

III.I Nucleation (*Wilson Line*)

III.I.1 Introduction

In gases and liquids statistical fluctuations of the pack density of the molecules take place, because of the *Brownian*-molecular motion. This leads to "short-time holes" or clusters in the liquid.

Consider the work of evolution W of a bubble with radius r in supersaturated liquid:

$$W(r) = 4\pi r^2 \sigma + \frac{4}{3} \pi r^3 (p_L - p_v) + (\mu_v - \mu_L) M_v \quad (1)$$

with σ : surface tension, μ : chemical potential per mass unit, M_v : mass of gas in bubble $M_v = 4/3 \pi r^3 \rho_v$.

The first term is the work, necessary to build the surface, the second the work against the forces of pressure and the third the molecular work.

III.I.2 The Wilson line

Nucleation theory implies that an initial step towards the build-up of critical nuclei involves the formation of a dimer. Incipient nucleation is therefore tied to ternary collisions. In the onset region of typical nozzle experiments triple collisions are about ten times as frequent as the value of the nucleation rate prior to measurable condensation. Thus, with the collision frequency depending strongly on pressure, it is expected that the supersaturation decreases at increased pressure, in particular if the critical point is approached. Moreover, the surface tension decreases to vanish at the critical temperature. This feature is well represented by nozzle and shock tube experiments with steam. To explain the term of the so-called "Wilson-line", as the line of maximal supersaturation is called, we shortly will treat a two-phase flow with phase transition in a Laval nozzle.

Imagine the moist air entering the Laval nozzle from the left. Somewhere behind the throat, in the supersonic part of the nozzle flow, saturation is attained as a result of cooling the gas by its expansion. Downstream from the saturation line, there is a rather extended zone in which the water vapor is supersaturated and

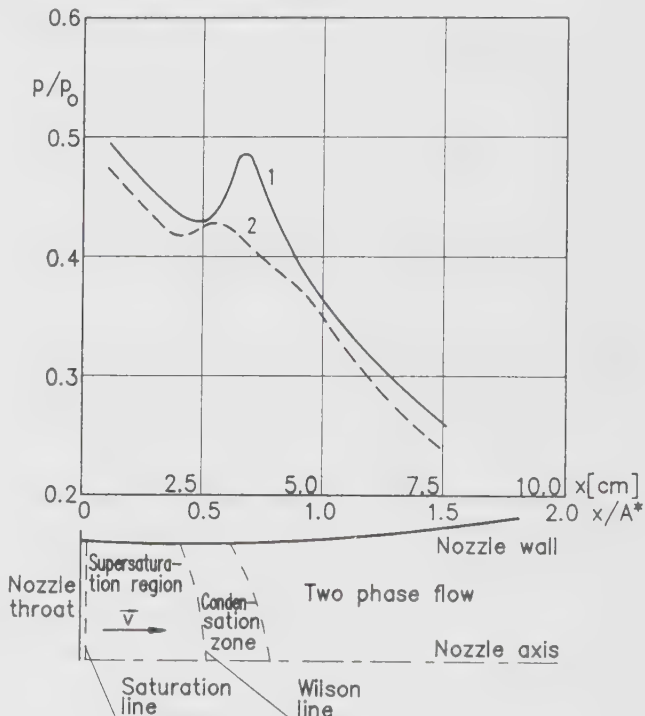
does not condense. In this region nucleation takes place but the nucleation rate is not high enough to compensate for the rate of cooling due to the expansion or, to put it in other words, the relaxation time of the phase transition does not keep pace with the characteristic time of the change of the flow parameters. Hence, the flow is nearly isentropic.

With increasing supersaturation the condensation is intensified and reaches the maximal value at the so-called Wilson line, whose position depends on the state of the entering gas and on the expansion rate.

The so-called condensation zone is defined here as a region of an intensive phase transition from the point of maximum supersaturation to the point of thermodynamic equilibrium. The condensation zone is characterized by a pressure increase compared to the pressure distribution for the isentropic flow. (see fig. 13)

In both the supersaturated region and in the condensation zone thermodynamic equilibrium is lost and is not restored until the region of two-phase flow is reached downstream.

Fig 13:
The dimensionless pressure distribution along the axis (curve 1) and along the wall of the nozzle (curve 2):
 $\varphi_0 = 58\%$, $T_0 = 290.8\text{ K}$,
 $p_0 = 753.1\text{ Torr}$



III. II Cavitation

III.II.1 Introduction

Cavitation is the rise of hollows or bubbles in fluids containing other gases or steam. First of all, of course, nucleation has to take place. Normally, e.g. water contains lots of nucleation embryos (oxygen, pollutions), so there will be heterogeneous nucleation. The number and size of the bubbles are dependent on the

local pressure in the fluid. Describing this coupling between the bubble radii and the pressure, the so-called bubble equation will be used. The mixture of the two phases will then be treated as a new homogeneous medium ruled by new terms of state [Rein 1987].

III.II.2 Static Bubbles And Embryos In Fluids

A. Steam bubbles:

Steam bubbles are filled with vapor of the surrounding fluid. That is the reason why the mass of the steam is able to vary by condensation or evaporation of fluid molecules at the bubble wall. Inside the bubble, the steam-pressure is $p_d = \text{const.}$, and we obtain the following equation called the *Laplace* equation:

$$p = p_d - \frac{2\sigma}{R} \quad (1)$$

with R : bubble radius, p : fluid pressure, σ : surface tension.

States of equilibrium are possible only at fluid-pressures lower than the steam-pressure.

At fixed pressure p_0 we will examine the influence of a quasistatic variation of the bubble radius. Reducing the radius causes increasing pressure in the bubble by decreasing the bubble volume and increasing surface tension (that is steam-pressure). Therefore a part of the steam will condense reducing the bubble radius even more. Again the equilibrium is disturbed. This process goes on until the whole bubble has vanished. The other way round, increasing the bubble radius leads to permanent growth of the bubble.

Fixing the bubble radius and varying the pressure, we still have the same phenomena: Increasing pressure causes condensation at the bubble walls and is therefore exactly the same as radius reducing: The bubble vanishes. Decreasing pressure leads the other way to permanent bubble-growth. Therefore the static state of a single steam bubble is an unstable one.

B: Static of gas-bubbles

A gas-bubble is an idealisation of a bubble filled with a non-condensable gas. Hence variation of the mass is only possible by diffusion, which should be neglected here, so that the mass can be taken as constant. The gas should be ruled by the barotropic equation of state:

$$p_i \rho_i^{-\kappa} = \text{const} \quad (2)$$

with κ : polytropic exponent, p_i : inner pressure of the bubble and ρ_i : vapor density. The coupling between the radius and pressure is determined by the equation:

$$p = p_i - \frac{2\sigma}{R} = \left(p_0 + \frac{2\sigma}{R} \right) \left(\frac{R_0}{R} \right)^{\kappa} - \frac{2\sigma}{R} \quad (3)$$

with p_0 and R_0 denoting pressure and the radius of a reference state. Taking

$$We = \frac{p_0 R_0}{\sigma} \quad (4)$$

the well-known *Weber* number, we obtain after scaling pressure p and radius R with p_0 and R_0 :

$$p = \left(1 + \frac{2}{We}\right) R^{-3\alpha} - \frac{2}{We R} \quad (5)$$

Evaluation of equation (5) exhibits stable states of equilibrium for bubble radii below a critical size R_b corresponding to a minimal pressure p_b .

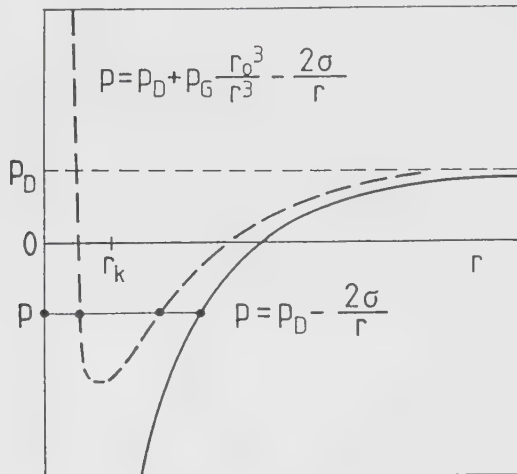


Fig 14: Stability curves for vapor bubbles (solid) and gas bubbles (dashed). P_d is the vapor pressure in the bubble, P is the gas pressure, r is the radius of the bubble and P is the pressure in the liquid. The gas content of the bubble is assumed to be constant.

III.II.3 Dynamic of Gas-Bubbles

In the following part three relatively simple models will be presented. In all three cases we will assume radial symmetry with the origin of the coordinates being in the middle of the bubble. The gas is assumed to follow equation (2), phase transitions being neglected (isentropic flow). Assuming the gas to be isothermal, a heat transfer takes place at the bubble wall, which will be neglected. The difference between the three models is found in the way they take into account the compressibility of the fluid.

A: The RPNNP Model

For a fluid with density ρ_i , and velocity v_i we have the radial symmetric continuity and impulse equation:

$$\frac{\partial \rho_i}{\partial t} + \nabla(\rho_i v_i) = \frac{\partial \rho_i}{\partial t} + \frac{1}{r^2} \frac{\partial}{\partial r} (r^2 \rho_i v_i) = 0 \quad (6)$$

$$\frac{\partial v_i}{\partial t} + v_i \frac{\partial v_i}{\partial r} = - \frac{1}{\rho_i} \frac{\partial P_i}{\partial r}. \quad (7)$$

Featuring a single bubble with radius R in infinite, incompressible fluid, we obtain

by introducing the fluid-velocity at the bubble walls

$$v_i(R) = \frac{dr}{dt} \Big|_R = \dot{R} \quad (8)$$

and a new form of equation (6):

$$v_i(r) = \frac{R^2 \dot{R}}{r^2}. \quad (9)$$

With respect to this equation we obtain after the integrating equation (7) in the area of $r = R$ to $r = \infty$:

$$p_\infty(t) = p(R) - \rho_{01}(R R + \frac{3}{2} R^2) \quad (10)$$

ρ_{01} being the constant density of the fluid. In static equilibrium the pressure $p(r)$ follows equation (3).

Assuming a bubble wall is movable an additional term of friction cannot be neglected. It was first introduced by *Poritzky* and could be written

$$2\mu \frac{\partial v}{\partial r} \Big|_R = -\frac{4\mu}{R} \dot{R} \quad (11)$$

where μ is the shear viscosity of the fluid. Using the equation of the pressure $p(R)$:

$$p(R) = \left(p_0 + \frac{2\sigma}{R_0} \right) \left(\frac{R_0}{R} \right)^{3/2} - \frac{2\sigma}{R} - \frac{4\mu}{R} \dot{R} \quad (12)$$

equation (10) varies to

$$(R \ddot{R} + \frac{3}{2} \dot{R}^2) = \frac{1}{\rho_{01}} \left(\left(p_0 + \frac{2\sigma}{R_0} \right) \left(\frac{R_0}{R} \right)^{3/2} - \frac{2\sigma}{R} - \frac{4\mu}{R} \dot{R} - p_\infty(t) \right). \quad (13)$$

This result is assuming constant pressure p_∞ and neglecting surface tension and time and tension dependent pressure $p_\infty(t)$. In 1950 *Noltingk and Neppiras* examined the equation with respect to sinusoidal pressure oscillations far away from the bubble. At last *Poritzky* added the viscosity term, so this equation is called RPNNP-equation. One obtains the natural frequency ω_R of a bubble of the linearized RPNNP equation as

$$\omega_R = \frac{1}{R_0} \sqrt{\frac{3 \times p_0}{\rho_{01}} + \frac{6 \times \sigma}{\rho_{01} R_0} - \frac{2 \sigma}{\rho_{01} R_0}} \quad (14)$$

neglecting the term of friction. A disturbed bubble is oscillating in this frequency.

B: The HT-Model

Because radiallysymmetric flows have no rotation a velocity-potential Φ exists:

$$v_i = -\frac{\partial \Phi}{\partial r} \quad (15)$$

Herring and Trilling (HT-Model !) assumed the approximation

$$\left(\frac{\partial}{\partial t} + c_i \frac{\partial}{\partial r} \right) (r \Phi) = 0 \quad (16)$$

to be true as long as velocities v_i are much smaller than the sonic speed c_i which should be held constant.

By integration of the momentum-equation one obtains:

$$\frac{\partial \Phi}{\partial t} = \frac{1}{2} v_i^2 + \int_{p_\infty}^{p(R)} \frac{dp}{\rho_i} . \quad (17)$$

This fits into the time-derivative of equation (16):

$$rv \frac{\partial v}{\partial t} + \frac{r}{\rho_{0i}} \frac{\partial p}{\partial t} + \frac{1}{2} c_i v^2 + c_i \int_{p_\infty}^{p(R)} \frac{dp}{\rho_i} + c_i rv \frac{\partial v}{\partial r} + \frac{c_i r}{\rho_i} \frac{\partial p}{\partial t} = 0 . \quad (18)$$

In this equation the partial derivatives of velocity and pressure with respect to time and location should be replaced by their terms at the bubble wall ($r = R$). This is aided by two conditions at the bubble wall:

$$\frac{dp}{dt} = \frac{\partial p}{\partial t} + \dot{R} \frac{\partial p}{\partial r} \quad \frac{dR}{dt} = \frac{\partial v}{\partial t} + \dot{R} \frac{\partial v}{\partial r} . \quad (19)$$

Derivations of density will be expressed by derivations of pressure. Neglecting quadratic terms in v/c_i with constant density, one obtains the *Herring-Trilling* equation:

$$R \ddot{R} \left(1 - 2 \frac{\dot{R}}{c_i} \right) + \frac{3}{2} \dot{R}^2 \left(1 - \frac{4}{3} \frac{\dot{R}}{c_i} \right) = \frac{1}{\rho_{0i}} \left(p(R) - p_\infty(t) + \frac{R}{c_i} \left[1 - \frac{\dot{R}}{c_i} \right] \frac{dp(R)}{dt} \right) . \quad (20)$$

This is mainly the RPNNP-equation with some added correction terms with respect to the compressibility of the fluid. Pressure is ruled again by equation (12).

C: The HTF-Model

Flynn developed a simplified form of the HT-equation by assuming a constant density of the fluid while the derivation of pressure with respect to density has a finite value. Equation (7) is again integrated and after a second partial integration we obtain:

$$\int_R^\infty \frac{\partial v_i}{\partial t} dr = \int_R^\infty \frac{1}{r^2} \frac{\partial}{\partial t} (r^2 v_i) dr = - \frac{1}{r} \frac{\partial}{\partial t} (r^2 v_i) \Big|_R^\infty + \int r \frac{\partial}{\partial t} \left(\frac{1}{r^2} \frac{\partial}{\partial t} (r^2 v_i) \right) dr . \quad (21)$$

After the introduction of the substantial derivation of v and paying attention to

$$\nabla v = \frac{1}{r} \frac{\partial}{\partial r} (r v_i) = \frac{\partial v_i}{\partial r} + \frac{v_i}{r} \quad (22)$$

we obtain:

$$\int_R^\infty \frac{\partial v_i}{\partial t} dr = R \ddot{R} - R \dot{R} \nabla v_i(R) + 2 \dot{R}^2 + \int_R^\infty r \frac{\partial (\nabla v_i)}{\partial t} dr . \quad (23)$$

With finite sonic speed at constant density we have:

$$\nabla v_i(R) = - \frac{1}{\rho_{0i}} \frac{dp_{0i}}{dt} = - \frac{1}{\rho_{0i} c_i^2} \frac{dp}{dt} . \quad (24)$$

If equation (23) is fitted into equation (21) with respect to the last transformation we obtain:

$$R \ddot{R} + \frac{3}{2} \dot{R}^2 = \frac{1}{\rho_{0i}} \left(p_\infty(t) - p(R) + \frac{R \dot{R}}{c_i^2} \frac{dp(R)}{dt} \right) + \int_R^\infty r \frac{\partial (\nabla v_i)}{\partial t} dr . \quad (25)$$

The remaining integral could be calculated by using the acoustical approximation in the form:

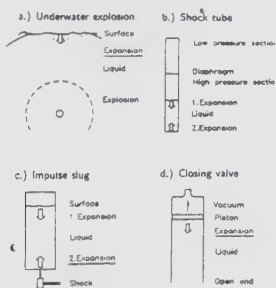
$$\left(\frac{\partial}{\partial t} + c_1 \frac{\partial}{\partial r} \right) (r \nabla v_i) = 0 . \quad (26)$$

Therefore we finally obtain the bubble-radius equation which is the same as the HT-equation with the exception of the missing correction term of inertia.

III.II.4 Shock Cavitation

Generation of nucleation in liquids and subsequent cavitation, can not only occur in flows or ultrasonic waves, but also in expansion waves. These waves, introducing negative pressures in the liquid, are often observed in connection with high pressure waves of underwater explosions, or water hammer effects in pipes. The reason for this dual appearance, is the phase change of the pressure pattern for reflection at high negative reactances.

Fig 15: a.)underwater explosion, b) closing valve



also arise, generating a large field of cavitation at the surface. In the case of water hammer, introduced by a closing valve (right scheme in Fig 15), the reflection of the occurring pressure wave at the open end, generates an expansion wave, which reduces the pressure first to the ambient in front of the end. When this expansion wave is later reflected at the mainly positive reactance of the closed valve, the superposition of the incoming and reflected expansion wave leads to very high, initially negative, pressures in the order of magnitude of the original water hammer wave. In consequence, high supersaturation, nucleation and cavitation with strong bubble oscillations occur. An apparatus for studying these phenomena is shown in Fig 16. A falling tube with the liquid under investigation in it, is abruptly stopped, for generating a strong compression wave, by a shock cylinder with suitable impedance. The wave pattern, observed after the impact, is shown in Fig 17. Especially the oscillations of the whole cavitation area, caused by subsequent wave reflections in the tube, by bubble oscillations, by bubble/bubble interference and by bubble disintegration are interesting.

Fig 18 shows a typical pressure pattern, taken close to the bottom of the tube at the side wall, for different repetitions n_{rep} of the experiment in second intervals. The high frequency oscillations (~ 10 kHz) of the bubbles (5), nearly disappear after 10 experiments. This indicates, as a corresponding theory does [Rein et al.], that the number of nucleation cores (submicroscopic bubbles) is increased by the process

Typical situations for shock cavitation are shown in Fig 15. The pressure wave of the underwater explosion is reflected at the surface, generating an expansion wave, which, in principle, reduces the overpressure to atmospheric conditions again. But by superposition of leading and subsequent parts, at the wave package negative pressures

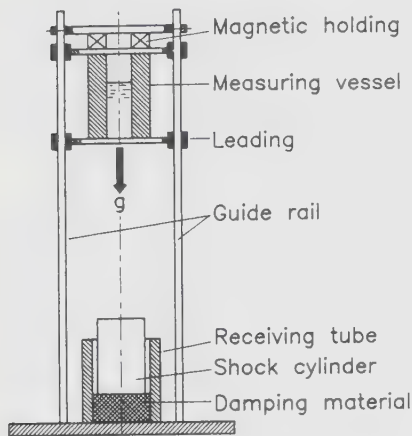
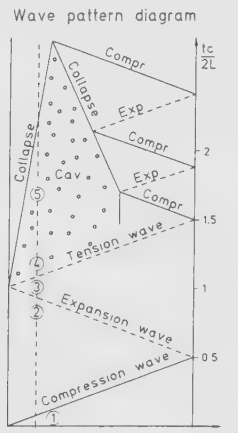
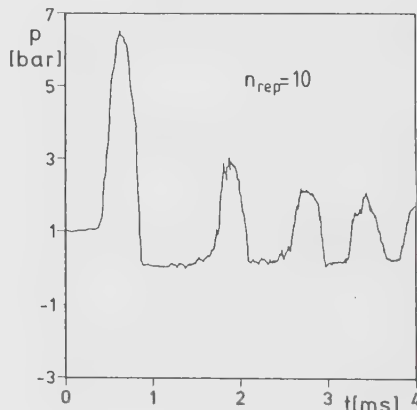
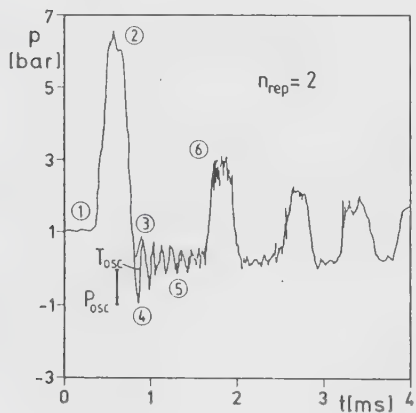


Fig 16: Falling tube

Fig 17:
Wave pattern
diagramFig 18: Dependence of the pressure signal on the repetition number n_{rep}

of bubble disintegration in the foregoing experiment.

This process is superimposed by an adverse bubble selection mechanism, which always tends to enlarge the larger bubbles of a field by surface tension effects [Meier, Bode].

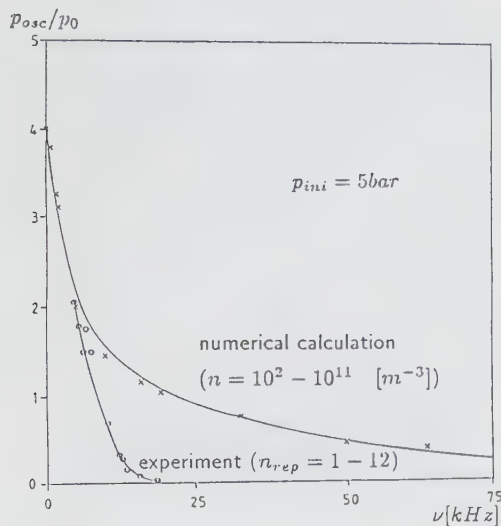
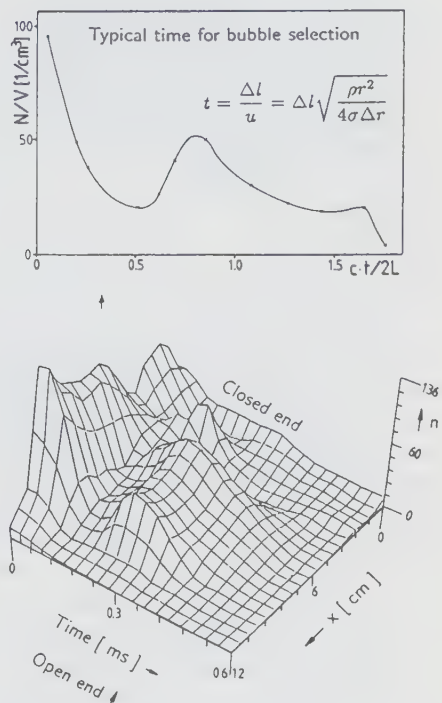


Fig 19: Comparison between experimental and numerical results for pressure oscillations of bubble clusters. (constant void fraction, variable nuclei density)

Fig 20: Dynamic nuclei density variation



III.III Superheated Jets

III.III.1 Introduction

Much effort has been put into the study of atomizing jets, mainly because of their application in fuel injection. Most of the experimental work is done under conditions where the liquid is not likely to evaporate. The theoretical interpretation of the results is based on mechanical or aerodynamic instabilities of the jet. However, if the exit pressure of the jet is below the saturation pressure of the liquid, evaporation comes to play an important role. Its effect can be much stronger than the disintegration effects caused by mechanical or aerodynamic forces. How large the effect of evaporation on a jet is, depends on the energy balance between internal energy of the fluid available for evaporation and its heat of evaporation. For fluids with a high molar specific heat the internal energy present in the hot liquid can be much larger than the heat of vaporization. Under adiabatic conditions such liquids can evaporate completely or the vapor can liquefy completely. Such behavior is called retrograde. It appears only at high temperatures -i.e. approximately greater than 0.7 times the critical temperature. Experiments with differential interferometers have shown the main point of

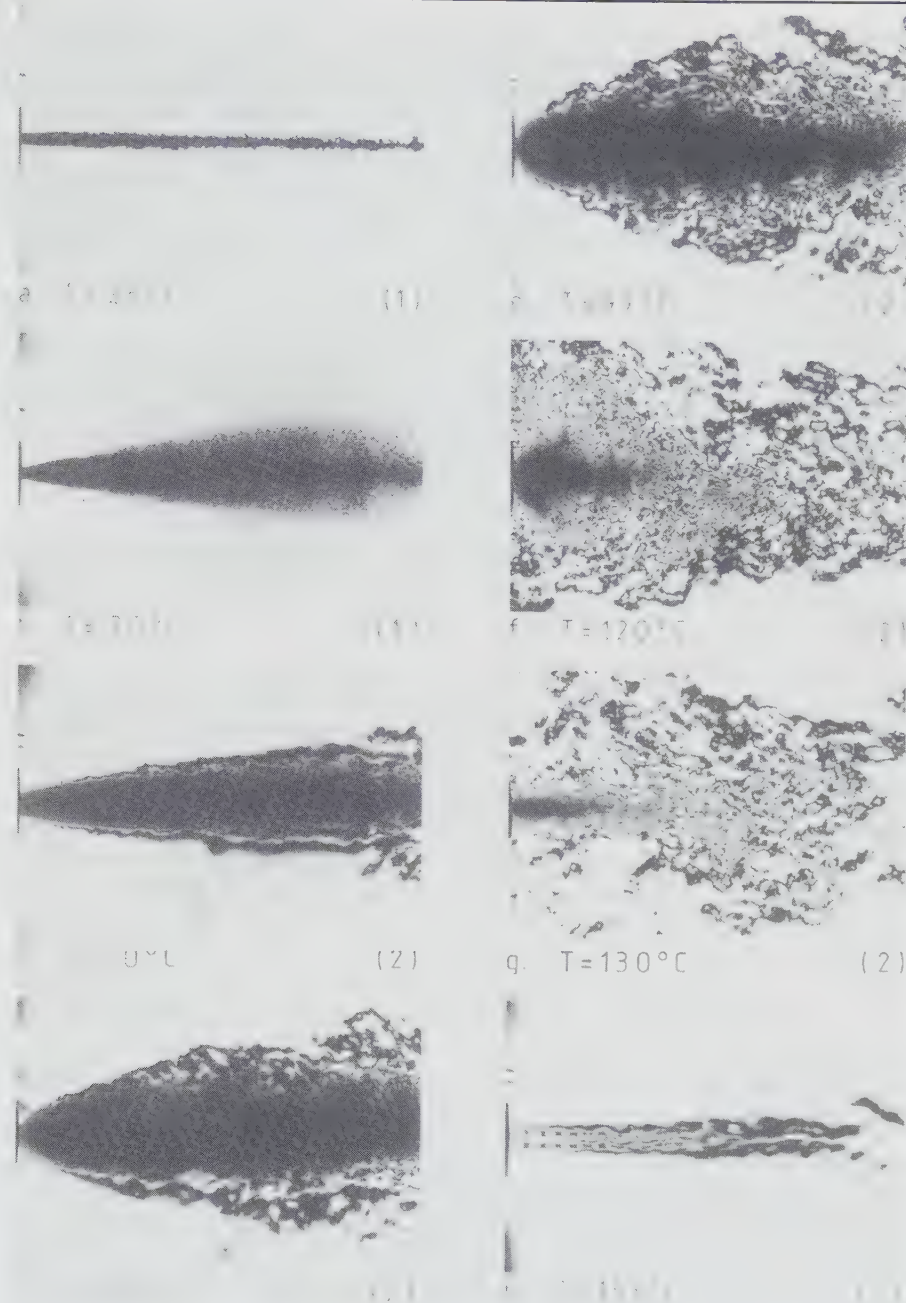
observation being the jet geometry. It is described by the following three parameters evaluated from the video image of the jet: the initial angle of expansion α , i.e. the angle of aperture of the jet immediately at the nozzle exit, the volume of the two-phase region of the jet V_z and the volume of the vapor region V_d . The volume of the vapor V_d and the two-phase parts V_z of the jet are calculated assuming axial symmetry of the jet. These volumes are normalized with the volume of a jet with no expansion V_0 (stable liquid jet). It is found that the measured jet angles increase sharply with an increasing degree of superheat and reach values which are limited in some case only by the geometry of the experimental set-up and not by the dynamics of the jet. The maximal jet angle is 180° since the nozzle hole is part of the injector tip, which is flat. In the range of temperatures used, the changes of the parameters typical of mechanical theories of jet atomization like viscosity, surface tension or density cannot explain this change in the jet angle.

Four regimes of jet phenomena can be distinguished.

In the first one, at high subcooling of the fluid in the nozzle the jet angle α is small and evaporation is not present. This regime of jet instability has been studied by many authors. In the presence of evaporation this becomes a second order effect, and one can assume that a velocity component perpendicular to the jet issuing from the nozzle is neglectable. The second regime of jet instability is observed at positive but small normalized temperatures (normalization by the critical temperature T_c). The jet consists of a liquid-vapor mixture, which creates a typical "bell" structure with relatively well defined boundaries. The angle of expansion α and volume V_z depend on the value of normalized temperature (superheat). In this regime the difference between retrograde and normal substances is very small.

The dependence of the initial jet angle on normalized temperature can be described qualitatively in the following way. The superheated liquid emerging from the nozzle contains a large number of bubbles formed by nucleation. These bubbles are very small and their number increases exponentially with increasing superheat. Although the mass fraction of liquid evaporated is very small, because of the low gas density, the void fraction of the two-phase mixture increases rapidly. This causes a global expansion of the jet, and therefore an increase of the jet angle. Even for the case when vapor bubbles are already present in the liquid within the nozzle, they are not in mechanical equilibrium with the ambient pressure and they grow very quickly expanding the jet. A void fraction of 0.5 is reached almost immediately after the exit of the nozzle, so that the two-phase flow changes from liquid-bubble to vapor-droplet flow. The global behavior of the initial jet angle as a function of initial temperature is not much different for all substances. Only a small amount of evaporation is needed to initially accelerate the droplets in the jet perpendicular to the nozzle axis. This is always possible even for fluids with low specific heat.

In the third case of jet behavior, observed at higher superheat values (normalized temperatures of about 0.7), the difference between retrograde and non-retrograde substances becomes apparent in the volumes of vapor in the jet. In the case of



PP1 JETS INTO THE ATMOSPHERE, INITIAL PRESSURE

$P_0 = 0.95 \text{ MPa}$, FOR VARYING INITIAL TEMPERATURE

(1) SHADOWGRAPH, (2) DIFFERENTIAL INTERFEROGRAM

Fig. 21: Short-time photos of PP1 jets in air.

retrograde substances jet evaporation has an explosive character, which completely disturbs the typical "bell shape" structure of the jet. At normalized temperatures close to one the fluid starts to evaporate within the nozzle. Especially when the value of the initial temperature is above 0.9 that of the critical temperature of the fluid, nucleation has to occur within the nozzle; this is because for reduced temperatures greater than 0.9 the liquid spinodal limit is at positive pressures and can easily be attained within the nozzle if the external pressure is low. Most likely nucleation would be homogeneous in these cases, because for a given pressure drop in the nozzle the attainable superheat is much greater than for low temperatures. The resulting number of nuclei formed by homogeneous nucleation is much larger than the possible number of heterogeneous nuclei likely present in the liquid. In these cases the fluid issuing from the nozzle is a liquid-vapor mixture (especially for long nozzles) and therefore its effective value of superheat is smaller than assumed when the evaporation begins outside the nozzle. It appears as a decreasing jet angle with increasing temperature observed for normalized temperature values above 0.7.

At values of normalized temperatures greater than one a supersonic gas (vapor) jet is observed. This is the fourth regime of jet phenomena, which is well-known in gas dynamics.

III.III.2 Basic Relations

With the help of a simple thermodynamic model the jet angles and the evaporated mass fraction can be calculated. This model is based on a direct interpretation of the initial jet angle α as a ratio of the jet expansion velocity u_i (due to evaporation from a superheated liquid state) to the jet exit velocity u_e . Since these velocities are perpendicular one can derive α in the following way:

$$\tan \alpha = u_i / u_e \quad (1)$$

The velocities u_i and u_e are calculated from the energy equations:

$$h_0 = h_{sup} + \frac{u_f^2}{2} \quad (2)$$

$$h_{sup} = h_e + \frac{u_e^2}{2} \quad (3)$$

where

$$h_e = \chi h_v + (1 - \chi) h_l . \quad (4)$$

Here h_0 is the reservoir specific enthalpy, h_{sup} is the enthalpy of the superheated liquid emerging from the nozzle, h_e is the enthalpy of the two-phase mixture at the end state after the expansion and evaporation of the jet took place, h_v is the specific enthalpy of the vapor, h_l the specific enthalpy of the liquid within the jet and χ is the mass fraction of vapor. The model assumes that at the end state the jet reaches an equilibrium as a homogeneous two-phase mixture and that the process is isentropic. This means that

$$s_e = s_0 = \chi s_v + (1 - \chi) s_l \quad (5)$$

where the subscript e means end state, 0 reservoir state and v,l vapor and liquid respectively.

Using the initial pressure p_0 and the initial temperature T_0 as independent variables and keeping the end or back pressure p_e constant, equation (5) can be modified to show the effect of the specific heat on the global expansion process. The initial entropy s_0 is then a function of the two independent variables. For constant initial pressure p_0 , equation (5) can be differentiated with respect to the initial temperature T_0 . The resulting equation for the change of quality χ of the two phase mixture with respect to the initial temperature is

$$\frac{\partial \chi}{\partial T_0} \Big|_{p_0} = \frac{\partial s_0}{\partial T_0} \Big|_{p_0} - \frac{1}{s_v - s_l} = \frac{C_{p0}}{T_0} - \frac{1}{s_v - s_l}. \quad (6)$$

The specific heat for constant pressure C_p of liquids depends only weakly on temperature and as long as the temperature range of the initial temperatures is not too large, this specific heat can be assumed constant. The evaporation entropy $s_v - s_l$ is constant for a given state. Integrating equation (6) one obtains

$$\chi = \frac{C_{p0}}{s_v - s_l} \ln \frac{T_0}{T_e}. \quad (7)$$

Since $0 \leq (T_0 - T_e)/T_e \ll 1$, then by expansion of the logarithm and using the Clausius-Clapeyron equation one gets

$$\chi = \frac{C_{p0}}{s_v - s_l} \ln \left(1 + \frac{T_0 - T_e}{T_e} \right) \quad (8)$$

$$\approx \frac{C_{p0}}{h_v - h_l} (T_0 - T_e). \quad (9)$$

Equation (8) shows that the mass fraction of vapor in the jet is directly proportional to the specific heat of the liquid and to the temperature difference between initial and end state. The temperature of the end state is the saturation temperature corresponding to the end or back pressure. The latent heat of evaporation $h_v - h_l$ is a function of the end temperature, or indirectly of back pressure. At the critical point the latent heat is zero and increases with decreasing temperature. At low temperature levels (cryogenic) therefore no complete evaporation is possible because the specific heat decreases with temperature. Equation (8) shows clearly the balance between internal energy and the heat of evaporation, although its range of usefulness is limited by the assumptions used to obtain it.

The theoretical results are only qualitatively comparable with the experimental curves, although they show that the basic physics of the problem of superheated jets can be described with the help of such an initially superheated liquid, which isentropically expands to a final homogeneous equilibrium mixture. The effect of an increased molar specific heat of the fluid on the jet is small for the initial jet angle, but very strong for the amount of liquid evaporated. The initial jet angle depends basically only on the initial degree of superheat of the liquid. This is given by the initial temperature and the end or back pressure for the jet. The jet angles attained by superheating the liquid are an order of magnitude larger than could be explained by mechanical instabilities of the jet. In a first estimate the quality of the two-phase mixture after expansion in the jet is linear with the specific heat of the fluid and with the difference between initial and end temperature (given by the end pressure). In reality the flow within the

nozzle is viscous (non-isentropic). The jet mixes with the surrounding gas, the droplets and the vapor separate (non-homogeneous) and thermodynamic equilibrium is only attained after a much longer period of time as assumed in the model. These phenomena should be the basis for further detailed work.

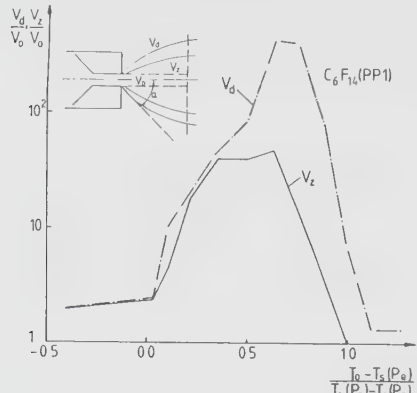


Fig. 22:
relative volumes of vapor
 V_d and two-phase mixture
 V_z versus relative superheat (subcooling)

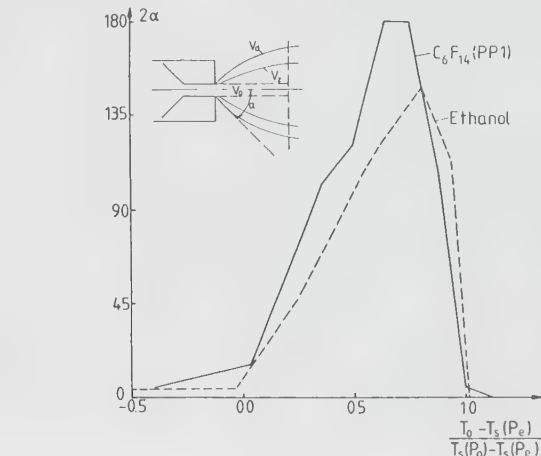
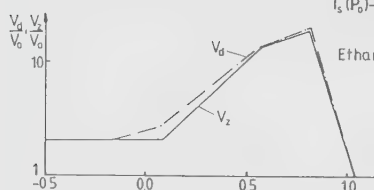


Fig. 23: initial jet angle α versus relative superheat (subcooling)
 T_0 initial liquid temperature
 $T_s(P_e)$ saturation temperature at end pressure
 $T_s(P_0)$ saturation temperature at initial pressure
 V_0 reference volume of jet
 V_z two-phase volume of jet
 V_d vapor volume of jet

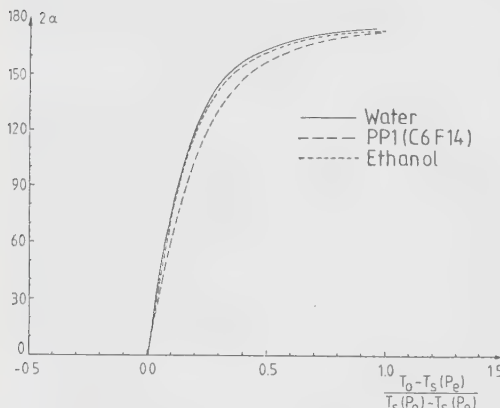


Fig. 24: calculated jet angle versus relative superheat

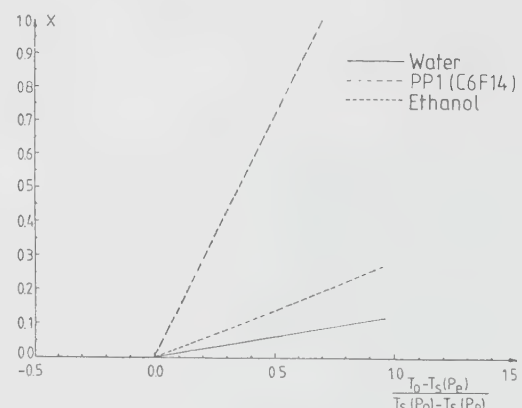


Fig. 25: calculated mass fraction X of vapor in the jet versus relative superheat for an initial pressure of 1.1 MPa and an end pressure of 0.1 MPa.

III.III.3 Flow of Superheated Liquid into Vacuum

If the receiver conditions for superheated liquid, emanating from conical nozzles, are close to vacuum conditions, super- or hypersonic jets occur. Especially in the case of retrograde substance behavior, this leads to spectacular phenomena.

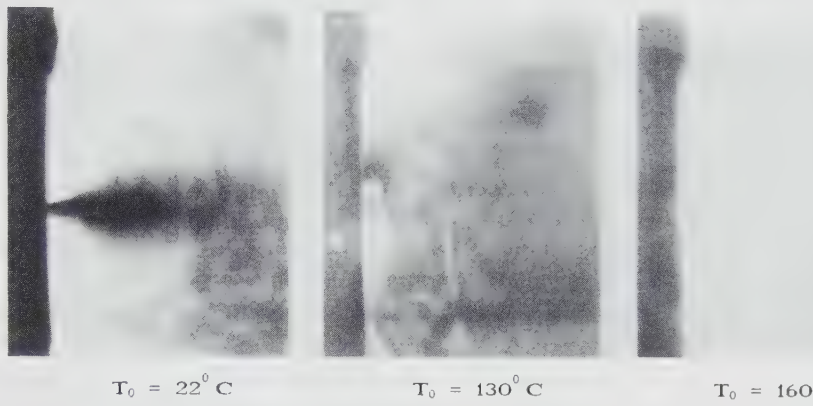


Fig 26: Hypersonic jet of a completely evaporated substance with high molar heat.
(PP1/C₆F₁₄) $T_{01} = 295 \text{ K}$, $T_{02} = 403 \text{ K}$, $T_{03} = 433 \text{ K}$, $p_0 = 1.06 \text{ MPa}$

The left frame in Fig 26 shows a comparatively normal case with an evaporating spray jet, which would be similar for normal or retrograde behavior. The spray is formed by initial evaporation of the superheated liquid and the gas flow forms a supersonic flow with a conical barrel shock and a spherical Mach-disk, which is already peculiar compared to normal supersonic gas jets. But for higher superheat, as shown in the middle frame of Fig 26, a completely different bowl shape of the barrel shock, a new conical shock and a very flat Mach-disk occur. This geometry is caused by a thin conical liquid core with an expansion discontinuity. At further increased superheat, a transition to the gas state is made already inside the nozzle, so the right frame in Fig 26 looks very similar to ordinary gas jets. A limit for liquid outflow is an initial temperature of $0.9 T_{\text{crit}}$.

Fig. 27:
geometry of
the model

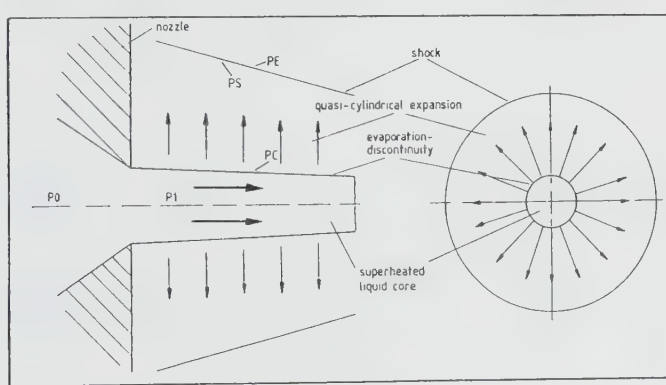
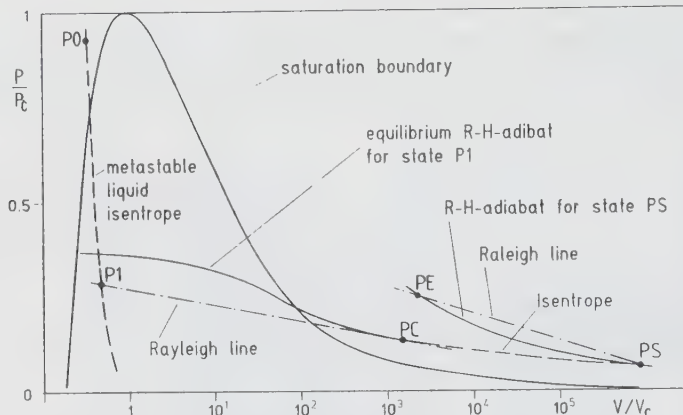


Fig 28:
Schematical
presentation
of the model



The geometry of the jet with a liquid core is shown in Fig 27 [Kurschat]. The existence of the conical shock PE results mainly from the existence of a liquid core, which evaporates in an expansion shock. The respective state changes are illustrated in Fig 28. Fig 29 shows the normalized distance of the lateral shock for different ratios of initial to receiver pressure. It is obvious from this diagram that for low pressure ratios the influence of the cylindrical liquid jet also determines the outer geometry of the supersonic flow field.

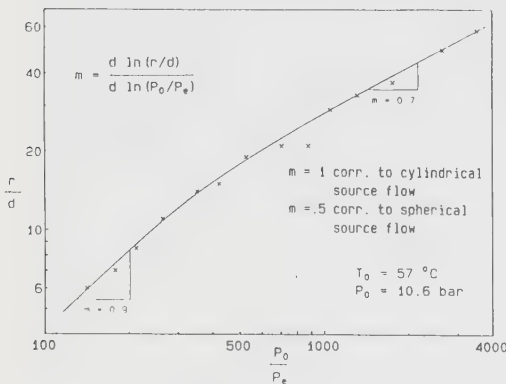


Fig 29: normalized distance of the lateral shock

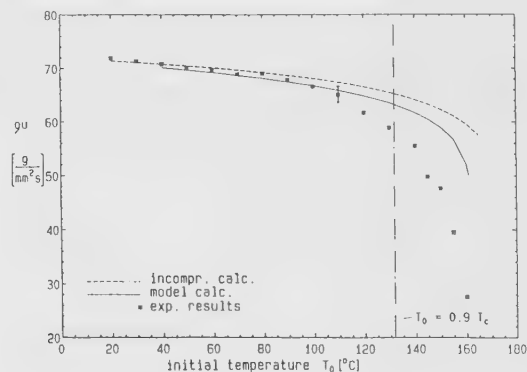


Fig 30: mass flow rate

The mass flow rate, which is plotted in Fig 30, indicates that for reduced temperatures above $0.9 T_{\text{crit}}$, no liquid core of the jet can be expected, because the complete evaporation takes place inside the nozzle. Also in the case of a non retrograde substance: in this case the atomization is completed inside the nozzle and a two phase flow is emitted from the nozzle exit. These flows have a different behavior, which is described by the initially given theory of expanding two phase flows, or, in the case of very high initial temperatures, by the gas dynamics of a pure gas flow.

III.IV Droplet Explosions

III.IV.1 Introduction

In the absence of bubble-forming nuclei, liquids may be heated to temperatures far above their boiling points. There is, however, an absolute limit of superheat, determined by the limit of mechanic stability of fluids, which for a pure substance is $(\partial p / \partial v)_T = 0$, and by a concomitant exponential growth of the level of phase fluctuations in the substance. The limit of superheat is only about 10% below the critical temperature of many substances, so superheats of more than 100 °C can in principle be attained. Heating to the superheat limit is made possible by suppressing heterogeneous nucleation and ordinary boiling by, for example, heating or depressurizing the liquid very rapidly (on a microsecond time scale), or by immersing the volatile liquid in another liquid, thus isolating it from rough solid surfaces containing gas nuclei. When such extreme superheats do occur, and boiling begins spontaneously by *homogeneous* nucleation, the ensuing evaporative fluxes, fluid accelerations and departures from thermodynamic equilibrium are orders of magnitude greater than in ordinary boiling. The resulting explosive process is known as a vapor explosion, and, when it occurs accidentally in industry or in nature, it can be very destructive.

As a detailed theory accounting for the full complexity of vapor explosions does not exist, we will report an investigation of the transient processes that take place just after a *single droplet* of metastable liquid at the superheat limit begins to boil [Shepard, Sturtevant, 1982].

III.IV.2 Instability Theory

It was found that the Landau mechanism of instability, originally described in connection with the instability of laminar flames, applies to rapid evaporation at the superheat limit. At early times, when the radius of the vapor bubble is still very small, surface tension stabilizes the bubble surface. During a later, thermally controlled stage of the vapor bubble growth the deceleration of the interface stabilizes the surface. Between these two regimes the presence of substantial mass flux across the interface may lead to instability. If the surface is initially slightly wrinkled, vorticity is produced by the baroclinic mechanism in the flow transition at the interface and appears in the vapor phase. This vorticity feeds back on the perturbed interface to further increase its distortion. The Landau theory yields a dispersion relation between the non-dimensional growth rate Ω and wave number K ,

$$\Omega^2 + \frac{2\alpha}{\alpha+1} \Omega K + \frac{1}{\alpha+1} \left(\alpha(\alpha-1) K^2 + \frac{2N_w K + K^3}{2N_i} \right) = 0 \quad (1)$$

where Ω and K are related to the corresponding dimensional quantities (ω, k) by

$$\Omega = \omega R / R \quad K = k R . \quad (2)$$

In equation (1) the effects of surface tension and acceleration are contained in the 'inertia number' and the Weber number

$$N_i = \frac{\rho_i R \dot{R}^2}{2\sigma} \quad (3)$$

$$N_w = \frac{(\rho_l - \rho_v) R^2 \dot{R}}{2\sigma} \quad (4)$$

and α is the density ratio ρ_v/ρ_l , ρ_l , ρ_v , σ , R , \dot{R} , and \ddot{R} are the liquid density, vapor density, surface tension, bubble radius, radial velocity, and radial acceleration, respectively.

In order to apply the planar theory (equation 1) to the spherical interface, the requirement that the perturbation wavelength must be smaller than the perimeter of the bubble ought to be imposed.

The Landau instability can be treated in an analysis which develops the perturbations in spherical harmonics. The contributions of harmonics of different index are assumed to be non-interacting. A simple dimensional argument shows that disturbances grow more slowly in a spherical system than for the planar case. If ε is the perturbation amplitude, λ the perturbation wavelength and U the radial velocity of the bubble, then

$$\frac{d\varepsilon}{dt} \sim \frac{\varepsilon U}{\lambda}. \quad (5)$$

For a plane interface λ is constant and equation (5) leads to exponential growth (with growth parameter $\omega \sim U/\lambda$) for ε . However, for a spherical bubble, if there is no energy transfer between modes the wavelength of a given spherical harmonic grows like the radius and equation (5) leads to algebraic growth in time for ε , i.e.,

$$\varepsilon \sim t^{\omega'} \quad (6)$$

where ω' is now the (non-dimensional) algebraic growth rate.

To apply the spherical analysis to the problem of rapid vaporization, the effects of acceleration and surface tension have been included in the boundary condition at the bubble surface. In this way a quasi-steady model may be formulated for bubbles that are growing with arbitrary velocity, assuming that the instability responds to the instantaneous acceleration and surface tension forces and that the previous history is not important. However, the surface tension terms introduce a coupling between different spherical harmonics and, hence, the assumption that the harmonics are non-interacting is not valid. The surface tension force becomes important at large values of the spherical harmonic index n , corresponding to small wavelengths. For large values of n , if one nevertheless neglects the coupling, the curvature of the interface x (and, hence, the surface tension force), can be modelled as a function of n , the perturbation amplitude ε , and the radius R , in the following simplified form:

$$x = -\varepsilon \frac{n(n+1)}{R^2}. \quad (7)$$

The resulting dispersion relation between ω' and n is:

$$\omega'^2 + b \omega' + c = 0 \quad (8)$$

$$b = 3 + \frac{n(1+2\alpha n)}{(n+1)\alpha + n} \quad (9)$$

$$C = 3 + \frac{\alpha(\alpha n + 1)(n^2 - 1) - \alpha n^2(n - 1)}{(n + 1)\alpha + n} - \frac{n(n + 1)[N_w - \frac{n(n + 1)}{2}]}{[(n + 1)\alpha + n]N_i}. \quad (10)$$

Positive values of ω' indicate that the perturbation amplitude grows more rapidly than the radius, leading to instability. The unstable region shrinks with increasing pressure and at atmospheric pressure the interface is predicted to be stable at all times. This is in disagreement with the experimental results, from which it is clear that the instability is present at atmospheric pressure. Apparently the instability occurs at such small wavelengths that the spherical constraint does not hold.

Because bubble growth rate depends strongly on the bubble surface temperature (and therefore on the ambient temperature), due to the temperature dependence of vapor pressure (density), the instability growth rates are also strongly temperature dependent. Therefore, in any real situation where temperature nonuniformities are present, departures from the quantitative predictions of the theory should be expected. In particular it is likely that in the regime of transitional stability, which might occur very frequently in practice, one of a number of different possible kinds of disturbances could serve to trigger a breakdown to violent instability.

IV Expansion Waves in Superheated Liquids

IV.I Nucleation Waves and Bubble Oscillations

IV.I.1 Introduction

In the splitting of expansion waves the rate of superheat is very important. Experimental investigations have shown that effects of relaxation in the process of nucleation lead to high rates of supersaturation. This rate is dependent on the steepness of the expansion wave, because of the theory of nucleation which predicts a dependence of the nucleation rate I on the supersaturation $p_v - p_l$ and the temperature T :

$$I = NB \exp(-16\sigma^3/3(p_v - p_l)kT) \quad \text{and} \quad t = 1/I \quad (11)$$

with N : number density of molecules and B : some sort of settling-frequency of molecules on an embryo. Surface tension σ and saturation pressure p_l are temperature dependent.

Therefore for rapid pressure drop to a pressure of the fluid p_l , that is steep wave fronts, the time t necessary for nucleation at low embryo density is not available. So we obtain very low pressures in the fluid with high numbers of embryos. Figure (1) exposes a picture of the changes of state caused by expansion wave initiated nucleation.

IV.I.2 Wave Splitting at Phase Boundaries in Retrograde Fluids

Wave splitting is a phenomenon first predicted by *Bethe*. Its reason is found in the fact that sonic speed in liquid or gas at the saturation boundary is higher than in the mixture near this border. Following the definition of the sonic speed,

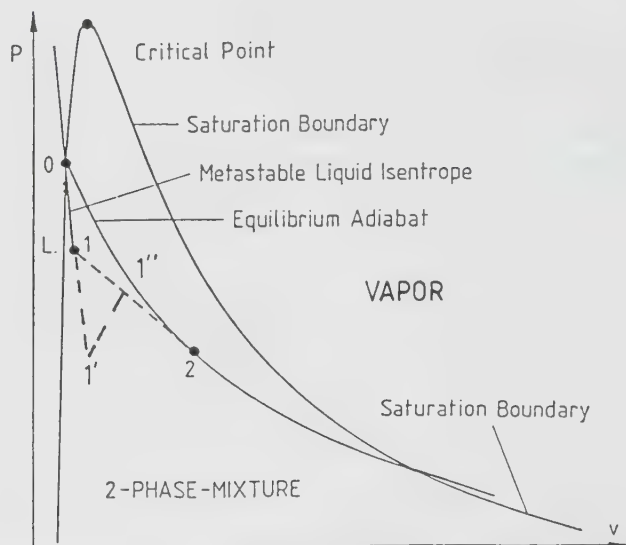


Fig. 31:
Pressure-volume-diagram
with metastable isentrope
and deflagration adiabat

the steepness of the isentrope in the p-V-diagram is a measure of the sonic speed :

$$c^2 = \frac{\partial p}{\partial \rho} \Big|_s = - V^2 \frac{\partial p}{\partial V} \Big|_s. \quad (2)$$

At the borderlines between vapor and mixture and on the other hand liquid and mixture a difference is found in the steepness of vapor- or fluid-isentrope and equilibrium-isentrope. A sound wave, initiating a change of state from pure phase to mixture, is confronted with a state with lower sonic speed (assuming an arbitrary fast transition to mixture). Part of the wave, existing in single-phase states, is propagating with the higher velocity u_1 . The other part of the wave in the region of mixture propagates with the lower speed u_2 . After a short time the first part of the wave is some distance s beyond the second:

$$s = t(u_1 - u_2). \quad (3)$$

This spatial divorce of a wave is called wave-splitting. Such a sonic wave with small amplitude cannot lead to phase transition. Phase boundary could be crossed but supersaturation would be too small for nucleation to take place.

It is necessary for wave propagation that the medium is homogeneous, that is inhomogeneities being small compared to the wavelength. For a two-phase mixture this means droplet or bubble radii and the distances between the bubbles are small compared to the characteristic length of the wave. Small bubble radii are coupled to high pressure gradients between vapor and liquid, so that a motion of a wave in the mixture requires high rates of supersaturation, and of nucleation. This is possible only for rapid expansion. An expansion wave starting from an initial state of saturated fluid, is limited by the pressure drop, possible for a given wave profile, set by nucleation. During a quick expansion the rate of nucleation first is

growing slowly and then, beyond a critical value, very quickly. The lifetime of the produced metastable state drops slowly out of infinity at saturation, later then much more quickly. In the first phase of expansion, the lifetime of the produced state is much longer than the duration in this state. The probability of generating an embryo is so small, that phase transition is negligible. If the duration time in the state is growing to the order of the averaged lifetime of the states, many embryos are produced in a very short time ($t \approx 10^{-9}$ s). Due to these embryos there is a depletion of the fluid. Out of the place of origin a little spherical increase of pressure is propagating in the liquid. If the number of embryos is large enough to let the regions of higher pressure overlap each other in a time shorter than the lifetime of the pressure increases, the supersaturation rate of the whole fluid is reduced a bit. Because of the strong temperature dependence of the nucleation rate, the probability of producing new embryos also drops strongly. In the first phase of inertial limited bubble growth, the growing velocity is the largest. Retrograde behavior strengthens this effect, so that supersaturation is further reduced. After a short time the probability of producing new embryos is so small that it can be neglected again. This self-limiting of nucleation at high densities of embryos and retrograde behavior leads to a peak-like distribution of the embryo radii, and to a nearly simultaneous production in a macroscopic time scale. In pressure this self-limiting effect of nucleation is expressed in a *Huygens-principle* of compression-waves added by the bubbles and embryos. A compression front is produced, running shortly after the expansion wave and, although having a smaller amplitude, limiting the pressure drop. However, a further drop of pressure is possible, but coupled with the bubble-growth and therefore pressed to propagate with the smaller sound velocity of the mixture, which itself is coupled with phase transition. The large pressure gradients involved lead to a sonic speed one order of magnitude smaller than in the fluid.

Altogether a given pressure profile of an expansion wave is distorted in the liquid. The first part of the pressure drop is able to propagate with sonic speed in the fluid, till self-limitation of nucleation begins. Immediately after, the compression wave with small amplitude, caused by production and first growing of the bubbles, follows, in spite of the bubbles, with local sonic speed. This apparent contradiction is solved by the reasons of origin of the wave. (The further pressure drop is following with lower speed.)

Watching this process in time, the different velocities of propagation lead to growing distances between the first part of pressure drop with a coupled compression wave and the further pressure decrease.

Wave-splitting is found in reality too, but not at a phase boundary, as could be obtained from equilibrium view; and is also different to a propagation in a gas with relaxation, because of the growing distance between the two parts of the waves. In a gas with relaxation the second wave is propagating with constant distance behind the first. The reason for this difference is found in the thermodynamic state between the two waves. The gaseous state between the waves is a limited (or metastable) one, changing, after a well-defined relaxation time τ of rotational and vibrational degrees of freedom, to an unlimited (stable)

state, which also is coupled with an increase of sonic speed. In the case of retrograde evaporation this is a state of superheated liquid with little bubbles, of course tending towards equilibrium, but stabilized by assimilation of temperature between fluid and vapor in the bubbles. Thus the pressure difference is conserved by the condition for a mechanical equilibrium of the bubble: $p_v - p_l = 2\sigma/r$. An analogous example in nature is simple fog; a mixture of air, steam and droplets in equilibrium with the steam.

IV.II Evaporation and Expansion Waves in Ducts

IV.II.1 Evaporation waves

The rapid depressurization of superheated liquids has often been investigated for normal liquids like water. In this case only a small percentage of the liquid can be evaporated because of the limited reservoir of evaporation heat. In the case of fluids with sufficiently high specific heat, they can be flash evaporated in case of sudden depressurization. The evaporation is after the experience of the recent experiments in expansion tubes of constant and increasing cross section clearly divided into the two steps of nucleation and bubble growth. An initial forerunner wave with the sound velocity of the liquid superheats the fluid. The sudden onset of nucleation limits the amplitude of this wave, because the mixture of liquid and bubbles produced by nucleation has a sound velocity much lower than that of the liquid. A further pressure decrease travels therefore with the mixture wave speed. This pressure decrease is a phase transition wave. Because of the large pressure and density changes involved with this wave, entropy production cannot be neglected. The final states after this wave are therefore described by a shock adiabat. This adiabat is similar to a detonation adiabat for shocks involving chemical reactions, but it is called a deflagration adiabat. The stability arguments valid for a normal detonation are also valid here. The final state, after the wave has attained its stable form, is determined by the Chapman-Jouget criterion (i.e. the wave travels with the local wave speed of the end state). In this case further disturbances behind the wave cannot influence its stability.

Measurements of these effects could be carried out in a duct of rectangular cross section, closed at one end and suddenly opened at the other end by rupturing a diaphragm adjoining a vacuum chamber. The vertical duct is partially filled with liquid, liquid at the bottom, and vapor on top, just below the diaphragm. At a given initial temperature the diaphragm is ruptured producing an expansion wave in the vapor above the liquid in the duct. This expansion wave is partly reflected, but mostly transmitted into the liquid. (The acoustic impedance of the liquid and of the vapor are close to each other due to the high initial temperature on the order of 90% of the critical temperature.) The forerunner wave can be seen as the initial pressure drop running down in the duct. It is reflected at the bottom of the duct, and again at the evaporation wave, which can be seen as a larger pressure drop moving slowly downwards in the duct. On reflection with the evaporation wave the forerunner wave changes phase (i.e. it is no longer an expansion wave but a compression wave because the evaporation wave behaves like an acoustic open end). The high pressure side of the wave has a high density and the low pressure side a low density. The

thermodynamic behavior of pressure and expansion waves at low temperatures is determined by the isentrope which is ruled by the initial state. At high amplitudes the behavior is described by the *Rankine-Hugoniot*-equation which is a relation between thermodynamic initial and end states of equilibrium. (see p.3, eqn. 1): This equation holds the classical conditions at the critical point:

$$\left(\frac{\partial \hat{p}}{\partial \hat{V}}\right)_C = \left(\frac{\partial^2 \hat{p}}{\partial \hat{V}^2}\right)_C = 0 \quad (1)$$

and the equation for an ideal gas for $\lim_{\hat{p} \rightarrow 0} p \hat{V} = \hat{R}f$.

There are two additional conditions which should hold in the regime of the equation:

- A: The critical factor of compressibility should be free for every substance
- B: The linearity of the critical isochore ($V = \text{const.} = 1$), which is observed by *Martin* and *Hou* near the critical point, should be expressed:

$$\left.\frac{\partial \hat{p}}{\partial \hat{V}}\right|_{\hat{V}=1} = \text{const.}, \hat{T} \approx 1. \quad (2)$$

Condition (2) leads to a temperature function Ω^3 , which is also already shown on page 3.

IV.II.2 Liquid Evaporation Wave Splitting

The splitting of a pressure releasing wave travelling through a liquid has already been described in section 1. A short recapitulation should follow here. After diaphragm rupture, an expansion (pressure release) wave propagates downward into the test section. This splits into two distinct waves, as shown by the pressure records; we will call these two waves the forerunner wave FW and evaporation wave EW, consistent with the description in section 1. The system of adiabats is shown in Fig 32. The initial liquid state 0 lies on the saturation boundary σ . The forerunner wave is a simple acoustic expansion wave which brings the liquid to the supersaturated state 1 on the metastable isentrope. Strictly speaking, this forerunner wave is subject to classical spreading characterized by the parameter $\Gamma/\rho c$. For liquids, however, this parameter has a small value compared to that of gases; the value for liquid water at STP is about 10^{-3} of that for air at STP, for example. It is thus not surprising that no spreading of the forerunner wave is observed in small scale experiments – the forerunner wave can indeed be characterized as a discontinuity, which propagates with the local liquid speed of sound. At higher temperatures, the nucleation rate in the supersaturated state 1 behind the forerunner wave is sufficiently high to produce rapid evaporation, leading to an evaporation wave with a propagation which is limited by the *Chapman-Jouguet* (sonic outflow) condition, as in classical deflagration, thus defining the two phase equilibrium state 2 behind the evaporation wave, as illustrated in Fig 32. States 0 and 2 then lie on a common deflagration adiabat (which has small departure from the equilibrium isentrope passing through 0).

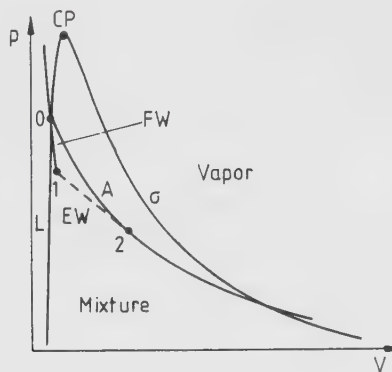


Fig. 32: Pressure-volume diagram for liquid-evaporation wave splitting in the test section and deflagration adiabat

The location of state 2 and the extent to which it satisfies the *Chapman-Jouguet* condition are experimentally established by the (redundant) measurements of the pressures p_1 and p_2 , the density ρ_2 and the wave velocity U_{EW} of the evaporation wave. These measurements could be compared with the calculated *Chapman-Jouguet* state, based on the *Abbot* equation of state (conf. eq.(5) section 1).

Experimental pressure records are shown in Fig 33. In Fig 33(a), the pressure signals $p(t)$ from transducers 1-6 are vertically separated in uniform steps so that the figure is similar to a wave diagram, with distance X on the vertical coordinate and time t on the horizontal. The path of the forerunner wave FW and its reflection from the closed bottom of the tube can be observed, as well as the path of the evaporation wave EW and its reflection EWR. The states between EW and EWR correspond to the *Chapman-Jouguet* state 2. One can infer from Fig 33(a) that the evaporation wave is triggered by the arrival of the reflected forerunner wave at the free surface. Diaphragm burst occurs at $t \approx 5$ ms in this experiment. Prior to burst, small amplitude pressure oscillations result from the downward displacement of the already activated arrow. This displacement produces weak pressure waves in the fluid. In Fig 33(b) the wave splitting can also be observed, but is not quite so distinct at the lower temperature. The amplitude of the forerunner wave is considerably greater. Fig 34 shows experimental and theoretical values of the wave propagation velocity for both the forerunner wave and the evaporation wave. The theoretical value of the forerunner velocity is simply the liquid speed of sound $(\partial p / \partial \rho)_s^{1/2}$; the evaporation wave calculation assumes a *Chapman-Jouguet* condition and is found from the slope of the *Rayleigh line* 1 \rightarrow 2:

$$U_{EW} = V_1 \left[\frac{p_1 - p_2}{V_2 - V_1} \right] \quad (8)$$

where $p_i(T_i)$ is a smoothed experimental value and the remaining properties are calculated from the *Abbot* equation of state.

Fig 35 shows the pressure amplitude of the forerunner wave and the evaporation wave compared to simple theoretical models. The experimental, normalized

forerunner amplitudes in Fig 35(a) are compared to curves of constant nucleation rate $I(T_0, \Delta p)$. At higher initial temperatures ($T_0 \geq 150^\circ\text{C}$, for instance) the curves of constant nucleation rate are nearly coincidental with the pressure amplitude data: this implies that the pressure p falls until the nucleation rate becomes large enough to generate an opposing compression in the liquid. At lower initial temperatures, nucleation is no longer controlling and the amplitude data depart from the constant nucleation rate curves. The amplitude curves for the evaporation wave in Fig 35(b) are calculated on the same basis as the evaporation wave velocity.

Fig 33:

pressure $p(t)$ from the numbered transducers along the length of the tube test section. The initial pressures are all equal to p_0 .

(a) $T_0 = 165^\circ\text{C}$, $p_0 = 14.7 \text{ bar}$
 (b) $T_0 = 155^\circ\text{C}$, $p_0 = 12.3 \text{ bar}$

FW = forerunner wave
 EW = evaporation wave
 EWR = reflected evaporation wave

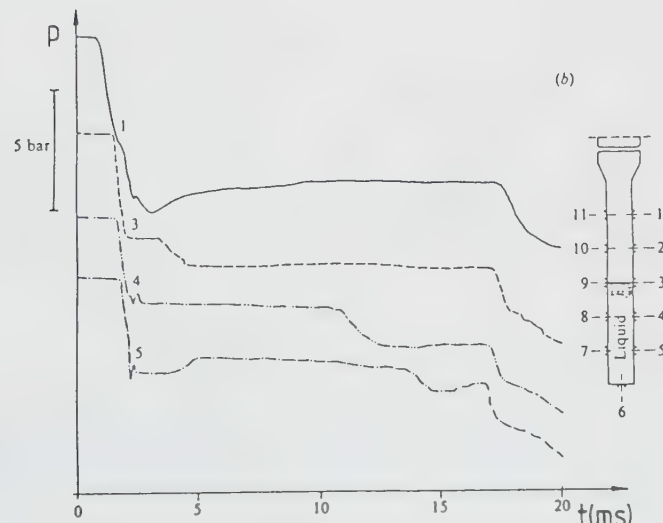
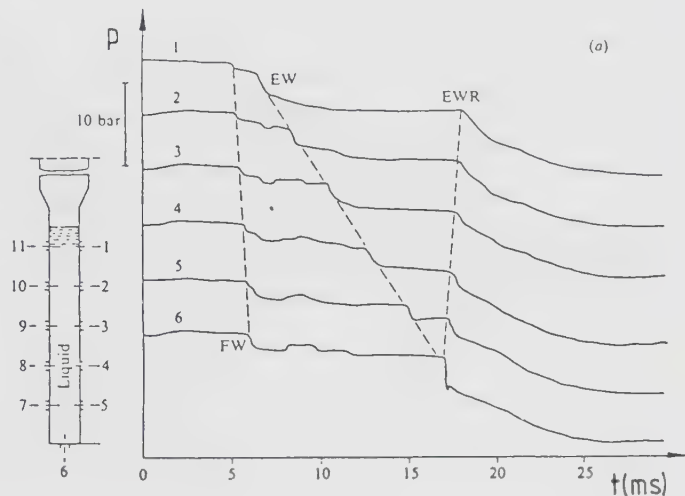


Fig. 34:

Propagation velocity U_{FW} of the forerunner wave (FW) in the liquid and of the evaporation wave (EW) as functions of the initial temperature T_0 . The solid curve for U_{FW} is the calculated speed of sound in the liquid.

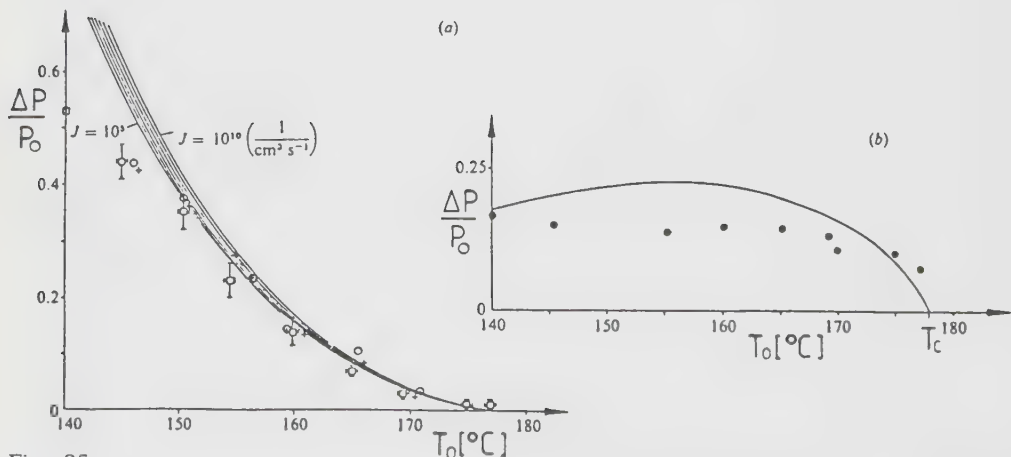
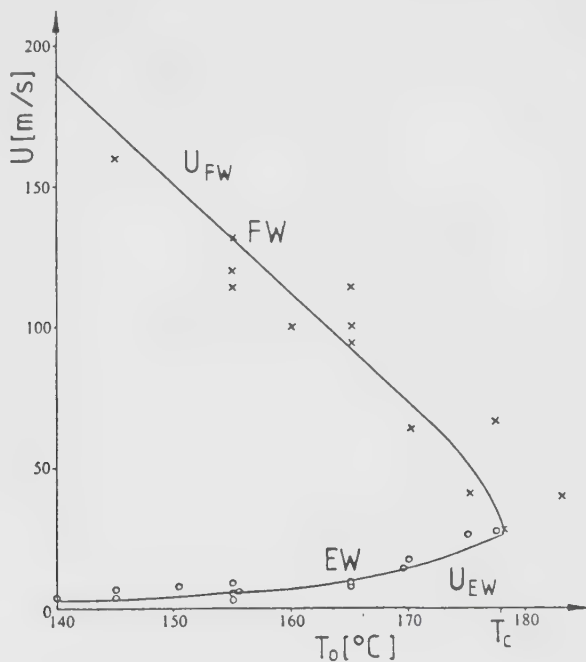


Fig. 35:

Normalized pressure amplitude Δp of the forerunner wave and the evaporation wave as a function of initial temperature T_0 . The pressure is normalized by the initial pressure p_0 . (a) Forerunner wave amplitude data compared to lines of constant nucleation rate. (b) Evaporation wave amplitude data and theoretical curve.

V Expansion Flows of Normal and Retrograde Substances

V.I Moisture Shocks in Steam

V.I.1 Introduction

Here we are concerned with a variant of compressible flow by describing the motion of a pure vapor, or a mixture of a vapor and an inert carrier gas, together with a liquid or solid condensate of variable mass fraction. While in this mixture transport phenomena may usually be neglected, the rate process of condensation and vaporization must be considered. This situation is different from the one where a condensate is initially present. Specifically we are concerned with condensation by homogeneous nucleation, a type of phase change which occurs in flow situations that exhibit a supersaturated state free of a liquid or solid phase before condensation sets in. Once the phase change occurs, however, the condensate is finely dispersed and the slip velocity between particles and gas can be neglected. A further simplification arises if the mass fraction of the condensate is small and the particle interaction is negligible. This mode of phase change is therefore noted primarily by the effects of a variable enthalpy derived from the latent heat of condensation or vaporization. Flows with condensation by homogeneous nucleation therefore model closely the diabatic flow of a thermally and calorical perfect gas.

V.I.2 Nonequilibrium Flow with Condensation [Wegener, 1975]

With the assumptions of the previous part and part I.III: Condensation, and omitting a discussion of discontinuities, the continuity equation

$$\frac{d\rho}{dt} + \rho (\nabla \cdot \mathbf{u}) = 0, \quad (1)$$

and the momentum equation for inviscid flow,

$$\rho \frac{d\mathbf{u}}{dt} + \nabla p = 0, \quad (2)$$

take their usual form in the absence of gravity. Here

$$\rho = \rho_i + \rho_v + \rho'_c, \quad (3)$$

the subscripts denote the inert gas, the vapor and the condensate (liquid or solid) respectively. The symbol, ρ'_c , implies that the condensate density is referred to as the same volume as that of the vapor. For pure vapors $\rho_i = 0$. The energy equation reads

$$\frac{d}{dt} \left(\frac{\mathbf{u}^2}{2} + h \right) - \frac{1}{\rho} \frac{\partial p}{\partial t} = 0, \quad (4)$$

with

$$h = \frac{m_i}{m} h_i + \frac{m_v}{m} h_v + g h_c \quad (5)$$

where g is the condensate mass fraction. Recalling the definition of the latent heat and assuming the condensate and the carrier to be at equal temperature, we have

$$h_c = h_v - L. \quad (6)$$

Combining equations 4, 5, and 6, we obtain

$$\frac{d}{dt} \left(\frac{u^2}{2} + \frac{m_i}{m} h_i + \frac{m_v - m_c}{m} h_v - gL \right) - \frac{1}{\rho} \frac{\partial p}{\partial t} = 0. \quad (7)$$

The solution of equations 1, 2, and 7 in conjunction with an appropriate equation governing the condensation process requires tabulated real gas values $h(p, \rho)$ for the participating species. The vapor and inert carrier gas may normally be taken individually as thermally and calorically perfect gases and this fact permits a simplification of the energy equation. With the definition of the specific humidity and with the specific heat of the vapor mixture in the supply, equation 7 becomes

$$\frac{d}{dt} \left(\frac{u^2}{2} + c_{p_0} T - gL \right) - \frac{1}{\rho} \frac{\partial p}{\partial t} = 0. \quad (8)$$

To complete our system of equations under the assumptions implicit in equation 8, we require an equation of state here given in the differential form.

$$\frac{dp}{p} = \frac{dp}{\rho} + \frac{dT}{T} - \frac{\mu}{\mu_v} \frac{dg}{1-g} \quad (9)$$

with the mixture molecular weight μ .

We now have a sufficient number of differential equations to solve the flows indicated in Figure 36 and labelled "no condensation", "equilibrium condensation", and "nonequilibrium" respectively.

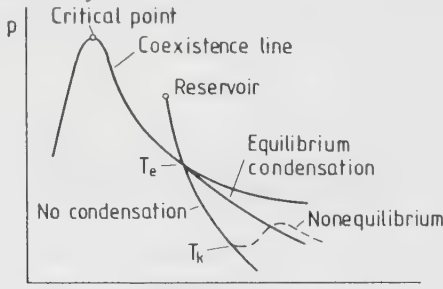


Fig. 36: Schematic pressure-volume diagram

V.II Retrograde Nozzle Flow

V.II.1 Introduction

Adiabatic evaporation of a retrograde fluid is possible only for considerable expansions of volume and pressure drops. This could be done by accelerating the substance in a Laval nozzle to supersonic velocities.

In the following we will treat a frictionless, steady and isentropic flow of a compressible fluid in a duct of variable cross section. The velocity u is assumed to be constant in every cross section F and gravity will be neglected. Due to the conservation of mass we obtain along the duct $\rho u F$ to be constant. The flow density $\Theta = \rho u$ is therefore inversely proportional to the cross section area F . In isentropic flows exists a unique relationship between velocity, pressure and density: growing velocity leads to pressure drop and therefore also to density drop. Hence the energy balance leads to $u^2/2 + h = \text{const}$ (h being the specific enthalpy) and therefore to:

$$dh = dp/\rho = c^2 d\rho/\rho \text{ and } d(u^2/2) = u du \rightarrow u du + c^2 d\rho/\rho = 0 \quad (1)$$

and

$$d\rho = -\frac{\rho u}{c^2} du. \quad (2)$$

With $d\Theta = d(\rho u) = u d\rho + \rho du$ follows

$$d\Theta = \rho du - \rho \frac{u^2}{c^2} du. \quad (3)$$

Being $M = u/c$ the Mach number one obtains

$$\frac{d\Theta}{du} = \rho(1 - M^2). \quad (4)$$

If the Mach number is $M \ll 1$, we obtain the flow-density rising with growing velocity of the fluid; that is, in $\Theta = \rho u$, prevails the growth of velocity. If $M \gg 1$, the density drop is dominant. The state of $M = 1$ is often called critical. We will skip this termination here to avoid confusion with the terms of state at the critical point. In nearly all cases M is growing monotonous with velocity (especially if the sonic speed decreases with decreasing pressure resp. increasing velocity, for example for the ideal gas), having a maximum at $M = 1$. Because of $\Theta F = \text{const}$ the cross sectional area of the duct has to be minimal. The pressure drop being sufficiently high, it is possible to generate a supersonic flow with a convergent – divergent nozzle (Laval nozzle).

If the sonic speed increases strongly with decreasing density, the case of a minimum at Mach number $M = 1$ is possible, corresponding with a maximum of the cross section area. This is possible if the second derivation of pressure with respect to the specific volume ($\partial^2 p / \partial V^2$)_s is negative, as for strongly retrograde substances in a small regime near the critical temperature and a bit less than critical pressure. For two-phase mixtures an exact treatment is difficult, because of the insecurity about the sonic speed ruling the fluid dynamics in this case.

In a small nozzle with transonic flow, changes of state take place at comparatively short times. Typically the time necessary for the fluid to pass the nozzle is of the order of milliseconds. Compared to the speed of changes in a shock-wave or a sound-wave of high frequency this time is very long. Evaporation of retrograde substances is very fast, so we assume the nozzle-flow to be nearly in equilibrium, that is, evaporation keeps up with pressure drop. Supposedly the Mach number M is one in the smallest cross section although it is uncertain which explicit sound speed should be assumed.

Considering the energy equation

$$\frac{u^2}{2} = - \int_{p_0}^p \frac{dp'}{\rho} \quad \text{with } u_0 = 0 \quad (5)$$

one can assume the relative pressure drop at the smallest cross section of the nozzle being comparatively small to that of a gas flow. Although $1/\rho$ and c are smaller by an order of magnitude than in gases, the lower sonic speed overwhelms them because of the quadratic contribution to the pressure drop. So the pressure

drop will take place mainly behind the smallest cross section, associated by a strong increase of the velocity u . As mentioned above the sonic speed increases just as strongly, so that the Mach number $M = u/c$ would not necessarily increase strongly. As we have assumed above, the substance being a mixture of liquid and vapor, streaming in the nozzle, we obtain the mixture of a retrograde fluid to evaporate completely if the initial temperature is sufficiently high and the pressure drop large enough.

A Laval nozzle, especially in its divergent part, has to fit exactly to the expanding flow, if an undisturbed flow should be obtained. In this case that is not necessary: the resulting disturbances like compression-shocks are desired to obtain informations about the behavior of the retrograde substance.

V.II.2 Critical Flux in a Nozzle

In all gasdynamic experiments with nozzle-flows and jets, sonic speed is reached at a certain pressure ratio at the smallest cross section of the Laval nozzle. This pressure ratio (end pressure/initial pressure) is almost always found at a value of about 1/2. The flux through a nozzle is limited with the reaching of sonic speed. A further increase of pressure ratio is followed only by a small increase of the flux. This remarkable fact should be investigated in detail.

First the case of an ideal-gas flow through a Laval nozzle should be mentioned. The associated flow density distribution versus pressure is shown in Fig 37(a). The reason for the reaching of maximal flow density and sonic speed is shown geometrically by the curve of the flow density at half of the rest-pressure. However, this fact cannot be drawn out of the formula given in Fig 37(b), which is derived from the equation of state and the energy equation. The rule, as shown in Fig 37(b), is nearly fulfilled for a variation of k (ratio of specific heats). Still the critical pressure ranges in the interesting region of 0.5 to 0.6. The shift to higher values for real gases with small k is strengthened for two-phase systems – as will be shown later.

Amazingly the rule of flux-limit at a lower rest-pressure than half holds even for fluids. This fact cannot be explained by the reaching of sonic speed as is done for gases, because sonic speeds of liquid are so large that the rule only would apply to values of rest-pressure nearly never occurring ($p_0 = 1000 \text{ MPa}$). It is all the more amazing to find the rule holding for nearly every liquid-nozzle in wide ranges. This could be explained only with some sort of real-gas effect which has already been discussed in chapter III.II. Nucleation and cavitation take place if the pressure in the nozzle falls short of the steam-pressure. Cavitation leads to a vapor-bubble mixture with comparatively small sonic speed limiting the flux through the nozzle. Phase transition leads here to a so-called Mach number unsteadiness which will be mentioned again in part three. With the aid of this mechanism all regulative valves for fluids are able to produce a flux proportional to the cross section area of the valve.

How could this behavior of the liquid-flows be explained? Fig 38(a) shows a Carnot-shock in a nozzle running into a wider duct. The pressures p , the velocities u and the areas F are pointed out in this figure. If one assumes cavitation to begin

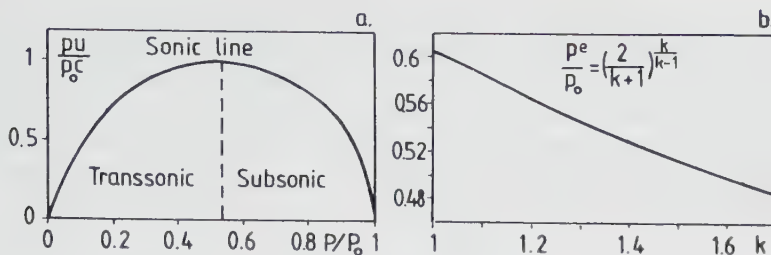


Fig. 37: a. Flow-density of an ideal gas flow in a Laval nozzle ($k = 1.4$)
b. critical pressure of an ideal gas flow as a function of the ratio

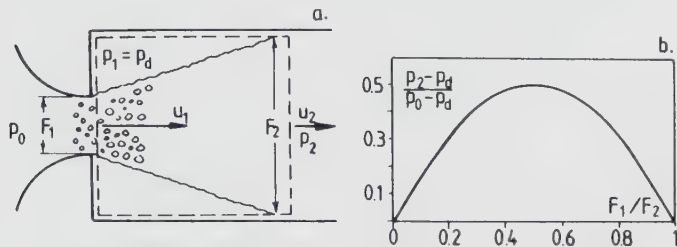


Fig. 38: a. schematic representation of nozzle flow in an expanding duct.
b. Pressure ratio, painted over area ratio (p_d : steam pressure)

at the cross section F_1 , one obtains $p_1 = p_d$. Also one assumes density to be constant both in cross section F_1 and in area F_2 , because of cavitation being still small in F_1 and already gone in area F_2 . The equations of conservation could thus be found as:

Continuity:

$$u_1 F_1 = u_2 F_2 \quad (6)$$

Momentum:

$$\rho (u_2^2 F_2 - u_1^2 F_1) = (p_1 - p_2) F_2 \quad (7)$$

Energy:

$$p_0 = p_1 + \rho u_1^2 / 2 \quad (8)$$

So one obtains for the pressure ratio:

$$(p_2 - p_d) / (p_0 - p_d) = 2 \left((F_1/F_2) - (F_1/F_2)^2 \right) \quad (9)$$

The evaluation of this quadratic relation between pressure and cross section ratio is shown in Fig 38(b). Looking a bit closer we recognize that the rule — like all rules of thumb — only holds approximately. Still, in a wide range of area ratios, the expected ratios of pressure are in the order of 0.4. The reason for taking the steam-pressure into account is found in the fact that cavitation takes place in heated fluids earlier than in cold ones with comparatively low steam-pressure. Water at room temperature has steam-pressures of about 20 hPa which can therefore be neglected. In the reduction of heated liquids we are talking about, steam-pressure is of the order of MPa and therefore not at all negligible.

V.II.3 Evaporation in nozzles

The mechanism of the flow through the nozzle runs as follows: The mixture of liquid and vapor accelerates in the divergent part of the Laval nozzle to transonic

speed. This corresponds to the location of the maximum of flow-density in the region of the mixture. Passing the phase boundary, the two-phase state retires and a vapor transonic flow remains. Being that the change of the Mach number is only small, there is little influence of the transition on the flow. More important are the compression shocks caused by reflection of the supersonic jet bordered by the barrel butt joints (barrel-shocks). These shocks together with the so-called Mach-shocks are able to lead the vapor back to states of mixture by compression.

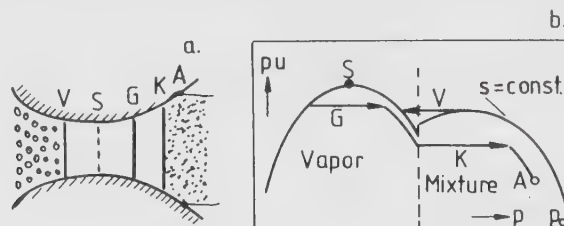


Fig. 39: a. Location of unsteadinesses in Laval nozzle. V: evaporation shock, S: sound barrier, G: compression shock in vapor, K: condensation shock, A: detaching b. Typical run of an expansion

The scheme of this should be explained in Fig 39. If the two maxima of the flow-density function are not of exactly the same value, complicated configurations of flow are possible. An example is given by Fig 39 showing a sonic expansion shock V in the contraction region of the nozzle, caused by a crossing of a relative maximum of flow-density. The second sonic state is located at S in the vapor state in the smallest cross section of the Laval nozzle. (The absolute maximum rules the flux!). In the transonic part of the expansion flow a normal vapor compression shock G is formed. After compression the phase boundary is reached and a condensation shock K leads to the isentrope of mixture, describing the increase of pressure to the place of detaching of the boundary layer.

Caused by mixtures in the store barrel and nozzle, constant conditions could be held a long time during the expansion of fluids with high specific energy. This too is in contradiction to the behavior of ideal gases.

VI Applications

VI.I Fuel Injection

VI.I.1 Introduction

In engines with direct cylinder injection of fuel, mixing of the fuel spray with surrounding air is of critical importance in determining the combustion characteristics of the engine [Oza, Sinnamon]. Flash-boiling injection offers a way of improving fuel-air mixing, reducing wall wetting by shortening spray-tip penetration and by improving atomization. Flash boiling occurs when a liquid, initially in a subcooled state, is rapidly depressurized to a pressure sufficiently below saturation pressure to initiate a rapid boiling process. The process is illustrated using the

pressure-enthalpy diagrams, Figs 40 (a) and (b). Referring to Fig 40 (a), subcooled liquid exists to the left of the liquid saturation line and superheated vapor exists to the right of the vapor saturation line, respectively. As mentioned above, superheated liquid can exist for a significant period of time without phase transition in a metastable condition between the liquid saturation line and the liquid spinodal. To the right of this line, there is no liquid metastable state, so that liquid and vapor must coexist.

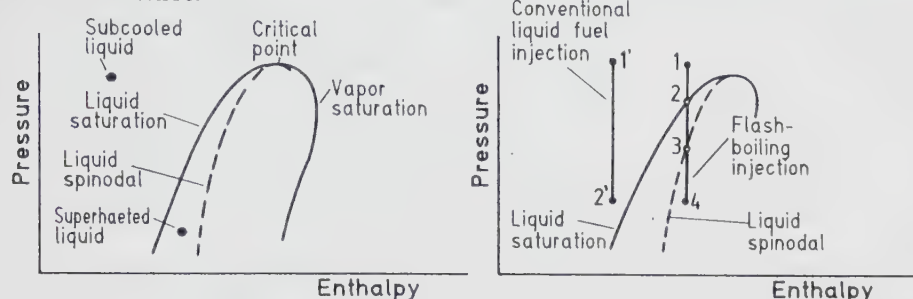


Fig 40: (a) pressure-enthalpy diagram (b) conventional and flash boiling injection compared for a pure substance

Consider a liquid fuel initially at point 1 in Fig 40(b) which undergoes a pressure reduction to point 4 while passing through an injector orifice. Given sufficient time between points 2 and 3, vapor bubbles will appear and grow until an equilibrium vapor fraction is achieved. The nucleation rate and the bubble-growth rate in the metastable zone depend upon a number of factors which will be discussed in detail later. As pressure is progressively reduced between points 2 and 3, nucleation and bubble growth rates increase until, as point 3 is approached, the nucleation becomes very large. Beyond this point the transition from liquid to vapor becomes explosively rapid. To initiate flash-boiling injection, fuel temperature, injection temperature and the pressure in the chamber into which fuel is injected are adjusted to obtain a process such as that described above. By contrast, points 1' and 2' illustrate a conventional "liquid to liquid" injection process.

Three potential benefits of flash-boiling injection are: 1) enhanced atomization, 2) increased initial spraycone angle for faster fuel-air mixing, and 3) reduced spray penetration. The above advantages could be attractive in direct injection engines (either diesel or stratified charge) in which fuel-air mixing rates and spray penetration rates must be carefully matched to the combustion chamber. In many of these engines, impingement of liquid fuel on the piston or chamber walls at high loads can be a particular problem. With flash-boiling, a low-penetration spray can be produced using a simple and reliable plain orifice, pencil-type injector.

It is also conjectured that enhanced atomization might alleviate the cold starting problems of alcohol-fuelled engines. Since methanol is a leading contender in the alternative fuels field, flash-boiling injection could also be of interest in this area.

VII.1.2 Regimes of Flash-Boiling Injection

Two regimes of flash-boiling injection can be observed in experiments. In the first, called the internal-flashing regime, a substantial number of fast-growing

bubbles is created within the nozzle, leading to two-phase flow within the nozzle. In the second, called the external-flashing regime, nucleation and growth of bubbles occur outside the nozzle.

In the internal-flashing regime, the flash-boiling within the nozzle is supported by two experimental observations. First, at relatively low values of superheat, the initial spray tip velocity near the orifice exit increases with an increasing degree of superheat, but the spray tip decelerates more rapidly. The higher initial velocity can be explained by a decrease in fluid density in the orifice due to increasing nucleation and bubble-growth rates. The higher spray tip deceleration can be explained by increasing nucleation rate, since a higher bubble number density should improve atomization and consequently increase the rate of air entrainment into the spray. Second, at relatively high superheats and low ratios of chamber pressure to injection pressure, the spray rapidly expands immediately upon leaving the orifice in the manner of an underexpanded, choked, compressible flow.

Phase separation during external expansion of the two-phase flow is observed when the degree of superheat is inadequate. It appears that a substantial part of the liquid is confined to a central core in the form of large droplets which are difficult to entrain in a predominant vapor phase that undergoes external expansion.

The external-flashing regime occurs when the fluid state at the chamber pressure lies between the saturation line and the liquid spinodal. Also, smooth nozzle entry geometry and/or low injection velocities must be used to avoid a region of locally low pressure within the nozzle. Rapid bubble growth occurring outside the nozzle shatters the initially intact liquid jet. The spray-cone angle increases and the intact length decreases as the degree of superheat increases.

Calculations performed using the bubble-growth rate theory are generally consistent with the experimental observations, and have led to a more complete understanding of the flash-boiling injection process. Bubble-growth-rate calculations indicate that flash-boiling of superheated fuel within an injector orifice can be obtained under typical fuel-injection conditions. The behavior of flashing injectors may then be explained on the basis of two-phase compressible flow within the orifice.

In agreement with experimental observations, the bubble-growth theory indicates that fuel jet atomization due to flashing can occur outside the nozzle if a smooth non-cavitating nozzle is used. The bubble-growth model yields intact lengths which are in reasonable agreement with experimental observations.

Application of the external-flashing regime in an engine should yield a spray with very low penetration, because a low injection velocity would be used. Careful matching of injection pressure and temperature conditions with combustion chamber pressure may be necessary because the degree of superheat, and hence the spray-cone angle, is very sensitive to the chamber pressure at the time of injection.

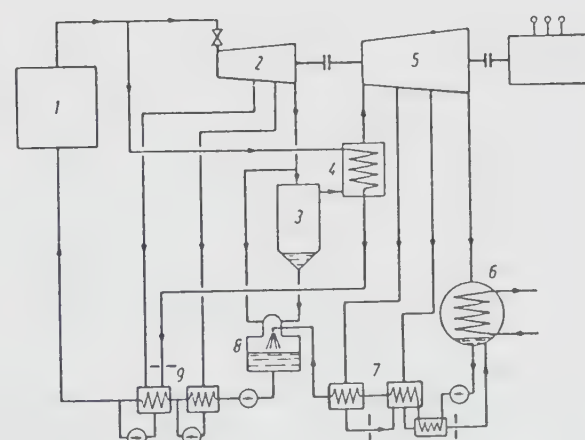
VI.II Steam Turbines

Even today steam turbines hold a pole position in technique. Although being the first machines using thermodynamics, because of their ability to yield the largest power they are therefore fundamental in the power supplying of the world [Traupel].

The intention to obtain a maximal efficiency leads to high temperatures, that is, evaporating the water at high pressures. Because of the quality of water to condense partly at the expansion of initially saturated vapor, even increasing with increasing initial pressure of the expansion, a too high moisture of the steam must be avoided with regard to efficiency and first of all erosion of the paddles. An increase of steam-pressure is possible only with the aid of superheating. The increase of temperature is limited by the material of the turbine itself. Hence, after a first partial expansion, one superheats a second time at lower pressures. This can be done two or even more times leading to an arbitrary pressure, and indeed even pressures of 300 bar have been used, heating the water beyond the critical point to superheated states without evaporation.

Figure 41 shows the diagram of a steam turbine normally used in atomic power plants with light-water reactors. These reactors are not able to work with high-pressure (superheated) steams. Hence the steam technique was pressed to saturated-steam turbines again, after the superheated steam had been usual for decades. In the scheme in symbol 1 the nuclear system of steam production is pointed out. The saturated steam is expanded in the high pressure turbine 2 to an intermediate pressure, producing moisture during this process which is separated in the water separator 3. The dried steam is superheated a second time in the intermediate superheater 4 with the energy obtained from a jet of fresh steam, condensing in the intermediate superheater, and is led to the preheating installation 9. This treatment is possible because the temperature of the initial saturated steam is much higher than the boiling point of the steam. The intermediately superheated steam is then expanded to the end pressure in the low pressure turbine 5 and condensed in the condensator 6. The following preheating installation is assembled from two preheaters in the low pressure regime 7, a mixture preheater 8 and two surface preheaters in the regime of high pressure with pumps 9.

Fig 41:
Scheme of a saturated steam turbine with intermediate superheating used in atomic-power plants.



VII. References

J. Bode:

Spontane Kavitation hinter starken Expansionswellen,
Max-Planck-Institut für Strömungsforschung, Göttingen, Bericht 110/1987

M. Bratos, G.E.A. Meier:

Shock Wave Induced Condensation in Retrograde Vapor
Archives of Mechanics, 31, 5, pp. 679-693, Warszawa 1979

M. Bratos, G.E.A. Meier:

Two-dimensional, Two-phase Flows in a Laval Nozzle with Nonequilibrium
Phase Transition
Arch. of Mech., 28, 5-6, pp. 1025-1037, Warszawa 1976

R. Brown, J.L. York:

Sprays Formed by Flashing Liquid Jets
A.I.Ch.E. Journal, Vol 8, No2, pp. 149-153

H. Chaves:

Expansion Waves in Retrograde Fluids
MPI, Bericht 7/1981

H. Chaves:

Phase Transitions and Waves in the Expansion of Fluids of High Specific Heat
MPI, Bericht 77/1984

H. Chaves et al.:

Adiabatic Phase Transitions and Wave Splitting in Fluids of High Specific Heat, in:
G.E.A. Meier, F. Obermeier (eds.): Flow of Real Fluids, Springer 1985

H. Chaves et al.:

Similarity in the Behavior of Initially Saturated or Subcooled Liquid Lets Discharging
Through a Nozzle
Chem. Phys. 126, 1988, pp. 137-143

A.Dillmann:

Theorie der homogenen Nukleation übersättigter Dämpfe
MPI, Bericht 93/1984

A. Dillmann, G.E.A. Meier:

Homogeneous Nucleation of Supersaturated Vapors
Chem. Phys. Letters 160, 1989, pp. 71-74

G.Gyarmathy, in:G.F. Hewitt, J.M. Delahaye and N. Zuber (eds):
Multiphase science and technology
Vol 1, Hemisphere, Washington, 1982, pp.99

R.E. Henry, H.K. Fauske:

The Two-phase Critical Flow of One Component Mixtures in Nozzles, Orifices and
Shock-tubes

Journal of Heat Transfer, May 1971, pp. 179-187

W.H. Isay:

Kavitation, Schiffahrtsverlag "Hansa", Hamburg 1984

Kurschat:

Vollständige adiabatische Verdampfung stark überhitzter Flüssigkeitsfreistrahlen,
MPI, Bericht 95/1990

J.H. Lienhard, J.B. Day:

The Breakup of Superheated Liquid Jets

Journal of Basic Engineering, Sept. 1970, pp. 515-521

G.E.A. Meier:

The Gas dynamics of Fluids of High Specific Heat

MPI, Bericht 89/1987

R.D. Oza, J.F. Sinnamon:

An Experimental and Analytical Study of Flash-boiling Fuel Injection

SAE technical paper series No 830590

M. Rein:

Numerical Investigation of the Dynamics of Heterogeneous Shock-cavitation
Max-Planck-Institut für Strömungsforschung, Bericht 86/1987

J.F. Shepard, B. Sturtevant:

Rapid Evaporation at the Superheat Limit

JFM, 1982, vol. 121, pp. 379-402

R.A. Sigsbee:

Vapor to Condensed-Phase Heterogeneous Nucleation in:

A.C. Zettlemoyer(Ed.): Nucleation

Dekker, New-York 1969

H.-D. Speckmann:

Spontane Kondensation von retrograden Gasen bei Verdichtungsstößen

MPI, Bericht 21/1978

H.-D. Speckmann:

Aufspaltung von Kondensationswellen in Fluiden hoher spezifischer Dichte

MPI, Bericht 76/1984

H. Tacke:

Lavaldüsenströmung eines binären retrograden Gemenges

JFM, Vol 185, 1987, pp. 385-414

P.A. Thompson et al.:

Wave Splitting in a Fluid of Large Heat Capacity

JFM, 1987, vol 185, pp. 385-414

W. Traupel:

Thermische Turbomaschinen Bd. 1

Springer, Berlin 1977

P.P. Wegener:

Nonequilibrium Flow with Condensation

Acta Mech., 1975, 21, pp. 65-91

WAVES IN SUPERFLUID HELIUM

W. Fiszdon

Polish Academy of Sciences

and

University of Warsaw, Warsaw, Poland

ABSTRACT.

A brief introduction to the basic hydrodynamic and thermodynamic properties and to quantum vortices is given. The two fluid flow equations are introduced. The second sound, temperature waves are considered, their specific properties and structure analysed. A brief account of third sound capillary and thin film waves as well as fourth sound waves is sketched. A geometrical treatment of the evolution of axisymmetric heat pulses is presented. The large influence of quantum turbulence on the evolution of second sound waves is illustrated analysing the evolution of moderate second sound heat pulses.

§1. Historical introduction.

Before attempting to tell you about certain wave phenomena in superfluid helium I would like to introduce to you this fluid, perhaps not so well known as other fluids, whose unique properties justify its selection to be included as a separate entity in this course on waves in real fluids.

Helium as a material element was first noticed in 1868 while analysing the spectrum observed during the eclipse of the sun and finding a line never before seen in the laboratory. This line was later confirmed as corresponding to a new element and given the name helium 4 after the Greek word for sun. About 30 years later Ramsay obtained a laboratory sample of this gas during his spectral analysis of the product of some minerals.

Helium 4 exists in the atmosphere with a volume concentration of about one part in 200000 and in much greater industrial concentrations in some natural gas wells. This gas was the last one to be liquefied and it is only in 1908 that Kamerlingh Onnes succeeded to liquefy it in the famous Leiden laboratory. In 1938 the journal Nature published the results of observations made by Kapitza and independently by Allen and Misener reporting that at temperatures below about 2 K the flow through capillaries (of about 10^{-4} cm diameter) of liquid helium took place without any measurable resistance. This important flow feature was called superfluidity.

These observations preceded by Keesom's earlier remarks made in 1928 that liquid helium must exist in two modifications led to a great interest of many eminent physicists (Kapitza, Feynman, Landau to name a few) in this non classical fluid. After WWII further research and possible cryogenic technological applications led to a better understanding of the observed phenomena and generated an explosion of published papers, but many questions still remain unanswered.

§2. General introduction.

There exist in nature 3 known isotopes of helium: ^3He , ^4He and ^6He . Helium 6 has a very short lifetime and helium 3 exhibits its superfluid properties at temperatures of the order of milikelvins and its concentration is extremely small, of the order of 1 part in 10^7 in well helium.

In what follows we will be concerned only with the more common isotope helium 4. A comparison of the phase diagram of ^4He with a corresponding diagram of a classical fluid, shown on Fig.2.1 illustrates some important differences between the two fluids. First of all the triple point, where the three states of matter meet, is absent in ^4He and helium remains liquid under its own saturated vapour pressure (SVP) down to absolute 0K . It is necessary to put it under a pressure of about 25 bars to solidify. This reluctance of helium to become solid is due to the very low mass of the atoms and the very weak interatomic forces. At these low temperatures on quantum mechanical grounds the zero point energy is sufficient to overcome the weak binding potential between the helium atoms.

Helium liquefies at 4.215K and has all properties of a classical fluid down to the temperature of the lambda-line shown on Fig.2.1. Observations made of the evaporation of liquid helium above T_λ show vigorous agitated nucleation boiling, but immediately the temperature is reduced below T_λ the bubbles disappear and the liquid surface becomes smooth. This suggests that the heat conductivity becomes so large that the liquid cannot support a temperature gradient necessary for the existence of a superheated vapour condition. It appears that crossing the λ -line a phase transformation of the liquid takes place. This can be also seen from the variation of the thermodynamic parameters with temperature as shown on Fig.2.2 e.g. for density, entropy, specific heat and latent heat of evaporation. Particularly the specific heat varies dramatically with temperature and its appearance gave its name to the λ -line marking the phase transition between the fluid of classical behaviour called HeI and the superfluid named HeII.

The non-classical behaviour of HeII can also be seen from the results of the viscosity measurements made with standard measuring and evaluation methods used for classical fluids. As can be seen on Fig.2.3 different apparent viscosities are obtained below T_λ depending on the apparatus used. This apparent contradiction can be avoided using a suitable theoretical model to describe the flow. As will be seen later the two-fluid model suggested by Tisza (1938) developed and substantiated using the microscopic theory by Landau (1941) explains the particularities of superfluid flows.

The flow in narrow capillary tubes without resistance can be justified invoking only the flow of the superfluid component with zero viscosity, whereas the two other viscometer methods correspond to flow conditions involving the entrainment only of this component part of the fluid whose viscosity is not zero. Indeed Andronikashvili (1946) measured the periods of oscillations of a set of metal discs suspended on a thin wire and spaced so as to insure that all the viscous fluid between the discs was entrained with them. Below T_λ the period of oscillations decreased with temperature indicating the reduction of the viscous fraction of the fluid which was entrained by the discs.

This substantiated the validity of the two fluid model, allowed the determination of the density of the normal component ρ_n and taking into account that the total density ρ is the sum of the two components $\rho = \rho_n + \rho_s$, to deduce the density of the superfluid component, ρ_s , see Fig.2.4.

A spectacular experiment illustrating the superfluid flow properties can be observed with a beaker partially filled with HeII in presence of a HeII bath, see Fig.2.5. When the levels of the free surfaces are uneven, owing to the formation of a thin film (which can be up to 30 μm thick) on the walls of the beakers the liquid levels inside tend to become even with the bulk level, the thin film is then acting as a capillary siphon for the superfluid with gravity as the driving force.

To complete the description of the main features of HeII I would like to mention briefly the so called thermo-mechanical effect. As the superfluid component has the properties of an ideal fluid it can not transport heat which is transported only by the normal component. Hence if we have two

vessels, connected by a capillary, or a tube filled tightly with very fine powder (called superleak), through which only the superfluid component can flow, a temperature head is accompanied by a pressure head. This occurs because as ρ_s/ρ increases when the temperature decreases the superfluid moves to the region of higher temperature to reduce the temperature difference. A spectacular experiment illustrating this effect is the so called helium fountain, see Fig.2.6. A container closed at one end by a powder pack acting as a superleak with a tube at the other end is immersed in a HeII bath. Heating the fluid in the container superfluid will flow through the powder pack and push out the liquid through the tube forming thus a fountain.

To explain the described observations it appears plausible to assume that the fluid is composed of two parts and only the superfluid component flows through the very narrow tubes, as the viscosity of the normal component prevents its flow. However I would like to emphasize that so far we have described phenomena and observations that could be classified as superfluid laminar flow, in analogy to the classical laminar flow. Beyond a certain range of flow parameters or and velocities which may be called critical velocities superfluid turbulence becomes of importance and affects strongly the character of the flow. We will come back to these flows at a later stage.

§3. The two fluid flow hydrodynamics of HeII.

The above described observations clearly indicate that, in the case of HeII it is necessary to modify the well known classical hydrodynamic model so as to be able to take into account its additional features observed in the macroscopic experiments.

A classical fluid macroscopically, i.e. on a scale much larger than the average distance between the particles, flows with some average velocity which varies continuously from point to point, whereas at the microscopic scale the molecules move randomly with velocities distributed over a wide range. These macroscopic random motions are responsible for the viscosity and thermal conductivity of the classical fluids.

In contrast the superfluid component of HeII, like a perfect fluid, flows apparently without the above mentioned random molecular motion effects. This is due to the quantum mechanical influence which becomes dominant at the very low temperatures we are interested in. A comparison of the de Broglie wave length ($\lambda_{deB} = h/(Tm k_B)^{1/2}$ where h , k_B are Planck's and Boltzmann's constants, m is the particle mass and the temperature is T) with the distance between the HeII molecules shows that, at a temperature of about 2K, it is of an order of magnitude larger than the distance between the particles which substantiates the importance of quantum effects. This is not the case in other fluids which remain liquid at much higher temperatures.

In what follows we will limit ourselves to the London-Landau most successful two fluid flow continuum theory and I think to avoid misunderstandings it is best to quote Landau: "*It should be emphasized that the treatment of the liquid as a 'mixture of normal and superfluid' 'parts' is simply a form of words convenient for the description of the phenomena in a quantum liquid. Like any description of quantum effects in classical terms, it is not entirely adequate. In reality we should say that in a quantum Bose liquid there can exist simultaneously two motions, each of which has a corresponding 'effective mass' such that the sum of these two masses is equal to the actual total mass of the liquid. One of these motions is 'normal', i.e. has the same properties as that of an ordinary viscous liquid; the other is 'superfluid'. The two motions occur without transfer of momentum from one to the other.*"

To obtain a consistent mathematical formal model based on the above considerations we use the laws of conservation of mass, momentum and energy, remembering that they must be invariant under a Galilean transformation and

the laws of thermodynamics must be obeyed. Note that in the case of a classical fluid 5 dependent variables i.e. 3 velocity components and 2 thermodynamic variables are necessary to define the flow and as there is in this case only one velocity field the Galilean principle is automatically satisfied. However in the case of a superfluid at least 3 more variables, the velocity components of the superfluid flow field, are required to determine the HeII flow.

Following Putterman, to obtain a closed system of equations for superfluid helium we will assume that:

- eight variables: the two velocity field vectors \mathbf{v}_n , \mathbf{v}_s , the pressure (or the density ρ) and the temperature T form a complete set.
- the linear stress strain and heat flow relations are satisfied as in the case of classical fluids.

The fluid flow equations are as follows:

- Conservation of mass:

$$\frac{\partial \rho}{\partial t} + \operatorname{div} \mathbf{j} = 0, \quad (3.1)$$

where the total density is the sum of the two component densities:

$$\rho = \rho_n + \rho_s \quad (3.2)$$

and the fluid flux \mathbf{j} is:

$$\mathbf{j} = \rho_n \mathbf{v}_n + \rho_s \mathbf{v}_s \quad (3.3)$$

and \mathbf{v}_n , \mathbf{v}_s are the normal and superfluid field velocities associated with the corresponding densities

- Conservation of momentum:

$$\frac{\partial \mathbf{j}_i}{\partial t} + \frac{\partial \Pi_{ik}}{\partial x_k} = - \frac{\partial \tau_{ik}^*}{\partial x_k}, \quad (3.4)$$

where Π_{ik} is the pressure tensor and τ_{ik}^* is the viscous stress tensor.

- Conservation of energy:

$$\frac{\partial E}{\partial t} + \operatorname{div} Q = \operatorname{div} Q^*, \quad (3.5)$$

where E is the energy per unit volume, Q is the energy flux and Q^* is the dissipation energy flux.

In the case of HeII, to form a complete set, these 5 equations have to be supplemented by the superfluid equation:

$$\frac{\partial \mathbf{v}_s}{\partial t} = \text{grad}(\frac{1}{2} v_s^2 + \mu) = - \text{grad } H^*, \quad (3.6)$$

where μ can be identified as the chemical potential and H^* is the off equilibrium correction to the chemical potential.

According to Landau's model in addition to the above we have the relation:

$$\text{rot } \mathbf{v}_s = 0. \quad (3.7)$$

Taking into account that heat is only transported by the normal component the entropy equation becomes:

$$\frac{\partial \rho s}{\partial t} + \text{div} (\rho s \mathbf{v}_n) = - \text{div } \frac{\mathbf{q}^*}{T} + \frac{\Sigma^*}{T}, \quad (3.8)$$

where the entropy flux \mathbf{q}^*/T and the entropy production Σ according to thermodynamic requirements must vanish at equilibrium.

Please note that we have included in the above equations terms denoted by stars which are due to dissipation. These terms are on the right hand side of the above equations and are identically zero in the case of the dissipationless flows originally described by Landau.

We have thus obtained an overdetermined set of equations since only 8 are necessary to form a complete set. Hence one of them say the energy equation must be implied by the remaining ones. We assume that the most general expression for the dissipative terms, which vanish at equilibrium and satisfy the Galilean principle, are first order with respect to deviations from equilibrium including also the velocity difference $\mathbf{v}_n - \mathbf{v}_s$. After rather very lengthy manipulations we deduce the relations necessary to close the analysed set of equations. Thus from the compatibility conditions in the cases of dissipationless and dissipative flow the following relations are deduced:

$$\left. \begin{aligned} \Pi_{ik} &= \rho \delta_{ik} + \rho_n v_{ni} v_{nk} + \rho_s v_{si} v_{sk}, \\ Q &= (\mu + v_s^2/2) j_i + \rho s T v_{ni} + \rho_n v_{ni} (\mathbf{v}_n \cdot (\mathbf{v}_n - \mathbf{v}_s)), \\ dE &= (\mu + v_s^2/2 - v_n v_s) d\rho + T d\rho s + \mathbf{v}_n d\mathbf{j} - \rho_s (\mathbf{v}_n - \mathbf{v}_s) d\mathbf{v}_s, \end{aligned} \right\} \quad (3.9)$$

$$d\mu = -sdT + dp/\rho - \frac{\rho_n}{2\rho} d(\mathbf{v}_n - \mathbf{v}_s)^2. \quad (3.10)$$

$$\left. \begin{aligned} \mathbf{q}^* &= -\mathbf{x} \operatorname{grad} T, \\ H^* &= \zeta_3 \operatorname{div} \rho_s (\mathbf{v}_n - \mathbf{v}_s) - \zeta_4 \operatorname{div} \mathbf{v}_n, \\ \tau_{ij}^* &= -\eta \left(\frac{\partial v_{n,i}}{\partial x_j} + \frac{\partial v_{n,j}}{\partial x_i} - 2\delta_{ij} \operatorname{div} \mathbf{v}_n / 3 \right) \\ &\quad + \delta_{ij} \left(\zeta_1 \operatorname{div} (\rho_s (\mathbf{v}_n - \mathbf{v}_s)) - \zeta_2 \operatorname{div} \mathbf{v}_n \right). \end{aligned} \right\} \quad (3.11)$$

$$\left. \begin{aligned} Q_i^* &= q_i + \tau_{ji} v_{nj} + H^* \rho_s (v_s - v_n), \\ \Sigma^* &= \zeta_2 (\operatorname{div} \mathbf{v}_n)^2 + \zeta_3 \left(\operatorname{div} (\mathbf{j} - \rho \mathbf{v}_n) \right)^2 + 2\zeta_1 \operatorname{div} \mathbf{v}_n \operatorname{div} (\mathbf{j} - \rho \mathbf{v}_n) + \\ &\quad + \frac{1}{2} \eta \left(\frac{\partial v_{ni}}{\partial r_k} + \frac{\partial v_{nk}}{\partial r_i} - \frac{2}{3} \delta_{ik} \frac{\partial v_{nl}}{\partial r_l} \right)^2 + \alpha (\Delta T)^2 / T, \end{aligned} \right\} \quad (3.12)$$

where η and α respectively are the classical viscosity and heat diffusion coefficients of the normal component. The coefficients ζ with indexes are second viscosity coefficients connected with the divergence terms. It appears that although the shear viscosity of the superfluid component is zero the bulk viscosities are finite. This is due generally speaking to the relaxation effects following a perturbation of the equilibrium state. It is also worth noting that $(\mathbf{v}_n - \mathbf{v}_s)^2$ is one of the thermodynamic variables.

For more details concerning the equations of superfluid flow I would like to recommend the monographs of Putterman and Khalatnikov.

§4. The dissipationless propagation of very small (acoustic) perturbations in Hell at rest.

In the case of very small deviations from the equilibrium values of all the hydro-thermodynamic variables we will assume that the quadratic and higher order terms in the conservation equations of § 3 can be neglected in comparison with the remaining first order terms. Assuming dissipationless flow, and taking ρs in the term $\text{div}(\rho s \mathbf{v}_n)$ as constant, equations (3.1), (3.4), (3.6) and (3.8) are reduced to the following simple linear form:

$$\frac{\partial \rho}{\partial t} + \text{div} \mathbf{j} = 0, \quad (4.1)$$

$$\frac{\partial \rho s}{\partial t} + \rho s \text{ div } \mathbf{v}_n = 0, \quad (4.2)$$

$$\frac{\partial L}{\partial t} + \text{grad } p = 0, \quad (4.3)$$

$$\frac{\partial \mathbf{v}_s}{\partial t} + \text{grad } \mu = 0. \quad (4.4)$$

The linearised thermodynamic relation for the chemical potential (3.11) becomes:

$$\partial \mu = - dT + \partial p / \rho \quad (4.5)$$

Subtracting from the time derivative of (4.1) the divergence of (4.3) there follows:

$$\frac{\partial^2 \rho}{\partial t^2} = \Delta p. \quad (4.6)$$

Taking into account the time derivative of (4.2) and the divergence of (4.3) and (4.4), eliminating the velocities and making use of the equations (4.5) and (4.6) we obtain finally:

$$\frac{\partial^2 s}{\partial t^2} = \frac{\rho_s}{\rho_n} s^2 \Delta T \quad (4.7)$$

Equations (4.6) and (4.7) determine the linearised variation of the hydro-thermo-dynamic quantities due to small perturbations such as sound waves.

Let us select as main variables the pressure and the temperature and represent them as the sum of their equilibrium values, with subscript zero, and their perturbation, with superscript prime:

$$p = p_0 + p', \quad T = T_0 + T' \quad (4.8)$$

Using the linear approximations we will have:

$$\rho' = \frac{\partial \rho}{\partial p} p' + \frac{\partial \rho}{\partial T} T', \quad s' = \frac{\partial s}{\partial p} p' + \frac{\partial s}{\partial T} T'. \quad (4.9)$$

Introducing the above relations in the hyperbolic equations (4.6), (4.7) there follows:

$$\left. \begin{aligned} \frac{\partial \rho}{\partial p} \frac{\partial^2 p'}{\partial t^2} - \Delta p' + \frac{\partial \rho}{\partial T} \frac{\partial^2 T'}{\partial t^2} &= 0, \\ \frac{\partial s}{\partial p} \frac{\partial^2 p'}{\partial t^2} + \frac{\partial s}{\partial T} \frac{\partial^2 T'}{\partial t^2} - \frac{s^2 \rho_s}{\rho_n} \Delta T' &= 0. \end{aligned} \right\} (4.10)$$

In the case of acoustic plane wave propagation in the x direction the solution of the above set of equations is obtained assuming that the dependent variables are proportional to:

$$\exp(i\omega(t - x/a)), \quad (4.11)$$

where ω is the frequency and a the velocity of propagation in the x direction.

$$\left. \begin{aligned} \left(\frac{\partial \rho}{\partial p} a^2 - 1 \right) p' + \frac{\partial \rho}{\partial T} a^2 T' &= 0, \\ \frac{\partial s}{\partial p} a^2 p' + \left(\frac{\partial s}{\partial T} a^2 - \frac{s^2 \rho_s}{\rho_n} \right) T' &= 0. \end{aligned} \right\} (4.12)$$

To obtain a non trivial solution the determinant of (4.12) must be equal zero. After some simple transformations the following compatibility condition is obtained:

$$(a_{10}^{-2} - a^2)(a_{20}^{-2} - a^2) = \left(1 - \frac{C_v}{C_p}\right) a_{10} a_{20}, \quad (4.13)$$

where:

$$a_{10}^{-2} = \left(\frac{\partial p}{\partial \rho} \right)_s, \quad (4.14)$$

$$a_{20}^{-2} = s^2 \rho_s \left(\rho_n \left(\frac{\partial s}{\partial T} \right)_p \right)^{-1}, \quad (4.15)$$

$$C_p = T \left(\frac{\partial s}{\partial T} \right)_p, \quad C_v = T \left(\frac{\partial s}{\partial T} \right)_\rho. \quad (4.16)$$

The compatibility condition (4.13) shows the very important property of HeII, i.e. the existence of two velocities of propagation of perturbations. As the thermal expansion coefficient, $(\partial\rho/\partial T)_P$, of HeII is extremely small, the two specific heats, C_p and C_v , except very close to T_λ , can be taken as equal. In this case the two velocities of propagation of small perturbations become a_{10} and a_{20} . The variation of these two velocities with temperature are shown on Fig.4.1 and it can be noticed that above $0.8K$ a_{10} is by an order of magnitude larger than a_{20} .

The nature of the two types of sound waves can be inferred by inspection of relations (4.4),(4.6) and (4.12) having inserted there the corresponding velocities of propagation a_{10} or a_{20} . The perturbation propagating with the velocity a_{10} , called first sound, corresponds to pressure and density variations and hence involves also mass transport as in classical fluids. The variation of the other thermodynamic parameters is in this case negligible. The perturbation propagating with the so called second sound, velocity a_{20} consists essentially of temperature and entropy variations with zero mass center of gravity displacements. The existence of these second sound temperature waves which are only very slightly damped, unlike in fluid mixtures, is a unique property of superfluids. It indicates also the possibility of wave like heat transmission.

So far we have considered the propagation of perturbations in an unbounded space. Due to the double nature of HeII as a combination of a "Navier Stokes" and an "Euler" fluid we can expect different cases of wave propagation depending on the additional restraints imposed by the boundaries. The different types of resulting waves have been given consecutive numbers such as third sound for waves of thin films or fourth sound when the flow of the normal component is restrained. We will come back to some of them later after having considered strong perturbations in an unlimited space.

§5. Dissipationless shock waves in HeII.

Similarly as in classical hydrodynamics when the velocity of propagation of perturbations depends on the local amplitude of the deviation from the equilibrium state a deformation of the shape of the wave occurs. At stronger perturbations this leads to the appearance of large gradients of the hydro-thermo-dynamic quantities in a narrow space range. This phenomenon, usually called a shock wave, exists also in superfluids. However similarly as in the case of acoustic waves we will expect in HeII the existence of the two types of waves: the classical pressure wave and temperature shock waves specific for superfluids. Under idealised dissipationless conditions the waves become simple discontinuities.

To describe this case we will use the original analysis due to Khalatnikov and consider the one dimensional plane wave, using a reference frame fixed to the wave so, as to have steady state conditions. The x axis is taken perpendicular to the surface of discontinuity.

The laws of conservation previously described must of course be satisfied, hence the difference between the conserved quantities on both sides of the shock wave must be zero. Denoting by square brackets the "jump" of the argument written within them the following relations must hold for the following density flows:

$$\text{- mass: } [\rho_n v_n + \rho_s v_s] = 0, \quad (5.1)$$

$$\text{- momentum: } [\rho_n v_n^2 + \rho_s v_s^2 + p] = 0, \quad (5.2)$$

- quantity under the gradient operator in the superfluid equation:

$$[\bar{\mu} + v_s^2/2] = 0, \quad (5.3)$$

- energy density flow taking into account (5.2) and (5.3)

$$[T\bar{\rho}\bar{s}v_n + \rho_n w v_n^2] = 0, \quad (5.4)$$

where, for convenience to facilitate further transformations, we indicated by dashes the thermodynamic parameters whose dependence on v_n , v_s should be

taken into account, and by $w = v_n - v_s$.

Changing to the laboratory rest frame, in which the shock wave moves with the velocity a into a quiescent fluid where $v_n = v_s = 0$, the velocities in the above equations must be changed as follows: in front of the shock wave both velocities must be equal a , i.e. $v_n = a$ $v_s = a$, behind the shock the corresponding velocities become $v_n - a$ and $v_s - a$. Denoting now by the index 1 the equilibrium quantities in front of the wave and leaving without index the quantities behind the wave eqs (5.1) to (5.4) become:

$$\rho_1 a = \bar{\rho}(a - v), \quad (5.5)$$

$$p_1 + \rho_1 a^2 = p + \bar{\rho}(a - v)^2 + \frac{\rho_s \rho_n}{\bar{\rho}} w^2, \quad (5.6)$$

$$\mu_1 + \frac{a^2}{2} = \bar{\mu} + \frac{1}{2} \left(a - v + \frac{\rho_n}{\bar{\rho}} w \right)^2, \quad (5.7)$$

$$\rho_1 T_1 s_1 a = \bar{\rho} s T \left(a - v - \frac{\rho_s}{\bar{\rho}} \right) + \rho_n w \left(a - v - \frac{\rho_s}{\bar{\rho}} w \right)^2, \quad (5.8)$$

where $v = j/\rho$.

The above set of equations is formally sufficient to obtain all the shock wave parameters behind the shock wave once the equilibrium values in front of the shock wave and the perturbation intensity are known. However to close this system of equations it is necessary to know the dependence of the thermodynamic variables, ρ, μ, s , on the other thermodynamic variables including w^2 . But this dependence is very complicated and at present the known data are limited to second order terms in w . Hence we must limit ourselves to moderate discontinuities for which this second order approximation is satisfactory.

From the thermodynamic relation which we repeat here for convenience:

$$d\mu = -sdT + \frac{dp}{\rho} - \frac{\rho_n}{2\rho} dw^2 \quad (3.10)$$

there follows:

$$\left. \begin{aligned} s(p, T, w) &= s(p, T) + \frac{1}{2} w^2 \frac{\partial}{\partial T} \frac{\rho_n}{\rho}, \\ \rho(p, T, w) &= \rho(p, T) + \frac{1}{2} w^2 \frac{\partial}{\partial p} \frac{\rho_n}{\rho}, \end{aligned} \right\} (5.9)$$

Using eqs (5.5),(5.9) and (3.10) and expanding all parameters in powers of $p' = p - p_1$, $T' = T - T_1$, up to second order and neglecting the variation of the density ρ with temperature after tedious transformations the following system of equations is obtained:

$$p'(1 - a^2 \frac{\partial \rho}{\partial p}) + p'^2 a^2 \left(\frac{1}{\rho} \left(\frac{\partial \rho}{\partial p} \right)^2 - \frac{1}{2} \frac{\partial^2 \rho}{\partial p^2} \right) + w^2 \left(\frac{\rho_n \rho_s}{\rho} - \frac{1}{2} \rho^2 a^2 \frac{\partial}{\partial p} \frac{\rho_n}{\rho} \right) = 0, \quad (5.10)$$

$$\begin{aligned} & \frac{p'}{\rho} \left(1 - a^2 \frac{\partial \rho}{\partial p} \right) + p'^2 \left(-\frac{1}{2\rho^2} \frac{\partial \rho}{\partial p} + \frac{3}{2\rho^2} \left(\frac{\partial \rho}{\partial p} \right)^2 a^2 - \frac{1}{2\rho} a^2 \frac{\partial^2 \rho}{\partial p^2} \right) - s T' + \frac{\rho_n}{\rho} a w + \\ & + p' w \frac{1}{\rho} \left(\frac{\partial \rho_n}{\partial p} - 2 \frac{\rho_n}{\rho} \frac{\partial \rho}{\partial p} \right) + w^2 \left(-\frac{\rho_n \rho_s}{2\rho^2} - \frac{\rho a^2}{2} \frac{\partial}{\partial p} \frac{\rho_n}{\rho} \right) - \frac{T'^2}{2} \frac{\partial s}{\partial T} + T' w a \frac{\partial \rho_n}{\partial T} \rho = 0, \end{aligned} \quad (5.11)$$

$$\begin{aligned} & T' \rho a \left(s + T \frac{\partial s}{\partial T} \right) - w \left(s T \rho_s + \rho_n a^2 \right) + T'^2 \rho a \left(\frac{\partial s}{\partial T} + \frac{T}{2} \frac{\partial^2 s}{\partial T^2} \right) - w T' \left(a^2 \frac{\partial \rho_n}{\partial T} + s \rho_s + T \frac{\partial(s \rho_s)}{\partial T} \right) \\ & - w p' \left(-\frac{\rho_n}{\rho} \frac{\partial \rho}{\partial p} a^2 + \frac{\partial \rho_n}{\partial p} a^2 + T s \frac{\partial \rho_s}{\partial p} \right) + w^2 a \left(T \frac{\partial \rho_n}{\partial T} + 2 \rho_s \rho_n \right) = 0. \end{aligned} \quad (5.12)$$

It can be checked that these equations reduce to the linear case described in §4 when the second order terms are neglected. It can also be seen that inserting in eqs (5.10)to (5.12) the first sound acoustic velocity, a_{10} , from (4.14), the pressure perturbation is of first order as compared with the temperature and countervelocity perturbations, whereas inserting the second sound acoustic velocity, a_{20} from (4.15) the pressure is of second order as compared with the two other variables. Furthermore in this last case the relation between the two first order quantities is:

$$T' = a_{20} \frac{\rho_n}{\rho_s} w. \quad (5.13)$$

Neglecting in (5.10) the higher order terms the following simple relation is obtained:

$$\left(1 - a^2 \frac{\partial \rho}{\partial p} \right) + \left(\frac{1}{\rho} \left(\frac{\partial \rho}{\partial p} \right)^2 - \frac{1}{2} \frac{\partial^2 \rho}{\partial p^2} \right) a^2 p' = 0, \quad (5.14)$$

from which the second order velocity of propagation of discontinuities results:

$$a_1 = a_{10} \left(1 + p' \frac{\partial}{\partial p} \ln(\rho a_{10}) \right) \quad (5.15)$$

Let us note also that for small values of the velocity jump at the discontinuity surface the pressure jump there can be approximated by the relation:

$$p' = \rho a_{10} v. \quad (5.16)$$

Using this expression in the previous equation we obtain a new relation for the second order velocity of propagation of pressure perturbations:

$$a_1 = a_{10} \left(1 + \frac{1}{2} v \frac{\partial}{\partial p} (\rho a_{10}) \right). \quad (5.17)$$

This relation coincides with the corresponding equation for the velocity of propagation of shock waves in classical fluids.

The correction term to the velocity of propagation of acoustical pressure perturbations in HeII is always positive and hence this class of shock waves can only be compression waves. It can also be checked by introducing the obtained relation for a_1 in (5.11), (5.12) that the jumps of T' and w are of second order as compared with the p' jumps.

To find the velocity of propagation of the temperature, second sound, waves we will first find the pressure increase from (5.10), which neglecting higher order terms leads to:

$$p' = -w^2 \left(\frac{\rho_n \rho_s}{\rho} - \frac{1}{2} a_{20}^2 \rho^2 \frac{\partial}{\partial p} \left(\frac{\rho_n}{\rho} \right) \right) \quad (5.18)$$

Introducing this relation in (5.11) and using (5.10), (5.12) to eliminate w , keeping only terms up to second order yields:

$$\rho \left(-s^2 \rho_2 + a^2 \frac{\partial s}{\partial T} \rho_n \right) + \rho_s s T T'^2 \left(-3 \frac{\partial s}{\partial T} + \frac{3}{2} s \frac{\rho}{\rho_n \rho_s} \frac{\partial \rho_n}{\partial T} - \frac{1}{2} s \frac{\partial T}{\partial s} \frac{\partial^2 s}{\partial T^2} \right) = 0. \quad (5.19)$$

From this equation we can deduce the velocity of propagation of temperature shock waves up to second order terms:

$$a_2 = a_{20} \left(1 + \frac{1}{2} \frac{\partial}{\partial T} \ln \left(a_{20}^3 \frac{\partial s}{\partial T} \right) T' \right), \quad (5.20)$$

this relation can be transformed to the following one:

$$a_2 = a_{20} \left(1 + \frac{\rho_n a_{20}^2}{2 \rho s} w \frac{\partial}{\partial T} \ln \left(a_{20}^3 \frac{\partial s}{\partial T} \right) \right). \quad (5.21)$$

In deriving these relations it was assumed that the counterflow velocity $\mathbf{w} = \mathbf{v}_n - \mathbf{v}_s = 0$ in front of the shock wave. When this relative velocity is $w_1 \neq 0$ before the shock wave and w_2 behind, taking into account (4.15) yields:

$$a_2 = a_{20} + \frac{1}{2} (w_1 + w_2) \frac{\rho_s s}{\rho} \frac{\partial T}{\partial s} \frac{\partial}{\partial T} \ln \left(a_{20}^3 \frac{\partial s}{\partial T} \right). \quad (5.22)$$

using instead of the relative velocities the velocities of the normal component, which in this case follows from the counterflow condition $j = 0$:

$$w = \frac{\rho}{\rho_s} v_n, \quad (5.23)$$

and denoting:

$$\alpha_2 = \frac{sT}{C} \frac{\partial}{\partial T} \ln \left(a_{20}^3 \frac{C}{T} \right). \quad (5.24)$$

where C is the specific heat, the velocity of propagation of second sound shock waves can then be written in the familiar form:

$$a_2 = a_{20} + \frac{1}{2} \alpha_2 (v_{n1} + v_{n2}) \quad (5.25)$$

It is important to note that the coefficient α_2 varies with temperature and changes sign at about $1.884K$ as shown on Fig.5.1 deduced theoretically by Khalatnikov and confirmed experimentally by Dessler and Fairbank. Thus, when a large amplitude disturbance propagates, points on the profile corresponding to larger deviations from the neutral position can move slower or faster depending on the sign of α_2 i.e. of the temperature of the fluid. This does not occur in classical fluids, where the peaks travel always faster than the troughs.

We will thus have in HeII the familiar front steepening shock waves when $1 < T < 1.884K$ or back steepening shock waves at $1.884 < T < T_\lambda$. This unique feature was already observed experimentally by Osborne and was very nicely visualised in Turners experiments reproduced on Fig.5.2 on which the remarkable existence of double shock pulses can be seen.

§6. Nonlinear second sound shock waves in HeII.

Following Turner we will use the Riemann method of characteristics to analyse nonlinear waves in HeII. Since the thermodynamic relations of superfluid helium with respect to the counterflow velocity are known only up to second order terms, i.e. w^2 terms, we limit present considerations to second order approximation. To start with we will assume that the motion is one-dimensional and reversible. We will select the velocities v, w and the thermodynamic variables p, t to describe the fluid flow. The thermodynamic relation (3.10), taking into account (5.9), will be used denoting

$$\xi_T = \frac{\partial}{\partial T} \left(\frac{\rho n}{\rho} \right) \text{ and } \xi_p = \frac{\partial}{\partial p} \left(\frac{\rho n}{\rho} \right). \quad (6.1)$$

$$\text{recalling (3.10): } d\mu = \frac{dp}{\rho} - s dT - \frac{1}{2} \frac{\rho_n}{\rho} dw^2,$$

$$\text{and } s = - \left(\frac{\partial \mu}{\partial T} \right)_{p,w^2}, \quad \frac{1}{\rho} = \left(\frac{\partial \mu}{\partial p} \right)_{T,w^2}, \quad \xi = \frac{\rho_n}{\rho} = - 2 \left(\frac{\partial \mu}{\partial (w^2)} \right)_{p,T},$$

$$\left(\frac{\partial s}{\partial (w^2)} \right)_p = - \left(\frac{\partial^2 \mu}{\partial T \partial (w^2)} \right)_p = \frac{1}{2} \xi_T, \quad \left(\frac{\partial (1/\rho)}{\partial (w^2)} \right)_T = \left(\frac{\partial^2 \mu}{\partial p \partial (w^2)} \right)_T = - \frac{1}{2} \xi_p,$$

the conservation equations up to second order terms become:

$$\text{continuity: } \frac{\partial \rho}{\partial t} + \rho^2 \xi_p w \frac{\partial w}{\partial t} + \rho \frac{\partial v}{\partial x} + v \frac{\partial p}{\partial x} = 0, \quad (6.2)$$

$$\text{bulk velocity: } \frac{\partial v}{\partial t} + \frac{1}{\rho} \frac{\partial p}{\partial x} + v \frac{\partial v}{\partial x} + 2 \frac{\rho_n \rho_s}{\rho^2} w \frac{\partial w}{\partial x} = 0, \quad (6.3)$$

$$\begin{aligned} \text{counterflow velocity: } & \frac{\partial w}{\partial t} + w \left(\frac{\rho_n}{\rho} \xi_T \frac{\partial T}{\partial t} + \frac{\rho_n}{\rho} \xi_p \frac{\partial p}{\partial t} \right) + \frac{\rho_s}{\rho_n} \frac{\partial T}{\partial x} \\ & + 3 \frac{\rho_s}{\rho} w \frac{\partial T}{\partial x} + v \frac{\partial w}{\partial x} + w \frac{\partial v}{\partial x} = 0, \end{aligned} \quad (6.4)$$

$$\begin{aligned} \text{entropy: } & \frac{\partial s}{\partial t} + \xi_T w \frac{\partial w}{\partial x} + \left(v + \frac{\rho_s}{\rho} w \right) \frac{\partial s}{\partial x} + \frac{\rho_s}{\rho} s \frac{\partial w}{\partial x} + \\ & - s w \left(\xi_T \frac{\partial T}{\partial x} + \xi_p \frac{\partial p}{\partial x} \right) + \frac{\rho_s s}{\rho^2} w \frac{\partial p}{\partial x} = 0. \end{aligned} \quad (6.5)$$

In principle these four equations could be solved using one of the standard methods, but the algebra involved, as they are coupled, nonlinear, complicated is overwhelming particularly as the characteristic equation is of fourth order. However if the thermodynamics is approximated by the linear relations with-

out the w^2 terms, i.e. if :

$$\left. \begin{aligned} d\rho &= \frac{\gamma}{a^2} dp - \rho \beta dT, \\ ds &= \frac{C_p}{T} dT - \frac{\beta}{\rho} dp, \end{aligned} \right\} \quad (6.6)$$

where: $\gamma = C_p/C_v$, $\beta = \frac{1}{1/\rho} \frac{\partial(1/\rho)}{\partial T}$

then the temperature and pressure variations decouple when β tends to zero. This condition is satisfied except at temperatures close to T_λ . Finite amplitude waves however still remain coupled through the counterflow velocity dependence implicit in the two velocity field hydrodynamics. Thus second sound waves produce p and v variations of order w^2 in addition to those of order βw . Fortunately if terms of order larger than two are neglected the continuity and bulk velocity equations uncouple from those of counterflow velocity and entropy.

Assuming that only II-nd sound waves are present they are described by the following two equations:

$$\begin{aligned} \frac{\rho_n}{\rho} \frac{\partial w}{\partial t} + w \xi_T \frac{\partial T}{\partial t} + s \frac{\partial T}{\partial x} + 3 \frac{\rho_n \rho}{\rho^2} w \frac{\partial w}{\partial x} &= 0, \\ \frac{C_p}{T} \frac{\partial T}{\partial t} + \xi_T w \frac{\partial w}{\partial t} + \left(\frac{\rho_s}{\rho} \frac{C_p}{T} - s \xi_T \right) w \frac{\partial T}{\partial x} + \frac{\rho_s}{\rho} s \frac{\partial w}{\partial x} &= 0. \end{aligned} \quad (6.7)$$

To put these equations in a characteristic form we multiply the first one by Λ/s and the second one by T/C_p and add them (Λ is in units of velocity).

$$\begin{aligned} \left(\Lambda \frac{\rho_n}{\rho_s} + T \xi_T \frac{w}{C_p} \right) \frac{\partial w}{\partial t} + \left(3 \frac{\rho_n \rho_s}{\rho^2} \frac{w}{s} + \frac{\rho_s}{\rho} \frac{T s}{C_p} \right) \frac{\partial w}{\partial t} + \left(\Lambda \frac{w}{s} \xi_T + 1 \right) \frac{\partial T}{\partial t} + \\ \left(\Lambda + \frac{\rho_s}{\rho} w - T \xi_T \frac{s}{C_p} w \right) \frac{\partial T}{\partial x} &= 0. \end{aligned} \quad (6.8)$$

The w and T derivatives must be then in the same direction in the $x-t$ space. This means that there exists a characteristic real velocity u which is identical for the variations of both w and T :

$$u = \frac{\Lambda + \frac{\rho_s}{\rho} w - T \xi_T \frac{s}{C_p} w}{\Lambda \frac{w}{s} \xi_T + 1} = \frac{3\Lambda \frac{\rho_n \rho_s}{\rho^2} \frac{w}{s} + \frac{\rho_s}{\rho} \frac{T s}{C_p}}{\Lambda \frac{\rho_n}{\rho s} + T \xi_T \frac{w}{C_p}} . \quad (6.9)$$

The following relation for Λ is obtained from the above equations:

$$\left(\frac{\rho_n}{\rho_s} - 3 \frac{\rho_n \rho}{\rho^2} \frac{w^2 \xi_T}{s^2} \right) \Lambda^2 - \left(2 \frac{\rho_n \rho_s}{\rho^2} \frac{w}{s} \right) \Lambda - \frac{\rho_s T s}{\rho C_p} + \left(\frac{\rho_s}{\rho} - T \xi_T \frac{s}{C_p} \right) T \xi_T \frac{w^2}{C_p} = 0. \quad (6.10)$$

Hence up to terms of first order in w :

$$\Lambda_{\pm} = \pm a_{20} + \frac{\rho_s}{\rho} w + O(w^2). \quad (6.11)$$

Substituting this value of Λ in (6.9) there follows:

$$u_{\pm} = \pm a_{20} + \left[2 \frac{\rho_s}{\rho} - \left(\frac{\rho}{\rho_n} T \xi_T \right) \frac{s}{C_p} \right] w + O(w^2). \quad (6.12)$$

The expression in square brackets can be considered as the entrainment of second sound by the counterflow velocity. It is interesting to note that C_p/s and $(\rho/\rho_n)T\xi_T$ are independent of T and very nearly equal at temperatures above $1.2K$. Hence the expression in square brackets becomes approximately:

$$\varphi \approx (\rho_s - \rho_n)/\rho \quad (6.13)$$

This coefficient, φ , is approximately equal to the Khalatnikov non-linearity coefficient obtained solving the full set of linear equations in a moving medium. At saturated vapour pressures $\rho_n = \rho_s$ at $1.97K$, hence at lower temperatures convection occurs in the direction of w and at higher temperatures in the opposite direction.

It can be seen, after some transformations using (6.12), that the equations for w and T can be written in the simple form:

$$\left(\frac{\partial}{\partial t} + u_{\pm} \frac{\partial}{\partial x} \right) w \pm \left(\frac{\rho_s}{\rho_n a_{20}} \right) \left(\frac{\partial}{\partial t} + u_{\pm} \frac{\partial}{\partial x} \right) T = 0. \quad (6.14)$$

This relation leads to the introduction of the Riemann invariants:

$$R_{\pm} = w + \int \frac{\rho_s}{\rho_n a_{20}} dT \quad (6.15)$$

and when $v \neq 0$ (6.14) can be written as follows:

$$\left(\frac{\partial}{\partial t} + (v + \varphi w \pm a) \frac{\partial}{\partial x} \right) R_{\pm} = 0. \quad (6.16)$$

The Riemann invariants as known vary from one characteristic to another but remain constant along each characteristic curve C_{\pm} in the x,t space given by:

$$\frac{dx}{dt} = u_{\pm} - v + \varphi w \pm a_{20}. \quad (6.17)$$

The approximate second order theory describes the evolution of non-steady compression and expansion shock waves. Consider e.g. a simple second sound wave, (ρ, φ are then constant) travelling along the x axis. Assume also that the counterflow condition $v=0$ is satisfied. Then along a characteristic R_+ will remain constant, hence (6.16), (6.15) yield

$$w = \int_{T_0}^T \frac{\rho s}{\rho_n a_{20}} dT \quad (6.18)$$

where $T=T_0$ corresponds to $w=0$. In the linear case we would have:

$$w = \left(\frac{\rho s}{\rho_n a_{20}} \right) (T - T_0) \quad (6.19)$$

The direct correspondence between w and T indicates that only one dependent variable is necessary to determine the flow produced by a simple wave:

$$R_+ = w + \int \frac{\rho s}{\rho_n a_{20}} dT = 2w. \quad (6.20)$$

Introducing this relation in (6.16) for w and T there follows;

$$\left. \begin{aligned} \frac{\partial w}{\partial t} + (\varphi w + a_{20}) \frac{\partial w}{\partial x} &= 0, \\ \frac{\partial T}{\partial x} + (\varphi w + a_{20}) \frac{\partial T}{\partial x} &= 0. \end{aligned} \right\} \quad (6.21)$$

As the characteristic velocity, which is a function only of T , remains constant along C_+ , hence the characteristic curve is a straight line. The velocity along the characteristic can be written in terms of w and $T-T_0$ approximately as follows:

$$u = u_0 + \left(\frac{\partial u}{\partial w} \right)_0 w + \left(\frac{\partial u}{\partial T} \right)_0 (T - T_0) + \dots \quad (6.22)$$

where

$$\left(\frac{\partial u}{\partial w} \right)_0 = \varphi, \quad \left(\frac{\partial u}{\partial T} \right)_0 = \frac{\partial a_{20}}{\partial T}, \quad \frac{\partial w}{\partial T} = \frac{\rho s}{\rho_n a_{20}},$$

and to first order in temperature:

$$u = a_0 (1 + b_0 \Theta), \quad \Theta = \frac{T - T_0}{T_0}. \quad (6.23)$$

The steepening coefficient is:

$$b_0 = \frac{T}{a_{20}} \left(\frac{\rho s}{\rho_n a_{20}} + \frac{\partial a_{20}}{\partial T} \right) = T \frac{\partial}{\partial T} \left[\log \left(a_{20}^3 \frac{C_p}{T} \right) \right], \quad (6.24)$$

hence

$$\frac{\partial \Theta}{\partial t} + a_{20}(1+b_0 \Theta) \frac{\partial \Theta}{\partial x} = 0. \quad (6.25)$$

The condition before the start of the perturbation is taken to be $w = 0, T = T_0$.

The front and rear steepening shock waves are shown on Figs 6.1, where the evolution of a trapezoidal temperature or velocity pulse is illustrated. The existence of temperature raising and temperature lowering shock waves is unique for HELL (in ordinary fluids only compression shocks are permissible except at a critical point or phase transition). Analysing the variation of the area under the wave profile (see Fig.6.2):

$$\int_{T_0}^{\infty} x(T) dT = \text{const.} \quad (6.26)$$

as the characteristic velocity of a point of a simple wave depends only on a single variable (T, w or s) and not on the local shape (gradients). Hence the function $x(T)$ does not change as the wave evolves as it depends only on the local value of the temperature. This is true also of w or s , hence the total entropy excess remains constant. Note that this approximate entropy conservation breaks down when $\text{grad } T$ and $\text{grad } w$ becomes very large and the local temperature depends also on the gradients and hence the length $x(T)$ will depend on them also.

As a second sound wave front steepnes the $\text{grad}(w, T)$ begin to generate appreciable entropy and the assumption of dissipationless flow breaks down. The growing dissipation tends to smooth out the large gradients. Eventually equilibrium between nonlinear steepening and irreversible dissipation is attained.

In shock waves, as known, the jump conditions are determined from the equilibrium states far ahead and behind the shock. It is not necessary to solve the much more difficult problem of the shock structure where non-equilibrium thermodynamics becomes important. Using a reference frame attached to the shock the jump relations are independent of time. They can be integrated perpendicularly to the shock and evaluated at the fore and aft equilibrium regions. The resulting set of algebraic equations can be solved for given jump conditions and shock velocity.

The full results of the second order shock theory are summarized below:

- shock wave Mach number

$$M_s = 1 + b_0 \Delta \Theta / 2 = u_s / a_{20} = (u_0 + u_1) / 2a_{20}, \quad (6.27)$$

- relative velocity jump

$$\Delta w = a_{20} \left(\frac{\rho C_p}{\rho_s s} \right) \Delta \Theta \left[1 + \frac{1}{2} \left(T \frac{\partial}{\partial T} \left(\log a_{20} \frac{C_p \rho^2}{T \rho_s^2} \right) \right)_0 \Delta \Theta \right], \quad (6.28)$$

- shock structure

$$T(x) = T_0 + \frac{1}{2} (T_1 - T_0) \left(1 + \tanh \frac{2x}{\delta} \right), \quad (6.29)$$

- shock thickness

$$\delta = \left(\frac{4D}{a_{20}} \right)_0 \frac{1}{b_0 \Delta \Theta} = \left(\frac{2D}{a_{20}} \right) \frac{1}{M_s - 1}, \quad (6.30)$$

- where

$$D = \frac{1}{\rho} \left[\frac{x}{C_p} + \frac{\rho_s}{\rho_n} \left(\frac{4}{3} \eta + \zeta_2 - 2\rho \zeta_1 + \rho^2 \zeta_3 \right) \right], \quad (6.31)$$

- irreversible entropy jump

$$\Delta s = \frac{1}{6} b_0 (\Delta \Theta)^3 C_p. \quad (6.32)$$

It should be noted that, although the above results correspond to the same order of approximation as for the unsteady reversible second sound waves, the difference results from the irreversibility assumption. The dissipation necessary to have a steady shock front invalidates the assumption of entropy conservation.

Plotting the shock wave thickness multiplied by the relative velocity jump, see Fig.6.3, it is noted that at $T=1.884\text{ K}$ when the steepness becomes zero the normalised shock thickness diverges even for an infinitesimally small shock strength. Let us examine approximately finite amplitude shock waves whose temperature is spanning the $b_0=0$ temperature which we will denote as T_b . We will use close to this temperature a linear approximation to the steepness coefficient:

$$b(p, T) = - B_b (T - T_b) / T_b. \quad (6.33)$$

The equation of the characteristic velocity near this region is:

$$\frac{u}{a_{20}} = 1 + b\Theta = 1 - B_b \left(\frac{T - T_b}{T_b} \right) \left(\frac{T - T_0}{T_0} \right). \quad (6.34)$$

This relation is illustrated on Fig.6.4 for a positive temperature pulse spanning the shock thickness divergence temperature T_b . For temperatures where $\partial u / \partial T > 0$ the front edge of the shock will steepen forming a temperature rising shock structure. At slightly larger T the wave front would tend to unsteepen but the characteristic velocity is still $u > u_s$. When the temperature increases to the value corresponding to $u < u_s$ an expansion wave appears. This results in a shock front and an expansion fan at the front of the shock pulse and similarly at its rear end a temperature lowering shock followed by another expansion fan evolve.

Such double shock configurations have also been observed in ultra strong shock waves in solids when phase changes occur. Complex configurations have also been found in fluids when $(\partial^2 p / \partial V^2)_s$ changes sign, as described in other lectures.

Double shocks in HELL occur close to T_b even if T_b is not spanned as illustrated on Fig. 6.5 when

$$0 < T_1 - (T_0 + T_b)/2 < \sqrt{2}(T_b - T_0)/4. \quad (6.35)$$

In this case there is no expansion wave between the temperature rising and temperature lowering shocks. The back steepened shock propagates then faster and eventually will overtake the front one.

The evolution of a double shock structure is quite involved and different scenarios can be expected depending on the shock strength and its closeness to the T_b temperature. If we follow for example a large amplitude shock crossing the T_b point this initially becomes a double shock with an expansion wave between its temperature raising and lowering branches. The expansion wave will move towards the rear branch of the shock overtaking it and decay in this process. The velocity of the rear shock, propagating initially slower than the front one and causing the double shock to spread, will increase as it decays. When the amplitude of the double shock decreases so much that the intermediate expansion wave disappears the rear shock will be travelling faster than the front one. The double shock will decay by decreasing in width until it disappears. What remains in this case is a decaying shock expansion pulse.

§7. The structure of moderate second sound shock waves in HeII.

In our previous analysis of the dissipationless shock wave problem the nonlinear terms implied the possible existence of a surface of discontinuity where the jump of the flow parameters takes place. The problem was thus greatly simplified and yielded, as we have seen, some important data on the main properties of the shock waves in HeII. However it is also of interest to have a closer look at the physical region of finite thickness where the transition between the two equilibrium states, existing at infinity on both sides of the shock wave, takes place. As the balance between the smoothing dissipative terms and the steepening nonlinear terms govern this region our analysis must be based on the set of the full nonlinear dissipative equations given in §3.

We will consider presently the case of plane waves and instead of using the classical approach, consisting mainly in solving the second order perturbation of the conservation and superflow equations applied very successfully e.g. by Turner, we will present the recently published third order development in series method of Atkin and Fox. Furthermore taking advantage of our gained experience on acoustic waves we will assume that the counterflow conditions are satisfied, i.e. $\rho v = 0$, and as estimated by the above authors viscosity as opposed to thermal conductivity can be neglected.

The conservation and superfluid equations concerning the dependent variables ρ , v , v_s , and the internal energy per unit mass, U , in a slightly different but equivalent form to those used in §3 can be written as follows:

$$\frac{\partial \rho}{\partial t} + \frac{\partial \rho v}{\partial x} = 0, \quad (7.1)$$

$$\rho \frac{\partial v}{\partial t} + v \frac{\partial v}{\partial x} - \frac{\partial P}{\partial x} = 0, \quad (7.2)$$

$$\rho \frac{\partial}{\partial t} \left(v^2/2 + U \right) + \rho \frac{\partial}{\partial x} \left(v^2/2 + U \right) + \frac{\partial}{\partial x} \left(Q + \Lambda - Pv \right), \quad (7.3)$$

$$\frac{\partial v_s}{\partial t} + v_s \frac{\partial v_s}{\partial x} + \frac{\partial u}{\partial x} = 0, \quad (7.4)$$

where: P is the normal stress acting on the surface perpendicular to the direction of the wave propagation x , the heat flux is Q . The total energy flux is $Q - Pv + \Lambda$, where Λ is the additional flux due to the superfluid component, the other two terms correspond to the classical energy flux. The remaining quantities used in the above set of equations are:

$$P = -p - \rho \gamma v_s^2, \quad (7.5)$$

where

$$\gamma = \rho_s / \rho_n.$$

$$Q = \rho T s \gamma v_s - \kappa \rho \frac{\partial T}{\partial x} \quad (7.6)$$

where $\kappa \rho$ is the thermal conductivity and

$$\Lambda = \rho \gamma^2 v_s^2. \quad (7.7)$$

As expansions in powers of the temperature variation will be used it is convenient to introduce the Helmholtz function:

$$F = U - Ts, \quad (7.8)$$

related to the chemical potential by the following relation;

$$\mu = F + p/\rho - (1/2 + \gamma) v_s^2 \quad (7.9)$$

We will look now for a travelling wave solution with a steady wave profile propagating with a constant velocity a in the x direction and use as the independent variable $\xi = x - at$, hence: and in this class of solutions the following

$$\rho = \rho(\xi), \quad v = v(\xi), \quad v_s = v_s(\xi), \quad T = T_1 + \Theta(\xi). \quad (7.10)$$

operator relations hold:

$$\frac{\partial}{\partial t} = -a \frac{\partial}{\partial \xi}, \quad \frac{\partial}{\partial x} = \frac{\partial}{\partial \xi}. \quad (7.11)$$

Equations (7.1) to (7.4) can now be integrated and using the relations (7.5) to (7.7) after some transformations reduced to the following set:

$$\rho(v - a) = \text{const.}, \quad (7.12)$$

$$-P + \rho(v - a) = \text{const.}, \quad (7.13)$$

$$\mu + \frac{1}{2}(v_s - a)^2 = \text{const.}, \quad (7.14)$$

$$\rho T s(v_n - a) - \kappa \rho \frac{\partial T}{\partial \xi} + \rho_n(v_n - a)^2 w = \text{const.} \quad (7.15)$$

Taking into account the counterflow condition $v = 0$, (7.11) implies $\rho = \text{const.}$ and to satisfy (7.13) we must have:

$$-P = p + \rho \gamma v_s^2 \quad (7.16)$$

Using this last relation and (7.9) in (7.14) and (7.15) yields:

$$av_s - F + 2\gamma v_s^2 = \text{const.} \quad (7.17)$$

$$a(F + Ts\gamma v_s) + \kappa \frac{\partial \vartheta}{\partial \xi} - \gamma^2 v_s^3 = \text{const.} \quad (7.18)$$

To describe a shock wave structure the solution of (7.17), (7.18) must satisfy the following conditions taking into account that equilibrium prevails at infinity on both sides of the shock wave.

$$\left. \begin{aligned} \vartheta &= 0, \quad \frac{\partial \vartheta}{\partial \xi} = 0, \quad w = 0, \quad \text{at } \xi = +\infty, \\ T_2 - T_1 &= h, \quad \frac{\partial \vartheta}{\partial \xi} = 0, \quad w = 0, \quad \text{at } \xi = -\infty. \end{aligned} \right\} (7.19)$$

where ϑ is the difference of the local temperature and its value at infinity ahead of the shock wave, and h is the difference of the temperatures at infinity on both sides of the shock. Since at infinity all flow parameters tend to uniform values hence, denoting by square brackets the jump of the corresponding arguments at $+\infty$ and $-\infty$, equations (7.17), (7.18) can be formulated as follows:

$$\left. \begin{aligned} [av_s - F + 2\gamma v_s^2] &= 0, \\ [a(F + Ts) + Ts\gamma v_s + \gamma^2 v_s^3] &= 0. \end{aligned} \right\} (7.20)$$

These relations agree, as they should, with those obtained in §5. To calculate now the structure of the shock wave it is necessary to use an approximate solution correct up to third order in h and v_s and therefore according to Atkins and Fox the following series development of the thermodynamic variables is used:

$$\left. \begin{aligned} F &= F_0 - s_0 \vartheta - \frac{1}{2} s_1 \vartheta - \frac{1}{6} s_2 \vartheta - \frac{1}{24} s_3 \vartheta + \frac{1}{2} (\gamma_0 + \gamma_1 \vartheta + \frac{1}{2} \gamma_2 \vartheta) v_s + \frac{\varepsilon}{2} v_s^2, \\ s &= s_0 + s_1 \vartheta + \frac{1}{2} s_2 \vartheta^2 + \frac{1}{6} s_3 \vartheta^3 - \frac{1}{2} (\gamma_1 + \gamma_2 \vartheta) v_s^2, \\ \gamma &= \gamma_0 + \gamma_1 \vartheta + \frac{1}{2} \gamma_2 \vartheta^2 + 2\varepsilon v_s^2, \end{aligned} \right\} (7.21)$$

where the numbers in the subscripts of s and γ indicate derivatives with respect

to ϑ evaluated at $T_1 = 0$, $v_s = 0$, e.g.

$$s_O = s(0,0), \quad s_i = -\frac{\partial^i s}{\partial \vartheta^i}(\vartheta, v_s^2) \text{ and } \varepsilon = \frac{1}{2} \frac{\partial \gamma}{\partial v_s^2}, \quad (7.22)$$

and the following thermodynamic relation of $F = F(\rho, T, v_s^2)$ are used

$$s = -\frac{\partial F}{\partial T}, \quad p = \rho^2 \frac{\partial F}{\partial \rho}, \quad \gamma = 2 \frac{\partial F}{\partial v_s^2}. \quad (7.23)$$

Substituting these expressions in (7.17) and taking into account the conditions at infinity yields a quadratic relation for v_s

$$-av_s + s_O\vartheta + \frac{1}{2}s_1\vartheta^2 + \frac{1}{6}s_2\vartheta^3 + \frac{3}{2}(\gamma_O + \gamma_1\vartheta)v_s^2 = 0. \quad (7.24)$$

The relevant solution developed in powers of ϑ is:

$$v_s = \frac{s_O}{a}\vartheta + \left(\frac{s_1}{2a} + \frac{3\gamma_O s_O^2}{2a^3} \right)\vartheta^2 + \left(\frac{s_2}{6a} + \frac{3s_O}{2a^3}(\gamma_O s_1 + \gamma_1 s_O) + \frac{9\gamma_O^2 s_O^3}{2a^5} \right)\vartheta^3 + O(\vartheta^4). \quad (7.25)$$

Substituting the obtained relation for v_s in (7.18), assuming x is constant and neglecting terms of higher order in ϑ the following equation for ϑ is obtained:

$$x \frac{d\vartheta}{d\xi} = \varphi_1\vartheta + \varphi_2\vartheta^2 + \varphi_3\vartheta^3 \quad (7.26)$$

where:

$$\varphi_1 = aT_O s_1 + a^{-1}T_1 s_O^2 \gamma_O,$$

$$\varphi_2 = -\frac{a}{2}(s_1 + T_O s_2) + \frac{a^{-1}}{2}(s_O^2 \gamma_O + 3s_O^2 T_O \gamma_1 + 3T_O s_O s_1 \gamma_O) + \frac{3}{2}a^{-3}T_O s_O^3 \gamma_O^2,$$

$$\varphi_3 = -a\left(\frac{1}{3}s_2 + \frac{1}{6}T_O s_3\right) + a^{-1}\left((s_O s_1 + \frac{2}{3}T_O s_O s_2 + \frac{1}{2}T_O s_1^2)\gamma_O + (2T_O s_O s_1 + s_O^2)\gamma_1\right) \quad (7.27)$$

$$+ T_O s_O^2 \gamma_2\right) + a^{-3}\left((3T_O s_O^2 s_1 + s_O^3)\gamma_O^2 + 4T_O s_O^3 \gamma_O \gamma_1 + 2T_O s_O^4 \varepsilon\right) + \frac{9}{2}a^{-5}T_O s_O^4 \gamma_O^3.$$

As shown by Atkin and Fox (7.20) leads to an expression for the second sound velocity :

$$a = u_O + u_1 h + u_2 h^2 + O(h^3), \quad (7.28)$$

where:

$$u_O = s_O \left(\frac{\gamma_O}{s_1} \right)^{1/2},$$

$$\left. \begin{aligned} u_1 &= \frac{u_0}{2} \left(\frac{3s_1}{s_0} + \frac{3\gamma_1}{2\gamma_0} - \frac{s_2}{2s_1} \right), \\ u_2 &= \frac{u_0}{2} \left(\frac{5s_1^2}{4s_0^2} - \frac{9\gamma_1^2}{16\gamma_0^2} + \frac{3s_2^2}{16s_1^2} + \frac{3s_1\gamma_1}{2s_0\gamma_0} - \frac{3s_2\gamma_1}{8s_1\gamma_0} + \frac{2s_2}{3s_0} + \frac{s_1}{2T_0s_0} \right. \\ &\quad \left. + \frac{\gamma_1}{4T_0\gamma_0} - \frac{s_2}{12T_0s_1} - \frac{s_3}{6s_1} + \frac{\gamma_2}{\gamma_0} + \frac{2s_1\varepsilon}{\gamma_0^2} \right), \end{aligned} \right\} (7.29)$$

and $u_0 = a_{20}$. The Khalatnikov coefficient α_2 corresponds to:

$$\alpha_2 = \frac{2u_1 s_0}{u_0 s_1}. \quad (7.30)$$

Substituting (7.28) into (7.27) yields:

$$\left. \begin{aligned} \varphi_1 &= \varphi_{11}h + \varphi_{12}h^2 + O(h^3), \\ \varphi_2 &= \varphi_{20}h + \varphi_{21}h + O(h^2), \\ \varphi_3 &= \varphi_{30} + O(h), \end{aligned} \right\} (7.31)$$

where:

$$\left. \begin{aligned} \varphi_{11} &= -2T s u, & \varphi_{12} &= T_0 s_1 \left(-2u_2 + \left(\frac{u_1^2}{u_0} \right) \right), \\ \varphi_{20} &= u_0 T_0 s_1 \left(-\frac{s_2}{2s_1} + \frac{3\gamma_1}{2\gamma_0} + \frac{3s_1}{s_0} \right), \\ \varphi_{21} &= -\frac{u_1 T_0 s_1}{2} \left(\frac{2}{T_0} + \frac{s_2}{s_1} + \frac{12s_1}{s_0} + \frac{3\gamma_1}{\gamma_0} \right), \\ \varphi_{30} &= u_0 \left(-\frac{s_2}{3} + \frac{T_0 s_3}{6} + \frac{2s_1^2}{s_0} + \frac{2T_0 s_1 s_2}{3s_0} + \frac{8T_0 s_1^3}{s_0^2} \right. \\ &\quad \left. + \frac{6T_0 s_1^2 \gamma_1}{s_0 \gamma_0} + \frac{\gamma_1 s_1}{\gamma_0} + \frac{T_0 s_1 \gamma_2}{\gamma_0} + \frac{2T_0 s_1^2 \varepsilon}{\gamma^2} \right) \end{aligned} \right\} (7.32)$$

$$\varphi_{11} + \varphi_{20} = 0, \quad \varphi_{12} + \varphi_{21} + \varphi_{30} = 0, \quad (7.33)$$

and it can be checked that $\partial \Rightarrow h = T_2 - T_1$ as $d\theta/d\xi \Rightarrow 0$.

Having now the relations for all the φ 's with indices (7.26) can be integrated to obtain the following approximate expression for the shock wave structure up to third order terms:

$$\frac{\xi}{\rho x} = \frac{\log|\vartheta|}{h(\varphi_{11} + \varphi_{12}h)} - \frac{\log|h-\vartheta|}{h(\varphi_{11} + (\varphi_{21} + 2\varphi_{12})h)} \\ - \frac{\varphi_{21} + \varphi_{12}}{(\varphi_{11} + \varphi_{12}h)(\varphi_{11} + (\varphi_{21} + 2\varphi_{12})h)} \times \log \left| \frac{\varphi_{11} + \varphi_{12}h}{\varphi_{21} + \varphi_{12}} + \vartheta \right| + \text{const.} \quad (7.34)$$

The constant in this last equation is determined by selecting the position of the origin say $\vartheta = h/2$ at $\xi = 0$.

The shock wave structure of the temperature as given by (7.34) is deduced using terms up to third order in ϑ . When the basic equations (7.17), (7.18) are third order terms then:

$$\varphi_{12} = \varphi_{21} = \varphi_{30} = 0 \quad (7.35)$$

taken neglecting and (7.34) is substantially simplified and reduced to the approximate form:

$$\left(\frac{\xi}{\rho x} \right)_2 = \frac{1}{h \varphi_{11}} \log \left(\frac{\vartheta}{h-\vartheta} \right) \quad (7.36)$$

However this approximation breaks down at $T_1 = 1.884K$ when $u_1 = \alpha_2 = \varphi_{11} = 0$, and also $\varphi_{11} = 0$, according to (7.32). It follows from (7.34), with third order terms, that at $T = 1.884K$ the shock wave shape is given by:

$$\left(\frac{\xi}{\rho x} \right)_3 = \frac{1}{2h^2 \varphi_{12}} \log \left| \frac{\vartheta^2}{h^2 - \vartheta^2} \right| \quad (7.37)$$

Knowing the shape of the shock wave we can determine its thickness, defined according to Prandtl as $\Lambda_s = h(\partial\vartheta/\partial\xi)_{\max}$. As can be seen from the last two relations at $T = 1.884K$

$$\Lambda_{s3} = \frac{3\sqrt{3}\rho x}{2h^2 \varphi_{12}} \quad (7.38)$$

and not too close to this temperature, say at T lower than 1.8 or higher than 1.95K, the shock wave thickness can be calculated from (7.36) yielding:

$$\Lambda_{s2} = \frac{4\rho x}{h\varphi_{11}} . \quad (7.39)$$

The calculated normalised shock wave structures at temperatures close to $T = 1.8K$ are shown illustrated in Fig.7.1.

§8. Clamped superfluid flows. Fourth sound.

As known in classical fluid mechanics (see e.g. Batchelor) there exist a certain length which characterises how far is the main flow influenced strongly by the viscous effects. For example how far does the no slip boundary condition have a predominant influence on the overall flow. This is the so called viscous penetration depth λ_v given by the relation:

$$\lambda_v = \sqrt{\left(\frac{2\eta_n}{\omega\varrho_n}\right)} \quad (8.1)$$

where we have introduced already the density and viscosity values of the normal component.

Having this background we can imagine that in channels or tubes whose semi width or radius l_d is smaller than the penetration depth the motion of the normal component will be restrained. Hence in the extreme cases when $l_d \ll \lambda_v$ the normal fluid will be stationary with respect to the stationary wall of the container filled with HeII. In this case only the flow of the superfluid component will be possible. The oscillatory flow in this case is called fourth sound.

The velocity of propagation of small perturbations in this idealised incompressible case can be obtained from the linearised system of Landau's equations assuming that the normal velocity component is zero, $v_n \equiv 0$. As in this case the number of unknown dependent variables is 5 the following set of equations is relevant:

$$\left. \begin{aligned} \frac{\partial \varrho}{\partial t} + \varrho \operatorname{div} \mathbf{v}_s &= 0, \\ \frac{\partial \mathbf{v}_s}{\partial t} + \operatorname{grad} \mu &= 0, \\ \frac{\partial \varrho s}{\partial t} &= 0. \end{aligned} \right\} \quad (8.2)$$

Eliminating v_s from the first two equations we obtain:

$$\frac{\partial^2 \rho}{\partial t^2} = \frac{\rho_s}{\rho} \Delta p - s \rho_s \Delta T. \quad (8.3)$$

Neglecting thermal expansion, $\partial \rho / \partial T = 0$, the third equation (8.2) be :

$$\rho \left(\frac{\partial s}{\partial T} \right) \Delta T + s \left(\frac{\partial \rho}{\partial p} \right) \Delta p = 0. \quad (8.4)$$

The last two equations yield the wave equation for p :

$$\frac{\partial^2 p}{\partial t^2} - \left[\frac{\rho_s}{\rho} \left(\frac{\partial p}{\partial \rho} \right) + \frac{\rho_s s^2}{\rho \left(\frac{\partial s}{\partial t} \right)} \right] \Delta p = 0. \quad (8.5)$$

The propagation velocity of a travelling wave solution to these last two equations is given by the following equation:

$$a_4 = (\rho_s / \rho) a_{10}^2 + (\rho_n / \rho) a_{20}^2, \quad (8.6)$$

where a_{10} and a_{20} are the first and second sound velocities given already in §4.

It can be noted that at the extreme temperatures close to T_λ : $a_4 \rightarrow a_{20}$ and at the lowest temperatures $a_4 \rightarrow a_{10}$. The variation of the fourth sound velocity with temperature as compared with first and second sound velocities is illustrated on Fig.4.1. We will not consider the more involved non linear fourth sound problem is considered in the paper of Torczynski and the case when v_n is not strictly equal zero and viscosity and heat conductivity is taken into account is given by Adamenko.

§9 Surface waves: capillary and thin film third sound waves.

At the free surface of a deep layer of superfluid helium or on thin films formed on a solid substrate there can exist waves propagating along the surface. These waves, similarly as in the case of fourth sound are restricted in their motion by viscosity effects.

We will consider first, following Khalatnikov, the case of small amplitude capillary waves. Of course in this case the linearised equations given in §4 will be relevant and neglecting the second order effects due to the presence of helium vapour above the free surface, the following boundary conditions must be satisfied.

- The mass conservation requirement at the free surface is satisfied writing that the total flux of the liquid across a unit area must be zero:

$$j_z - \rho \frac{\partial \zeta}{\partial t} = \rho_s v_{sz} + \rho_n v_{nz} - \rho \frac{\partial \zeta}{\partial t} = 0, \quad (9.1)$$

where ζ is the displacement, of a point on the surface of the liquid from its equilibrium position, in the z direction normal to the free undisturbed surface, (x,y) , see Fig.9.1 – Neglecting evaporation and heat transfer the entropy flux across the surface must

$$s(v_{nz} - \partial \zeta / \partial t) = 0. \quad (9.2)$$

- The pressure at the free surface must be balanced by the force due to surface tension:

$$p = \gamma(\partial^2 \zeta / \partial x^2 + \partial^2 \zeta / \partial z^2), \quad (9.3)$$

where γ is the coefficient of surface tension.

From (9.1) and (9.2) it can be seen that the z components of both velocities must be equal to the velocity of the free surface:

$$v = v = \partial \zeta / \partial t. \quad (9.4)$$

Let us now seek a travelling wave solution propagating in the x direction and decaying in the z direction. In this case all dependent quantities will vary as:

$$e^{-\alpha z} \exp(ikx - i\omega t) \quad (9.5)$$

where α is the decay coefficient in the direction perpendicular to the free surface.

The linearised hydrodynamic equations become wave equations and the frequency ω and the wave number k are related by the dispersion relation:

$$\omega^2/a^2 = k^2 - \alpha^2. \quad (9.6)$$

Note that in the limit of very small frequencies, $\omega \rightarrow 0$, we have $\alpha = k$.

The momentum conservation equation (4.3) in the z direction yield the following relation which should be also satisfied at the free surface:

$$i\omega j_z = \alpha p. \quad (9.7)$$

It should be noted that j and p correspond to the perturbation of these variables from their equilibrium values produced by the capillary waves.

From (9.3) there follows:

$$p + \gamma k^2 \zeta = 0. \quad (9.8)$$

Equations (9.1), (9.8) and (9.7) yield the following dispersion relation:

$$\omega^2 = (\gamma/\rho)k^3. \quad (9.9)$$

As could be expected from (9.4) the dispersion is the same as for classical fluids.

Let us now, following Puterman, consider the case of thin films (of the order of 10 μm thick) formed on a solid surface being in contact with the vapour of HeII. This is due to the short range Van der Waals attraction forces acting between the molecules of a substrate and the vapour. In the case of HeII a "part" of the film will behave like a superfluid and the remaining part like a normal fluid. The viscosity of the normal fluid component will prevent

its motion in the thin layer of the film.

The superfluid component will flow towards the lower chemical potential position according to its equation of motion (4.4) supplemented by an additional term due to the existence of external forces having a potential Ω :

$$D_s \mathbf{v}_s / Dt = - \operatorname{grad}(\mu + \Omega). \quad (9.10)$$

Unlike in the case of fourth sound (in a capillary) the velocity of the normal component is not restricted in the direction perpendicular to the wall, $v_{n\perp} \neq 0$. To describe the motion of the fluid we will need hence 6 equations. The additional required equation will be the momentum conservation equation in the direction perpendicular to the wall. The full set of equations in this case is:

$$\left. \begin{aligned} \partial \rho / \partial t + \operatorname{div} \rho_s \mathbf{v}_s + \operatorname{grad}_{\perp} \rho_n v_{n\perp} &= 0, \\ \partial \rho_s / \partial t + \operatorname{grad}_{\perp} \rho_s v_{n\perp} &= 0, \\ D_s \mathbf{v}_s / Dt = - \operatorname{grad}(\mu + \Omega) & \\ \frac{\partial}{\partial t} (\rho_s \mathbf{v}_s + \rho_n \mathbf{v}_n)_{\perp} + \operatorname{grad}_{\perp} p + \operatorname{grad}(\rho_n v_{n\perp} v_{n\perp}) + \frac{\partial}{\partial r_{\alpha}} (\rho_s v_{s\perp} v_{s\perp}) + \rho \operatorname{grad}_{\perp} \Omega &= 0, \end{aligned} \right\} \quad (9.11)$$

where

$$d\mu = -sdt + dp/\rho - \rho_n d(v_s^2 + v_{n\perp}^2 - 2v_{s\perp}v_{n\perp}). \quad (9.12)$$

The potential Ω will generally consist of a gravity and a Van der Waals component:

$$\Omega = \Omega_g + \Omega_{vw}. \quad (9.13)$$

The so called third sound waves in superfluid films, analogous to long gravity waves in a classical fluid, can exist due to the Wan der Waals forces. To derive the velocity of propagation of the third sound waves we seek the solution in the travelling wave class whose wavelength will be assumed to be much longer than the film thickness l , i.e.

$$1/k \gg 1. \quad (9.14)$$

In this case the fluid oscillations perpendicular to the substrate can be neglected with respect to the longitudinal ones, parallel to the substrate's sur-

face.

The mass conservation requirement in a volume element dx (see Fig. 9.1) implies that:

$$\rho \frac{\partial \delta\zeta}{\partial t} + \bar{\rho}_s l \frac{\partial v_s}{\partial x} = 0, \quad (9.15)$$

where $\bar{\rho}_s$ is the average density over the film of thickness l and v_s must in some sense be averaged over z . The deviation $\delta\zeta$ of the thickness ζ from its equilibrium value due to third sound perturbation satisfies the relation:

$$\zeta(x,t) = 1 + \delta\zeta(x,t). \quad (9.16)$$

As the first sound velocity is much larger than the third sound velocity the density ρ can be taken as constant. The momentum conservation equation (9.11) in the direction perpendicular to the substrate, disregarding the small gravitational force, yields:

$$\frac{\partial p}{\partial z} = -\rho \frac{\partial \Omega_{vw}}{\partial z} \quad \text{and} \quad \frac{\partial T}{\partial z} = 0, \quad (9.17)$$

hence the temperature depends only on x and t :

$$T = T_0 + \delta T(x,t). \quad (9.18)$$

Integrating the entropy equation over the distance dx and neglecting the small term $\frac{\partial \delta p}{\partial t} \frac{\partial s}{\partial p}$ we obtain:

$$s \frac{\partial \delta\zeta}{\partial t} + l \frac{\partial s}{\partial T} \frac{\partial \delta T}{\partial t} = 0. \quad (9.19)$$

As the pressure at the film-vapour interface must be continuous and equal to the vapour pressure p_g their follows integrating (9.13):

$$p = \int_1^{\zeta} \rho \frac{\partial \Omega_{vw}}{\partial z'} dz' + p_g. \quad (9.20)$$

The variation of pressure in a third sound wave is due to the variation of ζ and it is independent of z . To first order we have:

$$\delta p = \rho \frac{\partial \Omega_{vw}}{\partial l} \delta\zeta \quad (9.21)$$

Averaging the component in the x direction of the superfluid equation (9.11) there follows:

$$\frac{\partial v_s}{\partial t} - \bar{s} \frac{\partial \delta T}{\partial x} + \frac{\partial \Omega_{vw}(l)}{\partial l} \frac{\partial \delta \zeta}{\partial x} = 0. \quad (9.22)$$

The set of equations (9.15), (9.19), (9.22) for the variables v_s , δT , $\delta \zeta$ describe the third sound wave. The following dispersion equation for the travelling wave solution is obtained using the standard procedure:

$$\frac{\omega^2}{k_0^2} = \frac{\bar{\rho}_s \bar{s}}{\rho} s \left(\frac{\partial s}{\partial T} \right)_p^{-1} + \frac{\bar{\rho}_s l}{\rho} \frac{\partial \Omega_v(l)}{\partial l}. \quad (9.23)$$

The temperature variation is due the flow of the superfluid component which can not transport entropy. Thus in troughs where the film is thinner the entropy is "condensed" and the temperature is increased whereas the opposite effect occurs at the mounds. However it should be mentioned that at a higher approximation this effect is greatly reduced.

Moreover as there are temperature variations of the film one can expect an influence of evaporation and condensation on the propagation of third sound waves. Of course under equilibrium conditions the net effect is zero. In the first order approximation one can assume that the evaporation rate per unit area is proportional to the local temperature deviation, δT , from its equilibrium value with K_{ec} as the proportionality coefficient. The mass conservation equation (9.15) must in this case be supplemented by an additional term which takes into account this effect and becomes:

$$\rho \frac{\partial \delta \zeta}{\partial t} + \bar{\rho}_s l \frac{\partial v_s}{\partial x} = -K_{ec} \delta T \quad (9.24)$$

As evaporation requires the supply of latent heat L in addition to the entropy carried away by the vapour (9.19) must be modified to include an additional term to take into account these additional requirements and becomes:

$$s \frac{\partial \delta \zeta}{\partial t} + l \frac{\partial \bar{s}}{\partial T} \frac{\partial \delta T}{\partial t} = - \frac{K_{ec}(L + sT)}{\rho T} \delta T. \quad (9.25)$$

The plane travelling wave solution to (9.22), (9.24), (9.25) yields the following dispersion relation:

$$a_3^2 = \frac{\omega^2}{k_0^2} = \frac{\bar{\rho}_s l}{\rho} \frac{\partial \Omega_v(l)}{\partial l} + \frac{\frac{\bar{\rho}_s s T}{\rho} \left(\bar{s} + \frac{i K_{ec}}{\rho \omega} \frac{\partial \Omega_v(l)}{\partial l} \right)}{T \frac{\partial s}{\partial T} + \frac{i K_{ec} L}{\rho \omega l}} \quad (9.26)$$

The coefficient K_{ec} can be determined experimentally or roughly estimated from kinetic theory as:

$$K_{ec} \approx \left(\frac{M}{2\pi R T} \right)^{1/2} \left(\frac{dp}{dT} \right)_{co} \quad (9.27)$$

where M is the molecular weight, R the gas constant and the subscript co indicates that the derivative should be taken along the phases coexistence curve.

As the terms involving K_{ec} dominate the fraction in (9.27) at $1K < T < 2K$ and $\omega < 10^4 \text{ sec}^{-1}$, the approximate expression for the velocity of propagation of third sound within this range of parameters becomes:

$$a_3^2 = \frac{\bar{\rho}_s l}{\rho} \frac{\partial \Omega_{vw}}{\partial l} \left(1 + \frac{sT}{l} \right) \quad (9.28)$$

The theoretical variation of the third sound velocity with the film thickness, expressed in atomic layers (equal 0.36nm) is illustrated on Fig. 9.2 for two temperatures. The strong decrease of a_3 with the increase of film thickness is noticeable and therefore a comparison of experimental and theoretical results requires a precise knowledge of the film thickness, which is a rather very difficult problem.

The thin superfluid film problem is a very interesting and involved problem and I would like to recommend to those interested to start by reading the review of Atkins and Rudnick and of Rudnick,

§10. Evolution of rectangular axisymmetric heat pulses in superfluid helium.

The analysis of the evolution of rectangular heat pulses, as compared with shock waves, although more involved theoretically, can often yield more information about real flow conditions. It gives also the possibility of a more detailed comparison with experimental available results, in particular those reported by Iznakian and Mezhov-Deglin and the recent results of von Schwerdtner and Stamm.

We will analyse the evolution of moderate cylindrical heat pulses. It is known (see e.g. Whitham) that unlike in the cases of plane and spherical symmetry it is impossible to obtain a closed analytical solution of the linear wave propagation problem in the axisymmetric case. We would like following Fiszdon, Peradzynski, Stamm to show an approximate theoretical approach which compares well with the experimental results.

Typical experimental results of the evolution of temperature pulse shapes at different distances from the heated cylindrical surface for two different heating times are shown on Fig.10.1. The geometrical shape of the heat pulses gives a hint how to build an approximate analytical model describing this evolution.

As we are interested in weak second sound waves we will assume that the counterflow condition, $\rho_s \mathbf{v}_s + \rho_n \mathbf{v}_n = 0$, is satisfied. It will be assumed that within the range of parameters considered the linear approximation is adequate and the flow can be taken as dissipationless. The relevant conservation equations in terms of the counterflow velocity \mathbf{w} and the perturbation temperature T of the bath temperature T_0 become then:

$$\frac{\partial T}{\partial t} + \frac{T_0 s \rho_s}{\rho C_p} \operatorname{div} \mathbf{w} = 0, \quad (10.1)$$

$$\frac{\partial \mathbf{w}}{\partial t} + \frac{\rho_s}{\rho_n} \operatorname{grad} T = 0. \quad (10.2)$$

Subtracting the divergence of (10.2) from the gradient of (10.1) there follows the wave equation for the temperature perturbation:

$$\frac{\partial^2 T}{\partial \xi^2} - \Delta T = 0, \quad (10.3)$$

where the time, $\xi = a_{20}t$, is now measured in length units related to the second sound velocity given by (4.15). The equation for the counterflow velocity becomes now:

$$\frac{\partial \mathbf{w}}{\partial \xi} + \text{grad } T = 0, \quad (10.4)$$

where

$$K = \rho(C_p / (\rho_n \rho_s T_0))^{1/2}$$

In the case of axisymmetric flow (10.3) becomes:

$$\frac{\partial^2 T}{\partial \xi^2} - \frac{1}{r} \frac{\partial}{\partial r} \left(r \frac{\partial T}{\partial r} \right) = 0. \quad (10.5)$$

The boundary conditions for the counterflow velocity are given at the heated surface of the cylinder of radius R :

$$w(r=R) = w_0(H(\xi) - H(\xi - \xi_0)), \quad (10.6)$$

where H is the Heaviside step function and w_0 is related to the constant heat flux,

$$w_0 = Q_0 / (\rho_s s T_0) \quad (10.7)$$

and ξ_0 corresponds to the heating time t_h :

$$\xi_0 = a_{20} t_h \quad (10.8)$$

We will begin by solving the single positive step problem i.e. instead of (10.6) the relevant boundary condition will be:

$$w_+(r=R) = w_0 H(\xi). \quad (10.9)$$

In the absence of a known exact closed form solution we will use an approximate asymptotic expansion for small distances from the heated surface r/R and small distances from the wave front $\tau = \xi - r$ (see e.g. Whitham):

$$T_+ = T_i \frac{H(\tau)}{\sqrt{(r/R)}} (1 + \alpha_1 \tau + \dots) \quad (10.10)$$

where T_i and α_1 are to be determined from the boundary conditions.

Integrating (10.4) after having introduced there (10.10) we obtain:

$$w_+ = K T_i \left(1 + \tau/2r + \alpha_1 \tau + \dots \right) \quad (10.11)$$

and to satisfy the conditions (10.7), (10.9) we must have:

$$\alpha_1 = -1/2R, \text{ and } T_i = w_o / K \quad (10.12)$$

finally up to second order terms we obtain for the single step problem:

$$T_+ = \frac{w_o}{K} (R/r)^{1/2} H(\tau) \left(1 - \tau/2R \right), \quad (10.13)$$

$$w_+ = w_o (R/r)^{1/2} H(\tau) \left(1 - \tau/2R + \tau/2r \right) \quad (10.14)$$

To obtain the solution for a rectangular, top hat pulse according to (10.6) we must add to (10.13), (10.14) for $\xi > \xi_o$ a similar solution with reversed sign, delayed in time by ξ_o . Thus we obtain:

$$\left. \begin{array}{l} T_+ = \frac{w_o}{K} (R/r)^{1/2} H(\tau) \left(1 - \tau/2R \right), \\ w_+ = w_o (R/r)^{1/2} H(\tau) \left(1 - \tau/2R + \tau/2r \right). \end{array} \right\} \text{for } \tau < \xi_o, \quad (10.15)$$

and

$$\left. \begin{array}{l} T_+ = \frac{w_o}{K} \frac{\xi_o}{2R} (R/r)^{1/2} \\ w_+ = w_o \frac{\xi_o}{2R} (R/r)^{1/2} \left(1 - R/r \right) \end{array} \right\} \text{for } \tau > \xi_o, \quad (10.16)$$

The slope of the temperature pulse follows from (10.15):

$$\beta(r) = -\frac{w_o}{2K\sqrt{Rr}} = \frac{T_i}{2\sqrt{Rr}} \quad (10.17)$$

A somewhat better approximate asymptotic expansion could be obtained introducing an additional term in the (10.10) expansion:

$$T_+ = T_i (R/r)^{1/2} H(\tau) \left(1 + \alpha_1 \tau + \alpha_2 \tau/r + \dots \right), \quad (10.18)$$

however this is a time consuming procedure.

To analyse the general case of nonlinear evolution of the temperature pulse we will use the general dissipationless Burgers equation. The dissipations become important at large evolution times and hence also larger distances from the heated surface. As the experimental data are for fairly short times and we are presently not looking at the detailed structure of the shock wave the used approximation seems reasonable. Furthermore as the experimental results are in the form of temperature variations in time at different positions it is convenient to use Burgers's equation in Mendousse's form as given e.g. by Sachdev:

$$\frac{\partial T}{\partial r} - \alpha_2 T \frac{\partial T}{\partial \tau} + \frac{T}{2r} = 0, \quad (10.19)$$

where α_2 is the nonlinearity coefficient of Khalatnikov.

We will consider first the simpler triangular pulse, say OPP_O on Fig.10.2 calling A the amplitude:

$$q = \int_{-\infty}^{+\infty} A(r) d\tau, \quad (10.20)$$

there follows from (10.19):

$$\frac{\partial q}{\partial r} + q/2r = 0, \text{ hence } q = q_O(R/r)^{1/2}. \quad (10.21)$$

Substituting $T = \beta(r)\tau$ in (10.19) it can be noticed that the slope $-\beta(r)$ of the line $(P_O P)$ satisfies the relation:

$$\frac{\partial \beta}{\partial r} + \alpha_2 \beta^2 + \beta/2r = 0. \quad (10.22)$$

Integrating this last equation and taking into account that the initial slope at $r = R$ is $A_O/l_O = \beta_O$ we obtain:

$$\beta = \frac{A_O}{l_O} \left(\frac{R}{r} \right)^{1/2} \left(1 + 2\alpha_2 A_O \frac{R}{l_O} (\sqrt{r/R} - 1) \right)^{-1} \quad (10.23)$$

using the obvious geometric relations:

$$q = A(r) l(r) \quad \text{and} \quad \beta = A(r)/l(r), \quad (10.24)$$

there follows for $\alpha_2 > 0$

$$A = A_0 \left(\frac{r}{R} \left(1 + 2\alpha_2 A_0 \frac{R}{l_0} (\gamma/(r/R) - 1) \right) \right)^{1/2}, \quad (10.25)$$

$$l = l_0 \left(1 + 2\alpha_2 A_0 \frac{R}{l_0} (\gamma/(r/R) - 1) \right)^{+1/2}. \quad (10.26)$$

Thus for small times when r is close to R the amplitude varies as $r^{-1/2}$ and for large times as $r^{-3/4}$.

Having the solution corresponding to the later stages of evolution of the rectangular pulse, when it becomes triangular, let us analyse the earlier stages of evolution. From (10.17) it follows that at $t = 0$ and $r = R$

$$\beta(R) = \beta_0 - T_i / 2R \quad (10.27)$$

and from the similarity of the triangles PP_1P_1 and P_0OP that at $t = 0$, $l = l_0 = 2R$. Hence the variation of the amplitude of the temperature and of the length l in the case of a forward steepening shock wave i.e. at $T_0 < 1.884K$ are given by:

$$\left. \begin{aligned} T &= T_a \left((r/R) \left(1 + \alpha_2 T_a ((r/R) - 1) \right) \right)^{-1/2}, \\ l &= 2R \left(1 + \alpha_2 T_a ((r/R) - 1) \right)^{1/2}. \end{aligned} \right\} \quad (10.28)$$

Recalling (5.25) it can be noted that when the amplitude at P_1 is larger than $A_0/2$ then the point P_1 will be moving faster than point P (see Fig.10.2) in front of the heat pulse, and as the area (OPP_1P_2) say S_a varies with r according to (10.21):

$$S_a = S_0 \gamma^2 (R/r), \quad (10.29)$$

we will hence have the idealised intermediate pulse shape shown on Fig.10.3 which is similar to some measured pulses shown on Fig.10.1. The slope of P_1P_2 relative to OP_2 called $-\beta$ is determined from (10.22) satisfying the condition $\tilde{\beta} = \infty$ when $r = R$ i.e.

$$\tilde{\beta}(r) = \left(2\alpha_2 R (1 - \gamma/(R/r)) \right)^{-1/2} \quad (10.30)$$

The evolution of the pulse shape as P_1 moves towards P will be from the quadrangle to the triangle $(O, (P \equiv P_1), P_2)$ of area $A^2 / (2\tilde{\beta}_{cr})$. The index "cr"

corresponds to the involved variables at the geometrical transition. As the areas of the starting and the triangular pulses must evolve according to (10.21), (10.29) there follows:

$$\frac{\beta(r_{cr})}{\tilde{\beta}(r_{cr})} = \frac{\xi_O}{r} \left(1 - \frac{\xi_O}{4r}\right) = \mu_O, \quad (10.31)$$

where $\beta(r)$ is given by (10.23) with $r = r_{cr}$ and $l_O = 2R$. the critical value of r when the quadrangular pulse shape changes into a triangular one is

$$\frac{r_{cr}}{R} = \left(\frac{\mu_O}{\alpha_2 A_O (1 - \mu_O)} + 1 \right)^2. \quad (10.32)$$

Thus for $r < r_{cr}$

$$T = T_a \left(\frac{r}{R} \left(1 + \alpha_2 T_a (r/R - 1) \right) \right)^{-1/2} \quad (10.33)$$

$$d = 2R \left(1 + \alpha_2 T_a (r/R - 1) \right)^{1/2} - (2R - \xi_O). \quad (10.34)$$

For $r > r_{cr}$ the formulae (10.25) (10.26) must be used. At $r = r_{cr}$, $T = T_{cr}$ using (10.32) there follows:

$$T_{cr} = T_a \left(\frac{r_{cr}}{R} \frac{1}{1 - \mu_O} \right)^{-1/2}, \quad (10.35)$$

$$d_{cr} = 2R \left(\left(\frac{1}{1 - \mu_O} \right)^{1/2} - 1 \right) + \xi_O, \quad (10.36)$$

and finally at $r > r_{cr}$:

$$T = T_{cr} \left(\frac{r}{r_{cr}} \left(1 + 2\alpha_2 \frac{T_{cr} r_{cr}}{d_{cr}} (\sqrt{r/r_{cr}} - 1) \right) \right)^{-1/2}. \quad (10.37)$$

As we have seen on the figures the shapes of the theoretical and experimental pulses of course agree by "definition". It is also interesting to compare the calculated and measured variation of the amplitude with distance from the heated surface. This is illustrated on Fig.10.4 . The agreement is very satisfactory showing also the critical distance where the pulse shape changes from quadrangular to triangular. however it should be noted that in the considered case the geometrical effects predominate and this may explain the good correlation between theory and experiment.

§ 11. Evolution of moderate plane rectangular heat pulses

as influenced by quantum turbulence.

Before describing the stated problem I think, that it would be appropriate to give a very brief introduction to superfluid turbulence. More details about it can be found in e.g. Donelly's monograph and in the listed literature.

The Landau assumption concerning superfluid vorticity ($\text{rot} \mathbf{v}_s = 0$) at its direct meaning suggests that superfluid vortices do not exist. However as shown by Onsager and Feynman this condition is not violated by the existence of quantised vortex lines, which are potential confined singularities. This explains the "rotation paradox" connected with the possibility of setting the superfluid component into a rotational motion. Osborne demonstrated that a cylindrical bucket filled with superfluid helium when rotated has a meniscus of exactly the same shape as that of a classical fluid. Hence the superfluid component must move together with the normal component. The entrainment of the superfluid component into rotation in a rotating bucket can be explained by the existence of parallel straight isolated vortex lines as shown schematically on Fig.11.1, which interact with the normal fluid. Using the property of vortex lines to trap electrons Williams and apacckard photographed configurations of vortex lines in a rotating bucket filled with helium.

The circulation along a closed contour containing n vortex lines is:

$$\int \mathbf{v}_s d\mathbf{l} = \int_A (\text{rot} \mathbf{v}_s) dA = nh/m_4 = nx,$$

where h is Planck's constant, m_4 the mass of a helium atom and x is the quantum of circulation ($x = 0.997 \text{ cm}^2 \text{sec}^{-1}$).

Let us note that in a cylinder, filled with superfluid helium, rotating at 1 rad/sec about 2000 vortex lines per sq.cm are generated. The presence of these quantised vortex lines leads to mutual friction between the two components. The experiments of Gorter Mellink and the extensive study of Vinen led to the idea of the existence of a mass of quantised vortex lines, with a properly averaged vorticity, which could be described as homogeneous "quantum turbulence" recently reviewed by Donelly and Swanson. The microscopic analysis, made by Schwarz, of the evolution of vortex lines, with an appropriate assumption concerning their intersection properties, led to the theoretical confirmation of the model of "tangled" vortex lines.

The theoretical properties of this model are consistent with Vinen's phenomenological deductions from his flow experiments in small diameter tubes. As reviewed by Tough this model describes properly the temperature and pressure gradients observed in tubes once the flow velocity becomes higher than a so called critical velocity.

These roughly described quantum turbulence effects on steady flow in tubes suggest, that it would be of some interest to look at the influence of quantum vorticity on the evolution of heat pulses. Turners extensive research on second sound waves has shown the existence of a critical heat flux above which the two fluid model including dissipation is insufficient to explain the observed character of the flow. Following Fiszdon and v.Schwerdtner the recent investigations concerning the evolution of moderate second sound pulses will be described.

Typical temperature evolutions of a rectangular pulse of 5 Watt/sq.cm. at a bath temperature of 1.4K at distances of 1, 2 and 5.4 mm. are shown on Fig.11.2 as measured using a superconducting (An,Sn) bolometer near its critical temperature. On Fig.11.3 the temperature evolutions at a constant distance of 1 mm. and different heat inputs are given. The striking feature of the temperature curve shapes is the existence of important temperature overshoots. Already Torczynski in his research on second sound waves in rotating superfluid helium has shown that the presence of quantum vorticity influences strongly the shape of the propagating shock wave.

To substantiate and understand better the prevailing mechanisms leading to the experimental observations an approximate theoretical model based on the following simplifying assumptions was used:

- the flow is incompressible, $\rho_s = \text{const.}$, $\rho_n = \text{const.}$ and the counterflow conditions, $\rho_s v_s + \rho_n v_n = 0$, are satisfied.
- the entropy related to the normal density, $s_n = s\rho/\rho_n = \text{const.}$
- the quantum turbulence behind the shock wave can be taken as homogeneous isotropic and measured by its local vortex line density (VLD).
- the main dissipative forces are due to the interaction between the quantised vortex lines and the normal fluid and viscosity and heat conductivity can be neglected in the time and space limits we are presently interested in.

Hence from the set of conservation equations of §3, using as dependent variables the counterflow velocity, w , and the temperature perturbation, T , the following equations are obtained keeping terms only up to second order:

$$\frac{\partial T}{\partial t} + \frac{\rho_s}{\rho} w \frac{\partial T}{\partial x} + \frac{T s \rho_s}{C_p \rho} \frac{\partial w}{\partial x} = \frac{\rho_s \rho_n}{C_p \rho} A w^4, \quad (11.1)$$

$$\frac{\partial w}{\partial t} + 3 \frac{\rho_s}{\rho} w \frac{\partial w}{\partial x} + \frac{\rho_s}{\rho_n} \frac{\partial T}{\partial x} = - \rho A w^3. \quad (11.2)$$

The terms on the r.h.s. of the above equations are due to the phenomenologically deduced mutual interaction force based on stationary flow experiments

$$F_{ns} = A \rho_s \rho_n (|v_s - v_n| - v_0)^2 (v_n - v_s), \quad (11.3)$$

where the so called GM coefficient A is directly related to the vortex line density L by Vinen's expression

$$A \rho w^3 = \chi B L w / 3 \quad (11.4)$$

and to the mutual friction parameter B introduced by Khalatnikov. This last relation shows that the terms on the r.h.s. of (11.1), (11.2) are actually not higher than second order and should not be neglected in these second order conservation equations. In our further considerations we neglected the small shift velocity v_0 .

As A is a function of the VLD it is necessary to add a relation for L to close our set of equations. We will use the equation deduced by Vinen as extended by Nemirovski and Lebedev

$$\frac{\partial L}{\partial t} + \frac{\partial (v_L L)}{\partial x} = \chi_1 \frac{B \rho_n}{2 \rho} L^{3/2} - \chi_2 \chi L^2, \quad (11.5)$$

where v_L is the drift velocity of the vortex tangle and χ_1, χ_2 are the VLD growth and decay coefficients given by Vinen. The problem of the drift velocity v_L , as noted by Donelly and Swanson is still open and we will assume that it is a constant small fraction of a_{20} .

Transforming the set of equations (11.1), (11.2), (11.5) to a non-dimensional form (primed variables) taking:

$$T = T_0 + S_n T / a_{20}, \quad w = w' a_{20}, \quad x = x_u x', \quad x_u = 1 \text{ cm.},$$

$$t = x_u t' / a_{20}, \quad v_L = v'_1 a_{20}, \quad \rho'_s = \rho_s / \rho, \quad \rho'_n = \rho_n / \rho,$$

$$b'_1 = \chi B / 3 a_{20}, \quad b'_2 / b'_1 = s \rho_s / (C_p \rho),$$

$$\chi'_1 = \chi_1 B \rho_s, \quad \chi'_2 = \chi \chi_2 / a_{20},$$

there follows the dimensionless set of equations:

$$\frac{\partial w'}{\partial t'} + \frac{\partial T'}{\partial x'} + 3\rho'_s w' \frac{\partial w'}{\partial x'} = -b'_1 L w', \quad (11.6)$$

$$\frac{\partial T'}{\partial t'} + \frac{\partial w'}{\partial x'} + \rho'_s w' \frac{\partial T'}{\partial x'} = b'_2 L w'^2 \quad (11.7)$$

$$\frac{\partial L}{\partial t'} + v' L \frac{\partial L}{\partial x'} = \chi'_1 w' L^{3/2} - \chi'_2 L^2 \quad (11.8)$$

We will assume that at $t < 0$ the medium is at rest and solving the above set of equations use the initial VLD, L_0 , as a parameter. As in §10 the boundary value for the counterflow velocity induced by the heat flux Q is:

$$\left. \begin{aligned} w_0(x=0, 0 < t \leq t_h) &= Q / (\rho_s s_0 T_0), \\ w_0(x=0, t > t_h) &= 0. \end{aligned} \right\} \quad (11.9)$$

It is necessary to formulate boundary conditions for L and T . We will make the simplest assumption, may be justified by symmetry considerations, that at the heated surface in the plane case considered, the Neumann conditions are satisfied i.e. the gradients are zero. However principally Dirichlet or mixed boundary conditions cannot be excluded.

Unfortunately no analytic solution could be found for the set of non-linear hyperbolic equations (11.6) – (11.8). To obtain a convergent numerical solution using a personal computer it was necessary to transform them to a divergent form. For this purpose the temperature perturbation T' had to be replaced by a new dependent variable,

$$\Theta = T' - \rho'_s w'^2 / 2. \quad (11.11)$$

and, as while deducing the conservation equations, third order terms were neglected. The resulting set of equations was solved using the Richtmayer two step version of the Lax-Wendorff method of solution of a non homogeneous set of partial differential equations.

The distribution in space of the temperature, velocity and VLD at the early stages of the wave propagation is illustrated in Fig.11.4 for different consecutive time intervals. It can be seen that the existence of quantum turbulence leads to a reduction of the counterflow velocity and hence of the velocity of the normal fluid thus reducing the heat flow away from the heated sur-

face. This leads to an increase of the temperature of the layer of fluid close to the heated surface during the heating period. Hence at a given distance from the heated surface, particularly close to it, an increase of temperature beyond its shock wave jump is obtained. This was seen on Fig.11.2 where the calculated temperature evolution is reproduced as well as the experimental one. We reproduce also on Fig.11.5 corresponding theoretical results obtained at a bath temperature $T_0 = 1.65K$ showing also a good qualitative correlation.

The satisfactory qualitative correlation between the measured and computed temperature evolutions confirms the validity of the model used. It must be however noted, that on the one hand to have a good correlation of the $T(t)$ curves it was necessary to assume a rather high initial VLD, L_0 of the order of $5 \cdot 10^5 \text{ cm}^{-2}$; on the other hand the experimental data correspond to averages over 5-10 pulses repeated keeping a constant rest time between each consecutive pulse.

A further analysis has shown as illustrated in Fig.11.6 that starting with an initial VLD two or three order of magnitude lower and following the evolution of the consecutive temperature pulses their amplitude increased reaching after a few pulses a steady state. The overshoot increases when the rest time between consecutive pulses is decreased as can be noticed on Fig.11.7. The calculated evolution agrees qualitatively with the experimental measurements when care is taken to start the first pulse in a background of a very low quantum turbulence level. Apparently the consecutive pulses evolve on the background of quantum turbulence left over from the previous pulse whose decay depends strongly on the time interval between each pulse if the rest time between pulses is not long enough. The analysis extended to the axisymmetric case has also produced a good qualitative agreement between the theoretical and experimental results as illustrated on Fig.11.8

It appears that the theoretical model describes qualitatively the real evolution of heat pulses and could be adapted to any initial pulse shape. However although we have a satisfactory picture of the evolution of quantum vorticity between the heater and the shockwave the problem where and how quantum vorticity is generated remains open. Also the phenomenological coefficients used in the numerical calculations are not known well enough to enable a good quantitative comparison of the theoretical and experimental results.

§12 Literature.

Books.

Atkins, K.R., Liquid Helium. Cambridge University Press, (1959).

Batchelor, G.K., AN Introduction to Fluid Dynamics. Cambridge University Press, (1967)

Benneman, K.H., Ketterson, J.B. (eds.), The Physics of Liquid and Solid Helium. J.Wiley, (1976)

Donnelly, R.J., Experimental Superfluidity. The Chicago University Press, (1967).

Donnelly, R.J., Vortices in Helium 4. Cambridge University Press, (to be published in 1990)

Keller, W.E., Helium-3 and Helium-4. Plenum Press, (1969).

Khalatnikov, I.M., Introduction to the Theory of Superfluidity. W.A. Benjamin, (1965).

Landau, L.D., Lifshitz, E.M., Fluid Mechanics. Pergamon Press, (1959).

London, F., Superfluids, Vol.II, Macroscopic Theory of Superfluid Helium. Dover Publications, (1954).

Puterman, S.J., Superfluid Hydrodynamics. North Holland, (1974).

Sachdev, P.L., Nonlinear Diffusive Waves. Cambridge University Press, (1987)

Van Sciver, S.W., Helium Cryogenics. Plenum Press, (1986).

Whitham, G.B., Linear and Nonlinear Waves. J.Wiley, (1974).

Wilks, J. The Properties of Liquid and Solid Helium. Clarendon Press, (1967).

Wilks, J., Betts, P.S., An Introduction to Liquid Helium. Clarendon Press, (1987)

Papers.

Adamenko, I.M., First and Second Sound Dispersion in Cylindrical Capillaries Filled with HeII (in Ukrainian). Ukrainian Physical Journal **13**, (1968), 1001-1009.

Atkin, R.J., Fox, N., Non Linear Waves in Helium II. J. Phys.: Solid State Phys. **C16**, (1983), 1615-1629.

Atkin, R.J., Fox N., Thermal Shock Structure in Superfluid Helium. J. Phys.: Solid State Phys. **C20**, (1987), 1937-1946

Atkins, K.R., Helium Films. Prog. Low Temp. Phys.II, (1959), 104-107.

Atkins, K.R., Rudnick, I., Third Sound. Prog. Low Temp. Phys.**VI**, (1970), 37-76.

Campbell, L.J., Superfluid Film Flow. The Helium Liquid, Armitage et al.eds, (1975), 127-174.

Donnelly, R.J., Swanson, C.E., Quantum Turbulence. J. Fluid Mech. **173**, (1986), 387-429.

Fetter, A.L., Vortices and Ions in Helium. The Physics of Liquid and Solid Helium, (1976), 207-306.

Feynman, R.P., Application of Quantum Mechanics to Liquid Helium. Prog. Low Temp. Phys.**I**, (1955), 17-53.

Fiszdon, W., Schwerdtner, M.v., Influence of Quantum Turbulence on the evolution of Moderate Plane Second Sound Heat Pulses in Helium II. J. Low Temp. Phys. **75**, (1989), 253-267.

Fiszdon, W., Peradzynski, Z., Stamm, G., The Evolution of Axisymmetric Rectangular Second Sound (heat) Pulses in Superfluid Helium. Phys. Fluids **A1**, (1989), 881-886.

Geurst, J.A., Hydrodynamics of Quantum Turbulence in HeII: Vinen's Equation Derived from Energy and Impulse of Vortex Tangle. Physica **B 154** (1989), 327-343.

Glaberson, W.I., Donnelly, R.J., Structure, Distributions and Dynamics of Vorti-

ces in Helium. *Prog. Low Temp. Phys.* **IX**, (1986), 1-147.

Gorter, C.J., Mellink, J.H., On the Irreversible Processes in Liquid Helium II. *Physica* **15**, (1949), 285-304.

Hills, R.N., Roberts, P.H., Superfluid Mechanics for a High Density of Vortex Lines. *Arch. Rat. Mech. Anal.*, **66**, (1977), 43-71.

Iznakian, A.Yu., Mezhov-Deglin, L.P., Shock Waves in Liquid Helium. *Sov. Phys. JETP* **57**, (1983), 801-808.

Langer, J.S., Reppy, J.D., Intrinsic Critical Velocities in Superfluid Helium. *Prog. Low Temp. Phys.* **VI**, (1970), 1-36.

Liepmann, H.W., Laguna, G.A., Nonlinear Interactions in the Fluid Mechanics of HeliumII. *Ann. Rev. Fluid Mech.* **16**, (1984), 139-177.

Liepmann, H.W., Torczynski, J.R., Shock Waves in Helium at Low Temperatures. Proc. XV Intern. Symp. on Shock Waves and Shock Tubes, (ed.) Bershadet et al. Stanford University Press, (1986), 87-96.

Nemirovskii, S.K., Propagation of Heat Pulses Generating Quantized Vortices in HeII. *Sov. Phys. JETP* **64**, (1986), 803-810.

Nemirovskii, S.K., Lebedev, V.V., The Hydrodynamics of Superfluid Turbulence. *Sov. Phys. JETP* **57**, (1983), 1009-1016.

Nemirovskii, S.K., Tsoi, A.N., Transient Thermal and Hydrodynamic Processes in Superfluid Helium. *Cryogenics* **29**, (1989), 985-994.

Roberts, P.H., Donnelly, R.J., Superfluid Mechanics. *Ann. Rev. Fluid Mech.* **6**, (1974), 179-225.

Rudnick, I., The Sounds of ${}^4\text{He}$ II, 75th Jubilee Conference on Helium-4, Armitage (ed.), World Scientific, (1983), 24-33.

Schwarz, K.W., Turbulence in superfluid Helium: Steady homogeneous Counterflow. *Phys. Rev.* **B18**, (1978), 24-33.

Schwarz, K.W., Three-dimensional Vortex Dynamics in Superfluid ${}^4\text{He}$: Homogeneous Superfluid Turbulence. *Phys. Rev.* **B38**, (1988), 2398-2417.

- Schwerdtner, M.v., Stamm, G., Schmidt, D.W., Evolution of Superfluid Vortex Line Density Behind a Heat Pulse in Helium II. *Phys. Rev. Lett.* **63**, (1989), 39-42.
- Swanson, C.E., Donelly, R.J., Vortex Dynamics and Scaling in Turbulent Counter-flowing Helium II. *J. Low Temp. Phys.* **61**, (1985), 363-399.
- Torczynski, J.R., Nonlinear Fourth Sound, Wave Motion **7**, (1985), 487-501.
- Torczynski, J.R., On the Interaction of Second Sound Shock Waves and Vorticity in Superfluid Helium. *Phys. Fluids*, **27**, (1984), 2636-2644.
- Torczynskii, J.R., Shock Vortex Interactions in Superfluid Helium. *Phys. Rev. B*, 2165-2172.
- Tough, J.T., Superfluid Turbulence. *Prog. Low Temp. Phys.* **VIII**, (1982), 134-219.
- Turner, T.N., Second sound Shock Waves and Critical Velocities in Liquid Helium II. Ph.D. Thesis. California Institute of Technology. (1979).
- Turner, T.N., Using Second Sound Shock Waves to Probe the Intrinsic Critical Velocity of Liquid Helium. *Phys. Fluids* **26**, (1983), 3227-3241.
- Vinen, W.F., Mutual Friction in a Heat Current in Liquid Helium II. iii. Theory of Mutual Friction. *Proc. Roy. Soc. Lond.* **A242**, (1957), 493-515.
- Williams, G.A., Packard, R.E., A Technic for Photographing Vortex Positions in Rotating Superfluid Helium. *J. Low Temp. Phys.* **39**, (1980), 553-577.

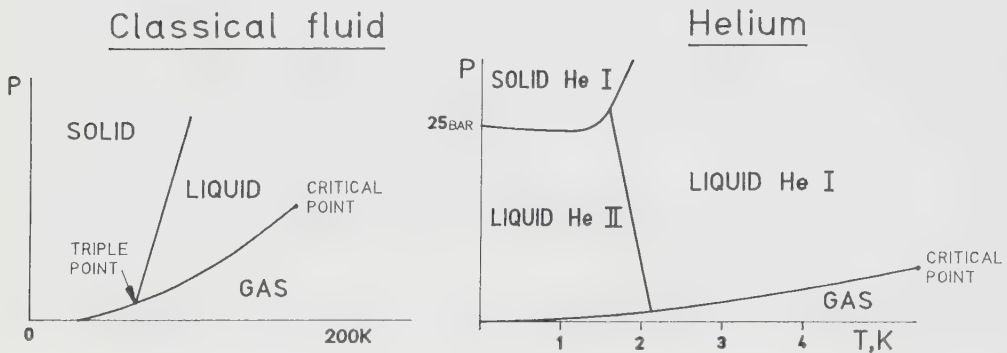


Fig.2.1 Comparison of phase diagrams of a classical liquid and He II.

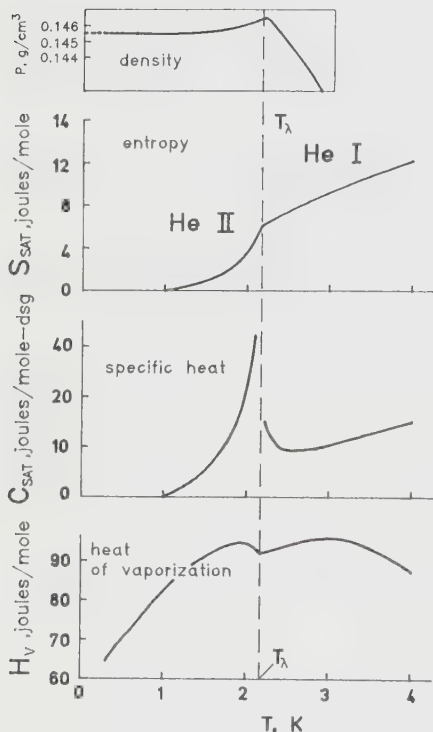


Fig.2.2 Variation of thermodynamic properties of helium with temperature.

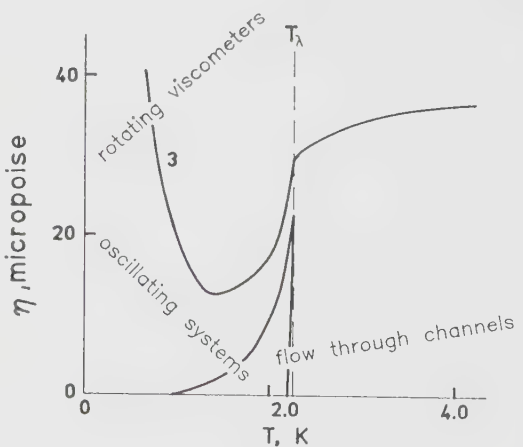


Fig.2.3 Apparent viscosities of liquid helium.

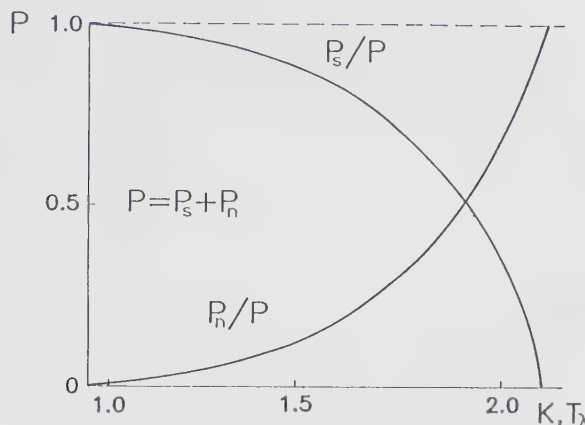


Fig. 2.4 Variation of normal and superfluid component densities with temperature.

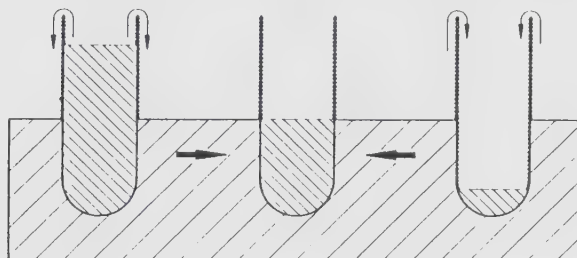


Fig. 2.5 "Connected vessels effect."

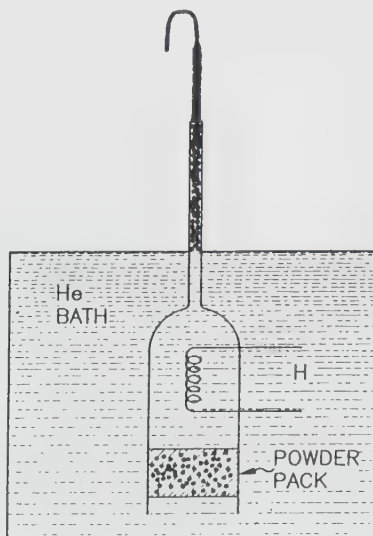


Fig. 2.6 "Helium fountain."

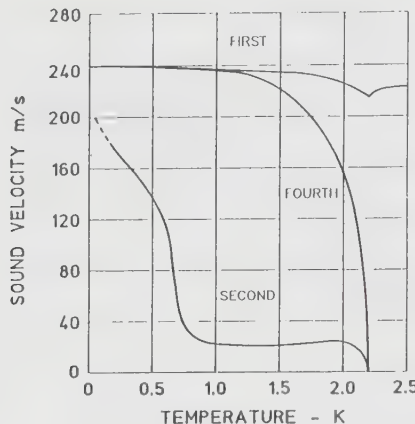


Fig. 4.1 First, second and fourth sound speeds of HeII.

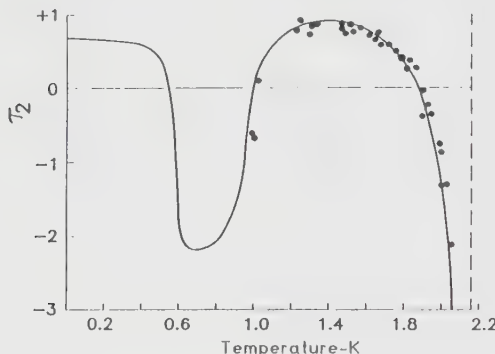


Fig. 5.1 Khalatnikov's nonlinearity coefficient.

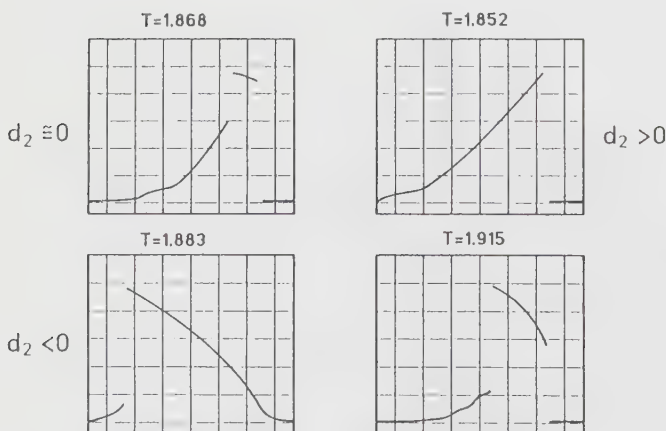


Fig. 5.2 Front steepening, double and rear steepening shock waves (Turner).

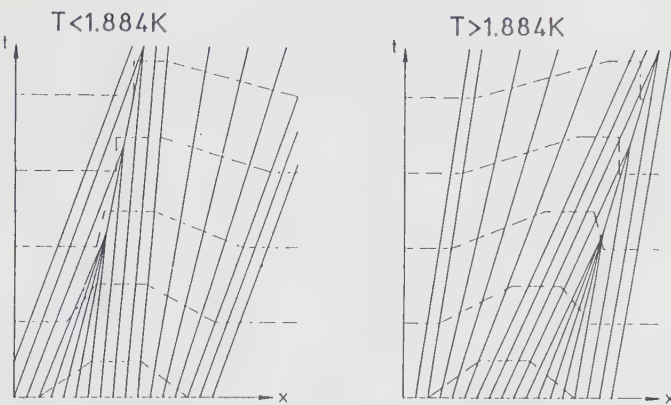


Fig. 6.1 Schematic evolution of trapezoidal temperature pulses using method of characteristics.

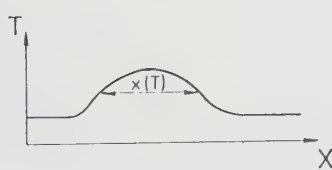


Fig. 6.2 Constant area shock wave.

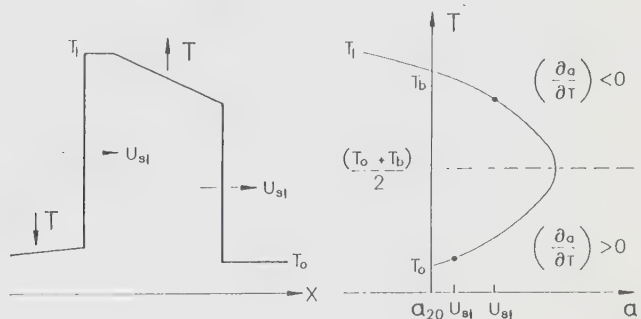


Fig. 6.4 Double shock spanning T_L .

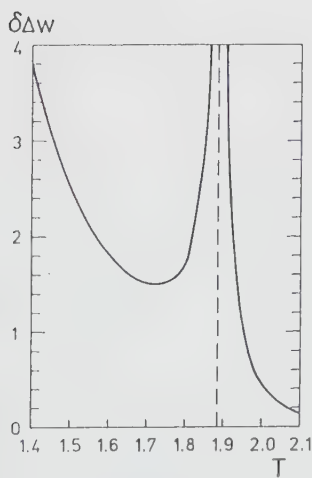


Fig. 6.3 Singularity of the normalised shock wave thickness.

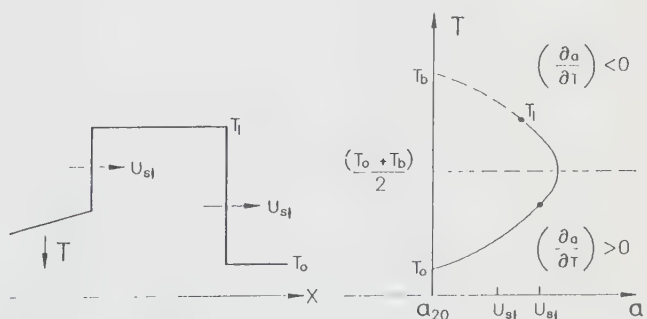


Fig. 6.5 Double shock not spanning T_b .

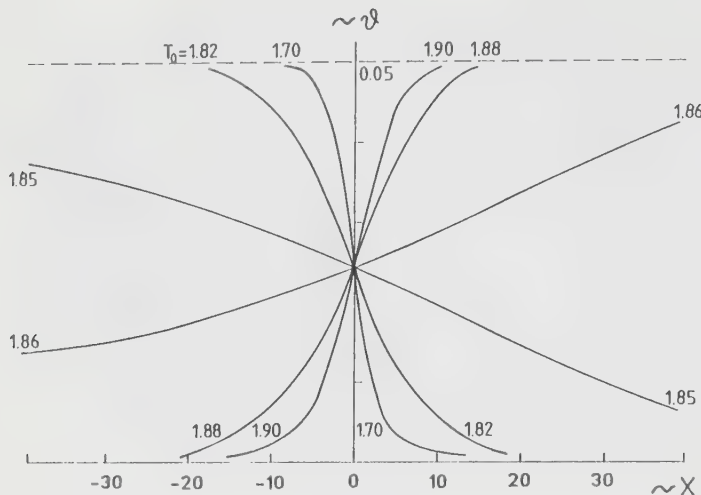
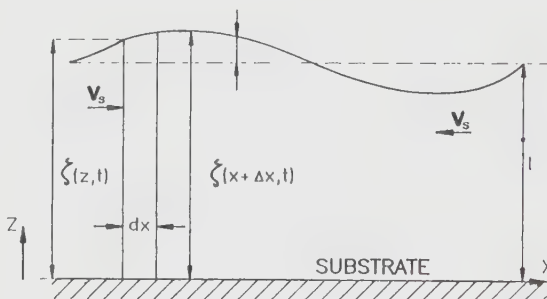
Fig. 7.1 Shock wave structure close to $T = 1.8K$.

Fig. 9.1 Thin film wave.

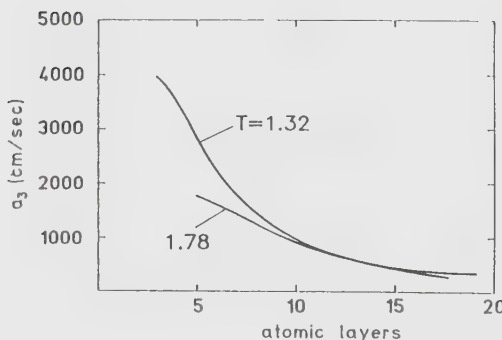


Fig. 9.2 Third sound velocity.

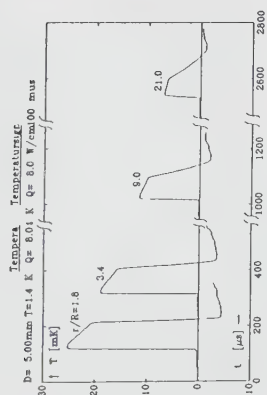


Fig. 10.1 Typical evolution of cylindrical temperature pulses.

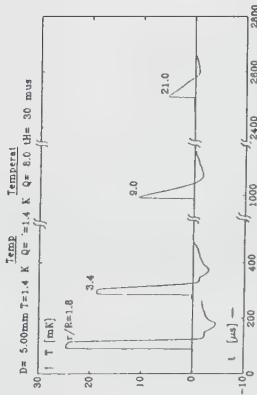


Fig. 10.2 Starting temperature pulse shape. Fig. 10.3 Intermediate temperature pulse shape.

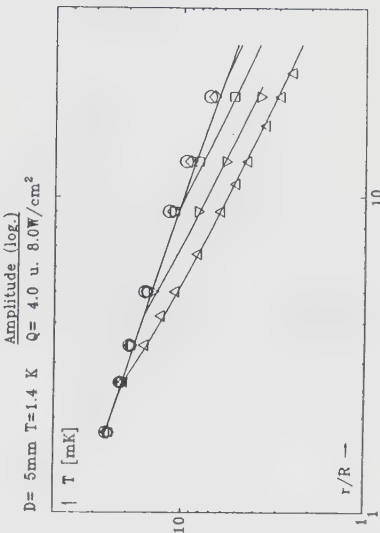
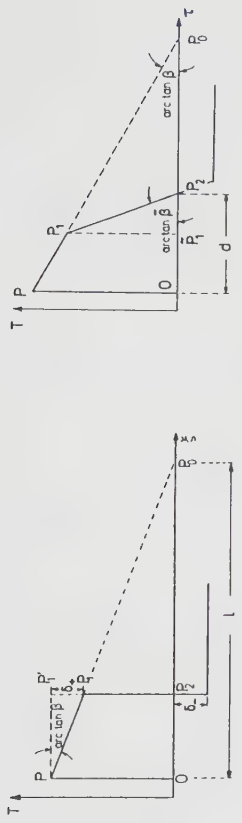


Fig. 10.4 Variation of the pulse amplitude with distance for different heating times.

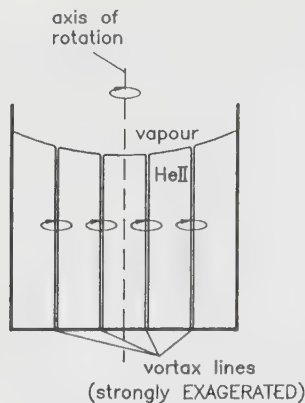


Fig. II.1 Quantum vortices in a rotating bucket filled with HeII.

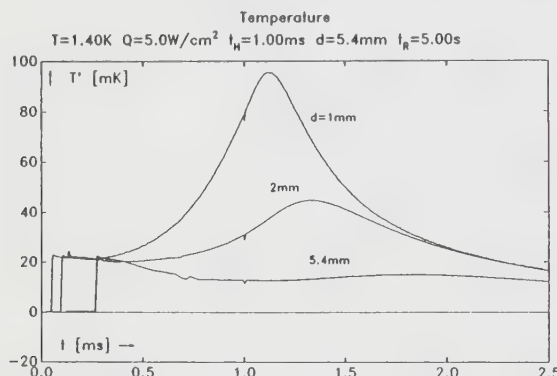


Fig. II.2 Typical temperature evolution at different distances from heated surface.

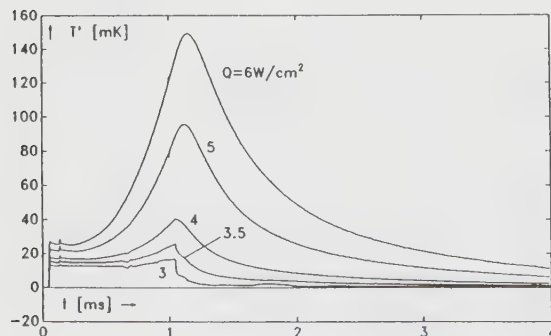


Fig. II.3 Typical temperature evolution at a distance of 1mm for different power inputs.

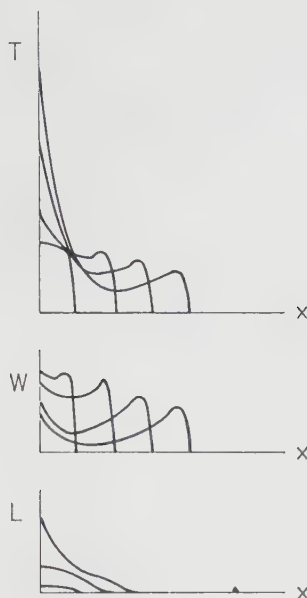


Fig. 11.4 Early stages of temperature, counterflow velocity and vortex line density evolution.

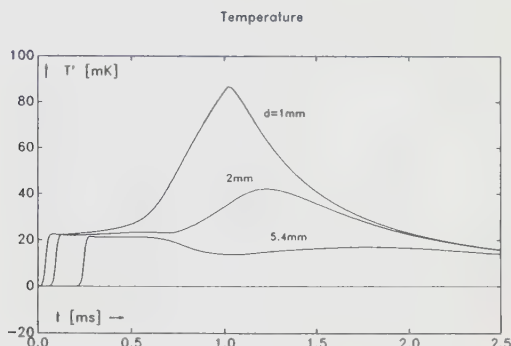


Fig. 11.5 Theoretical temperature evolution at 1, 2 and 5.4 mm from heated surface and 1ms duration heat pulse.

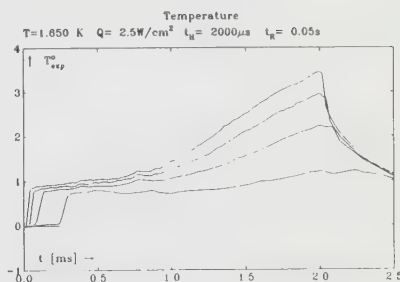
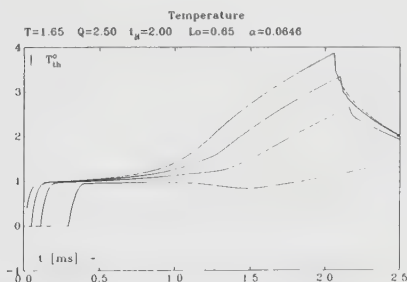


Fig. 11.6 Calculated and measured temperatures at $T_0=1.65 \text{ K}$, 2ms pulses at 1, 2, 3 and 5 mm from heater.

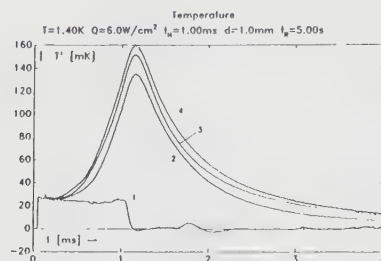


Fig. II.7 Consecutive pulses after "90°" rest time.

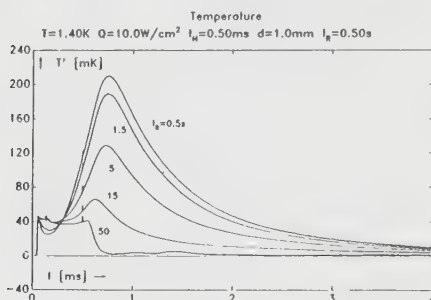


Fig. II.8 Influence of rest time on overshoot.

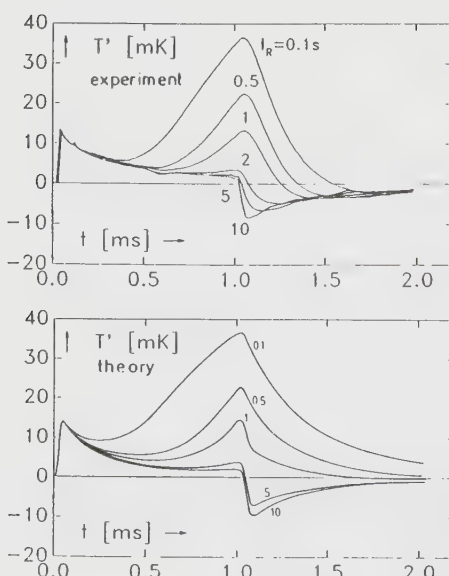
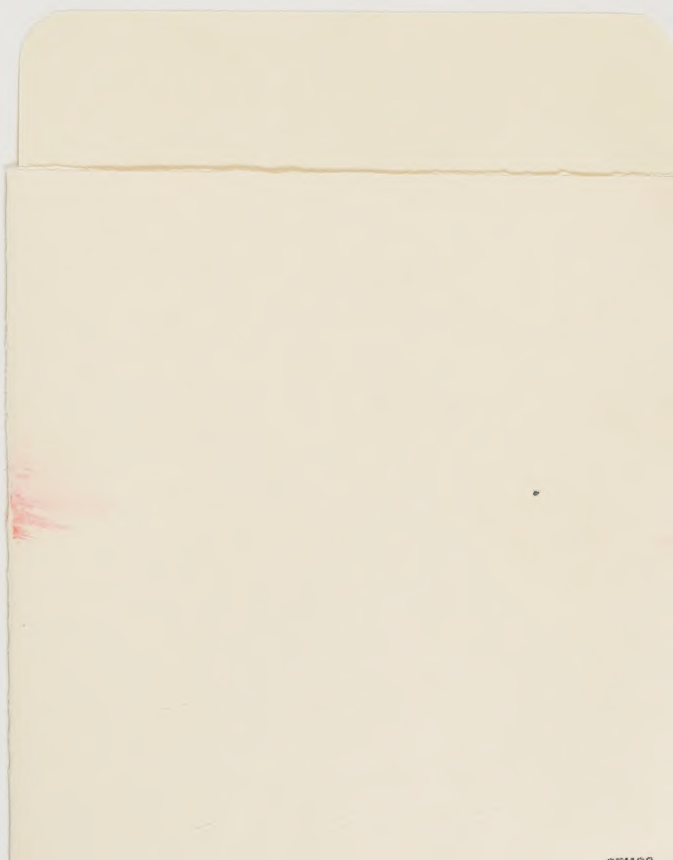


Fig. II.9 Influence of rest time on overshoot in the axisymmetrical case.

R02189 29595



ISBN 3-211-82277-1

ISBN 0-387-82277-1